University of Southern Queensland

School of Agricultural, Computational and Environmental Sciences

Magneto-Inductive Wireless Underground Sensor Networks: Novel Longevity Model, Communication Concepts and Workarounds to Key Theoretical Issues using Analogical Thinking

A thesis submitted by

Vinod Parameswaran

in fulfilment of the requirements of

Doctor of Philosophy

Submitted: March, 2016

Abstract

This research has attempted to devise novel workarounds to key theoretical issues in magneto-inductive wireless underground sensor networks (WUSNs), founded on *analogical thinking* (Gassmann & Zeschky 2008). The problem statement for this research can be summarized as follows. There has been a substantial output of research publications in the past 5 years, devoted to theoretically analysing and resolving the issues pertaining to deployment of MI based WUSNs. However, no alternate solution approaches to such theoretical analyses have been considered. The goal of this research was to explore such alternate solution approaches. This research has used the principle of analogical thinking in devising such alternate solution approaches.

This research has made several key contributions to the existing body of work. **First,** this research is the first of its kind to demonstrate by means of review of state-of-the-art research on MI based WUSNs, the largely theoretical genus of the research to the exclusion of alternate solution approaches to circumvent key theoretical issues. **Second,** this research is the first of its kind to introduce the notion of analogical thinking as a solution approach in finding viable workarounds to theoretical impediments in MI based WUSNs, and validate such solution approach by means of simulations. **Third,** this research is the first of its kind to explore novel communication concepts in the realm of MI based WUSNs, based on analogical thinking. **Fourth,** this research is the first of its kind to explore a novel longevity model in the realm of MI based WUSNs, based on analogical thinking. **Fifth,** this research is also the first to extend the notion of analogical thinking to futuristic directions in MI based WUSNs research, by means of providing possible indicators drawn from various other areas of contemporary research.

In essence, the author believes that the findings of this research mark a paradigm shift in the research on MI based WUSNs.

Associated Publications

The following publications were produced during the period of candidature:

Parameswaran, V., Zhou, H., & Zhang, Z. (2012, December). Irrigation control using wireless underground sensor networks. In Sensing Technology (ICST), 2012 Sixth International Conference on (pp. 653-659). IEEE

Parameswaran, V., Zhou, H., & Zhang, Z. (2013, December). Wireless underground sensor network design for irrigation control: Simulation of RFID deployment. In Sensing Technology (ICST), 2013 Seventh International Conference on (pp.842-849). IEEE

Parameswaran, V., Zhou, H., & Zhang, Z. (2014, September). Numerical Terrain Modelling for Wireless Underground Sensor Networks A Prototype for Nut Tree Plantations. In Sensing Technology (ICST), 2014 Eighth International Conference on (pp.296-300).

Parameswaran, V. (2014 November). Heuristic Deployment Model for Magneto-Inductive Wireless Underground Sensor Networks in Pecan Farm. Submitted to IEEE Sensors Journal (Manuscript No. Sensors-11126-2014).

Certification of Dissertation

I certify that the ideas, designs and experimental work, results, analyses and conclusions set out in this dissertation are entirely my own effort, except where otherwise indicated and acknowledged.

I further certify that the work is original and has not been previously submitted for assessment in any other course or institution, except where specifically stated.

Vinod Parameswaran

00610033416

Signature of Candidate

Date

ENDORSEMENT

Signature of Supervisor/s

Date

Acknowledgments

I would like to begin with a quote from Leo Burnett, which I first came across in a Reader's Digest issue during my pre-university days: “If you reach for the stars, you might not quite get one, but you won't end up with a handful of mud, either”. So, have I achieved everything that one could possibly achieve during the course of this journey? Probably not. Having said that, I have not ended up in a wasteland either. Essentially, this is in the spirit of every voyage and discovery. You set out with a destination, veer course en route due to setbacks or circumstances, but end up in a place where no man has been before. I am reminded of the quote from Albert Einstein “If we knew what it was we were doing, it would not be called research, would it?”, when I look back on my journey.

During this journey, many have tried to take the wind out of my sails or try and dissuade my purpose, but those are the ones that do not deserve mention at this juncture. So let me dwell on those who have made my days, directly or otherwise. My brother's support and love comes above everything else, which has been my constant source of courage and encouragement amidst many a rough weather. One of my friends who is a gifted writer, wrote recently on his Facebook page that he would like to thank his teachers as much for what they did not tell him, as what they did. I would like to extend that sentiment to both my supervisors, for granting me the privilege to experience this journey on my own terms. I would like to thank the university for supporting my research with a scholarship. I have benefited immensely from the library and its DocEx service, so this is the time to register a deep acknowledgement. I would also like to thank my department for the convenient office space taking my special needs into consideration. This is also the moment to register my deep acknowledgement to the support group at TEX and MATLAB Central for the countless occasions of timely resolution of Latex and MATLAB issues, some minor and some not so. Without their kind favour sans any reservations, this work would never have seen the light of this day.

Well, to sum it all up, let me take a leaf out of the bard, and say "All's well, that ends well".

Vinod Parameswaran

Contents

List of Figures

List of Tables

Acronyms & Abbreviations

AC	Alternating Current
ADC	Analog-to-Digital Converter
AI	Artificial Intelligence
AG2UG	Aboveground to Underground
ARPT	Active Reader Passive Tag
ASBCP	Aggregator Sensor Serial Bus Communication Protocol
BER	Bit Error Rate
BZ	Beach Zone
C	Coulomb
CDS	Connected Dominant Set
cm	centimetre
CMS	Crash Management System
CRIM	Complex Refractive Index Model
CSI	Channel State Information
CSMA	Carrier Sense Multiple Access
CTO	Chief Technological Officer
dB	Decibel
dBi	Decibel(isotropic)
dBm	Decibel-milliwatts
DC	Direct Current

DEM	Digital Elevation Model
EaT	Energy and Throughput
ELF	Extremely Low Frequency
EM	Electromagnetic
EMF	Electromotive Force
EMI	Electromagnetic Induction
EMI	Electro-Magnetic Interference
F	Fahrenheit
F	Farad
FDM	Frequency Division Multiplexing
FEC	Forward Error Correction
ft.	foot
FW	Full-Wave
GHz	Giga Hertz
H	Henries
Hz	Hertz
IACS	International Annealed Copper Standard
IEEE	Institute of Electrical and Electronics Engineers
IETF	Internet Engineering Task Force
IoT	Internet of Things
ISI	Inter-Symbol Interference
ISM	Industrial, Scientific and Medical
ISO	International Organization for Standardization
ITU	International Telecommunication Union
ITU-T	ITU Telecommunication Standardization Sector
kg	Kilogram
kHz	Kilo Hertz

kW	Kilowatt
LHS	Left Hand Side
LW	Lateral Waves
m	metre
MAC	Medium Access Control
MDM	Mobile Data Mule
Mg	Megagram
MHz	Mega Hertz
MI	Magnetic Induction
MICC	Mineral-Insulated Copper-clad Cable
MIV	Mean Index Value
mm	millimetre
MMSE-DFE	Minimum Mean Squared Error-Decision-Feedback Equalization
m/s	metre per second
MRI	Magnetic Resonance Imaging
MSE	Mean Squared Error
MST	Minimum Spanning Tree
N	Newton
NFC	Near Field Communications
NFPA	National Fire Protection Association®
NP	Non-deterministic Polynomial-time
NSW	New South Wales
1D	One Dimensional
OSI	Open Systems Interconnection
PA	Precision Agriculture
PCB	Printed Circuit Board
PDF	Portable Document Format

PER	Packet Error Rate
pF	Picofarad
PTE	Power Transfer Efficiency
PTF	PedoTransfer Function
PVC	Poly(Vinyl Chloride)
QAM	Quadrature Amplitude Modulation
QoS	Quality of Service
R&D	Research and Development
RF	Radio Frequency
RFC	Request for Comments
RFID	Radio-Frequency Identification
RHS	Right Hand Side
RMS	Root Mean Square
RSS	Received Signal Strength
SCA	Sink Connectivity Area
SCE	Synchronous Charge Extraction
SEA	Single Ended Elliptical Antenna
SER	Symbol Error Rate
SINR	Signal-to-Interference-plus-Noise-Ratio
SIP	Session Initiation Protocol
SN	South-North
SNR	Signal-to-Noise-Ratio
SR	Spread Resonance
SRR	Split Ring Resonator
SSHI	Synchronized Switch Harvesting on Inductor
SSRR	Split Squared Ring Resonator
SZ	Surf Zone

TC	Triangle-Centroid
TDMA	Time Division Multiple Access
TTE	Through-the-Earth
3D	Three Dimensional
2D	Two Dimensional
UBV	Underwater Bottom Vehicle
UG2AG	Underground to Aboveground
UG2UG	Underground to Underground
UHF	Ultra High Frequency
USB	Universal Serial Bus
USB-IF	USB Implementers Forum
UWB	Ultra-Wideband
V	Volt
VoIP	Voice over Internet Protocol
VSD	Visio Drawing
VSW	Very Shallow Water
VWC	Volumetric Water Content
W	watt
WE	West-East
WPT	Wireless Power Transfer
WSN	Wireless Sensor Network
WSNs	Wireless Sensor Networks
WUSN	Wireless Underground Sensor Network
WUSNs	Wireless Underground Sensor Networks

Chapter 1

Introduction

If one were to look back on the progress of humankind over the centuries, there are definite technological milestones that stand out. Breakthroughs such as the X-ray, the steam engine, the automobile, the aeroplane, the DNA, the penicillin, the theory of evolution, computers and microprocessor chips have not only revolutionized human lives; they have turned distinct chapters in the history of humanity. The next such paradigm shift in human life is going to happen due to a technological innovation collectively referred to as the *Internet of Things (IoT)*. To extract a characterization from (Kopetz 2011):
"According to the IoT vision, a *smart planet* will evolve, where many of the everyday things around us have an identity in cyberspace, acquire intelligence, and mash-up information from diverse sources. On the *smart planet*, the world economy and support systems will operate more smoothly and efficiently. But the life of the average citizen will also be affected by changing the relation of power between those that have access to the acquired information and can control the information and those that do not."
It is not before long that scenarios that would be relegated to science fiction now could be facts of life, thanks to IoT. For instance, IoT would be able to turn off the lights sensing that no one is home, or close the tap from which water has been dripping, or help locate an object that has been misplaced inside home. These examples merely scratch the surface of the vast potential of IoT, glimpses of which are already emerging in the aspects of modern life. WSNs as a part of IoT have been finding an increasing role in diverse areas ranging from military and civilian surveillance to tracking systems, from environmental and

structural monitoring to home and building automation, from agriculture and industrial settings to health care (Oppermann, Boano & RÃűmer 2014). Of great relevance related to the status quo of WSNs, is the following quote from (Oppermann et al. 2014):
"Until today, most WSN deployments have a strong scientific background. Their main purpose is the demonstration of new technologies and the exploration of remaining limitations; the requirements of the actual application at hand are often secondary. Consequently, most deployments are carried out by computer scientists and not by the intended end-users...... In spite of such promising examples, the number of WSN applications outside the scientific community is still limited. Most deployments remain prototypical in character and are conducted by researchers working on sensor network technologies. Commercial applications tend to be conceptually simple and not to exploit the full potential of scientific innovations."
The above quote points to the fact WSNs are still a largely developing technology, despite all the research output during the past decade. The realm of WUSNs is even less charted territory, owing to the fact that significant research on WUSNs has commenced only during the latter half of the previous decade (Akyildiz & Stuntebeck 2006). Early findings pointed to the unreliability of Electromagnetic (EM) waves for WUSNs, with suggestions of alternate options such as Magnetic Induction (MI). The research on MI based WUSNs is relatively more recent, with the first reported work dating back to only 2009 (Sun & Akyildiz 2009). This report engendered further interest in this area, resulting in a flurry of research output on the topic in the following years. However, all of this research output has been focused exclusively on the theoretical aspect of MI based WUSNs. Analysis of the previous research output on MI based WUSNs can be found under Chapter 4. *So far, no work has reported any design/model suggesting alternate workarounds to the issues unearthed by theoretical research. Considering this fact, the author has focused on the same in this research. More specifically, the author has used analogical thinking (Gassmann & Zeschky 2008) principles in devising innovative workarounds to specific issues highlighted by the theoretical research.* Analogical thinking has been adopted by many research streams previously to solve critical problems innovatively, sometimes without explicitly stating so, and the author has devoted an entire chapter to drive home this point. During the preliminary phase of this research, the author used simulations to validate the theoretical models using selective simulations within the chosen application context. The study undertaken during the preliminary phase eventually led the author to the novel

workarounds, which were further investigated during the second phase by means of prototypical concepts and corresponding simulations. The nature of the proposed workarounds and other innovative concepts and models rooted in analogical thinking, has also been intended to encourage and instil outside the box thinking in the research on MI based WUSNs. It is also intended to introduce a novel approach in problem solving within the domain, combining innovative workarounds with theoretical understanding, with the objective of expediting the full-fledged deployment of MI based WUSNs in the coming years.

1.1 Overview of Research Scope and Objectives

Ideally, WUSN embodies the notion of tiny sensors strewn across a deployment space underground. These sensors are capable of wireless communication with an aboveground sink. There is no wired connection implied in such design (Akyildiz & Stuntebeck 2006). However, the notion of wireless sensors deployed underground and connected by means of wire to aboveground sink, also constitutes WUSN paradigm (Silva & Vuran 2009). (Vuran & Akyildiz 2010) also point to a similar deployment paradigm (Martinez, Ong & Hart 2004), albeit for an application context dissimilar to this research. In the proposed design discussed in a later chapter, the author uses wired connection for UG2AG and AG2UG communication, and partially in UG2UG communication as well. Wireless communication is the predominant aspect of UG2UG communication. The proposed architecture has been used as a temporary workaround; further innovative pointers towards a novel conceptual paradigm shift for WUSNs and rooted in analogical thinking, have been proposed in the concluding section of this thesis. The WUSN layout used in this research can be characterized as follows:

- the underground nodes communicate among one another (UG2UG communication) by means of either wired or wireless mode (predominantly wireless mode)
- the underground nodes communicate with aboveground nodes (UG2AG/AG2UG communication) by means of wired mode

The author presents an extensive review of the state-of-the-art literature from the research on MI based WUSNs under Chapter 4. It will be quite evident from this review that MI as an alternative for EM communication underground has not progressed beyond the theoretical realm. As of now, alternate workarounds to theoretical issues have not emerged from the current research. The review of current research shows that independent research endeavours have followed divergent paths in arriving at theoretical models for MI based WUSNs. More often than not, such models have been highly influenced by the domain of traditional wireless communication aboveground, although it has been an acknowledged fact that the realm of MI based WUSNs has very little in common with the domain (Sun & Akyildiz 2012), (Kisseleff, Gerstacker, Sun & Akyildiz 2013). Many of the theoretical issues in MI based WUSNs stem from the borrowing of concepts inherent to the domain of traditional wireless communication aboveground; this research has embraced a different point of view in circumventing such issues. It is that, rather than looking for purely theoretical solutions to such issues in the underground environment, which is vastly different from the aboveground environment, it would be worthwhile to explore alternate solution approaches aimed at identifying possible workarounds to some of the theoretical issues. The author also extends this conceptual difference into the future, by means of pointers towards novel solution approaches that bring in a new dimension to the research on MI based WUSNs.

During the course of the narrative presented in this dissertation, the author also questions certain preconceptions well-entrenched in the realm of MI based WUSNs, especially in the context of the MI waveguide system (Sun & Akyildiz 2010*c*). For instance, the practice of embedding the relay coils directly in the soil medium, which presents both deployment complexity and is causative to performance attenuation. The novel workarounds suggested in this thesis also address this particular deployment aspect. The objective of this research has also been to engender a paradigm shift in the research on MI based WUSNs, by laying the emphasis on the significance of further similar innovative workarounds to both theoretical and deployment issues in MI based WUSNs, rooted in analogical thinking. Based on both extensive study and relevant simulations, the author holds the firm view that this is the best way forward in realizing rapid progress in the widespread deployment of MI based WUSNs in the coming years.

1.1.1 Simulations

The author presents the simulations and results achieved as part of this research under the **Research Output** part of this dissertation. A quick word of elucidation on these simulations and their corresponding results. The preliminary investigations and corresponding simulations outlined under Chapter 7 had been the result of the author's study to identify the applicability of current theoretical models in MI waveguide communication for the chosen application context. Due to the results of these preliminary simulations, the need for alternate workarounds based on analogical thinking was revealed. The novel workarounds for MI waveguide communication underground presented under Chapter 8 have been aimed at circumventing key theoretical issues, and the corresponding simulation results have been provided to corroborate the efficacy of the workarounds rooted in analogical thinking. ***The technology of MI waveguide WUSNs, based on its theoretical status quo, is still too premature to be deployed on field and as such the validation of the theoretical models and the proposed workarounds had to be confined to simulations. However, the directions for innovative workarounds which emerged can be eventually tested on the field, as part of a standardized deployment framework, which is yet to emerge.***

Before closing this subsection, the author would like to explicate that all the simulations carried out during the preliminary investigations outlined under Chapter 7 have been confined to MI UG2UG communication, as this has been the primary focus of the research study. However, the proposed innovations under Chapter 8, which stemmed from the results of the preliminary investigations, surpass the premise of UG2UG communication and deal with a total deployment scenario involving both AG2UG/UG2AG communication as well, within the context of addressing other aspects such as network longevity and deployment complexity. The simulation results presented under Chapter 8 again mainly deal with demonstrating how the proposed novel workarounds make up for the theoretical deficiencies in MI UG2UG communication, although attention has also been devoted to the aspect of deployment complexity characteristic of theoretical models reviewed under Chapter 4, and how the proposed workarounds drastically curtail the deployment complexity at no cost to network efficiency. In short, the crux of this study has been the aspect of MI as an alternative for UG2UG communication and how certain key theoretical issues therein can be circumvented by means of an alternate solution approach based on workarounds devised using analogical thinking; however UG2UG communication by itself does not complete the picture when it comes to MI based WUSNs, unless AG2UG/UG2AG communication is also addressed adequately. Towards this end, due attention and time have also been devoted to both these aspects all along this dissertation, at relevant junctures.

1.1.2 Summary of Research Objectives, Methodology and Contribution

The following is a summary of the relevant points from the above discussion.
The primary focus of this research lies on the following:

1. Theoretical research has pointed to key theoretical issues in the realization of MI based WUSNs. This research focuses on novel workarounds to these issues, rooted in the concept of analogical thinking.

2. This research also aims at creating a paradigm shift in the research on MI based WUSNs, by instilling and advocating the notion of exploring novel workarounds rooted in analogical thinking, to circumvent theoretical stalemates.

The methodology adopted by this research to both validate current theoretical findings, as well as the proposed innovations as workarounds to theoretical limitations, has been using simulations carried out primarily using MATLAB. The limitations pertaining to actual field deployment and testing as highlighted above, have played a crucial role in this selection.
The key contributions of this research to the existing body of work are as follows:

1. This research is the first of its kind to critically evaluate the state-of-the-art theoretical findings in MI based WUSNs, with the aim of demonstrating how the exclusive focus on theoretical research has prevented the adoption of alternate solution approaches to certain key theoretical issues.

2. This research treads an untrodden path in the research on MI based WUSNs, in that it introduces the notion of analogical thinking into this domain, and examines an alternate route to circumventing some of the critical and performance mitigating

theoretical bottlenecks in MI based WUSNs, by adapting proven solution approaches from other technological domains.

3. This research presents some novel concepts in underground communication adapted from other technological domains.

4. This research presents a novel longevity model for MI based WUSNs.

5. This research presents novel pointers rooted in analogical thinking towards futuristic research on MI based WUSNs.

1.2 Overview of the Dissertation

This dissertation has been divided into three distinct parts. In Part I, the relevant research output from previous work has been covered. This essentially lays down the material upon which the discussion in Part II has been built. Part I also includes a chapter devoted to analogical thinking, aimed at demonstrating how the concept has been the mainstay of many research and engineering initiatives in diverse domains for long.

Part II begins with the work done as part of the preliminary phase of this research. This phase is mostly exploratory in nature, but nevertheless vital to the innovations developed during the latter phase. Glimpses of analogical thinking can be discerned even during the preliminary phase. The innovations developed during the second phase of the research are subsequently detailed, with the relevant models and simulation output.

Part III concludes the dissertation with an outlook into future directions in the research on MI based WUSNs.

All the relevant source code has been provided in the subsequent appendix.

The following is a chapter-wise demarcation of the dissertation:

Part I : Chapter 2 provides a brief overview of WSNs. This chapter forms a prelude to the next chapter, which discusses WUSNs. The intend of the chapter is to highlight the key aspects of WSN functionality, in order to contrast it with the WUSN challenges outlined in the next chapter. The extent of topics covered under this chapter is also significant, considering the penchant in current theoretical research on MI based WUSNs to use principles from wireless communication aboveground in analysing MI based WUSN communication, which as pointed out earlier is not suitable, due to the vast difference between the two communication environments.

Part I : Chapter 3 discusses WUSNs and associated challenges. This discussion leverages on the discussion in the previous chapter, in terms of contrasting the WSN and WUSN deployment scenarios and corresponding demands. The key objective of this chapter is to demonstrate how the challenges in WSN communication are magnified multifold, when transposed to the underground environment.

Part I : Chapter 4 introduces the concept of MI and MI based WUSNs. This chapter also details the theoretical research output on MI based WUSNs till date. This chapter aims at demonstrating by means of reviewing the state-of-the-art research on MI based WUSNs, how the preoccupation has been largely theoretical in nature, to the exclusion of alternate approaches seeking workarounds to key theoretical issues.

Part I : Chapter 5 touches upon chosen prototypical deployment examples involving UG2AG and AG2UG communication. This chapter is also aimed at demonstrating how UG2UG communication has never been experimented with, in previous research conducted.

Part I : Chapter 6 is devoted to the concept of analogical thinking and how it has come into play in a lot of innovative ideas across domains. This chapter is intended as ushering in a departure from the previous research focus on MI based WUSNs, largely preoccupied with theoretical models. The chapter is devoted to the possibilities unleashed by analogical thinking in other domains, and thereby preparing the reader for a similar paradigm shift in the research on MI based WUSNs unveiled in the next part of the thesis.

Part II : Chapter 7 describes the research conducted as part of the preliminary phase, and the corresponding simulations and results. As mentioned before, the simulations discussed in this chapter are exploratory in nature, leading to the workarounds rooted in analogical thinking discussed under the next chapter.

Part II : Chapter 8 describes the research conducted as part of the secondary phase. The novel workarounds to circumvent key theoretical issues are presented at length; selective simulation results with their implications are also discussed. Additionally, novel longevity model and communication concepts for MI based WUSNs are also introduced.

Part III : Chapter 9 discusses the import of the research findings, and points to future directions of research. This chapter introduces some novel research directions in MI based WUSNs rooted in analogical thinking. This chapter concludes the dissertation.

Appendix A reproduces the source code used in the simulation tests performed during both research phases.

Appendix B provides a brief primer on MI. This addendum has been included as aid for the reader in better grasping some of the technical material presented in this dissertation.

Appendix C provides a brief technical overview of MI waveguide system with its variations. This addendum has been included as aid for the reader in better grasping some of the technical material presented in this dissertation.

Part I

Review

Chapter 2

Wireless Sensor Networks (WSNs)

2.1 Chapter Overview

In this chapter, the author covers certain key issues related to WSNs. These are the issues that bear relevance to the context of immediate WUSN deployment. Besides, the discussion presented under Chapter 4 also is related to the following discussion, since the theoretical research on MI based WUSNs has made use of conepts from aboveground wireless communication, as pointed out in the previous chapter. The subject matter in this chapter has drawn on a recent volume (Ammari 2014), apart from other sources.

2.2 Issues related to WSNs

The following subsections cover the issues related to WSNs, which are applicable to WUSN deployment as well.

2.2.1 Deployment Constraints

(Silva, Moghaddam & Liu 2014) introduce three fundamental metrics viz., low cost, reliability and scalability, as parameters to assess the *effectiveness* of a WSN solution. By means of analysis, the study points out how all of the above parameters are interdependent. A low cost deployment is impacted by maintenance and operational costs. The starting point to minimizing these costs is to identify the relevant networking aspects. In turn, such identification defines the scope of network reliability. Scalability can be a function of density or coverage, and based on the application context, is often a function of both. The aspect of scalability impacts the network reliability, in terms of data-rate, duty-cycle, data latency, communication errors, and energy consumption, determined by the architecture, hardware, and protocols in use (Silva et al. 2014). A fallout of area scalability (coverage scalability) is the reduced number of multi-hop paths between two different points, which adversely impacts the network reliability. In order to address this in real-time application contexts involving large areas, such as environment monitoring or precision agriculture, often there arises a need to strike a compromise between density scaling and area scaling. Considering the limited number of nodes, placement becomes crucial under such compromise. Judicious placement of the nodes so as to achieve maximum coverage at maximum density then becomes the key to *effective* WSN deployment. However, such prospect can be further marred due to the presence of adverse environmental factors. To reproduce an observation from (Silva et al. 2014):

"The connectivity challenge becomes more complicated when non-uniform deployments, obstacles, and environmental issues are considered. In this case, well-known multi-hop and collaborative protocols may not work properly in even relatively small areas."

This observation is crucial in the context of WUSNs, and the author will revisit this in the next chapter.

2.2.2 Physical Layer Issues

Interference is the major performance deterrent in the physical layer. If the WSN shares the frequency spectrum with another network, each network could interfere with the other. In the case of a dedicated spectrum, two nodes within communication range can interfere with each other's transmission.

The study reported in (Li, Wang & Liang 2014) is about capacity optimization of an Ultra-Wideband (UWB) network co-existing with an IEEE 802.11 n network (with the WSN deployed on UWB). This study is a case in point of the first category of physical layer interference. The three-fold objectives of the study are *communication capacity*, *estimation accuracy*, and *power efficiency*. The first objective depends on interference minimization through optimal spectrum allocation. The second and the third objectives depend on throughput and power optimization, respectively. The third objective is a function of the first, as shown by the derivations. The second objective is achieved through minimizing distortion of the estimate at the decoder (sink) of the distributed sensor readings. This is achieved by selecting readings from a subgroup of sensors with the best channel conditions/power level. This is shown to be a function of the third objective. Thus in the case of the first category of physical layer interference, optimal spectrum allocation holds the key to WSN system performance.

In the case of the second category of physical layer interference, the conventional outlook ties interference to connectivity. In other words, if two transceivers are within mutual connectivity range, they are bound to cause interference to each other. However, a different perspective to interference involving transceivers was demonstrated in (Zhou, He, Stankovic & Abdelzaher 2005). According to this work, both the notions of *interference-connectivity* (implying that interference is determined by connectivity range), and *connectivity-interference* (implying that connectivity leads to interference in a scenario involving multiple transceivers) are factually incorrect. The related experiments in (Zhou et al. 2005) show that the only determinant of interference in a scenario involving multiple transceivers, is the link quality. In other words, if a transmitter's signal is strong, it cannot be interfered with by a relatively weak signal from another source in or about the connectivity range. Alternately, if a transmitter's signal is weak, even a source outside of the connectivity range can interfere with it. These results show that the transmission power determines the nature of interference in the WSN channel between two nodes. Consequently, optimization algorithms similar to those in the case of the first category of physical interference, should be applicable in this case as well.

The study in (Kusy, Abbott, Richter, Huynh, Afanasyev, Hu, Brünig, Ostry & Jurdak 2014) highlights the efficiency gain for WSN based on a distinct dual frequency band with no overlapping. In effect, this study is complementary to (Li, Wang & Liang 2014). Both the studies are indicative of multi-radio being the norm for WSN deployment in the coming years.

Even though the author has devoted separate subsections for deployment and physical layer issues, in practice they impact each other. In (Younis, Lee, Senturk & Akkaya 2014), several deployment algorithms have been analysed that are aimed at optimizing both coverage and connectivity of WSN. Network coding also impacts the performance of the physical layer. Efficient network coding can reduce the number of bits over the physical layer. A survey of network coding techniques suitable for WSN can be found in (Huang, Xiao, Soltani, Mutka & Xi 2013). Network coding is topology dependent as well.

2.2.3 MAC Layer Issues

The MAC layer controls the physical layer. An efficient MAC protocol is a prerequisite to streamlined physical layer access, in both single and multi-radio environments. A recent survey (Huang et al. 2013) highlights the complexity of WSN MAC protocol algorithms. This study shows how WSN MAC protocol design has become increasingly intricate over the last decade. One of the reasons is the broadened scope of such design to achieve optimum throughput and delay as well, in addition to energy efficiency. The analysis of various protocols shows that a design change to improve one performance aspect could degrade another. This design problem is shown to be common to the identified classes of MAC protocols: *asynchronous*, *synchronous*, *frame-slotted*, and *multichannel*. As cases in point, the author draws on typical examples provided in the study.

The asynchronous *Preamble Sampling* method reduces delay and the duty-cycle, but the downside involves wasted node energy due to overhearing. The improvements suggested come with their own shortcomings. For instance, *Continuous Preamble Sampling* reduces per-hop latency and the duty cycle, at the cost of a long preamble. *Strobed Preamble Sampling* reduces the preamble length, but wastes node energy in channel sampling and reduces channel capacity. A combination of both, viz., *Dual Channel Sampling*, cuts down the channel sampling at the cost of increased packet length. *Schedule Learning* approach uses a short preamble to reduce node overhearing and increase channel capacity, at the cost of increased processing at the sender node. The alternate *Receiver Initiated Transmission* potentially gives rise to collisions among multiple senders, while increasing expended energy at the senders. The approach to *Estimate the Wake-up Time of the Receiver* for avoiding sender collisions, can lead to prediction errors effected by system parameters such as clock-drift. Besides, the method is susceptible to consistency issues arising in a dynamic system, and expends higher node energy.

The synchronous algorithms focus on improving throughput and reducing delay. The *Adaptive Listening* algorithm has a limited packet throughput efficiency of 2 hops per relay cycle. The *Future Request to Send* algorithm improves the throughput to 3 hops per cycle, with potential packet collision. The *Shifting Data Transmission to Sleep Period* algorithm and its proposed improvements are meant to reduce latency, but fail in the event of non-synchronization arising from repeated packet collisions, and reduce energy efficiency. The *Staggered Schedule* algorithm uses a data gathering tree for synchronization and throughput efficiency, at the cost of increased idle listening and reduced energy efficiency. *Adaptive Duty Cycling* is intended to reduce delay by dynamic proportionate channel assignment, but could fail due to contention issues and incur more energy consumption.

Frame-slotted MAC protocols are Time Division Multiple Access (TDMA) based, and are tailor-made for hierarchical networks with typically a master-slave architecture. *Slot Stealing* uses Carrier Sense Multiple Access (CSMA) to improve channel utilization. The algorithm enables a sender node to contend for unused slots, in addition to its own. This comes at the expense of increased energy consumption. *Adaptive Assignment* uses a mix of scheduled and random channel assignment to improve channel utilization, at the expense of energy efficiency, spatial reuse of vacant slots and increased delay. A proposed improvement does not guarantee minimum number of slots for the nodes. The *Maximize Throughput at the Sink* algorithm allocates slots to the nodes of a data gathering tree based on data flow rather than fairness, for maximizing throughput at the sink. This algorithm works only for a stable tree structure; dynamic tree growth results in new nodes getting low preference. Besides, wastage of slots is also a by-product. The *Reduce Duty Cycle by Switching Sending Slots to Receiving Slots* algorithm models the sleep-wakeup schedule on receiving nodes, rather than senders. The variants proposed use innovative slot allocation to minimize contention and potential collision characteristic of the algorithm.

Multichannel algorithms are applicable to multi-radio WSN systems supporting bursty traffic and multi-tasking. The key issues involved are channel allocation and cross-channel communication. *Address Cross-channel Communication* and its variants use novel channel assignment methods. These include improved TDMA schemes covering channel sensing and communication slots fitted into a single beacon interval, dynamic slot intervals, static channel allocation and channel switching. These schemes suffer from high control overhead, packet collision and reduced energy efficiency. *Channel Assignment based on Metric Optimization* algorithm is based on dividing the network according to a suitable logic, such as group of communicating nodes and node trees that share a channel. Such algorithms involve channel switching which is energy consuming. Packet loss is another by-product of channel switching. Certain variants model node tree channel assignment after game theory. Such approaches may involve excessive overhead under dynamic conditions. The logic of combining time slots and frequency channel is the basis of *TDMA/FDMA for Sending* and *TDMA/FDMA for Receiving* algorithms. These algorithms incur a large overhead in terms of broadcasting slot occupancy and channel switching. Hence their use is justified only if the throughput demand compensates for the overhead. These algorithms also suffer from under-usage of channels/slots under low contention. Besides, the issues of sender contention and collision also exist in some variants for same channel receivers.

These examples reveal the enormous challenge involved in achieving a balanced WSN MAC protocol. They also drive home the fundamental principle underlying WSN MAC design, which is that it is highly application specific.

2.2.4 Routing Issues

Similar to the MAC layer, routing in WSN is a constantly improving process. Each algorithmic improvement also brings new issues to be addressed. In the following discussion, the author presents a concise overview of the WSN routing protocols to highlight this fact. Routing in WSN can be classified under the heads *energy-centric* (Abdulla, Nishiyama, Ansari & Kato 2014) and *utility-based* (Li & Wu 2014). The former holds significance since WSN nodes are energy-constrained. The latter is determined by the application needs. Communication in WSN is an energy-intensive activity. Due to the hardware limitations, sensors can transmit only to a certain maximum distance. The longer the transmission distance, the greater the energy expended. For these reasons, multi-hop routing involving shorter transmission distances is usually preferred in WSN.

2.2.4.1 Energy-centric Routing

Energy-centric routing can further be classified as *flat multi-hop*, *hierarchical multi-hop*, *hybrid*, *data-centric* and *location-based*.

In flat multi-hop, the least energy consuming path is chosen for communication between two nodes. One of the tenets in flat multi-hop routing is to devise paths such that the communication load is divided equally among all sensors. Network life time has been a major preoccupation with many flat multi-hop variants. An off-shoot of such preoccupation has been the application of sleep-wakeup patterns to prolong network life time. Network life time has been variously defined as the time when the first sensor dies, the time until a sensor is able to monitor a local event, or alternately the time at which the sensor is not able to monitor a local event. One disadvantage of the flat multi-hop algorithm is its inability to capitalize on the redundancy in node data.

This disadvantage has been addressed in hierarchical multi-hop, wherein the nodes form role-based hierarchies to reduce the data flow, and consequently energy consumption in communication. A hierarchy is formed by a group of sensor nodes and a special node termed the *gateway* node. The gateway node is a sensor node that communicates with an adjacent group. Each hierarchical group is termed a *cluster*, each sensor node in the cluster becomes a *cluster member*, and the gateway node for the cluster is termed the *cluster head*. The cluster heads perform *data aggregation* on the data collected from the cluster members, capitalizing on the redundancy. Consequently, communication becomes more energy efficient within the WSN. The hierarchical multi-hop algorithm poses its own disadvantages. The cluster formation could result in uneven distribution of cluster heads, creating energy imbalance within the network. To overcome this, a grid based approach has been suggested. Still, there is the issue of the cluster head expending higher energy than the cluster members. Several algorithms have been suggested to select the most appropriate node as the cluster head. Use of data predictors is another improvement suggested to curtail the energy expended in cluster members. Data predictors predict the sensors' future readings from the past. Data predicting can be computation-intensive, depending on the degree of data correlation. Some approaches suggest implementing the data predictors in cluster heads, but this can be energy efficient only under conditions of high data correlation.

The hybrid routing algorithm combines the above two algorithms, in order to mitigate the *energy hole* problem. The energy hole problem manifests in multi-hop WSNs. In multi-hop WSNs, the sensors close to the sink node expend more energy in forwarding traffic. Consequently, these sensors could die out eventually, isolating the sink. Hybrid routing addresses this problem by combining hierarchical and flat multi-hop routing algorithms. The area within the maximum transmission range of the sink is termed the Sink Connectivity Area (SCA). In hybrid routing, sensors in the SCA use flat multi-hop routing, as opposed to the rest of the network set up using hierarchical multi-hop. This arrangement serves to minimize the energy expended by the sensors in the SCA, thus mitigating the energy hole problem. Implementing the hybrid routing method is not straightforward, considering the routing algorithm switch.

In data-centric routing, in-network data aggregation is performed to reduce the energy consumption in communication. The idea is to optimize the traffic based on unique data elements instead of sensor IDs. One advantage of this approach is the elimination of data redundancy. A variant of the algorithm uses the concept of application-specific *meta-data* to avoid data redundancy and consequent energy overhead. Another variant uses a query based mechanism to generate a single, optimal, aggregation-enabled routing path for each source to sink communication. Several improvements have been proposed for the above method. These include selective data acquisition based on relevance, routing based on maximum battery life-time of the nodes, preferential route based on high residual sensor energy density, routing based on minimal collision, and routing based on maximum aggregation. Definition of accurate meta-data scheme for complex data attributes can be challenging and can impact the algorithmic efficiency.

In location-based routing, location information of the nodes is used to reduce energy consumption in communication. Several variants of the algorithm have targeted improved energy efficiency. These include leveraging on spatial redundancy for selective sensor activation, targeted message routing, network partitioning for optimum routing to avoid *holes*, differential routing techniques for effectively negotiating holes, and sensor communication optimized for redundancy.

Energy efficiency is mainly a function of communication in WSNs. To reproduce an observation from (Abdulla et al. 2014):

"Practically, sending a bit over 10 or 100m can consume as much energy as millions of computational operations conducted in the processing unit of the sensor, referred to as the R4 signal energy drop-off."

Thus the sleep-wakeup schedule of the sensors determines the energy efficiency of the network. A schedule that ensures low duty-cycle radio operation is the most energy efficient (Abdulla et al. 2014). Based on this benchmark, all of the algorithms mentioned above lack in total energy efficiency. In terms of data-aggregation, hierarchical multi-hop can be energy efficient only in the case of high data correlation. Similarly, a data-centric algorithm ceases to be energy efficient if the data overlap among sensor readings is nil or negligible; lack of overlap impacts the energy efficiency of data-aggregation in the algorithm. Except for hybrid multi-hop, all the other algorithms are susceptible to the energy hole problem. However, as pointed out previously, the inherent algorithm switching in hybrid multi-hop makes it complex. All of the algorithms depend on route/information updates for energy efficient operation. Frequent updates can be energy intensive and degrade the energy efficiency. Besides, none of the algorithms are exempt from collision effects and consequent energy wastage due to retransmissions.

2.2.4.2 Utility-based Routing

Utility based routing is a function of the system parameters *cost* (in terms of hop count and energy), *delay* and *packet delivery ratio* (Li & Wu 2014). Additionally, it can also be *continuous*, *event-driven*, *query-driven*, or a *hybrid*. Network topology determined by node deployment impacts utility based routing. The author focuses on low duty-cycle WSN in this discussion, which pertains to the chosen application prototype for simulations and innovations. Utility based routing can either emphasize a single system parameter, or a combination. In the former case, different routing algorithms adopt different methods to evaluate performance. In the case of packet delivery ratio, these methods include

- *expected delivery ratio*, which is the sum probability of successful delivery of a packet by each neighbour of a given node.
- *link correlation*, which captures the level of link redundancy between two neighbours of a given node; here link redundancy defines the probability that a packet received by one link can equally be received by the other.
- *expected transmission count*, which is the minimum expected number of transmissions (including retransmissions) required to deliver a packet to its destination.

- *quality of forwarding*, which is the ratio of the data delivery to the transmission count.

All of the above methods can be impacted by delay, and also the associated route cost. The three delay factors are *transmission delay*, *propagation delay*, and *sleeping latency*. Sleeping latency denotes the delay incurred due to waiting on neighbouring nodes to wake up. This delay is the longest of the three. Sleep-wakeup randomness eliminates static routes. Various algorithms are used in delay-centric routing to minimize delay. *Sleep scheduling* focuses on synchronizing the sleep-wakeup schedule of neighbouring nodes. This synchronization incurs a cost. *Pipeline scheduling* focuses on enabling alternate routes between neighbouring nodes to reduce sleep latency. *Collaborative sensing* uses a prediction error bound for turning off specific nodes in a neighbourhood. In addition to delay, cost efficiency is also an objective. The routing concept of *end-to-end delay* has been used in sleep latency reduction. This denotes the multi-hop delay incurred in delivering a packet from source to destination. Various related algorithms include sleep-wakeup coordination among neighbours, and coordinated multiple routes between neighbours, extended to random walk and stochastic models. Augmenting the active instances of neighbours is an algorithm used to reduce communication delay. Evidently, this can incur a higher cost. Since the sleep-wakeup pattern is not conducive to flooding, *opportunistic flooding* is used as a cost-effective substitute. This algorithm uses a combination of probabilistic node wakeup times, forwarding based on link quality, and multiple senders to reduce latency.

Energy cost is a factor of both data processing and transmission. This cost is impacted by the network data and topology. Scenarios such as real-time data, expected energy consumption, energy optimization through suitable route selection, and balancing reliability with overhead, have been studied in this context.

Often, a combination of the utility parameters is adopted as the basis for routing. Thus packet delivery can be combined with energy efficiency, or delay can be combined with packet delivery. This is termed *composite utility-based routing* (Li & Wu 2014). Composite routing impacts the route adopted from the source to the destination. Composite routing is about achieving minimum performance benchmarks for all the involved parameters.

It is evident from the above discussion that utility-based routing in WSNs is deeply integrated with the network topology. Irrespective of the algorithmic variant, a thorough understanding of the network layout and node placements is a prerequisite for routing.

It is also clear that any algorithmic routing involves trade-offs. Emphasis on a particular parameter can only be at the cost of the remaining parameters.

2.2.4.3 Remarks

Routing in WSNs is highly network-centred. Without a well planned and demarcated network, efficient routing cannot be accomplished. Such routing also favours multi-hops in terms of small groups. As in the case of MAC, routing in WSNs is application specific as well.

2.2.5 Longevity Issues

Network lifetime determines the longevity of WSN. This aspect has been defined in multifarious ways. (Dietrich & Dressler 2009) review the cross-section of such definitions, in addition to putting forth a comprehensive definition. According to this definition, a variety of factors impact network lifetime. These include

- *Mobility*, which is even applicable to stationary networks. A stationary network is susceptible to node failures. The environment could also alter the location of the nodes. Both of these issues impact the network topology, akin to node mobility.
- *Heterogeneity*, which includes node differentiators (power, processing, modality, coverage) and data volume associated with a node.
- *Application characteristics*, which include task distribution, routing, and node activity (sensing, processing, communication), which can be regular, event-driven, or request-based.
- *Quality of Service (QoS)*, which includes timeliness and accuracy of data, optimality of network resources (nodes), and continuity of service.
- *Interdependency*, which correlates two or more of the above factors.

Based on the above factors, the complete criterion framed by (Dietrich & Dressler 2009) to define network lifetime includes the parameters *portion of alive nodes*, *maximum tolerable*

latency, *delivery ratio*, *portion of nodes with path to a sink*, *connected area coverage* and *service disruption tolerance*. It is obvious from this set that network lifetime is impacted by each of the relevant ISO/OSI layers (Akyildiz & Stuntebeck 2006). A fundamental definition of network lifetime provided in (Chen & Zhao 2005) is as follows:
"We ignore the continuous energy consumption in the network and define the network lifetime as the time span until any sensor in the network dies (the first death) or no sensor has enough energy for transmission during a data collection (the first failure in data collection), whichever occurs first."
This definition underlies the assumptions for network lifetime outlined in (Dietrich & Dressler 2009). Thus it can be stated without any loss of generality that node lifetime is the basic prerequisite for network lifetime. Two prevalent methods for enhancing node lifetime are *topology management* and *sensor selection*. Both aim at achieving maximum network coverage with connectivity, at maximum energy efficiency of the nodes. However, the techniques used are different.

2.2.5.1 Topology Management

(Younis et al. 2014) provide a review of the topology management techniques. These include *node discovery*, *sleep cycle management*, *clustering*, *power control* and *movement control*. In a given WSN, either a single node or multiple nodes could fail. In the former case, the failure of a cut-vertex node can split the network. So a durable network design should avoid cut-vertices. Failure recovery can be either reactive or proactive. Multiple node failures present a greater challenge both in terms of scope and restoration. The general taxonomy of recovery mechanisms has been analysed in (Younis et al. 2014). This includes *coverage vs. connectivity*, *scope*, *approach*, *methodology* and *objective*. Coverage and/or connectivity sets the context for the remaining terms.
In coverage vs. connectivity, emphasis is laid on either coverage or connectivity. Coverage-centric restoration mechanisms include node redundancy and substitution methods. In most of the related research, substitution involves relocation of nodes to cover a hole. Hole detection and substitution can be complex, depending on the topology. Coverage-centric methods in previous works include strategic node positioning using Voronoi tessellation

or grid, energy-efficient node re-positioning algorithms to cover a potential hole, timely identification of redundant nodes for relocation, load balancing among nodes, metrics to determine the criticality of a failed node, et al. The following observation from (Younis et al. 2014) underscores the advantage of a localized topology structure for failure recovery:

"Localized schemes limit the involvements of the nodes in the recovery and thus reduce the impact that a node failure and the associate recovery process have on the normal network operation."

The coverage-centric methods listed above involve different levels of complexity, and thus should benefit from a localized topology.

Connectivity-centric algorithms can be classified as *proactive* and *reactive*. Proactive algorithms integrate tolerance to connectivity failure into the network architecture using redundancy. Optimal node placement in such redundant architecture is a challenge. A workaround suggested in many works is using *bi-connectivity*. In this context, relays have been used to advantage. Certain proactive algorithms nominate backup nodes for critical nodes. This reduces the node relocation overhead and delay incurred upon failure, at the cost of additional nodes. The node location could have application level significance as well. The backup node method has also been used to address this dependency. Such dependency restricts the scope of node relocation within a locality. Another variant considers coverage as well, while assigning backup nodes.

Reactive algorithms rely heavily on node relocation. The algorithms can vary depending on the criticality of the failed node, target restored network state, connectivity restoration approach, nature of target network connectivity, and underlying basic restoration logic. In most cases, ascertaining the criticality of a node, for instance whether a node is cut-vertex, requires a complex network analysis. Bi-connectivity has been used in many works to prevent interim network failure during restoration. Another challenge is to restore the bi-connectivity after restoration. The notion of a backbone connection, viz., the Connected Dominant Set (CDS), has been used in some works to maintain basic connectivity during restoration. CDS also helps to minimize the number of nodes and their relocation distance, since only non-CDS nodes are relocated. However, even relocation of non-CDS nodes could necessitate a network re-structuring. A class of distributed restoration algorithms involve single-hop relocation of a set of neighbouring nodes. The neighbours converge in on the failed node, thus restoring interconnectivity. This strategy can be effective in small networks, wherein the network re-organization resulting from node relocation is minimal. In the case of large networks, this can incur a heavy cost. A peculiar variant of the algorithm provides intermittent coverage and connectivity restoration, by alternatively relocating each neighbouring node back and forth depending on its location. Multi-node failures constitute the greatest challenge for restoration. The adopted methods include network re-structuring, relay nodes, and mobile nodes. The restoration is determined by cost, connectivity and application QoS demand. The three factors impact one another. Restoration through node relocation is extremely complex for multi-node failures. Backup nodes can obviate the need for such relocation, at additional cost. Two different methods are generally used for relocation. One way is to move the remaining nodes towards the center of the deployment area. The other is to designate a leader node to move towards the isolated nodes, based on pre-failure route information. Yet another recovery method depends on relay nodes. However, optimal deployment of relay nodes is NP-hard in the wake of multi-node failure. Application QoS demands add another dimension to the complexity of restoring multi-node failures. This is because any pre-existent QoS distribution for a heterogeneous network has to be restored. In this scenario, a compromise can be achieved by populating selected network segments with additional relay nodes, even by means of relocation. However, identifying such segments itself is part of the challenge. *Mobile Data Mules (MDMs)*, which are mobile robots, have been used in various works as data relays, data collectors and data sinks.

The above discussion underlines the enormous challenges associated with topology management in WSNs. Almost all of the techniques require a thorough understanding of the topology. Even such understanding can be inadequate in the case of multi-node failures. Node relocation to address coverage or connectivity issues can result in re-organization of a portion or whole network, depending on the topology. This can incur a heavy cost. In many networks, node relocation may not be a feasible option. Other methods involving mobile robots cannot be implemented in many practical scenarios. Thus a highly localized network architecture is the most effective way to simple yet efficient topology management.

2.2.5.2 Sensor Selection

Sensor selection aims to alternate the sleep-wakeup schedules of sensors to prolong their lifetime. (Rowaihy, Eswaran, Johnson, Verma, Bar-Noy, Brown & La Porta 2007) evaluate the various sensor selection schemes. The schemes have been classified based on *coverage*, *target tracking and localization* and *mission assignment*. The problem of sensor selection has been defined in (Rowaihy et al. 2007) as follows:

"The goal of a sensor selection scheme is to select k sensors such that the total utility is maximized while the overall cost is less than a certain budget. In most cases, this problem becomes equivalent to the Knapsack problem which is known to be NP-complete. This means that there is no solution that can run in polynomial time (in number of sensors). This is clearly not desirable, especially if we consider a network with large number of sensors. Hence, approximation and heuristics are mostly used to solve this problem."

This statement captures the complexity of the sensor selection problem in WSNs. All the sensor selection schemes aim to balance the specific utility with the corresponding cost involved.

Typical coverage-centric algorithms for static nodes aim for balance between active sensors and total coverage, or a chosen parameter such as bandwidth. Such algorithms involve complex processing logic. For instance, a variant that deals with disjoint sets of sensors is NP-complete (Rowaihy et al. 2007). Distributed implementation of such algorithms is also hard. Additionally, a great deal of coordination among the sensors is required in most cases. Similarly, coverage-centric algorithms for mobile nodes can be computation-intensive as well. Deciding on which nodes to move so as to achieve the maximum energy efficiency, is a case in point. The related algorithms balance the mobile node selection against its distance from a given hole and residual energy.

Target tracking is not relevant to this research, but the author briefly covers it here for the sake of completeness. The three different schemes are based on *entropy*, *mean squared error*, and *dynamic information*. The first aims at reducing the entropy of a target by means of sensor selection. The method is computation-intensive and non-distributed. The second method makes use of dynamic information pertaining to target and sensor location to minimize entropy and energy cost. This method is computation-intensive as well. The third method uses Mean Squared Error (MSE) instead of entropy, and is both computation and communication intensive.

Mission assignment algorithms are driven by application demands rather than network logistics. The primary objective is to maximize the utility of the sensors while minimizing the cost. The utility is dependent on the application and sensor modality. Variants of the algorithm support both single and multiple missions. A processing overhead is involved dependent on the complexity of the algorithm and network topology.

2.2.5.3 Remarks

It is evident from the above discussion that optimizing the longevity of the network is a non-trivial process. Both topology management and sensor selection operate on trade-off involving maximum sensor utility against incurred cost. Distributive implementation is a prerequisite for optimal trade-off in many scenarios, as is a thorough understanding of the topology. In most cases, the complexity of the algorithm spirals out of control with increasing network size and node density. Due to this reason, the optimal solution becomes NP-complete and heuristic approximations are required. All these factors point to the suitability of localized topology in optimizing the trade-off involved.

2.3 Chapter Summary

In this chapter, the author focused on the issues involved in designing a cost-effective and efficient WSN. The range of topics covered in order to highlight the complex issues involved were the following:

- Issues pertaining to deployment
- Issues to pertaining to physical and MAC layer design
- Issues pertaining to routing
- Issues pertaining to longevity

All of the above topics have a direct bearing on WUSNs as well. In addition, the extent and scope of the discussion presented under the above topics, are also relevant in relation to many theoretical research directions in MI based WUSNs, which will be covered at length under Chapter 4. Thus the primary objective of this chapter has been to lay the background for the discussions that follow in the next two chapters. The next chapter would correlate the topics covered in this chapter to WUSN design and deployment.

Chapter 3

Wireless Underground Sensor Networks (WUSNs)

3.1 Chapter Overview

In this chapter, the author analyses the issues that confront WUSN deployment. These issues are largely due to the underground environment. Subsequently, the author correlates the issues outlined in the previous chapter to the underground environment. The objective of this chapter is to demonstrate the unprecedented challenges visiting WSN deployment underground.

3.2 Introduction

In the following discussion, the author first presents the theoretical analysis of EM wave communication underground. Subsequently, the author looks at certain studies involving WUSN communication. The author concludes the discussion with a correlation of the WSN issues presented in the previous chapter to WUSN.

3.3 Underground Environment and EM Wave Propagation

Many studies during the previous decade have detailed the unprecedented challenges posed by the underground environment for EM wave communication. Among these, (Akyildiz & Stuntebeck 2006) originally characterized the underground environment and related issues. This study classified the problem of WUSN design under four heads: *power conservation*, *topology design*, *antenna design*, and *environmental extremes*.

Power conservation becomes inevitable, since the WUSN nodes cannot be easily replaced or recharged after deployment. In view of this fact, power scavenging (Roundy, Steingart, Frechette, Wright & Rabaey 2004) has been studied as alternate source of energy to WUSN nodes. Topology design is instrumental to power conservation. Efficient topology design should architecture WUSN communication in terms of short multi-hops. Such communication pattern can save node energy. Deployment cost is another factor that is impacted by topology design. WUSN deployment can be expensive depending on the depth, and efficient topology design can minimize the cost of deployment and maintenance. WUSN topology design is highly application-specific. (Akyildiz & Stuntebeck 2006) suggest a choice between underground and hybrid topologies based on the application context. Antenna design becomes complex for underground environments, considering the low communication frequency and variable deployment depths. The antenna size is inversely proportional to the communication frequency. Directionality can also be impaired due to the three dimensional deployment space. Environmental extremities present the single most formidable challenge in WUSN deployment and communication. In terms of deployment, factors such as water, temperature extremes, animals, insects, vegetation growth et al., can interfere with the sensor node hardware and location. Many of these factors also figure adversely in WUSN communication.

(Akyildiz & Stuntebeck 2006) identify five key factors that impact WUSN communication: *extreme path loss*, *reflection/refraction*, *multi-path fading*, *reduced propagation velocity* and *noise*. Path loss is determined to a very large extent by the soil type and its water content. Soil type is impacted by its percentage of sand, silt and clay, or a combination thereof. EM waves propagating from ground to air or air to ground experience reflection, refraction and multi-path fading. Such propagation is necessitated due to UG2AG and AG2UG communication. Multi-path fading also occurs due to the environmental impediments such as scattered rocks, plant roots et al. Consequently, it impacts UG2UG communication as well. EM waves are considerably slowed down by the underground environment. EM waves are also impacted by the noise underground caused due to the atmosphere, apart from other possible factors like power lines and electric motors. Soil dielectric constant is a complex factor of its *water content*, *particle size*, *density* and *temperature*. All of these properties impact the EM wave propagation. Soil properties can vary over short distances, which renders link quality assessment even more difficult. This impacts deployment planning.

(Tiusanen 2005) proposes a signal attenuation model for UG2AG communication based on dielectric loss (soil dielectric properties), and reflection and refraction at the soil-air interface. (Li, Vuran & Akyildiz 2007) and (Akyildiz, Sun & Vuran 2009) propose a two path channel model for WUSN based on burial depth, and provide path loss equations for both single (high depth) and two (low depth) path models. In both cases, the path loss is shown to be a function of the frequency, the soil composition, density and volumetric water content (VWC). (Bogena, Huisman, Meier, Rosenbaum & Weuthen 2009) use the complex refractive index model (CRIM) to calculate the soil dielectric properties, and apply Fresnel equations to determine the signal attenuation. Besides, this model also considers the attenuation due to bulk electrical conductivity of the soil.

(Dong & Vuran 2011) propose a model for EM wave propagation underground taking *lateral waves* also into consideration, in addition to direct and reflected waves. The model also concurs with the broad level observations in (Li et al. 2007) and (Akyildiz et al. 2009) about the impact of soil VWC and burial depth on EM wave propagation. (Yoon, Cheng, Ghazanfari, Pamukcu & Suleiman 2011) propose a model to account for factors such as permittivity and electrical conductivity of the soil, which impact EM wave propagation underground. These factors have not been considered in either the two path model or the lateral wave model. Theoretical bounds for connectivity probability in WUSN have been derived in (Sun & Akyildiz 2010*a*) and (Sun, Akyildiz & Hancke 2011), as functions of system and environment variables such as node density, soil VWC, burial depth, tolerable latency, number of aboveground sink nodes, and aboveground sink node antenna height. (Sun et al. 2011) also include the impact of multipath fading in their derivations for UG2AG and AG2UG communication.

The above discussion points to the still evolving nature of characterization of EM wave propagation underground.

3.4 WUSN Deployment Studies

The purpose of this section is to highlight the complexity involved in WUSN deployment, by drawing on previous research reports. The following discussion examines the cross-section of deployment related issues for WUSN, reported in recent research. In addition to deployment issues, the discussion also uncovers critical performance issues reported in recent research for WUSN system prototypes.

In general, preparing a test bed for WUSN is a very complicated task. (Silva & Vuran 2010*b*) detail the prerequisites and variables that need to be addressed in this regard. These include

- line of sight deployment of the sender and the receiver nodes
- inter-node interference impacting the positioning of multiple sender/receiver nodes
- the meticulous planning and rigour that accompanies digging holes for node placement underground
- positioning aids such as paper or PVC pipes to facilitate underground node deployment, and corresponding logistics
- additional signal attenuation caused due to the positioning aids
- knowledge of soil composition across deployment space and depth
- the knowledge of soil VWC variations across deployment space and depth
- antenna orientation to minimize packet error rate (PER) for each inter-node communication
- pre-deployment evaluation of nodes for compatible radio frequency (RF) sensitivity, required for optimal network route determination
- knowledge of *transitional regions* applicable to inter-node communication wherein the signal strength decays with increasing distance, eventually leading to a point of no connectivity

- understanding of any sensor device electronics design aspects such as the *clipping effect*, a limitation in the RF circuitry resulting in the same reported received signal strength (RSS) value beyond a cap, which could impact interpretation of test data

It is quite evident from the above points that deploying WUSN presents a formidable challenge. The above points also convey the significance of processing the deployment in terms of small, stand-alone spaces.

(Akyildiz & Stuntebeck 2006) show using a link budget equation for WUSN and corresponding simulations that only short communication hops are possible. This fact has to be considered for any deployment. Moreover, lower frequencies in the MHz range reduce the signal attenuation. However, this results in a larger antenna size infeasible for WUSN devices. Low frequency also reduces the effective bandwidth, which is compounded by the extreme channel loss in the underground environment.

(Tiusanen 2005) compares field simulation (laboratory tests) results with values obtained from the proposed attenuation model. The set-up uses a discone dipole antenna underground (at various depths) and a precision dipole antenna aboveground (at varied heights and at 15 m horizontal distance) to measure signal attenuation using a 14 dBm signal at 869.5 MHz frequency radiation from UG2AG. The results verify that compared to free air, signal propagation from UG2AG through soil medium causes additional attenuation of 15-60 dB depending on the underground burial depth and the aboveground antenna height. In addition, soil permittivity and VWC, and antenna installation (orientation, depth, compaction, et al.) are also mentioned to have a decisive impact on signal attenuation. An interesting observation is the positive impact on refraction and signal attenuation with increased soil dielectric factor, after a rain or surface irrigation. Besides these results, most of which concur with (Akyildiz & Stuntebeck 2006), (Tiusanen 2005) also provides glimpses of certain unique problems visiting WUSN deployment. In relation to antenna deployment underground, (Tiusanen 2005) documents:

"Before any laboratory measurements the antenna was wrapped in a plastic bag and paper tape to protect it from mechanical damage. Thus there was air inside and soil outside the cone, causing a poor coefficient of transmission, seen as a return loss as high as -12.5 dB."

This is characteristic of the dilemma inherent in WUSN deployments. On the one hand, the electronic equipment and accompanying circuitry of the sensor nodes need to be protected from the harsh environment. But in the absence of careful foresight, such protection mechanisms could interfere with the system performance. The peculiarity of this problem renders WUSN deployment even more challenging.

(Tiusanen 2007) presents further field and laboratory tests to validate the model, under two different soil compositions. A number of highly significant conclusions pertaining to WUSN deployment have been drawn in the study, based on the similarity and discrepancy between the model and the test results. The significance of choosing the optimal operating frequency is one. In keeping with the required miniature antenna size, the frequency of 869.5 MHz had been chosen for the study. To reproduce a contextual observation from (Tiusanen 2007):

"The chosen frequency is the most common in present single-chip radio technology and also a licence-free band. Another, almost as popular frequency band is 433 MHz, but here the underground antenna would have been twice the size of the present one (some 20 cm in diameter), which would have made the measurements very difficult to carry out."

This statement also confirms the stricture mentioned in (Akyildiz & Stuntebeck 2006). The complexity concerning accurate analysis of underground system fluctuations for particular instances is another. Specifically in relation to the observed variation (of signal attenuation) to the tune of 8 dB between the model and the test result at 40 cm depth, obtained using restoration of soil layered structure and bulk density by means of "refilling the hole", (Tiusanen 2007) makes the following comment:

"Still, the soil layers must have been somewhat corrupted. ... As soil dry bulk density should not influence permittivity significantly when there are tens of percents volumetric moisture in the soil, this observation is hard to explain."

A third difficulty pertains to the accurate approximation of layer demarcations in underground soil medium. Since soil properties vary according to layer, this could have significant impact on signal attenuation. The related observation from (Tiusanen 2007) is as follows:

"A transition from 'plough layer' to bottom soil was noticed during the tests at 25 cm. The soil texture did not change there, but the topsoil probably contained more organic matter."

Another interesting observation in (Tiusanen 2007) pertains to the problem of defining the maximum allowed attenuation for a WUSN link. Examining the difficulty involved, (Tiusanen 2007) makes the following comment:

"In this study another approach is taken. As the attenuation increases dramatically by depth, a Soil Scout with an extension cord to the sensor part can be constructed. The Soil Scout can be installed just below the ploughing depth and the sensor anywhere else. Connecting several sensors to one Soil Scout is also possible. Altogether, placing an extended Soil Scout 25cm underground enables all field activities without a risk of mechanical violation."

The above approach for combining multiple sensors using a single transmitting soil scout by means of cabling, is very similar to one of the solution approaches adopted in this research, which will be explained in a later chapter. ***Nevertheless, this coincidence is a vindication of the relevant research approach in general***. The above observations point to the challenges that are hard to overcome while devising WUSN deployment solutions.

Based on actual field test data collected over 5 months, (Tiusanen 2009) examines the possible causes for discrepancies that could creep in between model estimate and actual results. There are some valuable insights related to WUSN deployment revealed during this examination, which both corroborate as well as extend the earlier inferences outlined in (Tiusanen 2007). The first lesson pertains to the impracticality of predicting fool-proof operation of underground nodes, in spite of careful analysis of weather and environment conditions, and planned deployment. The results show that all the nodes ran out of battery power eventually. There is also a very keen related observation about device accessories in this regard. To reproduce the same from (Tiusanen 2009):

"The Soil Scout prototypes were waterproofed by coating the devices with a two component epoxy adhesive. This turned out to be a poor decision. The moisture probe cable lead-ins perished rapidly in the underground conditions and the prototypes suffered from short-circuit caused by water intake."

This statement is testament to how WUSN deployment at this juncture, owing to the relative novelty of the paradigm, is often a trial-and-error procedure. It also underscores the deployment dilemma highlighted in (Tiusanen 2005). Again, in relation to the discrepancy between the modelled and observed receiver threshold potential to the tune of -10 dB, no reasonable explanation could be formed. As (Tiusanen 2009) observes:

"The intended system specification was to overcome -110 dB of attenuation. Comparing to attenuation estimates, this was not achieved. However, there is no evidence on whether the difference is caused by instrument properties or model inaccuracy."

This is akin to the inconclusive signal attenuation to the tune of 8 dB observed at 40 cm depth, as reported in (Tiusanen 2007). The overall results point to the infeasibility of the devised and deployed system for large scale irrigation purpose.

The WUSN deployment set-up complete with aboveground infrastructure for monitoring and reporting soil moisture in an 18-hole golf course has been detailed in (Ritsema, Kuipers, Kleiboer, van den Elsen, Oostindie, Wesseling, Wolthuis & Havinga 2009). The report emphasizes on the usage of commercial off-the-shelf products for both underground and aboveground deployment. Even though the overall performance of the system has been reported to be according to set benchmarks, with UG2AG communication from depths of 4 cm and 10 cm respectively, no description has been provided about the UG2AG communication mechanism. Specifically, the report mentions about usage of EC-5 soil moisture sensors; however such sensors need a serial port connection to a EM-50 series data logger device (Decagon 2014*b*), (Decagon 2014*c*). The normal practice with these products is to use the data logger aboveground with the wired underground sensors. There is reference to a housing mechanism for lodging the sensor nodes underground. On a broad level, this is conceptually similar to an innovation proposed as part of this research, discussed in a later chapter.

(Stuntebeck, Pompili & Melodia 2006) present field experiment results conducted using commodity MicaZ motes operating at 2.4 GHz, with transmit power of 0 dBm and receiving threshold of -90 dBm. The results reveal the infeasibility of UG2UG communication under this configuration, and the limited range achievable for both UG2AG and AG2UG communication. In addition, the results also agree with the broad level challenges and limitations outlined in (Akyildiz & Stuntebeck 2006), including that current commercial sensors are ill-equipped to meet the challenges posed by UG2UG communication.

(Bogena et al. 2009) present laboratory experiment results for a hybrid WUSN set-up operating at 2.44 GHz, and verify the same against the predictions using the proposed CRIM-Fresnel model. The results show pointed increase in signal attenuation with burial depth, operating frequency, and soil VWC, porosity and electrical conductivity. These results agree with the findings in (Akyildiz & Stuntebeck 2006).

(Li et al. 2007), (Akyildiz et al. 2009) and (Vuran & Akyildiz 2010) present some interesting simulation results for single and two path propagation models underground. The frequencies considered are in the 300-900 MHz range. The transmission power range assumed is in the range 10-30 dBm. The average noise level assumed is -103 dBm. One result shows that for a given operating frequency, the optimal path loss is a function of the burial depth. Another result shows that even though the bit error rate (BER) decreases with transmission power, such reduction is minimal. It has also been shown that the BER increases dramatically with a minimal increase in soil VWC. This result demonstrates the soil VWC as the single most determinant of BER in EM wave propagation underground. Further, the two path model fares better in terms of BER for the same transmission power and soil VWC. A fourth result shows the impact of soil composition and seasonal variations of VWC on maximum communication range with a target BER. The system performance exhibits pronounced variations due to both factors. The maximum communication range reported across the results does not exceed 5 m for a minimum target BER. All the results agree with the propositions in (Akyildiz & Stuntebeck 2006), including short multi-hop communication links, and the need for cross-layer design to adapt best to the environmental impact on the physical layer.

(Silva & Vuran 2009) present results from field experiments conducted in the *subsoil region* (burial depth >40 cm) to corroborate the results in (Li et al. 2007), (Akyildiz et al. 2009) and (Vuran & Akyildiz 2010). In addition, the study also highlights antenna orientation as an additional constraint in WUSN multi-hop communication. The study also points to how existing sensor nodes are incapable of achieving any meaningful communication in the underground environment. The study concludes:

"Consequently, a new generation of nodes with more powerful transceivers and/or more efficient antennas are required for the actual deployment of WUSN applications."

More efficient antenna design for UG2AG and AG2UG communication has been addressed in (Silva & Vuran 2010*c*). The study proposes a full-wave (FW) antenna for aboveground nodes and single ended elliptical antenna (SEA) for underground nodes, both operating at 433 MHz frequency. For a burial depth of 35 cm, the antenna scheme is shown to achieve a range of 22 m and 11 m respectively, for UG2AG and AG2UG communication. For a burial depth of 15 cm, the range for UG2AG and AG2UG communication is shown to improve by 40% and 300% respectively. The study also analyses the adverse impact of soil moisture on UG2AG and AG2UG communication range using the proposed antenna scheme. An interesting observation based on the field tests conducted is the existence of a *symmetric region* within the communication range, wherein bi-directional communication is possible. The rest of the communication range is shown to be unidirectional. The communication range claimed in the study is suitable for short multi-hop communication. However the challenges posed by burial depth and soil moisture render node deployment complex. The unidirectional communication limitation further complicates this matter. Simulation results presented in (Dong & Vuran 2011) show that their model is more accurate than the two path model, based on the field test data from (Silva & Vuran 2009). Both laboratory and field test data have been provided in (Yoon et al. 2011) to validate the proposed theoretical model based on permittivity and electrical conductivity of the soil medium. The adopted parameters include a frequency of 2.4 GHz, transmission power of 0 dBm, communication range of 0.05 - 1 m, and burial depth of 140 cm for the field tests. The chosen communication range falls way short of practical application scenarios, even using short multi-hops. Besides, the burial depth too does not match practical scenarios, usually less than 100 cm (Silva & Vuran 2010*b*). So these results have to be viewed purely as expository in significance. An interesting fact about the tests is the use of a PVC box to host the sensor nodes. This bears resemblance to an analogical solution approach proposed in this research, detailed in a later chapter.

The simulation results presented in (Silva & Vuran 2010*b*) for UG2UG, UG2AG and AG2UG communication at 40 cm burial depth and transmit power range of -3 to 10 dBm, show a maximum range of 1 m under typical soil composition.

(Sun & Akyildiz 2010*a*) and (Sun et al. 2011) present simulation results under controlled environment and system settings. These simulations show that connectivity probability in WUSN is impacted by soil VWC, sink node density, application specific tolerable latency, sensor node burial depth and sink node antenna height. The simulation results point to the WUSN deployment complexity, as all of these parameters need to be optimized to achieve maximum connectivity probability.

3.5 Correlation to WSN Issues

(Akyildiz & Stuntebeck 2006) do a high-level analysis of the suitability of WSN protocol stack to WUSN. The analysis reveals that existing WSN stack needs to be modified across layers to meet WUSN challenges. Typical issues have been pointed out across layers to highlight this fact. For instance, transmission and modulation at the physical layer need to adjust dynamically to changing water content of the soil. Optimal trade-off is needed between various factors at the MAC layer. Cases in point are between the overhead caused due to contention or synchronization based access schemes, and between energy saved due to packet size and consequent latency. Routing protocols need to adapt to the dynamically changing link quality due to soil water content, and reduce the overall signalling overhead. Similar modifications are required at the transport layer as well. Packets dropped due to channel conditions need to be distinguished from congestion. Distinguishing between differentiated services based on priority is another challenge. The unique challenges of underground environment also demand cross-layer approaches. Examples include correlation of channel link quality at the physical layer to soil water content measured at the application layer, and mapping channel link state information at the physical layer to optimized packet scheduling, routing and channel access at the corresponding layers.

(Vuran & Akyildiz 2008) present a seminal framework for cross-layer packet size optimization in WSN, and its extension to WUSN. The framework for WSN is centred on the objectives of optimum *packet throughput*, *energy per useful bit*, and *resource utilization*. In turn these objectives are optimized as functions of inter-node distance, path loss exponent, shadow fading factor, and error correction code (block code) components $((n, k, t))$, where n denotes the block length, k denotes the payload length, and t denotes the error correcting capability in bits. Several important results have been presented for WSN based on the framework. These include energy efficiency (energy per bit) as a function of minimum signal-to-noise-ratio (SNR) threshold and packet size, non-feasibility of optimal packet size for current commercial node design and consequent energy inefficiency, and suitability of a specific error correcting code depending on the application specific compromise between end-to-end latency and energy efficiency. These results indicate the complex permutations inherent to cross-layer packet optimization in WSN. However, when the framework is transposed to the WUSN environment, matters get further complicated. The simulation results show that optimum packet size, energy efficiency, and packet throughput are all adversely impacted by soil VWC. The results also show that end-to-end latency does not impact energy efficiency beyond a point. These results clearly point to the additional complexity imposed on the system configuration and layout by the underground environment. Further, they also corroborate the unsuitability of WSN layered solution approach to WUSN, as highlighted in (Akyildiz & Stuntebeck 2006).

3.6 Remarks

In the preceding sections, the author elaborated on the technical issues involved in the propagation of EM waves underground, and the related theoretical research. These discussions reveal the theory of EM wave propagation underground itself as an evolving research area, with succeeding interpretations either improving on the previous ones, or tracking a new trajectory. The author also discussed at length about the tremendous challenges visiting WUSN deployment underground, by reviewing related work on this topic. The review shows conclusively that as of now, WUSN communication using EM waves is impractical, even for application contexts with moderate QoS expectations. The review also clearly shows how UG2UG communication has never been attempted thus far in any of the experimental studies. The author will further dwell on this aspect in a subsequent chapter, in the context of WUSN application scenarios pertaining to irrigation control. Next, the author reviewed the complexity involved in cross-layer solution approaches for WUSNs. The discussion showed how WSN solutions fall way short of the requirements at each layer, and how a revamped approach is necessitated by the unique challenges posed by the WUSN deployment environment.

In the previous chapter, the author detailed the various issues applicable to WSNs in general, with the objective of highlighting how the involved complexity is augmented many-fold when it comes WUSNs. The author also demonstrated by means of relevant reviews how WSN itself is just an emerging paradigm. It should thus be evident from the discussion presented in this chapter that how much more that perspective is factual in the case of WUSNs, which has been actively researched only for a decade now.

In the previous chapter, the author reproduced a quote from (Silva et al. 2014), promising to revisit the same after the discussion on WUSN. So here the author would like to reproduce that observation one more time:

"The connectivity challenge becomes more complicated when non-uniform deployments, obstacles, and environmental issues are considered. In this case, well-known multi-hop and collaborative protocols may not work properly in even relatively small areas."

The author would like to state that the veracity of the above quote in relation to WUSNs is quite evident from the discussion presented in this chapter, accompanied by review of related research. The environment and related deployment challenges highlighted in the above observation are typical of WUSNs, as demonstrated by the reviews and discussion presented in this chapter.

In the next chapter, the author will introduce a novel twist in the WUSN paradigm, which proposes to eliminate the usage of EM waves altogether in UG2UG communication. This proposition also forms the crux of the study undertaken as part of this research.

3.7 Chapter Summary

In this chapter the author outlined the theoretical issues pertaining to EM wave communication underground and analysed the corresponding WUSN deployment issues. The author also covered the complexity of cross-layer solution approaches for WUSNs, and showed how WSN solution approaches are inadequate to meet the novel challenges. These observations and conclusions were supported by remarks and results reproduced from relevant previous research reports. In the next chapter, the author will introduce an alternate technology to EM waves for WUSNs.

Chapter 4

Magnetic Induction (MI)

4.1 Chapter Overview

In this chapter, the author introduces the alternative to EM wave communication underground: Magnetic Induction (MI). MI has been increasingly looked at as a viable alternative for WUSN communication over the past 5 years. An offshoot of this evaluation process has been the emergence of an innovative paradigm to improve the range and efficiency of MI communication underground. During the course of this brief evolution, certain initial preconceptions about MI communication underground have also undergone redefinition. The author will touch upon all of these aspects during the course of this chapter. The discussion will also demonstrate how MI communication for WUSNs is at its very stage of inception. Consequently, most of the research output thus far has been preoccupied with the theoretical aspects of MI communication for WUSNs, and corresponding simulation results. The direction pursued in this research has been to look at novel workarounds to circumvent some of the key theoretical issues in MI communication for WUSNs. The subject matter presented in this chapter forms the foundation for such novel workarounds presented in a later chapter. Hence this is the most crucial chapter under the Review part of this dissertation.

In the following sections, author first introduces the preliminary work on MI and MI based WUSNs, leading up to what is currently referred to as the *MI waveguide system*. Subsequently, the MI waveguide system for WUSNs has been discussed in detail. Finally, the state-of-the-art research on MI has been reviewed, with the objective of demonstrating the purely theoretical nature of the research.

NOTE

The reader could benefit from a brief primer on MI as a technology provided under Appendix B, and a quick overview of the technical aspects of the MI waveguide system provided under Appendix C, of this document. It is advised that the reader be familiar with the subject matter covered in both the appendices, before proceeding with the technical review presented under the remaining sections of this chapter. Such familiarity is a prerequisite for fully comprehending the ensuing technical discussion under the subsequent sections.

4.2 Preliminary Work on MI

As a technology, MI has long-standing application in various contexts. An example of the same can be found in (Adler 1974). The applicability of MI to WUSN context has been actively researched only during the past 5 years. However, there have also been intermittent works earlier in this direction. In the following subsections, the author examines the earlier work both in terms of theoretical and practical aspects. It needs to be made clear that by practical aspects, experiments conducted largely using simulations and on field to a limited extent is implied.

4.2.1 Theoretical Output

(Sojdehei, Wrathall & Dinn 2001) is the first work to report on the theoretical aspects of MI communication for WUSNs, albeit in the context of underwater communications. The following are some of the key theoretical observations outlined in the work pertaining to MI communication:

NOTE

(Sojdehei et al. 2001) report on MI communication by means of a magnetic-dipole field generated using alternating current (AC).

- at extremely low frequency (ELF), there is little or no electric field generated for the magnetic-dipole; consequently, the magnetic field is *non-propagating*.

  NOTE

  The magnetic field is a quasi-static field in air, and chiefly a diffusion field in a conductive medium (Sojdehei et al. 2001).

- due their non-propagative attribute, MI waves are not subject to multipath fading.
- similar to EM waves, the MI field can be modulated for data transmission.
- the magnetic permeability does not vary significantly from aboveground (air) to underground (any medium, including soil); everywhere, the MI field strength attenuates according to $\frac{1}{R^3}$, where R denotes the transmitting antenna (coil) range.
- in addition, in very shallow water (VSW), the magnetic field is susceptible to further attenuation due to eddy currents.

  NOTE

  The observation about eddy currents is key to underground propagation as well, and as the author shall point out later, was rediscovered in the context of underground communication by research conducted during recent years.

- the magnetic-dipole field strength of an MI transmitter coil is determined by its magnetic moment defined as $m = NIA$, where N denotes the number of turns of the coil, I denotes the current through the turns, and A denotes the cross-sectional area of the coil; if a magnetically permeable core were to be used, the field strength is increased to $m = \mu_E NIA$, where μ_E denotes the effective permeability of the core and the coil; μ_E is a strong function of the coil geometry.
- the formula $m = \mu_E NIA$ is impacted by the inherent trade-offs in coil design; assuming copper coils, increasing N increases coupled core and copper losses, and the

overall coil weight; increasing I increases power loss due to copper resistance and core; increasing A increases the overall coil size and weight; increasing μ_E involves modifying the coil geometry, which impacts the overall coil size and weight, in addition to the core power loss.

- similarly, receiver coil sensitivity and inductance are also impacted by μ_E, the antenna cross-sectional area, and the number of coil turns; the root mean square (RMS) voltage induced on the receiver coil by the AC magnetic field is given by $V = \mu_E 2\Pi BAfN$, where B denotes the RMS sinusoidal flux density, f denotes the carrier frequency, and the rest of the terms are as defined above; the receiver antenna coil needs to be tuned for optimal power transfer, noise reduction and bandwidth; at low frequencies, it becomes necessary to increase the number of coil turns to optimize the above tuning in order to achieve adequate sensitivity; this in turn can lead to increase in the coil parasitic capacitance, an issue that has been highlighted in the most recent research as well, as will be explained later.

The above points underline the fact that (Sojdehei et al. 2001) identified some of the most fundamental theoretical issues pertaining to MI communication for WUSNs. These theoretical aspects continue to be the preoccupation of the state-of-the-art research on the topic, as will be evinced later.

NOTE

As an aside, roundabout the same time (Bunszel 2001) highlighted the tremendous advantages presented by MI over RF communication in the near-field (< 3 m), in terms of several operational parameters including BER (interference), transmit power, complexity (system), and cost. The write-up had been highly upbeat about the future of MI communication in the mainstream:

"By the end of this year, several RF and magnetic induction solutions will be available for wireless voice and data networks within the 100-meter space ...... MI is poised to be the backbone for close-proximity, low-power, low-cost, wireless devices."

However, the technology could not penetrate a lot of application scenarios due to theoretical impediments. The author shall demonstrate a case-in-point based on the review of MI based WUSN research in this chapter; such impediments mark the point of departure to the research and innovation direction that has been pursued in this research.

A realistic review of the progress of MI as the technology for near field communications (NFC) for diverse application contexts, has been provided in (Evans-Pughe 2005). As the author rightly sums up:

"The NFC Forum describes near field communications as "the perfect solution for exchanging data in our increasingly complex and connected world". They've a little way to go to justify such claims, but it looks as though they're on to something...".

MI waveguides as a concept was introduced in (Shamonina, Kalinin, Ringhofer & Solymar 2002*b*), with the purported primary application scope of magnetic resonance imaging (MRI). This is a revolutionary concept that could be integrated with the proposition of *relay-mode* operation put forth in (Sojdehei et al. 2001) and referenced under the next subsection. The concept of MI waveguides forms the crux of the current research on MI communication underground. Further theoretical investigations on MI waveguides have been pursued in (Shamonina, Kalinin, Ringhofer & Solymar 2002*a*). The theoretical MI waveguide aspects covered in the report include dispersion and propagation of MI waves, current distribution (for finite lines), the Poynting vector analysis, and the impact of non-synchronous inter-element resonance due to manufacturing leniency. In the case of one-dimensional waveguides, both axial and planar coil alignments have been investigated. In addition, the work also provides useful theoretical insights on unique planar waveguide coil arrangements in one dimension, and three-dimensional waveguides with restricted configuration. These findings are highly relevant to the MI waveguide design for WUSNs. The vein of theoretical approach adopted in (Shamonina et al. 2002*b*) and (Shamonina et al. 2002*a*) has been extended in various subsequent reports for miscellaneous waveguide concepts. These theoretical findings have a significant bearing on the practical aspects of MI waveguide solutions.

(Wiltshire, Shamonina, Young & Solymar 2004) extend the theory of MI waveguides originally proposed in (Shamonina et al. 2002*b*) to an one-dimensional array of "swiss rolls", operating under a given frequency range. A very significant theoretical observation in this work is about the higher-order coupling resulting in a relatively slow decline of the magnetic field compared to loops examined in (Shamonina et al. 2002*b*). The relevant theoretical precept from (Wiltshire et al. 2004) can be reproduced as follows:

"...... higher-order coupling is more significant for swiss rolls. They differ from loops by having a third dimension as well. ...... Hence, the magnetic field distribution generated by the swiss rolls is quite different from that of loops: the decline of the magnetic field along the axis of the array is much slower."

This theoretical fact about the rolls had been stated previously in the case of solenoids as well, as observed in (Wiltshire et al. 2004).

(Shamonina & Solymar 2004) provide a detailed theoretical analysis of one-dimensional MI waveguides (both planar and axial configurations), and contrast the theory of MI waveguides with that of traditional transmission lines. This is a very useful study as far as examining the possibility of accomplishing the same objectives by means of MI waveguides as by using transmission lines, albeit on a reduced scale.

(Freire, MarquÃľs, Medina, Laso & MartÃŋn 2004) examine the theory of microwave delay lines using planar waveguides.

(Syms, Shamonina, Kalinin & Solymar 2005) use conventional transmission line equations to theorize on the behaviour of metamaterials consisting of split ring resonators (SRRs) and metallic rods. They claim based on the derivations that the previous notion of negative material parameters implicit in the derivation of such models is not factually correct; rather such notion needs to be replaced by the notion of *backward waves*. To reproduce the contextual observation from (Syms, Shamonina, Kalinin & Solymar 2005):

"It would, however, be desirable to answer the question whether negative parameter materials have any deeper meaning, i.e., are there any physical phenomena, which can only be explained by negative material parameters or is it simply a useful artifice that often helps physical intuition? We believed the latter to be true, and are prepared to go even further and offer the following conjecture: any experimental results explained by negative material parameters can also be explained without any recourse to them. The crucial point is to look at the properties of backward waves."

This reference might seem to be a digression, but actually it is topical. The larger point is that both metamaterials and their associated properties (such as negative permittivity) have been explored in novel theoretical approaches to certain complex electromagnetic phenomena. However, such sentiment has not percolated to the theoretical study of MI based WUSNs. This is an observation the author would revisit at the conclusion of this dissertation.

(Syms, Solymar & Shamonina 2005) examine the theoretical problem of broadband reflection absorption in a lossless finite one-dimensional waveguide. They propose the algorithm of incrementing resistances loaded in successive loops in gradations, for maximum reduction of reflection.

(Syms, Shamonina & Solymar 2006) analyse the coaxial waveguide configuration for critical multi-port devices in radio engineering, based on the corresponding reflection/transmission theorization of MI waves and the applicable power dependency. The devices studied include mirrors, resonators, reflectors, tapers, splitters, and directional couplers. (Syms, Young & Solymar 2006) propose a theoretical model for reducing the effect of higher-order coupling in solenoid MI waveguide. The model proposes the reduction of higher-order coupling as the inverse exponential function of magnetic field strength along the axis. Such a model in turn can increase the adjacent neighbour coupling, leading to lower propagation loss. In addition, theoretical analysis has also been provided for controlling reflections in similar waveguide structures using varied mutual induction between adjacent coils.

4.2.2 Experiments and Observations

In the context of WUSNs, the earliest reported application of MI can be traced back to (Sojdehei et al. 2001) for underwater communications. This work is noticeable for both the nature and extent of the experiments conducted using MI communication, as well as the ground-breaking results and novel solution pointers. The reported field tests were conducted in a range of environments including VSW, surf zone (SZ) and beach zone (BZ), involving various deployment depths, transmission ranges, operating frequencies, magnetic moments, modulation schemes, bandwidths, receiver sensitivities (SNRs), antenna models and orientations. The reported results show communication ranges between 300-600 m with varying, yet tolerable BER. Although these results indicate encouraging possibilities for underwater MI communication, they do not speak for the possibilities underground through soil medium, as conveyed by simulation results unearthed by later research. These will be reviewed in a later subsection. However, there are some very interesting inferences drawn in (Sojdehei et al. 2001), which are echoed in terms of relevance for underground communication through soil medium as well. To reproduce the relevant excerpt:

"The ratio of the magnetic moment ($A - m^2$) required to the power (W) consumed to produce it can be used as a figure of merit for a MI transmitter. Parametric analysis indicates that the figure of merit is proportional to the weight of copper used in the coil. Because of the $\frac{1}{R^3}$ law relating field strength and range R, the power consumed by a MI transmitter must increase if longer ranges are desired. Field strength is a direct function of antenna current (I); thus the power loss (I^2r) in the copper resistance (r) is a 6^{th}-order function of range. Consequently, for long-range signalling, the weight of copper wire used in the transmitter must increase (larger wire cross-section or more turns) if a high figure of merit is to be achieved; otherwise additional power must be consumed. From this we conclude that for long-range communication, a system of MI transceivers operating in relay-mode has significant merit when there is a need to keep the weight low and the size small, e.g., as in the UBV application."

This is perhaps the single most crucial observation to emerge from the earlier research on MI communication for WUSNs, which turned out to be highly prognostic, as vindicated by the more recent research in the area. The gravity of this observation will be more evident, as this discussion progresses with the review of the state-of-the-art research on MI communication for WUSNs.

Experiment result for the seminal MI waveguide concept was presented in (Shamonina et al. 2002*b*). The result highlighted the possibility of relay-mode transfer of power from a source to the destination using magnetically coupled, resonant, axially-aligned coils loaded with a suitable capacitance. This result had a lasting impact on the evolution of MI communication underground, and is at the centre of the state-of-the-art research on the topic. (Shamonina et al. 2002*a*) present simulation results based on theoretical derivations of MI waveguide properties in one, two and three dimensions, as well as in planar and axial configurations. The waveguide models and the results presented are relevant to WUSNs. The one-dimensional waveguide model presented in the work has been adapted to WSUNs by later research.

(Wiltshire, Shamonina, Young & Solymar 2003) validate the theoretical waveguide models presented in (Shamonina et al. 2002*b*) and (Shamonina et al. 2002*a*), using simulations for bandpass region, amplitude and phase variations, and dispersion of the MI waves under specific system (frequency) and device configurations. The results reveal a close match with the theoretical model, thus indicating the possibility of using variants of the model to emulate different radio systems based on MI wave attributes. Such possibility has been further corroborated in (Syms, Shamonina & Solymar 2006). The simulations presented in (Syms, Shamonina & Solymar 2006) show that MI waveguides can be used to reproduce the transmission/reflection characteristics and corresponding power attributes of common device structures in radio technology. These results are suggestive of the potential of MI waveguides in reproducing the radio wave aspects of a given structural paradigm. However, this concept has not gained prevalence in later research, especially in the context of WUSNs.

(Wiltshire et al. 2004) compare the theoretical model to the experimental results obtained for an one-dimensional array of "swiss rolls" constrained by operational parameters including frequency. Their theoretical observation highlighted the higher-order coupling of this waveguide structure, resulting in a relatively slower attenuation of the magnetic field. The experimental results validate this observation by means of the inverse cube relationship (which is the relationship $\frac{1}{R^3}$ originally touched upon during the review of (Sojdehei et al. 2001)). Based on the experimental data obtained from an array comprising of 31 rolls, (Wiltshire et al. 2004) make the following observation in this regard::

"As expected, the higher the order of the coupling, the smaller the coupling coefficient. Note that, if the distance between the two elements is large enough, the decay of the coupling coefficient should be proportional to the cube of the distance. This is because, when observed from a sufficiently large distance, a swiss roll (or a solenoid) appears as an infinitely small magnetic dipole. The magnetic field in the vicinity of the swiss roll, ..., declines much more slowly due to the finite length of the element. ......It can be clearly seen that the cubic law starts to become valid at around the 24th element ...... an indication of the significance of higher-order coupling."

Elsewhere, the same report continues:

"A separate experiment, involving only two elements, was performed in order to derive the coupling coefficient between any two elements of the array. We find that these coefficients fall off quite slowly as a function of distance, only tending asymptotically to inverse cube behavior for >24th-neighbor spacing. The key point here is that the rolls are extended resonators, and only at large separation is the point dipole behavior recovered. This, of course, is well known from the mutual inductance of finite solenoids ...... A remarkable feature of the array, in contrast to any other array we have come across, is the relevance of the higher-order coupling between the elements which is due to the fact that the magnetic field generated by a swiss roll decays relatively slowly away from the element."

Irrespective of this finding, as will be shown later based on the review of current research on MI communication for WUSNs, there has not been any foray in the direction of replacing loops in the waveguide with either "swiss rolls" or even solenoids in order to investigate the impact on certain theoretical snags due only to the relay coils.

(Shamonina & Solymar 2004) present simulation results for power transfer to a load, either matched or unmatched, using various arrangements of one-dimensional arrays (both planar and axial configurations). The arrangements used include a single waveguide, junctions of two different axial waveguides, two identical planar waveguides fully inter-coupled (coupler), and partially inter-coupled (directional coupler). The key aspects investigated include the dispersion characteristics and wave reflection arising due to composite waveguide. A significant observation in the case of waveguide junctions is the notion of "tunnelling" power between two identical waveguides using a different bridge. The amount of power transferred can be controlled by means of the bridge configuration, upto a theoretical maximum. A similar effect has been demonstrated in the case of directional coupling as well. This is an idea that can be creatively applied to many of the theoretical issues in MI waveguide communication for WUSNs, such as for instance channel demarcation in multi-waveguide WUSNs. However, this has not been explored in any of the current research so far. The simulation results also reveal striking similarities between MI waveguides and traditional transmission lines, apart from a few quintessential differences. This is again a major revelation, indicating the tremendous possibility of exploring the time-tested solution space of traditional transmission for possible answers to some of the technical snags in MI waveguide communication for WUSNs. This approach, true to the concept of *analogical thinking* (Gassmann & Zeschky 2008), has been overlooked as well in the current research.

(Freire et al. 2004) use experiment results to demonstrate microwave delay lines using planar waveguides photo etched on a PCB. The results validate the theory. The concept of a delay line can be employed in mitigating interference related issues in multi-waveguide WUSNs, although current research has not explored this solution approach.

(Syms, Solymar & Shamonina 2005) present simulation results to show that broadband reflection in one-dimensional lossless finite waveguides is considerably reduced, by means of equipping successive loops with resistor values which increment according to a gradation. The results are mentioned to be applicable to lossy waveguides as well. This finding can be very useful in the context of multi-user interference in MI waveguides for WUSNs, but so far no current research has explored this direction.

(Syms, Young & Solymar 2006) present a novel solenoid waveguide design using PCB coils and corresponding experiment results for several practical applications. The PCB design is used to devise both single and double layered coils, in order to investigate their impact on reducing the higher-order coupling effect (denoted by ξ), based on the theoretical analysis. For frequencies in the 40-500 MHz range. the results show a 30% reduction in ξ in the case of the double-layered coils. To quote (Syms, Young & Solymar 2006):

"... for single- and double-sided coils operating at.....frequencies in the range 50-400 MHz.....For the single-sided coils, the variation follows an inverse square law, to a reasonable approximation. However, the rate of decay is lower at small separations and higher at larger ones.....Double-layer coils have a consistently higher coupling coefficient than single layer coils over this range. The data were then used to estimate the coupling ratio ξ.....Double-sided coils clearly show a significant reduction in ξ, by around 30%. Based on the above, double-sided coils offer significant advantages for MI waveguides."

This result, along with the possibility of a "controlled reflector" by means of adjusting the mutual inductance between adjacent coils, has been used to demonstrate increased S_{21} and reduced S_{11} parameters for path-breaking application concepts such as coupling the MI waveguide to a standard 50 Ω transmission line, and the design of a recursive filter based on solenoid MI waveguide. These significant design and implementation concepts and corresponding results have not been considered in any of the research output related to MI communication for WUSNs.

NOTE

The author would like to note an exception to the above statement, and mention that as will be pointed out during the review in a subsequent section, multilayer coils have indeed been considered in the many recent theoretical research outputs on MI waveguide WUSNs. However, this has not been the norm, and there have been exceptions as well. In other words, the broader significance of discarding single layer coils in favour double layer coils as outlined in (Syms, Young & Solymar 2006) has not been well received. The author shall take up this thread again during the course of the discussion under Chapter 8.

(Hesmer, Tatartschuk, Zhuromskyy, Radkovskaya, Shamonin, Hao, Stevens, Faulkner, Edwards & Shamonina 2007) present simulation and experiment results for electric and magnetic coupling between SRRs constructed using different metamaterials, with different yet comparable physical dimensions but varied resonant frequencies. Four different gap orientations viz., *equal (0°)*, *reversed (90°)*, *near* and *far* have been used in the experiments. The results show that the magnetic coupling is stronger for reversed than equal orientation. To quote (Hesmer et al. 2007) on this aspect:

"The strength of the electric coupling (near orientation,...) in the case of flat SRRs can be seen to be reduced more than the strength of the magnetic coupling (reversed orientation)....For all types of elements the reversed orientation can be seen to provide a stronger coupling than the equal orientation in which the electric and the magnetic coupling mechanisms tend to compensate each other ... Thus if a chain of nanostructured split rings is to be used as a near field guide for magnetic field based on the propagation of slow waves of coupling, ..., then the reversed orientation of the elements would be a better choice and not the equal orientation."

This result is highly relevant to the deployment of MI waveguide for WUSNs, and has been adopted to benefit in the related theoretical studies as will be discussed shortly. The author has also adopted this guideline in research related modelling.

4.2.3 Remarks

The author endeavoured to present a comprehensive review of the early research on MI and MI waveguides in the preceding subsections. There could have been omissions in bringing in the entirety of the work involved, but certainly the cross-section should have been covered. It is evident from the above review that almost entirely, with very few exceptions, the founding research on MI and MI waveguide had very little to do with WUSNs. In fact, in almost all of the works reviewed, the preoccupation is with NFC in mm or cm ranges, which is more suitable for applications such as MRI. There is not even a remote preoccupation with an application context akin to WUSNs, which would involve communication ranges exceeding hundreds of metres. Among the works reviewed, the single exception to this claim is (Sojdehei et al. 2001). However, as pointed out earlier, most of the claims pertaining to MI underwater communication put forth in (Sojdehei et al. 2001) have not been in agreement with MI communication underground, as will be shown in the following sections. This is due to the fact that the underground environment is dissimilar to the underwater environment. Additionally, the notion of waveguides was only hinted at as a possibility in (Sojdehei et al. 2001), which is the pivot of the current research on MI communication underground. It will be evident from the review of current research on MI communication for WUSNs, that as in the case of (Sojdehei et al. 2001), even the ideas and solution approaches which stemmed from other preliminary research outcomes, such as MI waveguide, had to be adapted to suit the underground environment. Also, the impact of the underground environment on the performance of these models could not be completely annulled by such adaptation, as will be shown in the following sections.

The author has also used the review under the previous subsections to point out how some of the innovative solution approaches presented in the earlier research have not found much favour with the current research on MI communication for WUSNs, despite their relevance. As cases in point, exploring the use of metamaterials in probable workarounds to some of the theoretical impediments, as well as using other innovative concepts like experimenting with alternate configurations such as "swiss rolls" (Wiltshire et al. 2004) instead of coil loops in MI waveguides, novel waveguide arrangements such as multi-waveguide junctions or directional couplers (Shamonina & Solymar 2004) in tandem with signalling techniques, or exploiting the similarity to traditional transmission for analogous solution approaches (Shamonina & Solymar 2004), and resistor gradients (Syms, Solymar & Shamonina 2005) to control reflection in a multi-user scenario, can be considered. These apparent oversights are testament to how the current research has been oblivious to alternate solution approaches that could be used to circumvent the theoretical bottlenecks, not only from other domains but even from research areas which serve as foundation to MI communication for WUSNs.

4.3 MI Waveguide System for WUSNs

MI in the context of WUSNs without the notion of a waveguide was originally proposed in (Akyildiz & Stuntebeck 2006) and (Akyildiz et al. 2009) due to its following inherent advantages over EM waves underground:

- Magnetic fields do not experience any attenuation due to the dense soil medium, as the magnetic permeability of soil is same as that of air.

  NOTE

  This conclusion was revisited in a later research, as will be pointed out shortly.

- In MI communication, transmission and reception of signals is achieved by means of a small coil of wire, thus obviating the need for complex antenna structures.

However, the above studies also point to the fact that MI path loss over a range (total path loss) is larger than that of EM waves, and propose the MI waveguide as the viable alternative to overcome this shortcoming.

MI waveguide has been studied in detail in subsequent research (Sun & Akyildiz 2010*c*), (Sun & Akyildiz 2010*b*), (Sun & Akyildiz 2012) wherein the MI relay point has been described as a simple coil devoid of any energy source or processing capability. Further, as in the case of the preliminary research on MI, each coil has been loaded with a capacitor whose value can be tuned to achieve resonance between consecutive coils. The MI waveguide performance figures based on the simulation results have been bound by very specific assumptions about the parameters.

4.3.1 Detailed Overview of MI Waveguide

The following detailed overview of the MI waveguide technical aspects has been provided to point out the system challenges and limitations, which have bearing on the ensuing discussion.

- In all the simulations, the magnetic permeability of soil is treated as a constant equivalent to $\mu = 4\pi \times 10^{-7}$ H/m.
- The simulations in (Sun & Akyildiz 2010*c*) consider finite system parameters including operating frequency (10 MHz), number of turns of the coil (5), minimum relay distance (4 m) and coil radius (0.15 m). The loaded capacitance is specified to be greater than 10 pF (35 pF is the actual value used) so as to make the value non-identifiable with coil parasitic capacitance. The coil is made of copper with a characteristic resistance of 0.01 Ω/m with a diameter of 1.45 mm. It has been shown by means of simulations that the path loss of the MI waveguide system is less than 100 dB for a transmission distance of 250 m. The BER of the MI waveguide system has been studied under two different noise levels of -103 dBm and -83 dBm for 10 dBm transmission power. The simulation results show that the BER of the MI waveguide is as efficient as those of the EM wave or MI transmission, for a transmission range enhanced by more than 25 times. Both the path loss and the transmission range of the MI waveguide calculated assume that the coils operate under resonance. For the chosen operating frequency of 10 MHz, the 3-dB bandwidth of the MI waveguide is shown to be between 1 KHz and 2 KHz. The above results are based on the assumption that the mutual inductance between consecutive coils is identical, which corresponds to the ideal deployment condition. It has been shown using simulations that a standard deviation of >10% from ideal deployment is accompanied by a dramatic increase in path loss and decrease in bandwidth of the MI waveguide.
- The simulations in (Sun & Akyildiz 2010*b*) study the optimum number of relay coils for the MI waveguide, based on the required bandwidth and the distance between nodes. The optimum coil deployment strategy is analysed for one and two-dimensional WUSNs. In both cases, the transmission power has been set to 4 dBm,

the minimum power for correct demodulation of a received signal has been set to -80 dBm, the bandwidth has been set to 1 KHz and the operating frequency has been set to 10 MHz. The radius of the relay coils have been set to a uniform value of 0.15 m, and the number of coil turns have been set to 20. The coil is made of copper wire with a characteristic resistance of 0.01 Ω/m, and a diameter of 1.45 mm. In the case of one-dimensional WUSNs, the simulation results show the relay distance as a decreasing function of the number of relay coils. For two-dimensional WUSNs, the deployment strategy is analysed for the hexagonal tessellation topology (full coverage of a given area) and random topology (selective coverage of a given area). Two algorithms viz., the Minimum Spanning Tree (MST) and TC (Triangle-Centroid) have been presented. In the case of both, a particular sensor density has been assumed. The MST algorithm is the same for both hexagonal tessellation and random topologies, and is concerned with connecting all the sensor nodes using the minimum number of relay coils. However, the MST is not robust to node failures, due to the single-point connectivity between two successive nodes. The TC algorithm is aimed at remedying this defect, and has two variants. In one variant, all the sensors at the vertices of the hexagon are connected to one another, by means of relay coils deployed at the edges (6-connected). An optimization to this model has also been discussed. It divides the hexagonal tessellation into non-overlapping triangles, and the number of relay coils is optimized by connecting the sensors at the vertices through the "three-pointed star" MI waveguide deployed along the centroid of every alternate triangle. For random topology, Voronoi diagrams have been used to organize the random nodes under a polygonal tessellation topology, which is then partitioned using the TC algorithm. Simulation results for 100 underground sensors in a given square area (sensor density) have been presented. The results show that the MST takes up the least number of coils, whereas the 6-connected hexagonal (polygonal) tessellation takes up the most. The optimized deployment strategy for the hexagonal (polygonal) tessellation takes up an in-between number of coils.

- The simulations in (Sun & Akyildiz 2012) study the channel capacity, and the network capacity and reliability of WUSNs implemented using the MI waveguide. Closed-form expressions for the MI waveguide path loss and bandwidth have been developed under the following assumptions:

1. The axial direction among successive coils is a straight line.
2. Successive coils resonate with each other.

The closed-form expression for the MI waveguide channel capacity is derived from path loss and bandwidth, using the classic channel capacity formula (Showers, Schulz & Lin 1981). The default simulation parameters include a transmission power of 10 dBm, operating frequency of 10 MHz, relay coil radius of 0.15 m and 20 coil turns. The simulation results show the optimum channel capacity as a function of relay coil density and resistance value. In addition, the channel capacity is also shown to be a dramatically decreasing function of transmission distance, for various coil sizes and number of coil turns. The channel capacity is then used to derive the network capacity for the deployment models outlined in (Sun & Akyildiz 2010*b*). In the case of the MST model, mathematical derivations of inter-node interference range and corresponding maximum number of interfering neighbours for a given node, are used to formulate a spatial and temporal transmission schedule for the WUSNs. The mathematical expression for the mean value for the number of routes served by each node is then derived. Correlating the expressions for channel capacity, the transmission schedule and mean value for routes served, the expression for the achievable throughput of each node is derived. In the case of the other two models (6-connected and TC) outlined in (Sun & Akyildiz 2010*b*), it is inferred that the network structure is similar to the traditional wireless networks, based on the fact that the interference and communication range of all the nodes is isotropic. However, since the channel capacity and the network capacity are different for WUSNs, the achievable node throughput is suitably adapted from the results presented in (Gupta & Kumar 2000). In the simulation results based on the above derivations, it has been shown that the network scaling capacity (a function of node throughput) of WUSNs modelled on MST is comparable to that of traditional wireless networks (ad hoc networks to be precise), whereas that of the WUSNs constructed using the other two models (6-connected or TC) fares slightly better. The above results are then used to analyse the WUSN reliability under the following conditions:

1. Sensor node failure
2. Relay coil missing
3. Relay coil misalignment

The channel capacity is not impacted due to the first condition, but the network geometry is affected. The network geometry is not impacted due to the remaining conditions, but the channel capacity is affected. In the case of the first condition (node failure), it has been stated based on logical analysis that the impact on MST-based WUSNs is 50% while the impact can be neglected for the other two WUSN models (6-connected or TC) for reasonably sized networks. The other two conditions are approximated for simulation by means of the following logic:

1. The probability of a relay coil is damaged or missing is assumed to be 10%.
2. The probability of axial misalignment (not aligned on a straight line) is assumed to be a zero-mean Gaussian variable with a standard deviation $10\% \times 90°$.
3. The probability of position change is assumed to be a zero-mean Gaussian variable with a standard deviation $10\% \times r$, where r denotes the relay distance.

Based on the simulation results averaged over 100 iterations, it has been shown that the channel capacity is impacted by the above three probabilities in the following order:

1. The probability of axial misalignment of coils has the most pronounced impact on channel capacity.
2. The probability of coil position deviation has the least impact on channel capacity.
3. The probability of damaged or missing coils has an in-between impact on channel capacity.

4.3.2 Shortcomings of the MI Waveguide

The author presented a very detailed overview of the MI waveguide theoretical model for WUSNs under the previous subsection. In this subsection, the author addresses certain shortcomings that are inherent to the model, which severely impact MI communication underground. Further theoretical improvements on the MI waveguide model outlined under the next section stem from these shortcomings.

The author would start with the basic MI waveguide model originally proposed in (Sun & Akyildiz 2010*c*). The model is subject to the following limitations:

1. In the MI waveguide, each coil is loaded with a capacitor, which is tuned to achieve resonance among the coils. For a given operating frequency (ω), specific number of turns of the coil (N), and coil radius (a), assuming that all the coils in the waveguide are uniform (each coil has the same resistance (R), self-inductance (L), and the mutual inductance (M) between two adjacent coils in the waveguide is the same), the value of the capacitance for resonance condition is given by

$$C = \frac{2}{\omega^2 N^2 \mu \pi a} \tag{4.1}$$

The path loss of such an MI waveguide is a monotonously increasing function of the variable $\frac{R}{\omega M}$, expressed as

$$\frac{R}{\omega M} = \frac{4R_0}{\omega N \mu \pi} \left(\frac{r}{a}\right)^3 \tag{4.2}$$

where in addition to the variables denoted above, R_0 denotes the coil wire resistance. The conditions imposed by (4.1) and (4.2) are counter to each other. In the case of (4.2), a reduced value for $\frac{R}{\omega M}$ should imply

   - Higher values for ω and N, since μ is considered as constant. However, increasing both the values beyond a certain limit can interfere with the required minimum value for C in (4.1), in order to achieve resonance condition in the waveguide. In addition, this minimum value of C makes it non-comparable to coil parasitic capacitance. Coil parasitic capacitance is a critical issue in MI waveguide performance, as will be evinced in the next section.
   - The value of R_0 has to be a minimum as well in (4.2), in order to avoid in-band signal fluctuation.
   - To maintain the cost advantage of the MI waveguide the ratio r/a has to be a minimum as well.

2. The MI waveguide resonance is subject to the condition that the system operates under a central frequency. Any deviation from the central frequency impacts the resonance condition and causes impedance mismatch at the receiver.

3. The MI waveguide system also presumes that the coils are uniformly distributed between the transceivers. A deviation from such an arrangement causes performance deterioration in terms of increased path loss and decreased bandwidth. It has been shown in (Sun & Akyildiz 2010*c*) that a standard deviation of 20% can drastically impact the system performance.

The deployment algorithms presented in (Sun & Akyildiz 2010*b*) are not readily implementable in an actual field environment. The least optimal and most straightforward of the algorithms presented, viz., MST, is an exception to this fact. However, MST is not optimal in terms of coverage potential and is not robust either to potential node failures. The other algorithms are quite intricate and cannot be easily realized in a practical deployment scenario, especially involving a large coverage area. The network scaling capacity model presented in (Sun & Akyildiz 2012) has been based on the TC algorithm presented in (Sun & Akyildiz 2010*b*), and hence cannot be applied to a real deployment scenario owing to the reason mentioned above. Besides, the channel model and the consequent network model for the MI waveguide have been based on a vertical axis coil deployment strategy. Apart from the fact this is suboptimal in comparison to the horizontal axis deployment strategy for WUSNs (Kisseleff, Gerstacker, Schober, Sun & Akyildiz 2013), this choice also renders the findings of (Sun & Akyildiz 2012) less generic.

4.4 Improvements to the MI Waveguide Model and MI Communication for WUSNs

In this section, the author critically examines the state-of-the-art research output aimed at addressing the shortcomings of both the MI waveguide model outlined under the previous section, as well as MI communication for WUSNs. At the very outset, the author would like to emphasize that all of the current research output on the topic have been of pure theoretical relevance. In addition to pointing at the relative infancy of this research area, this fact also hints at the fact that no alternate solution approaches have been considered to circumvent the theoretical issues. This research is intended to bridge this gap using simulations targeted at specific issues stemming from the theoretical research. The research direction adopted also engenders a paradigm shift by means of the overall solution approach rooted in *analogical thinking* (Gassmann & Zeschky 2008) to circumvent key theoretical limitations, and instigate outside the box thinking in finding novel solutions to other issues as well within the research domain. In order to appreciate this point of difference, a good insight into the state-of-the-art in the theoretical research is a pre-requisite, which purpose would be served by the review undertaken in this section.

4.4.1 Critical Analysis of Theoretical Models

In this subsection, pertinent analysis of each proposed improvement to the MI waveguide model or MI communication for WUSNs has been provided in a chronological order, while highlighting its assumptions, merits and demerits. The demerits have to be perceived within the larger premise of the original MI waveguide model, and consequently also point to the unresolved issues within the system.

(I) The study in (Kisseleff, Gerstacker, Schober, Sun & Akyildiz 2013) revisits the theoretical channel capacity bounds for MI waveguide. In this study, several theoretical assumptions made in (Sun & Akyildiz 2010*c*) and (Sun & Akyildiz 2012) have been discarded, in favour of more accurate system specifications. A significant omission in the previous models addressed herein is the attenuation of the magnetic fields in soil caused due to eddy currents. This omission had been alluded to in the discussion on the original MI waveguide model proposed in (Sun & Akyildiz 2010*c*). The simulation results in (Kisseleff, Gerstacker, Schober, Sun & Akyildiz 2013) vastly depart from those presented in (Sun & Akyildiz 2010*c*) and (Sun & Akyildiz 2012).

Assumptions: Besides the system parameters chosen for simulation, it has been assumed that the waveguide would be deployed in a homogeneous conductive medium (soil), uniform across space and time. It has also been assumed that the magnetic field would be propagated by means of multilayer air core coils. The coil axial direction is assumed to be horizontal (coil axis is identical to the waveguide axis).

Merits: Several aspects bearing on the MI waveguide performance have been considered in this study, which had been overlooked in (Sun & Akyildiz 2010*c*) and (Sun & Akyildiz 2012), including

- The issue of conductivity based losses in soil (the eddy current factor).
- Frequency-selective path loss and corresponding received noise power.
- Channel capacity as a function of optimal system parameters.

Demerits: The simulation results show that in contrast to the unconstrained MI waveguide, the channel capacity of capacitance constrained MI waveguide (Sun & Akyildiz 2010*c*) deteriorates with increasing frequency or number of turns of the coil. Thus both these parameters have to be jointly optimized for best system performance.

> **NOTE**
>
> It needs to be pointed out here that the effect of parasitic capacitance has been totally neglected in this model, which should reflect unfavourably on its overall findings. The implication is that the impact of parasitic capacitance should further demote the performance benchmarks projected by this model.

Subsequent simulations after such optimization show that due to the impact of soil conductivity, the capacitance constrained MI waveguide has a low path loss at high frequency in dry soil or for short relay distance. In contrast, the unconstrained MI waveguide has low path loss at low frequency in wet soil or long relay distance. A capacitance constrained MI waveguide has to operate at low frequency (Sun & Akyildiz 2010*c*), and this dramatically reduces its channel capacity in dry soil. Further simulations show that the channel capacity of the MI waveguide is inferior to direct MI transmission for low density coil deployment (relay distance >3 m). For high density coil deployment (relay distance ≤ 3 m), the channel capacity of MI waveguide is superior for distances greater than 45 m.

(II) In (Kisseleff, Akyildiz & Gerstacker 2013), inter-node interference minimization in an MI system (no waveguide) by means of tactical coil deployment in 3 dimensional (3D) space is investigated, by leveraging on the fact that magnetic polarization of power radiation is cancelled out at certain angles of orientation. To achieve the exact orientation of the coils required for interference polarization, the coil relative positions are modified on a 3D grid space to achieve maximum throughput and the optimal carrier frequency. The proposed algorithm uses an iterative approach to integrate the network in terms of groups of adjacent nodes for interference polarization.

Assumptions: Besides the system parameters chosen for simulation, the following assumptions have been made:

- All network devices are assumed to contain the same passive circuit elements.
- A minimum angle separation of 45° is assumed between the adjacent coil directions.
- It has been assumed that the MI direct transmission system would be deployed in a homogeneous conductive medium (soil), uniform across space and time. It has also been assumed that the magnetic field would be propagated by means of multilayer air core coils.
- It has been assumed that no bit errors occur at the output of the decoder.

Merits: The simulation results show that optimal coil alignment based on interference polarization can significantly increase network throughput.

Demerits: The interference polarization based deployment strategy is intricate and would involve careful planning of the network to achieve optimum results. In the complex underground terrain, this should imply a substantial amount of trial deployments, before a fully functional network can be put in place. Besides, no guarantees can be provided for how the fluctuations in the underground environment could degrade the performance of such a delicately balanced network.

(III) In (Kisseleff, Gerstacker, Sun & Akyildiz 2013), the problem of maximizing the network throughput of inter-connected MI waveguides for orchestrated multi-node transmissions has been examined as a function of optimum identical system specifications, where each node transmission is subject to inter-node interference and inter-waveguide reflections. In addition, the cumulative noise power at a receiver node due to the interconnection has also been taken into consideration.

Assumptions: Besides the system parameters chosen for simulation, the following assumptions have been made:

- The frequency is assumed to be identical for all links.
- The number of windings is assumed to be equal for all coils.
- The transmit power of all nodes is assumed to be uniform.

- The interconnected waveguide is assumed to be capacitance-constrained.
- Distinct circuitry has been assumed for transceiver and relay nodes.
- A uniform distribution of nodes has been assumed.
- The minimum inter-node distance is assumed to be 21 m and the minimum relay distance is assumed to be 3 m.
- It has been assumed that the MI waveguide would be deployed in a homogeneous conductive medium (soil), uniform across space and time. It has been also been assumed that the magnetic field would be propagated by means of multilayer air core coils.

Merits: The simulation results show that the MST algorithm used to optimize the links in the network based on the minimum number of relay nodes and maximum throughput, can identify and circumvent bottleneck links in favour of more optimal links. The more involved optimization logic for frequency and corresponding number of turns of the coil by means of a two dimensional (2D) grid in (Kisseleff, Gerstacker, Schober, Sun & Akyildiz 2013) has been replaced by a simpler logic of calculating frequency as a function of the capacitance-constraint. Even though uniform distribution of nodes has been assumed, the performance of the MST algorithm for a non-uniform distribution of the nodes has also been considered.

Demerits: One of the main shortcomings of the MST algorithm is that since the system specifications of frequency and the number of turns of the coil are tightly coupled with the optimization logic, any preferred link for its throughput rate would also necessitate a change of the corresponding system specifications. This severely limits the practicality of the MST algorithm. The simulation results show throughput degradation with increasing node density or total coverage area. Yet another result is that the required number of turns of the coil increase in proportion with the transmission distance. Overall, the results show very low throughput for the capacitance constrained interconnected MI waveguide using the MST algorithm. A suggestion to even out the overall network throughput using energy harvested from interference signals may not be realized without complex device circuitry.

(IV) In (Sun, Akyildiz, Kisseleff & Gerstacker 2013), the problem of optimizing the transmission range for a loosely coupled MI waveguide has been studied. The concept Spread Resonance (SR) has been proposed as the solution to achieve a ϵ-outage channel capacity. The SR method aims at achieving unique resonance between adjacent coils along the waveguide, using frequency bands that deviate from the central frequency by predetermined gradations.

Assumptions: None other than the system parameters considered for simulation.

Merits: The simulation results show that an MI waveguide based on the SR method could achieve much greater transmission range than a single centralized resonant frequency.

Demerits: The SR method introduces enormous complexity into the waveguide, by means of predetermining the central frequency gradations and their corresponding capacitance values, to achieve unique inter-coil resonance. Each chosen central frequency and its range of gradations would be adversely impacted by medium (soil) conductivity and coil direction deviations. Simulation results show that the inter-coil resonance is a drastically decreasing function of both parasitic capacitance (which is taken on par with the loaded capacitance in resonant coils unlike in (Sun & Akyildiz 2010*c*)) and medium conductivity. In a nutshell, the SR method presents too much complexity and many challenges to be considered as an option for a practical deployment scenario.

(V) In (Kisseleff, Akyildiz & Gerstacker 2014*a*), optimized modulation schemes for uncoded transmission using both direct MI and MI waveguide have been examined. The problem of long impulse response of the direct MI channel has been studied, and a solution approach similar to Frequency Division Multiplexing (FDM) has been proposed. In the case of the MI waveguide, the high SNR enables an impractically high order Quadrature Amplitude Modulation (QAM), and resorting to the most practical 1024-QAM reduces the achievable data rate by more than half, an effect termed as *clipping*. In order to overcome this effect, and considering the fact that the MI waveguide is a low bandwidth system, the bandwidth is increased beyond the optimum limit so as to enable a higher order modulation. Since this would adversely impact the SNR and the Symbol Error Rate (SER), the bandwidth increase of the system is bounded by a target SER.

Assumptions: Besides the system parameters chosen for simulation, the following assumptions have been made:

- Coil axial direction is assumed to be horizontal (coil axis is identical to the waveguide axis, or $\theta_t = \theta_r = 90°$ for direct MI transmission).
- Parasitic effects in coils (including parasitic capacitance) have been ignored, under the assumption that they should have negligible impact under the frequency band used for transmission.
- It has been assumed that the MI waveguide would be deployed in a homogeneous conductive medium (soil), uniform across space and time. It has also been assumed that the magnetic field would be propagated by means of multilayer air core coils.

Merits: Simulation results show that the proposed FDM based approach for direct MI transmission achieves up to 85% of the theoretical limit of transmission using a single frequency band. In the case of the MI waveguide, the bandwidth expansion technique has been shown to dramatically enhance the achievable data rate close to the channel capacity. The findings of this study, along with that of (Kisseleff, Akyildiz & Gerstacker 2014*b*), provide some preliminary insights into the transceiver design aspects for MI based WUSNs.

Demerits: The study mentions that if the FDM based approach is not resorted to, there could be a diminution of the achievable data rate of up to 95% for a practical MI direct transmission system of reduced bandwidth. This points to the non-feasibility of MI direct transmission for single frequency band systems. The import of this study is purely theoretical for present day WUSNs.

(VI) In (Kisseleff et al. 2014*b*), the theoretical problem of estimating the Channel State Information (CSI) at the receiver from the transmitter end, without the associated signalling, has been studied for MI based networks (both direct transmission and waveguide). The uncoded signalling system for MI based WUSNs in (Kisseleff et al. 2014*a*) has been made the basis for the theoretical study. An innovative algorithm has been proposed for channel estimation, wherein the impulse response of the system is used to deduce the mutual induction of the channel depending on the conductivity of the medium of transmission. The channel equalization is done using the Minimum Mean Squared Error-Decision-Feedback Equalization (MMSE-DFE) scheme adapted to the algorithm, and two different methods of channel estimation have been derived based on the resultant Inter-Symbol Interference (ISI).

Assumptions: Besides the system parameters chosen for simulation, it has been assumed that the CSI is known perfectly at the receiver due to the relatively larger coherence time at the receiver for the stationary WUSN channel.

Merits: This study provides some early insights into the transceiver design aspects for emergent WUSNs.

Demerits: The outcome of this study has purely theoretical relevance from the point-of-view of present day WUSNs.

(VII) In (Lin, Akyildiz, Wang & Sun 2014), a cross-layer protocol Xlayer for achieving maximum throughput at minimal energy cost in MI based interconnected WUSNs has been proposed. The protocol selects the optimum algorithms for each layer functionality, such as modulation, Forward Error Correction (FEC) and routing, to provide a minimum Quality of Service (QoS) guarantee in terms of a minimum Signal-to-Interference-plus-Noise-Ratio (SINR) per transmission per link. A careful distinction is made between application requirements of energy conservation vs. efficient data throughput, and the cross-layer optimization framework has been designed to address both these requirements by means of a combined weightage factor EaT (Energy and Throughput).

Assumptions: Besides the system parameters considered for simulation, uniformity of coil dimensions has been assumed across the network.

Merits: The simulation results show that in general the cross-layer framework of Xlayer achieves much better performance than layered protocols for which interaction is confined between the same layers, in terms of energy consumption, and throughput bit rate.

Demerits: As in the case of (Kisseleff et al. 2014*b*), the relevance of Xlayer is purely theoretical in relation to the present day WUSNs. Moreover, cross-layer optimization is an ongoing research area even in the relatively mature traditional wireless networks (Fu, Xiao, Deng & Zeng 2014). Thus it shouldn't be incorrect to surmise that the proposition of a cross-layer approach for the emergent MI based WUSNs can only be prognostic at its best.

4.4.2 Commentary

The review presented in the above subsection on the cross-section of the state-of-the-art research on MI and MI waveguide based communication for WUSNs, clearly brings the aforementioned preoccupation with the theoretical improvement of the system to the fore. There has hardly been any attention paid to circumvent the key theoretical limitations by means of suitable workarounds. One crucial aspect of the theoretical research that should not be missed is that, as the review shows, most of the models have resorted to highly specific conditions for their simulations, often overlooking even some of the most crucial parameters. For instance, it was pointed out in the review how some of the models have totally ignored the factor of parasitic capacitance, whereas others have emphasized its adverse impact on the performance of the MI system. On another level, assumptions such as air core coils, uniform soil conductivity, uniform coil dimensions and inter-node distances cannot be accepted at face value. It was pointed out during the review on WUSN research that soil properties do not remain constant, and can vary even over short distances depending on the terrain. Thus uniform medium conductivity is an assumption that goes contrary to typical field conditions underground. Further, a recent study (Stadler, Rudolph, Kupisch, Langensiepen, van der Kruk & Ewert 2015) points to the close affinity of the electromagnetic conductivity of soil to its properties. The study observes

"....Here, we use an electromagnetic induction (EMI) sensor to measure the apparent electromagnetic conductivity of the soil (ECa), which can be used as a proxy for the relative spatial variability of the prevailing soil properties. We evaluate relationships between ECa and soil and crop characteristics assuming that measured ECa patterns relate to observed growth patterns in the field.....Good correlations between ECa and soil texture and soil moisture confirmed that ECa measurements are suitable for characterizing spatial differences in soil properties for our test sites.....We conclude that ECa measurements are suitable for detecting spatial patterns in soil characteristics that influence the spatial crop growth patterns for the region, years and crops considered."

Thus there is every reason to conclude that any study based on the assumption of uniform medium conductivity underground has a very high probability of being factually incorrect. The other parameters noted are some of the system aspects that can be tweaked at the deployment stage to customize system performance in keeping with terrain conditions. Assuming uniformity in their case tends to restrict the flexibility of the system to adapt to the ground conditions. Such adaptability is imperative and hence assumptions to the contrary can only be of theoretical relevance by any stretch of imagination. A broad level characterization of the theoretical research so far can be as a study on the optimization of MI field propagation underground, by means of permutation and combination of the various environmental and technical aspects such as field characteristics, soil properties, coil specifications and deployment algorithms. A very glaring fact about each of these aspects is that taken by itself, it is bound by very specific limitations. Thus any permutation and combination of all of the above aspects is also bound to be limited. The discrepancies between the ground realities and theoretical assumptions pointed out earlier, taken together with the highly challenging underground environment, could imply that the least limited solution that could be arrived at by means of the permutation and combination of the above mentioned aspects, should still fall short of the minimum working system required for any meaningful application envisaged underground. This is a very good possibility, considering the direction and progress of the theoretical research on MI communication underground in the past 5 odd years. The limitations concerning the multiple aspects mentioned above cannot be changed. So it should pay to look at alternate ways of circumventing them, by using novel solution approaches that are a blend of the understanding of theoretical limitations, and application of suitable contrivances to achieve feasible workarounds for a functional system. This can be a more pragmatic approach leading to speedier deployment of MI based WUSNs in real-time contexts, rather than the current approach of making the theory work by exhausting all the permutations and combinations of the related dependencies, as stated before. This is precisely the approach that has been adopted in this research, as will be shown in the Research part of this dissertation.

4.5 Remarks

Earlier in the chapter, the author shared a highly optimistic forecast for MI communication in (Bunszel 2001). Albeit this prognosis had been in a more generic context, and not specifically related to WUSNs, it is yet appropriate to position it within the premise of the review presented under the previous sections on the MI communication research so far for WUSNs.

(Bunszel 2001) had highlighted the *consortium factor* as a crucial differentiator in the success or failure of an emergent technology. Since the technology of MI communication for WUSNs is at its inception, such consortium factor is yet to emerge. The review presented in this chapter showed how most of the contemporary research outputs have followed independent paths. Moreover, the sole focus of contemporary research has been on theoretical analysis and consequent improvement of MI communication for WUSNs. The author is of the view that a consortium factor for the domain should encompass more than theoretical research; it should also bring under the aegis alternate solution approaches that are complementary to theoretical research. Such synergy should lend the much required momentum for research in the domain towards a minimal deployment solution for MI waveguide WUSNs. The author shall revisit this topic at the conclusion of this dissertation.

In the case of MI communication for WUSNs, based on the review, the author would like to observe that the amount of progress achieved on the domain in the past 5 years could have been more, had the exclusive focus been not on the theoretical aspect of underground communication through soil. The main thread of current research on MI communication for WUSNs appears to be focused on augmenting the system performance solely through theoretical improvements, without pausing to consider alternate solution approaches. One such alternative could be searching other domains or fields of study for insights or pointers to possible novel solution approaches for some of the more pressing theoretical issues. In the context of the preliminary research on MI, the author pointed out how some of the innovative concepts thereof have never been explored within the context of MI communication underground. The review of the current research on MI based WUSNs substantiated this claim.

A more balanced approach should also look at innovative ways to solve the problem of achieving a minimal working solution for MI communication underground, by means of novel solution approaches that are based on the theoretical understanding. When it comes to this, it is essential to look for novel ideas outside the theoretical framework, both within and without the domain of MI communication. This is the fundamental philosophy of *analogical thinking* (Gassmann & Zeschky 2008) that has been espoused in this dissertation, and demonstrated by means of simulations.

4.6 Chapter Summary

In this chapter, the author laid out the cross-section of the research development so far on the front of MI communication for WUSNs, starting with the preliminary output related to NFC and related application contexts, and showing how some of the fundamental precepts of this early research have impacted the current research on MI communication for WUSNs. The author further showed by means of reviewing the state-of-the-art research output on MI communication for WUSNs, how the topic has been largely focused on theoretical analysis and corresponding simulations, at the cost of completely ignoring alternate solution approaches and corresponding workarounds. A more balanced approach calls for a blend of both theoretical understanding and novel workarounds adapted from within or without the domain of MI based WUSNs. The author maintained that this combined approach was fundamental to *analogical thinking* (Gassmann & Zeschky 2008), which is the guiding principle underlying the novel ideas and models presented in this thesis. The Research part of this thesis would dwell at length on those aspects.

In the next chapter, a brief discussion on the deployment examples of WUSNs in irrigation control has been presented. The topic is a logical follow-up to the discussions so far, since the related discussion is used to demonstrate how UG2UG communication has never been attempted in the relevant application context, due largely to the theoretical issues in WUSN communication highlighted in this and the preceding chapter.

Chapter 5

WUSNs in Irrigation Control

In this short chapter, the author takes a quick look at some of the applications of WUSNs in irrigation control. The purpose of this chapter is to demonstrate by means of such review, how UG2UG communication has never been attempted in the corresponding applications. This fact is the fallout of the theoretical impediments pertaining to both EM wave and MI communication underground, as outlined in the previous chapters.

5.1 Chapter Overview

In the previous chapters, the author dwelt at length on the theoretical impediments visiting both EM wave and MI communication underground. During the course of those discussions, the author alluded to the non-feasibility of UG2UG communication using EM waves due to the theoretical impediments; subsequently, the author also presented a detailed review of the state-of-the-art research on MI communication underground, making it evident that this alternative too fell way short of the minimum requirements for a UG2UG communication system of practical relevance. This fact can be readily perceived, upon a cursory review of the application of WUSNs in irrigation control. The purpose of the review in this chapter is to drive home the fact that owing to the insurmountable obstacles posed by the theoretical premise, UG2UG communication has never been attempted thus far in any application scenario of irrigation control or precision agriculture involving

WUSNs. This review has been intended as an exercise in further highlighting how theoretical approach alone to resolving the issues confronting MI communication in WUSNs is not sufficient; a more balanced approach should complement it with alternatives involving novel workarounds.

5.2 Application of WUSNs in Irrigation Control or Precision Agriculture

In this section, the author considers a cross-section of WUSN application scenarios in irrigation control. The method of review is rather brief, without delving too much into the details of the particular application; this is quite apt as the sole purpose of the review is to highlight the different modes of communication used in each application context, which could be either the set of UG2UG, UG2UG and AG2UG, or a subset.

NOTE

A word of clarification before proceeding with the review: the following review only considers hybrid topologies (Akyildiz & Stuntebeck 2006); any other paradigm does not fall within its scope.

The author would like to begin with certain observations in (da Silva, Moghaddam & Liu 2014) on the feasibility of EM wave or MI communication for UG2UG, UG2AG, and AG2UG communication in WUSNs. These observations set the right expectation for the subsequent review of WUSN applications in irrigation control; in other words, the observations in (da Silva et al. 2014) preclude the feasibility of UG2UG communication for large scale coverage (which is typical of irrigation control) under the technological status quo, using either EM wave of MI communication. The key observations in (da Silva et al. 2014) in relation to WUSNs (UG2UG communication) can be summarized as follows:

NOTE

Some of the points below might be a repetition of review results presented under previous chapters.

- In the case of EM waves, signal attenuation in soil is a complex function of soil composition and VWC.
- Through-the-Earth (TTE) solutions cannot be adapted to WUSNs due to the inherent differences in the two paradigms.
- A single communication model does not suit UG2UG, UG2AG and AG2UG communication due to distinct characteristics.
- Two problems, viz., the propagation problem and the antenna problem, need to be simultaneously resolved for effective WUSN communication.
- The empirical results for UG2UG communication thus far using EM waves have been limited to short inter-node distances (<3 m). However, a majority of WUSN implementations would require a large inter-node distance, e.g., 5-50 m.
- Experiment results thus far indicate that UG2AG and AG2UG communication using EM waves is feasible under shallow burial depths.
- In WUSNs, antenna size confines communication to the VHF band.
- The antenna problem in WUSNs, which includes its operational parameters and specifications, has not been effectively considered in UG2UG communication modelling. In these models, antennas have wrongly been assumed to have the same behaviour as in free space. More specifically, the effects of the directivity and other performance parameters have been simplified by the introduction of a *fixed* term in the antenna gain. At the moment, there are no best antenna design practices for a given WUSN scenario. The current set of models also do not fully address another antenna factor, involving the negative impact due to parameters such as soil moisture on antenna impedance, at least not in analytical form.
- Even though lateral waves (LW) present the possibility of improving the UG2UG communication range using EM waves, its feasibility would require antennas with

very high directivity which are hard to build.

- Long range AG2UG/UG2AG communication has been demonstrated only for shallow deployments. This is due to the fact that the above mentioned antenna factor has to be considered as a dynamic component in any theoretical model for deep deployments. Only for long range communication in shallow regions is this problem not applicable.
- Path loss exists for MI communication underground as well due to magnetic coupling.
- Implementation aspects of relay coils have not been thoroughly researched for MI communication underground.
- MI can be an alternative to EM waves in UG2UG communication, especially considering the communication range. However, no implementation guidelines for MI communication underground have been put forth in contemporary research.

The above points indicate that transmission range is a major bottleneck in the case of EM wave communication for all the applicable links in a hybrid WUSN model.

NOTE

This fact had been highlighted during the review under previous chapters as well.

Even though MI is an alternative, there are no practicable models in place to substitute for EM wave communication. These observations aptly summarize the limitations visiting WUSN communication at present, which are reflected in the WUSN applications for irrigation control as well.

Table 5.1 lists the cross-section of WUSN applications reviewed, with an overview of their scope and particular reference to the communication methods employed (from among the relevant methods for a hybrid topology as mentioned above); wherever applicable, additional remarks have been provided to highlight important aspects.

NOTE

In order to optimize space, the author does not adhere to a chronological order in the table. For the same reason, the author has chosen to place the caption at the top instead of bottom as in the case of the remaining tables in this document.

Table 5.1: Review of WUSN Applications in Irrigation Control

Application	Remarks
(Silva & Vuran 2010*a*) describe the regulation of a centralized pivot irrigation system by means of a hybrid WUSN. The laboratory experiments performed have been confined to the subsoil region (>30 cm depth). The WUSN system includes 433 MHz Mica2 motes (Crossbow 2007) deployed underground and communicating with an aboveground node installed on the pivot's structure.	Both UG2AG and AG2UG communication are involved. Customized antenna designs (a FW for AG2UG and SEA for UG2AG) are used in such communication.

Continued on next page

Table 5.1 – continued from previous page

Application	Remarks
(Dong, Vuran & Irmak 2013) extend (Silva & Vuran 2010*a*) to actual field experiments. Based on the results, an improvement to the original antenna scheme comprising of a circular planar antenna for UG2AG communication and a Yagi antenna for AG2UG communication, has also been proposed for extended range.	Both UG2AG and AG2UG communication have been considered as in the case of (Silva & Vuran 2010*a*).
(Dursun & Ozden 2014) describe an application for regulating irrigation pumps in a drip irrigation system, powered by solar panels and deployed in an orchard, based on the soil moisture content reported by 10 HS (Decagon 2014*a*) soil moisture sensors deployed at shallow depths (<30 cm). The sensor data is communicated aboveground at 434 MHz using a UFM-M11 (udea 2011) RF modem, whose range is augmented by means of a UGPA-434 (udea 2014) antenna.	Only UG2AG communication has been used.
(Wang, George & Green 2014) describe the prototypical design of a ARPT mechanism for powering underground sensors (no burial depth has been specified, although it would be safe to assume shallow burial depth considering the application design) *without* a battery, by means of query generated by a reader mounted on a tractor; the sensor node is envisaged to harvest power from the query, and use this power to report its readings back to the reader (at a proposed frequency of 915 MHz) through backscatter modulation. The readings are in turn used to control a spray boom mounted on the rear of the tractor.	Both UG2AG and AG2UG communication have been envisaged. The model bears similarity to the ARPT model that the author has experimented with in this research, which will be outlined in a subsequent chapter. In this research, the ARPT model has been envisaged in a UG2UG communication context.

Continued on next page

Table 5.1 – continued from previous page

Application	Remarks
(Huang, Kumar, El-Sayed Kamal & Eber 2008) detail the hardware, software and communication characteristics of a WUSN system prototype for soil moisture sensing at shallow burial depths. Of particular interest is the proposed simple antenna design "made of twisted wire of one quarter wavelength (about 2.8 meters) for underground wireless communication". There is also mention about use of a custom bit-oriented protocol for data communication. An ISM frequency of 27.145 MHz has been used for communication.	This work stands out because of its mention about attempting both UG2UG as well as UG2AG communication. According to the authors, "We have carried out the field tests for both above-ground and underground transmissions. For the former, sender and receiver were placed in line of sight. Reliable communications could be established up to a distance of 120 yards at a baud rate of 256 bits/second ...... For the underground transmission tests, both sender and receiver were buried at the depth of about 30cm. Received data were logged to check the communication quality. With baud rate of 256 bits/second, the frame error rates were found to be 17.14% and 35.14% at the distance of 66 feet and 91 feet, respectively." In addition, the authors also mention about accomplishing an UG2AG communication range of 120 meters, for line-of-sight communication between the underground and aboveground nodes. Even though these claims are really impressive even by today's standards of UG2UG communication, the work undertaken does not seem to have been carried forward by further research endeavours.

Continued on next page

Table 5.1 – continued from previous page

Application	Remarks
	Moreover, the claims made for UG2UG communication have not been substantiated using any graphs plotted based on the experiment conditions. Thus even though the authors' claims could be well justified, its applicability to any future research is very limited in scope. Certain aspects such as the antenna design and bit-oriented protocol bear close resemblance to the paradigms experimented with, in UG2UG communication for WUSN at present.
(Soontornpipit, Furse, Chung & Lin 2006) present the prototype design and implementation of a dual purpose microstrip antenna which could perform both sensing and communication functions at different frequencies (1350 MHz and 1850 MHz respectively). The basic design principle requires that the antenna communication band is not detuned by soil moisture fluctuations, whereas the sensing band should be strongly impacted by these changes. A cost function based on the magnitude of the reflection coefficient is fundamental to the antenna tuning, guided by this design principle. The soil moisture data communicated by the antenna is ultimately intended to regulate a sprinkler system. A stacked design of the antenna model has also been proposed with two layers, for which a communication frequency of 410 MHz is assumed.	

Continued on next page

Table 5.1 – continued from previous page

Application	Remarks
A similar multi-frequency (1-30 MHz for sensing and 915 MHz for communication) metamaterial dual purpose antenna design has also been reported in a more recent work (Pandey, Kumar & Weber 2014).	Based on the description provided in the reports, only UG2AG communication has been assumed using the proposed antenna designs.
(Bogena et al. 2009) present the results of laboratory experiments conducted using soil moisture sensors deployed at shallow depths (<4 cm) for studying the impact of signal transmission through soil, with the end-objective being the study of hydrological processes in small watersheds. The communication frequency used for a low-cost ZigBee radio network is 2.44 GHz.	Only UG2AG communication has been considered in the experiments.
(Zhang, Wu, Han & Yu 2012) describe the prototypical design and test results of a hybrid WUSN system for soil moisture sensing and reporting. The frequencies of 433/868/915 MHz in the ISM band have been envisaged for the WUSN communication. Different burial depths (0.2-2 m) and soil VWC (5-25%) have been considered for the tests. A related report (Yu, Wu, Han & Zhang 2012) also specifies use of mobile aboveground sink nodes for data gathering.	Based on the description provided in the report, only UG2AG communication has been envisaged for the hybrid WUSN prototype.

Continued on next page

Table 5.1 – continued from previous page

Application	Remarks
(Li, Wang, Franzen, Taher, Godsey, Zhang & Li 2014) present the deployment study of WUSN in a wheat field for monitoring soil properties including VWC, temperature and bulk electrical conductivity. The study has been conducted involving both shallow and deep burial depths using EC-5 (Decagon 2014*b*) and EC-TE (Decagon 2008) sensors communicating their readings aboveground using IRIS mote (Crossbow 2007).	Only UG2AG communication has been employed in the application.
(Tiusanen 2013) discusses the design and experimental evaluation of *soil scouts* at shallow burial depth (15 cm), which are "palm-size wireless underground sensor nodes for monitoring of agriculture soil parameters." The soil scouts comprise of sensing and communication subsystems; the sensing system is equipped with a 12 bit ADC, soil moisture sensors and a temperature sensor; the communication subsystem consists of a wide-band printed circuit monopole antenna for communication at 869.4 MHz ISM-band.	Only UG2AG communication has been attempted in the experiments.

Continued on next page

Table 5.1 – concluded from previous page

Application	Remarks
(Adel & Norsheila 2013) present the design and corresponding simulation results for an optimized routing protocol in a hybrid WUSN topology. The proposed set up uses both underground nodes and relay nodes for optimal UG2AG communication. All the simulation results have been presented in shallow burial depths (0-20 cm of clayey soil), using TELOSB motes (Crossbow 2013) for underground sensor/relay nodes, with the relay nodes deployed at 0 cm depth and sensor nodes distributed in different orientations throughout the applicable depth range.	Even though the paradigm of using relay nodes presented in this work is novel, in effect the communication between the underground nodes is effected by means of the relay nodes deployed close to the ground, thus eliminating UG2UG communication and restricting the scope to UG2AG communication.

5.2.1 Commentary

The review of the cross-section of WUSN applications in irrigation control presented under Table 5.1, clearly demonstrates that practically UG2UG communication has never been experimented with so far in almost all of the applications considered. A unique exception to this generality has been the work reported in (Huang et al. 2008). As mentioned during the course of the review, the claimed results of this report have neither been substantiated by means of experimental data (plots), nor has there been any further related report carrying the work forward. These observations matter considering the fact that the UG2UG communication reported in (Huang et al. 2008) has been based on EM waves, the non-feasibility of which for UG2UG communication has been highlighted in many related studies of late, which have been discussed previously under Chapter 3. One among such reports, (da Silva et al. 2014), was also referenced in this chapter to drive home this aspect. The same report also pointed to the lack of specific implementation guidelines when it comes to MI communication for WUSNs.

In the previous chapter, the author had critically examined the ongoing theoretical research output on MI communication for WUSNs, and concluded based on such evaluation that for innovatively circumventing key theoretical issues, alternate complementary solution approaches rooted in *analogical thinking* (Gassmann & Zeschky 2008) should be explored. In the view of the author, such novel approaches could also generate valuable pointers in terms of practical guidelines, the lack of which has been pointed out in (da Silva et al. 2014). As a case in point, one such novel workaround presented under Chapter 8 of this thesis can be viewed as a pointer to a possible future practical guideline.

Before closing this chapter, the author would also like to point out that the review presented under Table 5.1, and the relevant observations from (da Silva et al. 2014), corroborate the earlier observation that theoretical research alone is not adequate for enabling the full-fledged application of WUSNs. Thus it should be worthwhile to explore alternate solution approaches based on analogical thinking to complement the theoretical understanding, and circumvent key theoretical issues.

5.3 Chapter Summary

In this chapter the author briefly reviewed the cross-section of applications of WUSNs in irrigation control, with the purpose of demonstrating how UG2UG communication has never been a preoccupation in all the contexts. The author also attributed such lack of preoccupation, to the difficulties posed by the underground environment for both EM wave and MI communication (in terms of theoretical impediments). The review also helped to corroborate the view outlined under the previous chapter, pertaining to theoretical research on MI communication for WUSNs. The view emphasized on how theoretical research may not be adequate in finding solutions to key communication and deployment issues; an alternate solution approach rooted in analogical thinking is required to explore novel workarounds.

In the next chapter, the author would discuss the concept of analogical thinking, and show how it has always been the mainstay of contemporary scientific and technological thought mechanism, and reason why it should find application in MI communication for WUSNs as well.

Chapter 6

Analogical Thinking

This chapter bridges the different thought patterns presented under the Review and the Research parts of this dissertation. The key purpose of this chapter is to drive home the extent to which analogical thinking has percolated the solution approaches in modern science and engineering. In order to do justice to such a vast and ever growing topic within the small confines of this chapter, the author has adopted a slightly different method for documenting the contents of this chapter, so as to ensure as much of the entire gamut of this fascinating topic as possible has been addressed, with its myriad strikingly innovative examples. Instead of delving deeper into the specifics of each innovation model, the author has provided a surface overview of the particular innovation covered by the reference under consideration, and would expect the reader to go to the particular reference for details. The reason for bringing in as many examples of analogical thinking from science and technology, has also been to demonstrate how the notion of analogical thinking, and its manifold manifestations have become the life force of modern scientific thinking and creativity; and reason why such thinking and consequent innovation should immensely benefit the research area of MI based WUSNs as well.

6.1 Upon the Relevance of this Chapter

Analogical thinking as a method for devising novel solution approaches has been at the very core of some of the key scientific and technological innovations across domains, in both previous and contemporary research. In addition, the approach has also been strongly recommended in scientific literature. This chapter presents a discussion on the above role played by analogical thinking in both science and technology. The author intends this discussion to set the stage for the paradigm shift in the thinking on MI communication for WUSNs, evinced in terms of the novel workarounds and ideas presented under Chapter 8. It is also the intended objective of the discussion to demonstrate how analogical thinking has proven to be effective, in the context of diverse research and technological endeavours. Hence the author believes that the positioning of this discussion as a separate chapter linking the two parts of this dissertation, presenting two different patterns of thought process, is more appropriate to the flow. This is also the reason this discussion has not been relegated to an appendix. It is the author's view that the reader of this dissertation would benefit from the familiarity gained, about the analogical thinking concepts and innovations presented under this chapter, in forming a better appreciation of the novelty of the workarounds and ideas presented under Chapter 8. Hence, the reader keen to follow the evolution of thought in this dissertation should read this chapter, before proceeding to the discussion in the next part. This logic also justifies the author's decision about the position of this chapter in the general flow of the dissertation.

6.2 Chapter Overview

The author has been referring to (Gassmann & Zeschky 2008) throughout the course of this dissertation thus far, as the technical definition of analogical thinking more congenial to the scope and dimension of the stated objectives of this research. However, that is just one of the myriad facets of the concept of analogical thinking in general. The author would cover (in more detail) the nature and scope of analogical thinking as outlined in (Gassmann & Zeschky 2008), during the course of this review. But the author would also like to provide glimpses of the other innovative manifestations of analogical thinking, which abound in the mainstream literature of scientific and engineering research.

In order to bring in a semblance of distinct order in judiciously covering the variant of analogical thinking discussed in (Gassmann & Zeschky 2008), and other specimens dealt with in other research outputs, the author has taken recourse to the method of addressing the more generic analysis or examples of analogical thinking first under each relevant section, followed by a more detailed discussion of the analysis or examples mentioned in (Gassmann & Zeschky 2008). The author has concluded this chapter with a very terse section on the import and implications of analogical thinking for MI based WUSNs.
For the sake of clarity, the author has classified the ensuing discussion under two distinct sections. Under the first section, the author has presented a theoretical analysis of analogical thinking based on relevant research output. This is aimed as an exercise in understanding what possibilities are offered by the application of the faculty of analogical thinking to any scientific or technological problem, and what could be the associated challenges and limitations. Besides, the theoretical analysis also serves as a touchstone for better evaluating and appreciating the practical examples of analogical thinking drawn from variegated disciplines of science and engineering (technology), presented under the subsequent section.

6.3 Analysis of Analogical Thinking

The author would like to begin with the seminal essay (Hadamard 1954) by Jacques Hadamard, which is replete with vivid examples of how analogy often functions as the cornerstone to inventive thinking. For the purpose of elucidating the role played by logic and chance in innovation, Hadamard invents the analogy of the *hunting cartridge* based on Poincaré's *comparison of projected atoms*, and aptly quotes Souriau, "In order to invent, one must think aside". This quotation has been further explained by means of additional statements, "... in mathematics and in experimental sciences ...... too stubbornly following an idea once conceived may lead to errors ... in both domains, the mathematical and the experimental, the fact of not sufficiently "thinking aside" is a most ordinary cause of failure i.e., the lack of success in finding a solution ..." The examples involving notable discoveries (including those of Hadamard himself) illustrate what Hadamard observes as "paradoxical" failures, "... viz., the failure of a research scholar to perceive an important immediate consequence of his own conclusions." Further, Hadamard reasons based on the examples, "Such instances show us that, in research, it may be detrimental to scatter our attention too much, while overstraining it too strongly in one particular direction may also be harmful to discovery...... We must notice, in that direction, that it is important for him who wants to discover not to confine himself to one chapter of science, but to keep in touch with various others." Hadamard also dwells at length on how the very nature of innovative thinking itself is analogical in its elements, and produces several examples to corroborate this notion. He cites the studies conducted by Alfred Binet on the remarkable ability of some chess players to play multiple simultaneous games without seeing the chess boards, and observes, "their results may be summed up by saying that for many of these players, each game has, so to say, a kind of physiognomy, which allows him to think of it as a unique thing, however complicated it may be; just as we see the face of a man. Now, such a phenomenon necessarily occurs in invention of any kind." Hadamard goes on to demonstrate this phenomenon using both instances of his own personal inventive thinking and those of other mathematicians, and men of science and art. To reproduce certain excerpts (starting with Hadamard's own thought process),

" We have, for instance, to prove that there is a prime greater than 11.

STEPS IN THE PROOF	MY MENTAL PICTURES
I consider all primes from 2 to 11, say 2, 3, 5, 7, 11.	I see a confused mass.
I form their product	N being a rather large number,
2X3X5X7X11 = N	I imagine a point rather remote
	from the confused mass.
...	...

"

"About the mathematicians born or resident in America, whom I asked, phenomena are mostly analogous to those which I have noticed in my own case. Practically all of them ... avoid not only the use of mental words but also, just as I do, the mental use of algebraic or any other precise signs ; also as in my case, they use vague images ...... The mental pictures of the mathematicians ... are most frequently visual, but they may also be of another kind for instance, kinetic. There can also be auditive ones, but even these, ... quite generally keep their vague character."

"We can say as much of the observations which Ribot has gathered by questioning mathematicians. Some of them have told him that they think in a purely algebraic way, with the help of signs ; others always need a "figurated representation," a "construction," even if this is "considered as pure fiction.""

"An instance quite analogous to our above description is that of the economist Sidgwick, ... His reasonings on economic questions were almost always accompanied by images, and "the images were often curiously arbitrary and sometimes almost undecipherably symbolic." "

"Also a most curious process occurs among musical composers, ... Several of them see their creations in their initial conception, in a visual form ... One of them perceives in that way, without any precise musical presentation, "the main line and main characteristics of his music...""

"Some scientists have told me of mental pictures quite analogous to those which we have described. For instance, Professor Claude Levi-Strauss, when thinking about a difficult question in his ethnographic studies, sees, as I do, unprecise and schematic pictures which, moreover, have the remarkable character of being three-dimensional. Also, asking a few chemists, all of them reported absolutely wordless thought, with the help of mental pictures."

Hadamard reproduces the related personal view of Albert Einstein in this regard, "The words or the language, as they are written or spoken, do not seem to play any role in my mechanism of thought. The psychical entities which seem to serve as elements in thought are certain signs and more or less clear images which can be "voluntarily" reproduced and combined. There is, of course, a certain connection between those elements and relevant logical concepts. It is also clear that the desire to arrive finally at logically connected concepts is the emotional basis of this rather vague play with the above mentioned elements."

Based on such striking examples of analogy intertwined with the very innovative thinking process, Hadamard presents certain interesting observations:

"It has been written that the shortest and best way between two truths of the real domain often passes through the imaginary one."

"We must add, however, that, conversely, application is useful and eventually essential to theory by the very fact that it opens new questions for the latter. One could say that application's constant relation to theory is the same as that of the leaf to the tree: one supports the other, but the former feeds the latter. Not to mention several important physical examples, the first mathematical foundation in Greek science, geometry, was suggested by practical necessity, as can be seen by its very name, which means "land-measuring.""

Certain interesting observations on analogical thinking also stem from the related research in cognitive psychology. In (Gick & Holyoak 1980), the authors align experiments designed to evaluate the analogical thinking capabilities of participants to the following guidelines (relevant excerpts from the cited work have been reproduced wherever convenient):

- "... fruitful analogies may be based on a mapping of relations between two very disparate domains."
- "... "semantic distance" between analogous domains can vary a great deal."
- "... anecdotal reports of the use of analogies typically involve problems that are much less well defined."
- For an "ill-defined" problem for which the desired goal is specified only at a relatively abstract level and the permissible operations are left open-ended, analogy from a remote domain might trigger a creative insight.
- "Indeed, there appear to be close ties between the concept of analogy and the concept of "schema," which has been widely applied in discussions of prose comprehension. In essence, both an analogy and a schema consist of an organized system of relations."
- "A system of representation for analogy must be able to describe a fundamental property of such relational systems, namely, that analogy may be defined at multiple levels of abstraction."
- "Similarly, we assume there is an optimal level of abstraction at which analogical relations may be represented in order to effectively guide the solution process. Indeed, an important empirical issue is to determine what factors influence this optimal level of abstraction."
- "It is probably the case that analogies used to guide problem solving are generally incomplete in some respects..."
- "... for use in solving a problem the optimal level of abstraction for representing an analogy may be that which maximizes the degree of correspondence between the two relational systems. In many cases a very detailed representation will include disanalogous relations, while a very abstract representation will omit information about important correspondences."

Several conclusions pertinent to the application of analogical thinking in any domain have been drawn in (Gick & Holyoak 1980), based on the experiment results:

- "... a solution to a problem can be developed by using an analogous problem from a very different domain."
- "Our results substantiate anecdotal descriptions of the role that analogical thinking may play in creative problem solving,..."
- "It is clear that our understanding of the use of analogies in problem solving remains severely limited in many important respects."
- "... we need to learn more about the ways in which the use of analogies may interact with other strategies (e.g., means-ends analysis) used in problem solving."
- "A potential analogy may often be encoded in a very different context from that in which the target problem appears. Indeed, the basic problem in using an analogy between remote domains is to connect two bodies of information from disparate semantic contexts. More generally, successful transfer of learning generally involves overcoming contextual barriers."
- "It may be possible to use a representation of the current problem as a retrieval cue for accessing analogous problems."
- "Theories in each domain must explain how abstract structures can be derived from a set of instances, and how instances can be related to each other and to abstract structures."
- "... an analogy may often serve as a model to guide the development of a new theory."

6.3.1 Analysis by Gassmann and Zeschky

(Gassmann & Zeschky 2008) study the notion of analogical thinking relevant to product innovation, which is more aligned with the applicability of analogical thinking to WUSNs as envisaged by this research. (Gassmann & Zeschky 2008) analyse the various aspects and agents of analogical thinking based on previous research output, and the author summarises below some of their key observations (the author finds it convenient to quote from the text directly as and when):

- "On the one hand, drawing analogies from an initial problem to distant but similar problem settings may reduce uncertainty as potential solutions have already proved to function in a similar context. On the other hand, non-obvious analogies may entail highly novel solutions because the combination of more distant pieces of knowledge is associated with higher innovative potential ... In fact, 'divergence and lack of shared experiences are critical for developing new ideas'..."
- "Analogical thinking is a creative method for a problem that needs a solution. Analogical thinking happens when a familiar problem is used to solve a novel problem of the same type ..."
- "Analogies can be drawn in different settings and directions. In some cases, a solution is found in one industry and applied to solve a problem in another industry. In other instances, the analogy is drawn from a solution looking for a problem ... In all cases, the search for a solution is stimulated by a rather specific problem. Within this 'problemistic search'... analogies to settings quite similar to the original problem can be drawn, potentially providing a solution."
- "Cognitive scientists commonly agree that innovation entails reassembling elements from existing knowledge bases in a novel fashion ... Thus, analogical thinking is a mechanism underlying creative tasks, in which people transfer information from a familiar setting and use it for the development of ideas in a new setting ... Similarity of concepts (such as problems or situations) at any level of abstraction is argued to enable analogical thinking ... Thus, similarity of some basic elements between the source where the problem originates (i.e., the problem source) and the source where the analogy is found (i.e., the solution source) is a vital pre- condition for analogies to be identified. Similarity has also been described in a continuum from 'near' or 'surface' analogies to 'far' or 'structural' analogies ... Near analogies are more easily identified than far analogies, as near analogies often entail obvious surface similarities such as similar design, while far analogies typically entail similarities in the structural relationships between source and target attributes. For instance,... the case of designing a new freeway system. A near analogy would entail looking at

an already existing freeway system in another city, whereas a far analogy would entail arriving at a solution by considering the human circulatory system. . . . . . The example intuitively shows that far analogies are more difficult to identify and require more cognitive effort. The identification of far analogies requires the identification of similarities in the relational (vs. surface) structure between the problem and the solution source, which is often difficult when surface similarities are completely absent. However, if successfully implemented, far or structural analogies serve as the base for 'mental leaps' and can lead to radical innovation . . . "

6.4 Analogical Thinking at Work

In this section, the author takes a look at some examples of innovation that are rooted in analogical thinking. It would be opprotune begin with the notion of analogical thinking at work as delineated by Margaret A. Boden within the context of Artificial Intelligence (AI), in her book (Boden 1987). Margaret A. Boden variously observes:

- "In Minsky's terminology of *frames*, one might say that useful analogical thinking involves the comparison of frames, wherein admittedly disparate frames are initially assimilated by virtue of certain points of likeness, and are thereafter scanned for further similarities in terms of which the relatively novel schema may be developed and understood with the help of the more familiar one."
- "For instance, Harvey approached the task of understanding the blood system with a well-developed conception of the water-pump already in his mind. His "hydraulics" frame apparently had terminals some of which matched specific observations of contemporary anatomists, such as that the blood flowed through tubes, spurted out if the tubes were broken, passed through a specially shaped structure connected to the tubes, and so on. . . . . . Observational comparison with the blood system confirmed the analogy at various points. . . . . . Not all the observations prompted by the hydraulic schema found a parallel: Harvey was unable to see the capillaries, since he had no microscope. Undeterred he posited the existence of capillaries, which were observed some years later by Malpighi. This example illustrates two important creative uses of analogy,. . . . . . The first is the use of the familiar frame to prompt inquiry

> at developing the novel (and initially often more sketchy) frame in an economical fashion...... The second creative use of analogy enables one not merely to gather new factual knowledge about the novel phenomenon, but correlatively to *understand* or *explain* it, by relating it to the concepts already accessible in the familiar frame."

In her book (Benyus 1997), the author Janine M Benyus dwells on the topic of "*not ... learn about nature ... but ... learn from nature*" for lasting solutions to harmonious human cohabitation of the earth with other species. During the course of this narrative, Janine M Benyus emphasizes on how human innovation has always been a very crude attempt at mimicking the more subtle and marvellously ingenious natural phenomena:
"When we stare this deeply into nature's eyes, it takes our breath away, and in a good way, it bursts our bubble. We realize that all our inventions have already appeared in nature in a more elegant form and at a lot less cost to the planet. Our most clever architectural struts and architectural beams are already featured in lily pads and bamboo stems. Our central heating and air-conditioning are bested by the termite tower's steady 86 degree F. Our most stealthy radar is hard of hearing compared to the bat's multifrequency transmission. And our new "smart materials" can't hold a candle to the dolphin's skin or the butterfly's proboscis. Even the wheel, which we always took to be a uniquely human creation, has been found in the tiny rotary motor that propels the flagellum of the world's most ancient bacteria."
Janine M Benyus goes a step beyond and insinuates that what has been accomplished by the humankind by means of such mimicry forms just the tip of the iceberg:
"Humbling also are the hordes of organisms casually performing feats we can only dream about. Bioluminescent algae splash chemicals together to light their body lanterns. Arctic fish and frogs freeze solid and then spring to life, having protected their organs from ice damage. Black bears hibernate all winter without poisoning themselves on their urea, while their polar cousins stay active, with a coat of transparent hollow hairs covering their skins like the panes of a greenhouse. Chameleons and cuttlefish hide without moving, changing the pattern of their skin to instantly blend with their surroundings. Bees, turtles, and birds navigate without maps, while whales and penguins dive without scuba gear. How do they do it? How do dragonflies outmaneuver our best helicopters? How do hummingbirds cross the Gulf of Mexico on less than one tenth of an ounce of fuel? How do ants carry the equivalent of hundreds of pounds in a dead heat through the jungle?

These individual achievements pale, however, when we consider the intricate interleaving that characterizes whole systems, communities like tidal marshes and saguaro forests. In ensemble, living things maintain a dynamic stability, like dancers in an arabesque, continually juggling resources without waste."

It is therefore not a coincidence at all that *biomimetics* has emerged as the next frontier in science and technology, which explores nature for analogous solutions to certain complex problems concerning human life. A very detailed survey of the rich possibilities presented by this branch of study can be found in (Bar-Cohen 2006). As the author of (Bhushan 2009) observes:

"Molecular-scale devices, superhydrophobicity, self-cleaning, drag reduction in fluid flow, energy conversion and conservation, high adhesion, reversible adhesion, aerodynamic lift, materials and fibres with high mechanical strength, biological self-assembly, antireflection, structural coloration, thermal insulation, self-healing and sensory-aid mechanisms are some of the examples found in nature that are of commercial interest."

The interested reader is also directed to (von Gleich, Pade, Petschow & Pissarskoi 2010) for a more detailed review of biomimetics and its recent advances.

On a different note, the notion of *fractals* (Mandelbrot 1983) was inspired by the rather arbitrary shapes found in nature that are beyond the scope of Euclidean geometry. As Benoit B. Mandelbrot observes in his work (Mandelbrot 1983):

"More generally, I claim that many patterns of Nature are so irregular and fragmented, that, compared with *Euclid*–a term used in this work to denote all of standard geometry–Nature exhibits not simply a higher degree but an altogether different level of complexity... The existence of these patterns challenges us to study those forms that Euclid leaves aside as being "formless", to investigate the morphology of the "amorphous" ... Responding to this challenge, I conceived and developed a new geometry of nature and implemented its use in a number of diverse fields. It describes many of the irregular and fragmented patterns around us, and leads to full-fledged theories, by identifying a family of shapes I call *fractals*."

Quite evidently, this is an example of analogical thinking at work in the reverse *direction compared to biomimetics;* for the solution space of fractals has been inspired by the complexity of natural shapes, whereas biomimetics looks to nature for solutions to complex problems.

6.4.1 The Gassmann and Zeschky Model

(Gassmann & Zeschky 2008) use case studies from firms in four different domains, to drive home the power and efficacy of analogical thinking in finding innovative solutions to unique problems. In all of these case studies, there is an underlying pattern of how for a unique problem in one domain, an innovative solution could be adapted from another *distant* domain. The following is a summary of the case studies outlined in (Gassmann & Zeschky 2008):

Case Study 1 AlpineCo: (Gassmann & Zeschky 2008) describe how AlpineCo could find the solution to the unique problem of damping the vibrations in skis at high velocities, by adapting an analogical solution in acoustics for filtering undesirable frequencies of bowed instruments. In this context, (Gassmann & Zeschky 2008) observe:

"From his background as a mechanical engineer, the head of R&D knew that vibrations were a recurring problem in settings such as machine or building construction. With the terms 'vibration', 'damping' and 'cushioning' unconsciously in mind, the team then decided to search for industries and applications where damping or elimination of vibrations were a problem ...... The search was only successful when one team member proposed to limit the search scope to include only frequencies above 1800 Hz, as this was the range of frequency found in the vibrating ski. This frequency is typically found in acoustics, and AlpineCo ultimately found a viable solution at an inventor who had for years researched on the elimination of undesirable frequencies of bowed instruments...... This technology is termed 'frequency tuning' and is today found in virtually every ski."

Case Study 2 AluCo: (Gassmann & Zeschky 2008) explain how AluCo could enable a paradigm shift in their design approach to crash management system (CMS), by resorting to analogical thinking. To quote (Gassmann & Zeschky 2008) within this context:

"For a long time, AluCo had been looking for alternative approaches to improve its crash management system (CMS)...... Somewhat frustrated with the hitherto 'conventional' approach, AluCo management realized that mere optimization of materials and tweaking geometric designs would not result in the major advancement that they hoped for ...... Before ‘prematurely jumping to solutions’..., a team of four R&D employees engaged in an in-depth investigation of the current crash-box ...... In the course of the analysis, AluCo developed key terms such as ‘energy absorption’ and ‘transformation of kinetic energy’. With these terms in mind, AluCo were able to build associations with different kinds of technologies, applications and industries where the absorption of energy was crucial. AluCo's R&D then started to search the internet with the focus on the previously developed key terms. In this way, they identified several promising technologies new to their industry, which today are subject for further development.”

Case Study 3 TextileCo: (Gassmann & Zeschky 2008) mention the lack of synchrony between material displacement and the speed of the sewing foot in TextileCo's sewing machine, “which resulted in inhomogeneous stitch lengths and spaces”, and how the company found a very simple yet highly effective analogical solution in the mechanics of the optical sensor of a computer mouse. To reproduce the relevant extract from (Gassmann & Zeschky 2008):

“TextileCo faced the problem that the speed of the material displacement was different from the speed of the sewing foot, which resulted in inhomogeneous stitch lengths and spaces ...... TextileCo's R&D concluded that the displacement of the material had to be gauged with high precision because of the high speed of the sewing foot ...... As gauging was outside their competence, TextileCo agreed to looking for external solutions ...... They approached an external technology service provider, who ultimately provided TextileCo with the optical sensor of a conventional computer mouse as a solution. As a result, because of the automation, even beginners are now able to quilt genuine artwork of high quality ......”

Case Study 4 PipesCo: (Gassmann & Zeschky 2008) share the fascinating episode of PipesCo, in which the serendipity of an employee rooted in analogical thinking revolutionized the company’s product line. The relevant excerpt of the story outlined in (Gassmann & Zeschky 2008) is as follows:

“The piping division of PipesCo has deep know-how in production techniques such as welding or gluing in combination with material optimization for the joining of pipes ...... One day an R&D employee was watering the flowers in his garden, when he realized that the hose and the sprinkler head were connected via a clicking system:

> 'It was a lucky accident. The basic principle is the same, it's about a medium flowing through a pipe, only the way the pipes are connected is different'. . . He introduced the idea into the company, and preliminary assessments convinced the chief technological officer (CTO) to pursue the idea, both because of the simplicity of the technology which would tremendously facilitate the joining of large pipes in construction, and because of the enormous cost savings involved with the new technology . . . . . . Today, the clicking technology has prevailed and led to significant competitive advantage for PipesCo."

Based on the above case studies, (Gassmann & Zeschky 2008) draw the following fundamental inferences which are instrumental to the effective application of analogical thinking for an innovative solution to a unique problem:

- ". . . the will to break with conventional boundaries is paramount when searching for solutions that are non-obvious and highly novel . . . "
- On knowledge reuse in relation to analogical thinking:
  ". . . the reusers in the more innovative cases needed to be aware of and open to non-traditional approaches that might lead to greater levels of innovation . . . . . . as analogous solutions typically originate outside known environments, an open attitude is pivotal for analogical thinking to be successful . . . "
- On analogical solution approaches where the problem and the solution source share either surface or structural similarities:
  ". . . also surface similarities can result in innovations of higher novelty . . . . When looking at structural analogies, the quality of the information might be more tacit in contrast to superficial similarities where the information is more explicit . . . . . . by abstracting the original problem to its structural relationships, the space for potential solutions is opened up . . . and the use of cognitive abilities is enabled or facilitated . . . . . . In this regard, 'problems can be defined very concretely or abstractly, with the former leading to less novelty . . . ' . . . "
- ". . . analogies entail limited risks while simultaneously having great impact in terms of radical innovations . . . "

- "...analogical thinking does not happen merely by accident but is supported by means of a systematic approach ..."

6.4.2 Further Examples

The scope of analogical thinking, the extent of its applicability in both science and technology, and its potential to enable novel solutions to unique problems, are indeed vast. In addition to the examples that the author discussed under the previous subsections, the reader can also refer to (Gordon 1961), (Vosniadou & Ortony 1989), (Holyoak 1996), and (Boden 2004) for further examples of analogical thinking. A very stimulating discussion on the influence of analogical thinking in major scientific discoveries can be found under *Chapter 8 The Analogical Scientist* of (Holyoak 1996).

6.5 Commentary

In the previous sections, the author presented both a theoretical analysis of the genesis of analogical thinking and its virtually unlimited creative calibre founded on mapping symbols, structures and concepts from both *near* and *distant* domains to devise highly novel solutions to specific problems, and showed how such faculty of analogical thinking has been practically the mainstay of the development of science and technology over the centuries, and continues to be so. This is further testament to Hadamard's characterization of seminal thinking itself as analogical in nature (Hadamard 1954). Moreover, the analysis of analogical thinking also emphasized on how resorting to analogical thinking, and its application to particular theoretical problems, can result in improvement of the theory itself. These are valuable takeaways that can be of immense advantage even in the solution space of WUSNs. In order to demonstrate this precept, the author would present novel solution approaches based on analogical thinking under the next part of the dissertation, as workarounds to certain theoretical snags inherent to the MI waveguide model (Sun & Akyildiz 2010*c*) (reviewed at length under Chapter 4). The author would also demonstrate by means of simulation results how the proposed workarounds provide instant and effective resolutions to these theoretical snags. In addition, the author would also describe a novel power harvesting and distribution model for WUSNs based on analogical thinking, which is aimed at perpetually self-sustained WUSN operation post-deployment. The model would also incorporate certain novel communication concepts based on analogical thinking for MI based WUSNs.

6.6 Chapter Summary

This chapter presented a very concise yet adequate review of the concept of analogical thinking, with the objective of marking a paradigm shift in the solution approach to MI based WUSNs, covered under the two parts of this dissertation. While the literature review covered under chapters 3-5 stressed on theoretical models and corresponding application bounds for MI based WUSNs, the discussion presented in the next part under chapter 8 would demonstrate how analogical thinking can be used to circumvent some of the key theoretical impediments. Thus the relevance of the discussion presented under this chapter as the *link* between the two parts of this dissertation, should be evident according to the author.

The author also brought to the fore by means of literature review, the undeniable impact analogical thinking has had, and continues to have, in scientific and technological advancement. The review provided glimpses of the enormous possibilities presented by analogical thinking in radically altering science and technology, and how the scientific community is constantly making use of this faculty and associated techniques to push back the frontiers. The purpose of the review was to highlight how analogical thinking can be similarly employed in circumventing key theoretical bottlenecks in MI based WUSNs, by means of novel solutions or workarounds. The author would use the next part of this dissertation in demonstrating examples of such workarounds.

Part II

Research Output

Chapter 7

Preliminary Investigations

7.1 Chapter Overview

In this chapter, the author would detail the preliminary investigations conducted in the form of simulations, to study the feasibility of the applying the relevant theoretical models on MI waveguide communication for the chosen application context. A detailed review of the theoretical research on MI waveguide for WUSNs was presented under Chapter 4.
The data elements of the application prototype upon which the simulations presented under this chapter have been based, have been derived from a large commercial pecan farm located in northern New South Wales, Australia (*vide* Fig. 7.1).

Figure 7.1: Aerial view of a section of the pecan farm

These data elements comprise of the following:

1. the arable land area of the farm, which has been used in simulation 3.
2. the unique requirements pertaining to pecan farming (Andersen & Crocker 2015), and the consequent planting pattern adopted in the farm (Plantation 2002), which have been considered for all simulations.
3. the underground terrain aspects of the farm, which have been used in simulation 3.
4. the soil covariance pattern of the farm, which has been used in simulation 3.

The validations carried out under simulation 1 and 2 apply the MI waveguide theoretical model (Sun & Akyildiz 2010*c*) to the data model constructed using the above elements. Simulation 3 has focused on prototyping the farm underground terrain characteristics for the topsoil region and the soil covariance across the arable land area, using a novel composite numerical model. The corresponding validation has been used to ascertain the combined impact on the MI waveguide theoretical model.
In simulation2, the Active Reader Passive Tag (ARPT) Radio-frequency identification (RFID) scheme has been validated using the MI waveguide theoretical model, for the chosen application context. The motivation for pursuing this direction had been the

prospect of figuring out whether ARPT RFID could be used as a means to achieve better power efficiency and consequently longevity of the deployed nodes.

Since the results obtained from the simulations largely pertain to the MI waveguide theoretical model, a direct correlation to the application context may not be immediately evident to the reader. Hence the author has supplemented each simulation result with suitable technical commentaries, in order to highlight its relevance to the chosen application context.

The simulations and their corresponding results presented under this chapter were instrumental in advising the author to explore alternate solution approaches rooted in *analogical thinking* (Gassmann & Zeschky 2008), presented under the next chapter. The insights gained from the simulations presented under this chapter are crucial in this regard as well, apart from validating the MI waveguide theoretical model. Hence the author would like to request the reader to maintain both these relevant perspectives, during the course of the ensuing discussion.

All of the simulation results presented in this chapter had been showcased in a major international conference on sensing technology. The corresponding references have been highlighted under the list of publications at the start of this dissertation, and would be recalled again within the appropriate contexts.

The entire source code related to all the simulations presented under this chapter have been reproduced for reference under Appendix A.

7.2 Simulation 1: MI Waveguide Performance Modelling

7.2.1 Related Publication

The simulations and results discussed under this section have been published in (Parameswaran, Zhou & Zhang 2012). The data and other relevant material from the same publication have been reused in the following discussion.

7.2.2 Description

The simulations presented under this section pertain to ascertaining the feasibility of the MI waveguide theoretical model (Sun & Akyildiz 2010*c*) and deployment algorithms (Sun & Akyildiz 2010*b*) for the chosen application context. The notion of a random topology familiarized in (Sun & Akyildiz 2010*b*) has been adopted for the simulation, since only specific sections of the farm underground needed to be monitored for soil moisture levels. The relevant equations presented in (Sun & Akyildiz 2010*c*) and (Sun & Akyildiz 2010*b*) have been reused in the source code.

7.2.3 Simulation Specific Data

The parameters and corresponding values used in the simulation, based on the data provided in (Sun & Akyildiz 2010*c*) and (Sun & Akyildiz 2010*b*) have been reproduced under Table 7.1. The parameters which would take on variable values in the simulation have been indicated using β. Of the variables, the three main parameters are the link distance (d), the transmission power (P_t) and the minimum power of the received signal (P_{th}). The remaining variables take on values determined by the values of the three main variables. The values for the rest of the parameters have been listed as constant values. The assumption in (Sun & Akyildiz 2010*c*) that all the coils have the same parameters (resistance, self and mutual induction), has been adopted for the simulation. The equations used in the simulation have been presented under Table 7.2. The equations have been borrowed from (Sun & Akyildiz 2010*c*) and (Sun & Akyildiz 2010*b*). A range of values was assigned to the three main variables d, P_t and P_{th} as part of the simulation. These values have been listed in Table 7.3. These values were adopted to enable a minimal configuration of the MI waveguide theoretical model, with a relay distance of < 130 m. Since the purpose of the simulation was a feasibility study for the chosen application context, this configuration was deemed sufficient.

Parameter	**Value**
Angular frequency of the transmitted signal (ω)	10 MHz
Required Bandwidth (B)	1 KHz
Transmission power (P_t)	β
Minimum received power for correct signal demodulation (P_{th})	β
Self-impedance of each coil (Z)	β
Mutual induction between adjacent coils (M)	β
Number of turns of each coil (N)	20
Radius of each coil (a)	0.15 m
Wire resistance of unit length of coil (copper wire with 1.45 mm diameter) (R)	0.01 Ω/m
Permeability of soil medium (μ)	$\mu = 4\pi \times 10^{-7}$ H/m
Link distance (d)	β
Optimum number of coils (n_{opt})	β
Relay interval (r)	β

Table 7.1: Parameters for Simulation 1

7.2.4 Simulation Results

The results obtained for the simulation conducted using the MI waveguide theoretical model (Sun & Akyildiz 2010*c*) have been presented under this subsection. For the sake of the simulation, a standard configuration was also considered, wherein fixed values were assigned to P_t and P_{th} and only the value of d was varied. The value of P_t was fixed as 10 dBm and that of P_{th} as −80 dBm.

Figure 7.2 shows the values for the optimum number of coils (n_{opt}) for the standard configuration, with varied values for d as listed under Table 7.3. Figure 7.3 shows the simulation results with varied values for d and P_t as listed under Table 7.3. The value of P_{th} was fixed at the value of −80 dBm for this simulation. Figure 7.4 shows the simulation results with varied values for d and P_{th} as listed under Table 7.3. In this case, the value of P_t was fixed at 10 dBm.

Equation	**Description**
$L_{MI}(d,n,\omega) = 6.02 + 20\lg\zeta(\frac{R}{\omega M}, n)$ $\frac{R}{\omega M} = 4\frac{R}{\omega N \mu\pi} \cdot (\frac{r}{a})^3$	The path loss of the MI waveguide system (L_{MI}) as a monotonically increasing function of $\frac{R}{\omega M}$. Note that R = Z, when $\omega = \omega_0$.
$M \approx \frac{\mu\pi N^2 a^4}{4(\frac{d}{n})^3}$	Approximation for the mutual inductance between adjacent coils.
$n_{opt}(d,B) = argmin_n\{P_t - L_{MI}(d,n,\omega_0 + 0.5dB) \geq P_{th}\}$	Optimum number of relay coils for covering a link distance d, to ensure a minimum received power. In the equation, the transmission signal frequency ω is assumed to deviate from the central signal frequency ω_0 by 50% of the required bandwidth B.

Table 7.2: Equations used in Simulation 1

Parameter	**Range**
Link distance (d)	100 – 125 meters
Transmission Power (P_t)	9 – 10 dBm
Minimum power of the received signal (P_{th})	−30 to −80 dBm

Table 7.3: Range of Parameter Values for Simulation 1

7.2.4.1 Commentary

Several valid inferences can be taken away from the simulation results presented under the previous subsection. Contrasting Fig. 7.4 with Fig. 7.3, the impact of the minimum receiver sensitivity threshold on the MI waveguide theoretical model is evident. Even for

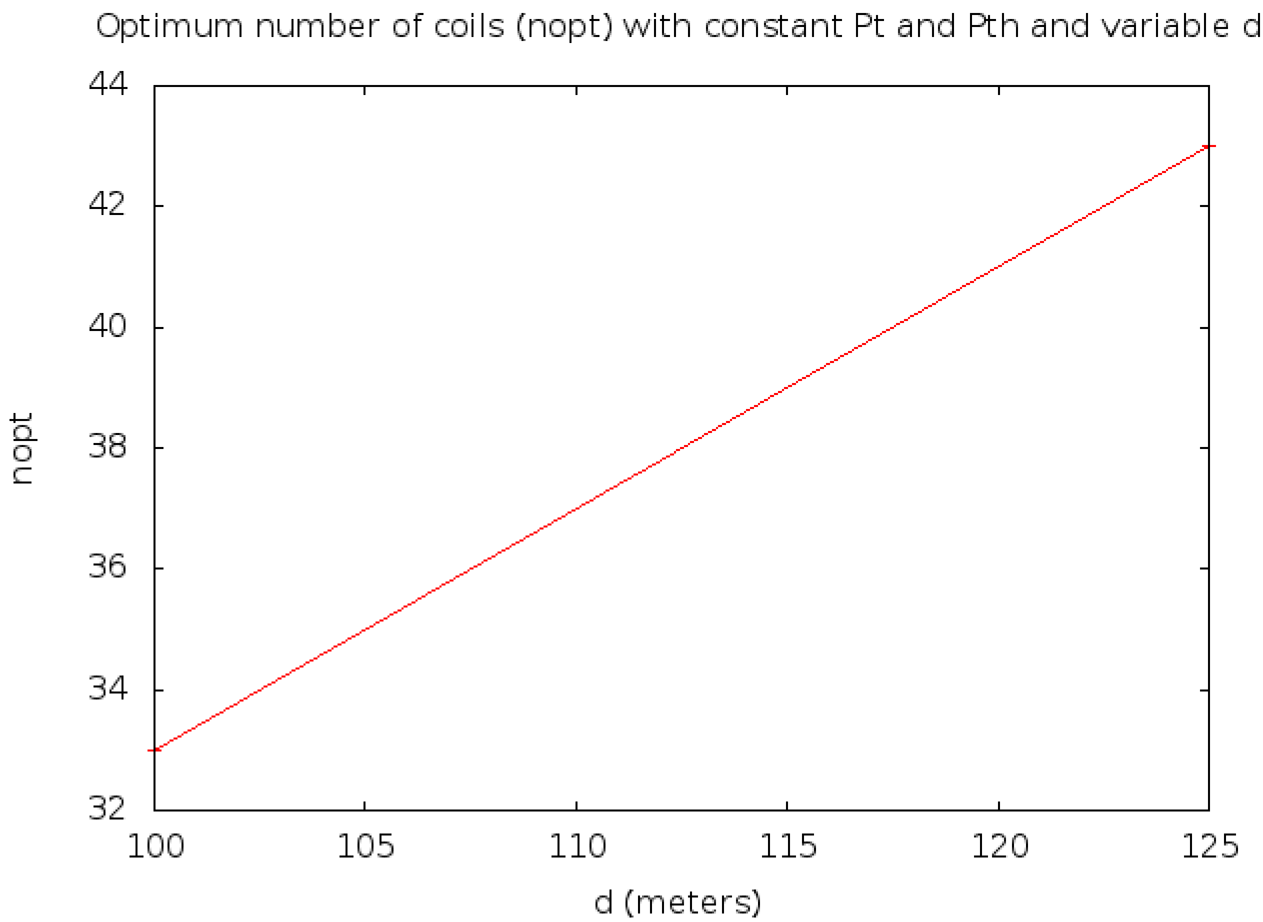

Figure 7.2: Simulation results for standard configuration

the minimal relay distance considered, and assuming constant mutual inductance between adjacent relay coils (which is a technical improbability for actual deployment conditions involving terrain variations), the difference in the number of relay coils is significant.

NOTE

The results from this simulation advised the author about further the validating the impact of underground terrain variations and soil covariance on the MI waveguide theoretical model. The corresponding validations have been listed as part of the discussions pertaining to Simulation 3.

Another takeaway from the results is that varying the transmission power by a very marginal value as evinced in Fig. 7.3, does not impact the system performance. This observation in the light of the minimal MI waveguide theoretical model adopted for the

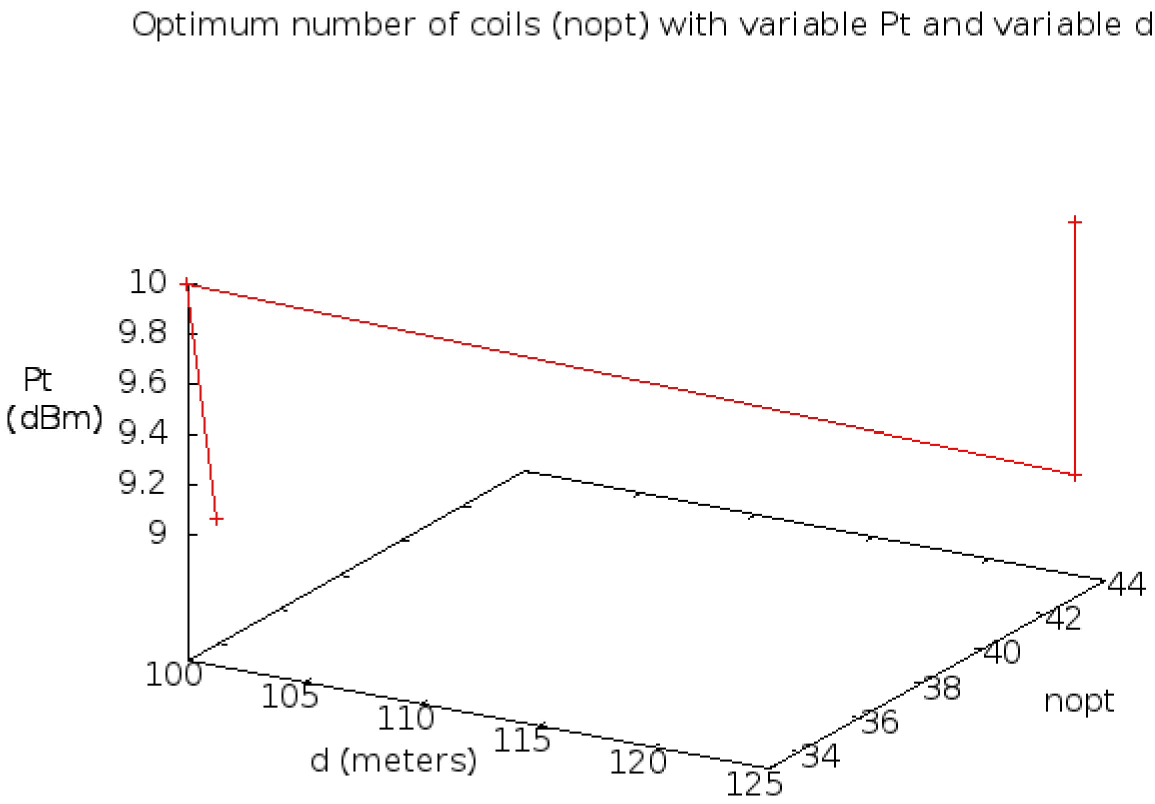

Figure 7.3: Simulation results with variable P_t and d

simulation, is indicative of the fact that taking into consideration the terrain irregularities as well on the field, which prohibit uniform mutual induction between adjacent coils, the transmission power would have to be augmented by a much higher factor for the chosen application context. This observation is also in accordance with a similar point related to power consuption for MI based WUSNs highlighted in (Sojdehei et al. 2001), which had been discussed under Chapter 4.

Even for the minimal MI waveguide theoretical model under consideration, more than 30 coils are required for a theoretically acceptable coverage, assuming uniform mutual induction. So the numbers should be much higher in the absence of such assumption. This could have a telling impact on the cost-efficiency of field deployment. Moreover, as pointed out during the theoretical review under Chapter 4, the effect of soil conductivity (eddy current factor) has not been factored into the equations in (Sun & Akyildiz 2010*c*), which have been the basis of the simulation results presented herein. The eddy current

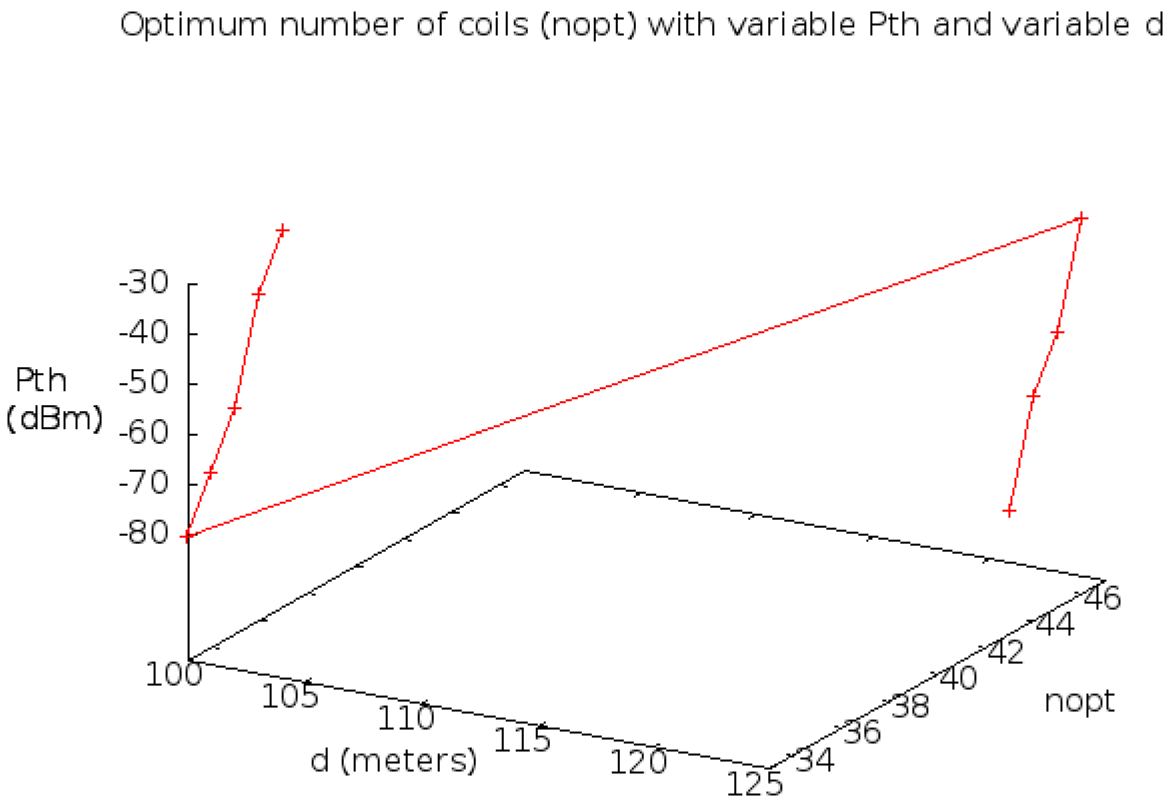

Figure 7.4: Simulation results with variable P_{th} and d

factor can be neglected for the chosen 10 MHz frequency for the minimal model; however, it comes into play for higher frequencies in the VHF or UHF range, as pointed out in (Kisseleff, Gerstacker, Schober, Sun & Akyildiz 2013) reviewed under Chapter 4. So assuming a direct deployment of coils beneath the ground by means of burial within the soil, the impact of the soil conductivity could further drag down the system performance by a few notches.

Regarding the frequency in UHF or VHF range relevant to the chosen application context; during the theoretical review under Chapter 4 the author had pointed to the two basic conditions imposed by the MI waveguide theoretical model, which are counter to each other and restrict the extent to which the system can be tuned to meet specific requirements. Since both the conditions are dependent on the operational frequency, it is not possible to merely transplant the minimal model considered for the above simulations to a UHF frequency range. This sheds light on the fragile balance inherent to the MI waveguide theoretical model, and how all the system parameters are closely dependent on one another. Consequently, results obtained under the unrealistic assumption of uniform mutual inductance may not have any bearing on the actual system performance, once deployed beneath the ground. This observation is a good demonstration of how theoretical models on MI waveguide WUSNs are not directly relevant to deployment on the field. The author had also highlighted this observation during the course of the review of the theoretical research on MI waveguide WUSNs presented under Chapter 4.

Based on the reasoning presented above, the simulation results indicate the infeasibility of the MI waveguide theoretical model proposed in (Sun & Akyildiz 2010*c*) for the chosen application context. The model could only be considered for such a scenario, if the inherent demerits reflected in the simulation results pertaining to coil alignment (uniform mutual inductance, which has been assumed without factual basis), and soil conductivity (which has not been considered, and could further mar the results if had been) could be effectively addressed. The MI waveguide theoretical model itself is very limited in its configuration options as pointed out above, and as such no possible reconfiguration or remodelling could render it more fool-proof to the issues brought to the fore by the simulation results. In other words, the author has hit the theoretical limit by means of this simple simulation.

7.2.5 Source Code

The source code for the simulation results presented under this section can be viewed under Appendix A. The source code has been authored using C programming language and gnuplot (Williams & Kelley 2015) has been used to generate the graphs from the source code.

7.3 Simulation 2: ARPT RFID Solution Model for MI waveguide WUSNs

7.3.1 Related Publication

The simulations and results discussed under this section have been published in (Parameswaran, Zhou & Zhang 2013). The data and other relevant material from the same publication have been reused in the following discussion.

7.3.2 Description

The basis of the simulations presented under this section, were originally mentioned in (Parameswaran et al. 2012). In that work, the notion of a polling mechanism between the participant sink and sensor nodes in UG2UG communication had been hinted at. This simulation also served as a harbinger to the research directions adopted later on, such as terrain modelling, as well as the sustained power generation and delivery model, and other novel workarounds based on *analogical thinking* (Gassmann & Zeschky 2008).
In fact, many instances of analogical thinking can be seen in the model adopted for this simulation. The author would like to start off on this discussion by elaborating on these elements of analogical thinking embedded in the simulation model:

1. The concept of ARPT RFID is analogous to the approach suggested previously in (Hamrita & Hoffacker 2005), with the following amendments:
    - A frequency in the UHF band (868 – 916 MHz) was considered for the model for longer read range (>8 m), based on the results indicated in prior studies (De Vita & Iannaccone 2005), (Mayordomo, Berenguer, Garcia-Alonso, Fernandez & Gutierrez 2009).
    - The notion of averaging over multiple readings was discarded in favour of instantaneous sensing (reading) coincident with polling.
2. In order to enable one-to-many communication, the design concept of a rotating antenna was incorporated for the reader analogous to the model originally devised

in (Barber & III 2000).

3. The aspect of link deviation due to coil misalignment was modelled on the *correlated random walk* algorithm proposed in (McCulloch & Cain 1989) for predicting an organism's rate of spread.

The simulations also laid the groundwork for the terrain modelling simulations undertaken subsequently. The particular aspects of the groundwork have been detailed below. These include several aspects founded on ground data such as:

- any hindrance presented to the line-of-sight coil alignment due to terrain peculiarities
- prediction of characteristic terrain pattern based on analysis of randomly chosen sectors (regions), and the possibility of extracting a uniform model from such random observations
- identification of a suitable range of link deviation (coil angular misalignment) for such uniform model (the chosen range for the simulation attuned to ground conditions falls between 30°– 45°, inclusive)
- approximating the geometric pattern of the terrain with the objective of accommodating the irregularities into a uniform geometric layout; a close polygonal pattern identified is shared in Fig. 7.5; the green dots (bordering dots in black and white) represent pecan trees

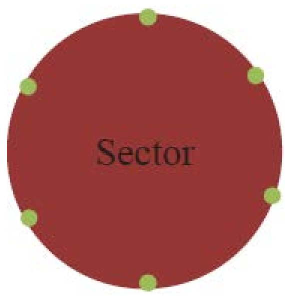

Figure 7.5: Approximate Geometrical representation of a sector

The modelling aspects outlined above were also driven by and instrumental to the following primary simulation objectives:

1. For a chosen range of relay distances for the ARPT RFID model for MI waveguide WUSN, what would approximately be the corresponding optimum number of coils?

2. Taking into account the link deviations effected by the terrain, what is the maximum approximate power efficiency achievable for a relay distance under consideration?

7.3.3 Simulation Specific Data

The algorithms adopted in the model have mainly been drawn from the following publications:

1. The power transfer efficiency between a reader and its set of tags has been approximated using the model derived in (Chen, Chu, Lin & Jou 2010). The model in (Chen et al. 2010) has been based on the model presented in (Kurs, Karalis, Moffatt, Joannopoulos, Fisher & Soljacic 2007).

2. The MI waveguide model and related algorithms proposed in (Sun & Akyildiz 2010*c*) and (Sun & Akyildiz 2013) have been reused.

3. As stated previously, the *correlated random walk* algorithm proposed in (McCulloch & Cain 1989) has been reused for modelling link deviations. However, the aspect of total deviation from the origin considered by the algorithm has been omitted. The author has also not taken into consideration the lateral displacement of the coils in the simulation. This is due to the fact that in the case of a relatively small displacement range (which assumption will be revisited later), the angular displacement tends to be dominant (Fotopoulou & Flynn 2011).

4. Equations and functions provided in (Knight 2013) and (Weaver 2012) have been used for approximation of mutual inductance dependent on chosen coil dimensions.

7.3.3.1 Equations

Table 7.4 lists the majority of equations used in the simulation. The equations and functions reused from (Knight 2013) and (Weaver 2012) have not been included under Table

7.4. The reader is advised to refer to the simulation source code reproduced under Appendix A for their evaluation. A glossary (constructed in logical order) of all the variables (including those used in the simulation source code reproduced under Appendix A) has been provided under Table 7.5.

Equation	Description
$C = \frac{2}{\omega^2 N^2 2\pi a}$	The capacitance loaded in each relay coil of the MI waveguide system (Sun & Akyildiz 2010*c*).
$\Delta = k_{SD}^2 Q_S Q_D$	The coupling regime (for loose coupling) between adjacent coils in the MI waveguide system (Chen et al. 2010).
$k = \frac{\omega k_{SD}}{2}$	The relation between the coupling coefficients adopted from (Chen et al. 2010) and (Kurs et al. 2007).
$k = \frac{\omega M}{2\left[(L_S L_D)^{\frac{1}{2}}\right]}$	Coupling coefficient (tight coupling) adopted from (Kurs et al. 2007).
$X_n = \sum_{i=1}^{n} l_i \cos \alpha_i$ $Y_n = \sum_{i=1}^{n} l_i \sin \alpha_i$ $\alpha_i = \alpha + \sum_{j=1}^{i-1} \theta_j$	The x and y coordinates corresponding to total displacement from the origin, for correlated random walk (McCulloch & Cain 1989). In this simulation, origin for a given link constituted by two adjacent coils is considered to be the position of the first coil. Hence, the value α_i should correspond to the angular displacement θ_j. l_i denotes the straight-line distance between the two coils of a given link (relay distance).

Continued on next page

Table 7.4 – concluded from previous page

Equation	Description
$M_i \cong \mu\pi\frac{a^4}{4ri^3} \cdot (2\sin\theta_{ti}\sin\theta_{ri} + 2\cos\theta_{ti}\cos\theta_{ri})$	Approximation of the mutual inductance between non-axially aligned and fixed adjacent coils (Sun & Akyildiz 2013).
$L_{MI}\left(d_i, n, \omega\right) \cong 6.02 + 20\lg\left[\prod_{i=1}^{n}\frac{R}{\omega M_i}\right]$	Approximation of path loss for a set of given links (n relays) under the mutual inductance condition stated for the previous equation (Sun & Akyildiz 2013).
$n_{opt}\left(d, B\right) = argmin_n\{P_t - L_{M_i}\left(d, n, \omega + 0.5B\right) \geq P_{th}\}$	Optimum number of relay coils for specified bandwidth and minimum receptivity threshold communication between a reader and its set of tags separated by a given relay distance (Sun & Akyildiz 2013).

Table 7.4: Equations used in Simulation 2

Parameter	**Value**
ω	Angular frequency of transmission
ω_0	Resonant frequency
Δ	Coupling regime between adjacent coils (for loose coupling)
S	Source (transmitter coil)
D	Destination (receiver coil)
L$_S$	Inductance of the source
L$_D$	Inductance of the destination
Continued on next page	

Table 7.5 – continued from previous page

Parameter	**Value**
Q_S	Quality factor of the source
Q_D	Quality factor of the destination
k	Coupling coefficient for theoretical tight coupling between source and destination
k_{SD}	Coupling coefficient for loose coupling between source and destination
r_i	Unit link interval (relay interval for a link formed between adjacent coils)
α_i	Angular displacement pertaining to the i^{th} link
θ_t, θ_r	Angle between the coil radial direction and the line connecting the coil centre for the transmitter and the receiver coil respectively of a given unit link
θ_j	Angular deviation between successive unit links
M_i	Mutual inductance between non-axially aligned (link deviation), fixed coils
L_{MI}	Path loss of the MI waveguide
B	Link bandwidth
P_t	Transmission power
P_{th}	Minimum received signal power for correct demodulation
d_i	Coaxial distance between two coils in a given unit link i
d	Relay distance between a reader and its set of tags

Continued on next page

Table 7.5 – concluded from previous page

Parameter	Value
R_o	Ohmic resistance of a coil
N	Number of turns of a coil
C	Capacitance loaded in a coil
μ	Permeability of the medium (soil)
a	Coil radius
l	Length of coil wire
n	Number of coils (non-optimal) in the MI waveguide
n_{opt}	Number of coils (optimal) in the MI waveguide

Table 7.5: Glossary of Variables for Simulation 2

7.3.3.2 Parameters

Table 7.6 lists all the parameters used in the simulation. The simulation has adopted the set of coil properties in accordance with International Annealed Copper Standard (IACS) (Stratton 1914) specifications for a cylindrical solenoid coil, with a fixed coil radius of *0.2 mm*. It has been assumed that all the deployed coils have uniform dimensions. The quality factor of the coil wire has been fixed at a maximum of **100**, which is typical of mass produced coil wires. The following is a brief note about the classification of the simulation parameters listed under Table 7.6:

- *Fixed (f)*, denotes parameters which take on constant values within the applicable range (based on ground data as well as relevance).
- *Calculated (c)*, denotes parameters calculated before the simulation, based on relevant equations.
- *Variable (x)*, denotes parameters whose values have been determined by the simulation.

Place-holder variables of α and β under Table 7.6 denote the corresponding unknown calculated and variable values.

Parameter	**Value**
μ (f)	$4\pi \times 10^{-7}$ H/m
ω (f)	868 – 916 MHz (858.6 MHz to be precise)
B (f)	1 – 3 KHz
P_t (f)	26.0206 dBm in accordance with the chosen value of ω
P_r (x)	β
P_{th} (f)	−150 dBm
k_{SD} (c)	α
L_S (x)	β
L_D (x)	same as L_S (based on the assumption of uniform coil dimensions)
Q_S, Q_D (f)	100
δ (c)	α
a (f)	0.2 mm
N (f)	20 – 40
l (c)	α
R_o (c)	α The resistivity of an IACS copper wire of length 1 metre and weighing 1 gram is fixed as 0.15328 Ω/meter-gram (Stratton 1914). The actual value was calculated based on this specification and the length of the coil, as determined by the number of turns.
	Continued on next page

Table 7.6 – continued from previous page

Parameter	Value
M_i (c)	α
r_i (c)	α
θ_t, θ_r (f)	30°– 45°as determined by field conditions (actual value sets considered were 30°and 35°, 40°and 45°respectively)
d_i (c)	α
d (f)	10 m - 30 m (for ARPT RFID simulation)
θ_j (f)	30°(average) as determined by field conditions
n_{opt} (x)	β

Table 7.6: Parameters used in Simulation 2

7.3.4 Simulation Results

The simulation results obtained for the ARPT RFID MI waveguide system have been reproduced below. The following is a brief note on the correlation of each graph to the corresponding test configuration:

Test Suite 1: This suite pertains to simulations for verifying the optimum number of coils (n_{opt}) corresponding to the number of coil turns (N) for the following configuration set:

1. $\theta_t = 30°$, $\theta_r = 35°$, d = 10 m (Simulation output 1) (*vide* Fig. 7.6)
2. $\theta_t = 30°$, $\theta_r = 35°$, d = 20 m (Simulation output 5) (*vide* Fig. 7.7)
3. $\theta_t = 30°$, $\theta_r = 35°$, d = 30 m (Simulation output 9) (*vide* Fig. 7.8)

Test Suite 2: This suite pertains to simulations for verifying the optimum number of coils (n_{opt}) corresponding to the number of coil turns (N) for the following configuration set:

1. $\theta_t = 40°$, $\theta_r = 45°$, d = 10 m (Simulation output 2) (*vide* Fig. 7.9)

2. $\theta_t = 40°$, $\theta_r = 45°$, d = 20 m (Simulation output 6) (*vide* Fig. 7.10)
3. $\theta_t = 40°$, $\theta_r = 45°$, d = 30 m (Simulation output 10) (*vide* Fig. 7.11)

Test Suite 3: This suite pertains to simulations for verifying the received power (P_r) corresponding to the the optimum number of coils (n_{opt}) for the following configuration set:

1. $\theta_t = 30°$, $\theta_r = 35°$, d = 10 m (Simulation output 3) (*vide* Fig. 7.12)
2. $\theta_t = 30°$, $\theta_r = 35°$, d = 20 m (Simulation output 7) (*vide* Fig. 7.13)
3. $\theta_t = 30°$, $\theta_r = 35°$, d = 30 m (Simulation output 11) (*vide* Fig. 7.14)

Test Suite 4: This suite pertains to simulations for verifying the received power (P_r) corresponding to the the optimum number of coils (n_{opt}) for the following configuration set:

1. $\theta_t = 40°$, $\theta_r = 45°$, d = 10 m (Simulation output 4) (*vide* Fig. 7.15)
2. $\theta_t = 40°$, $\theta_r = 45°$, d = 20 m (Simulation output 8) (*vide* Fig. 7.16)
3. $\theta_t = 40°$, $\theta_r = 45°$, d = 30 m (Simulation output 12) (*vide* Fig. 7.17)

7.3.4.1 Commentary

The results obtained from the simulation call for a very engaging discussion. First of all, certain aspects of the simulation results agree well with the theoretical predictions. One of them is the observation that the path loss of the MI waveguide is inversely proportional to the number of turns of the coil (Please refer to Chapter 4 for more details). This observation is directly vindicated by the relationship between the optimum number of relay coils and the corresponding number of coil turns, for both test suites 1 and 2.

NOTE

The author has chosen a very limited range for N, considering the dependency binding on the loaded capacitance to achieve resonance, as highlighted under Chapter 4.

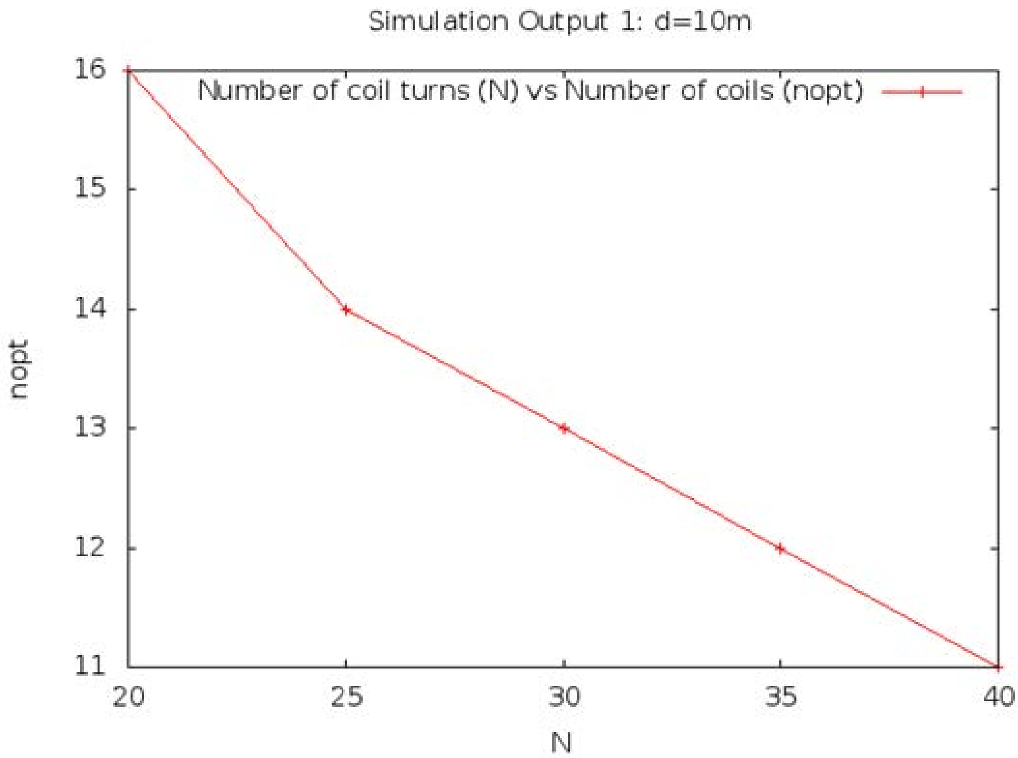

Figure 7.6: Simulation 2, Test suite 1: $\theta_t = 30°$, $\theta_r = 35°$, d = 10 m

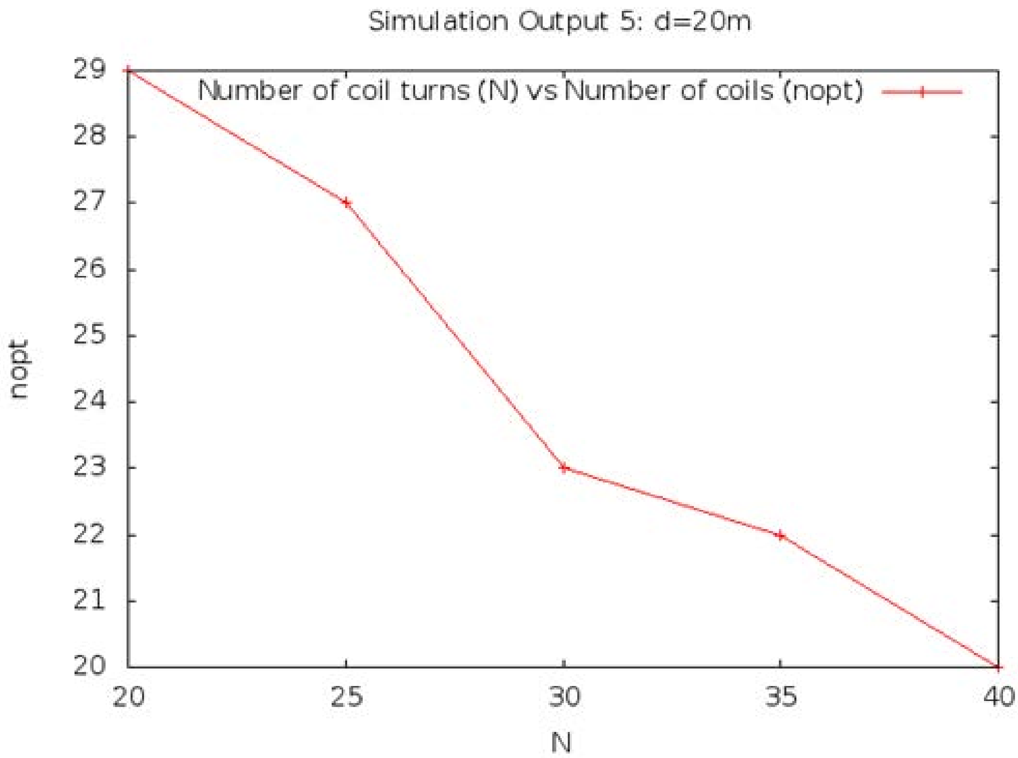

Figure 7.7: Simulation 2, Test suite 1: $\theta_t = 30°$, $\theta_r = 35°$, d = 20 m

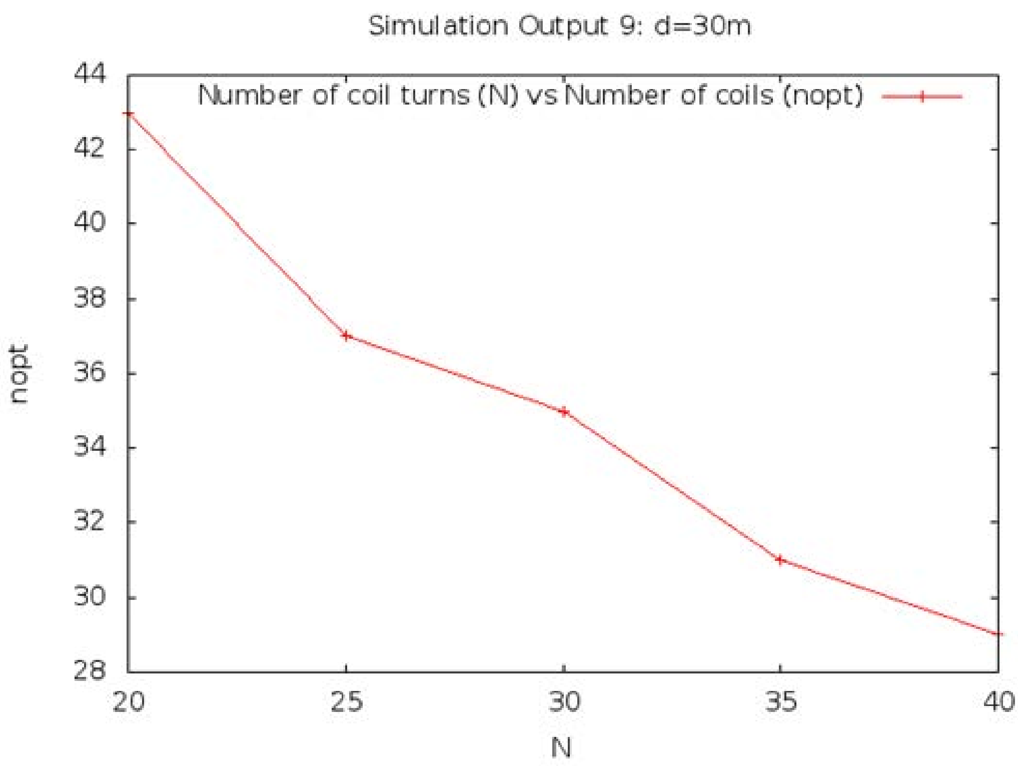

Figure 7.8: Simulation 2, Test suite 1: $\theta_t = 30°$, $\theta_r = 35°$, d = 30 m

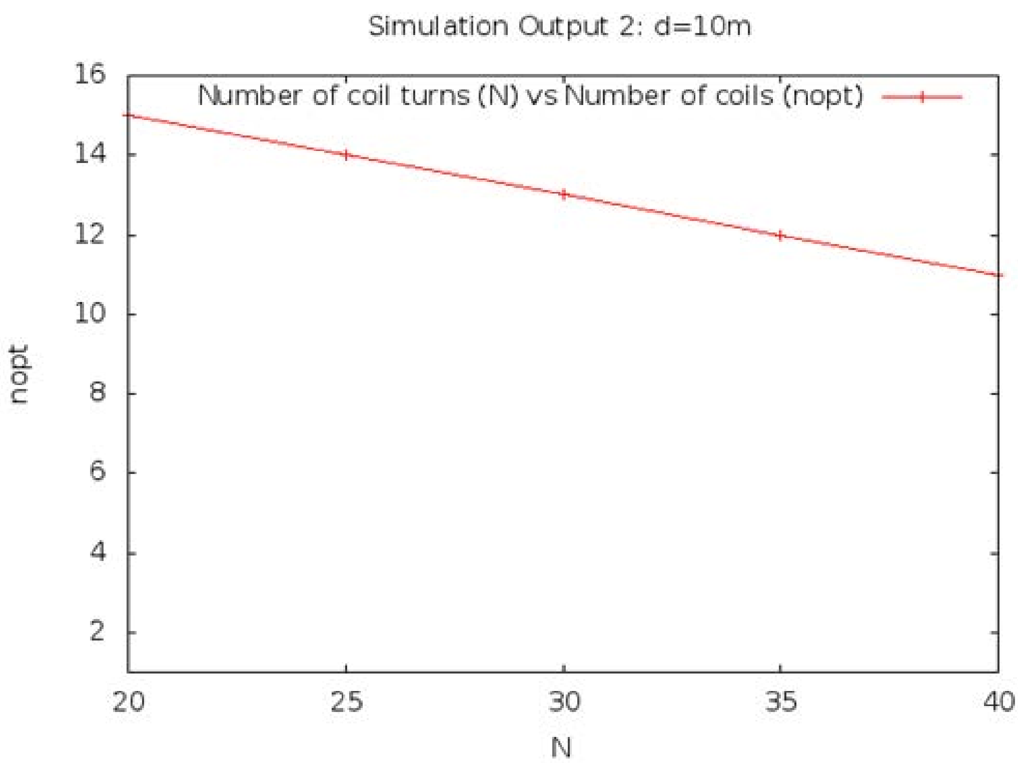

Figure 7.9: Simulation 2, Test suite 2: $\theta_t = 40°$, $\theta_r = 45°$, d = 10 m

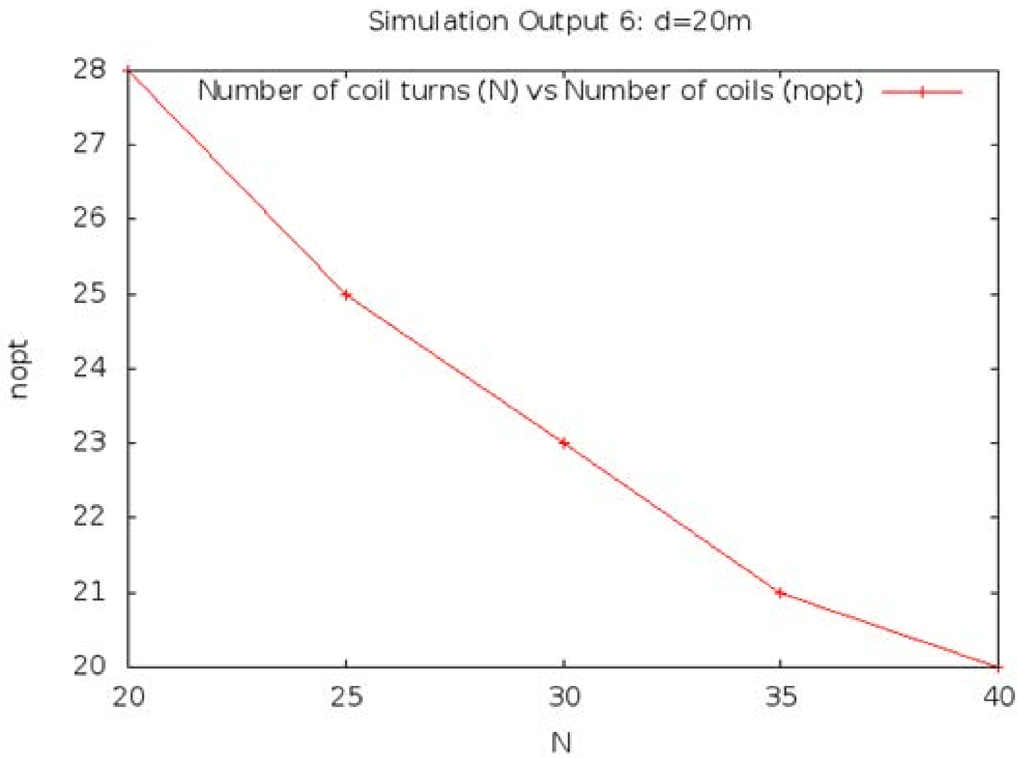

Figure 7.10: Simulation 2, Test suite 2: $\theta_t = 40°$, $\theta_r = 45°$, d = 20 m

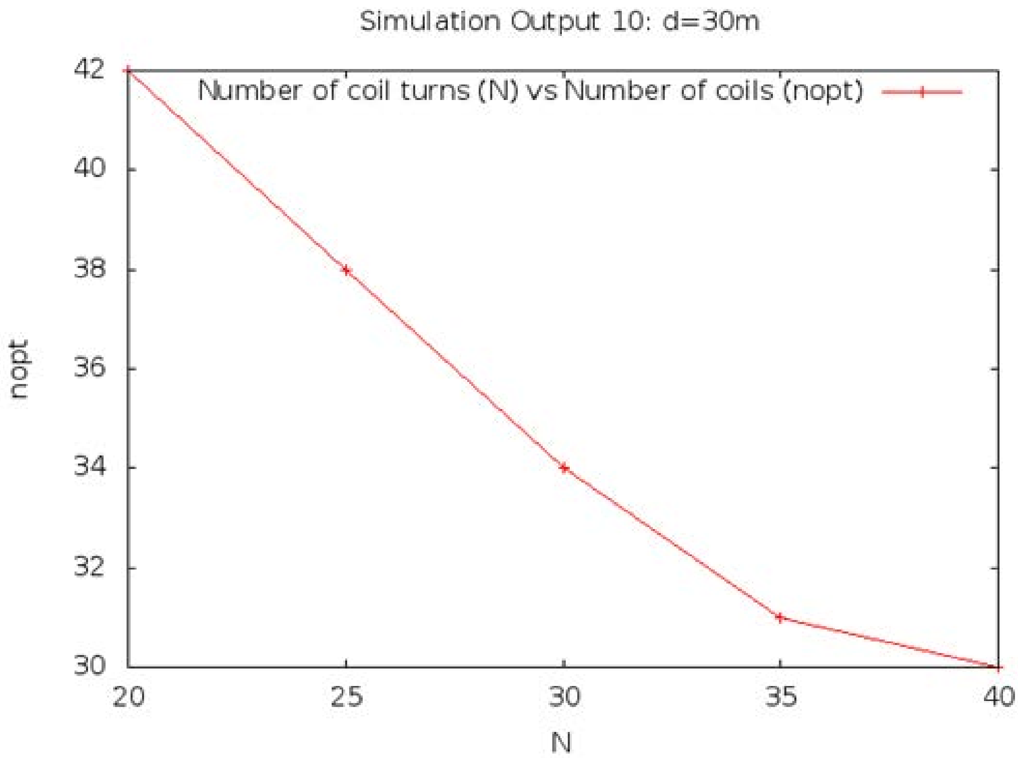

Figure 7.11: Simulation 2, Test suite 2: $\theta_t = 40°$, $\theta_r = 45°$, d = 30 m

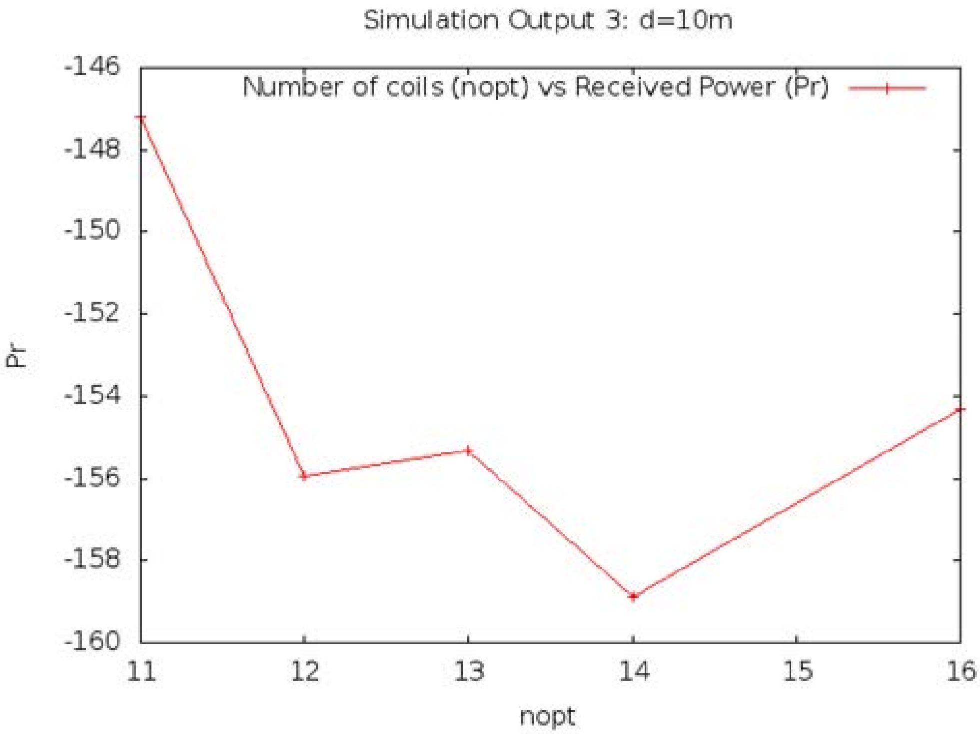

Figure 7.12: Simulation 2, Test suite 3: $\theta_t = 30°$, $\theta_r = 35°$, d = 10 m

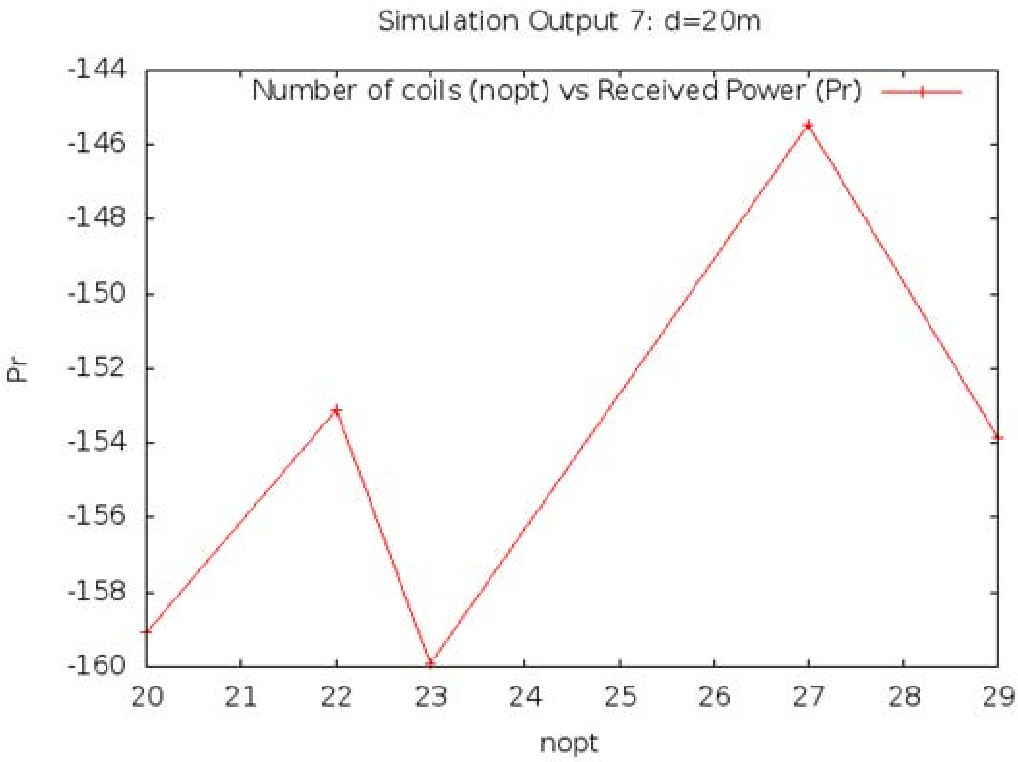

Figure 7.13: Simulation 2, Test suite 3: $\theta_t = 30°$, $\theta_r = 35°$, d = 20 m

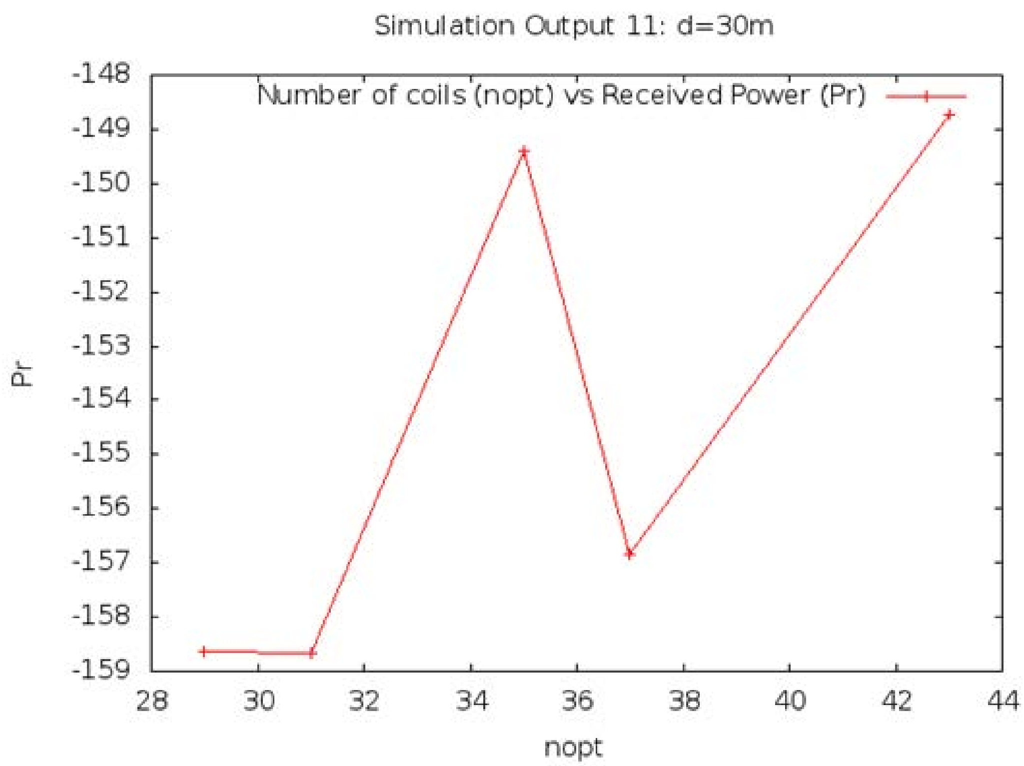

Figure 7.14: Simulation 2, Test suite 3: $\theta_t = 30°$, $\theta_r = 35°$, d = 30 m

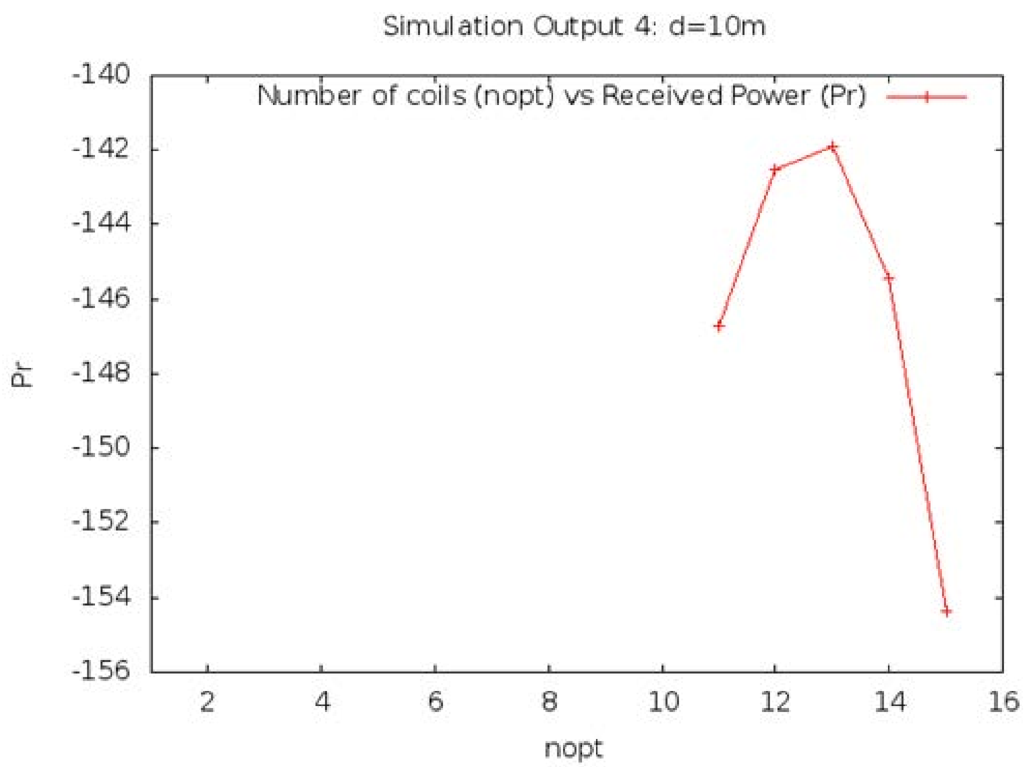

Figure 7.15: Simulation 2, Test suite 4: $\theta_t = 40°$, $\theta_r = 45°$, d = 10 m

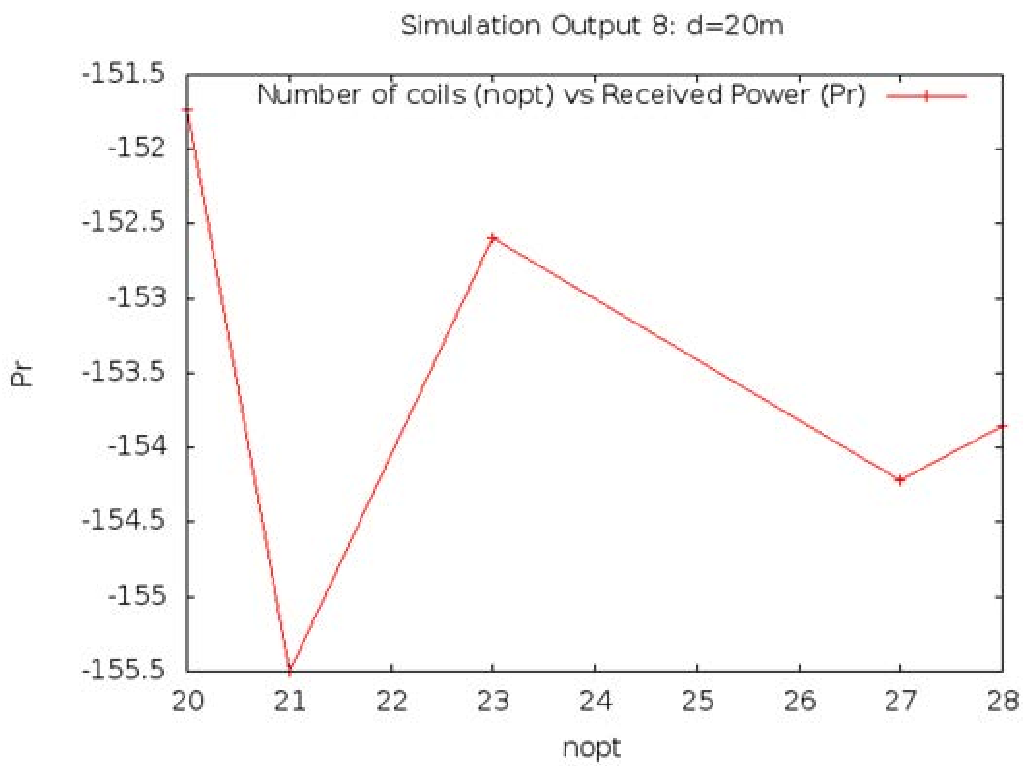

Figure 7.16: Simulation 2, Test suite 4: $\theta_t = 40°$, $\theta_r = 45°$, d = 20 m

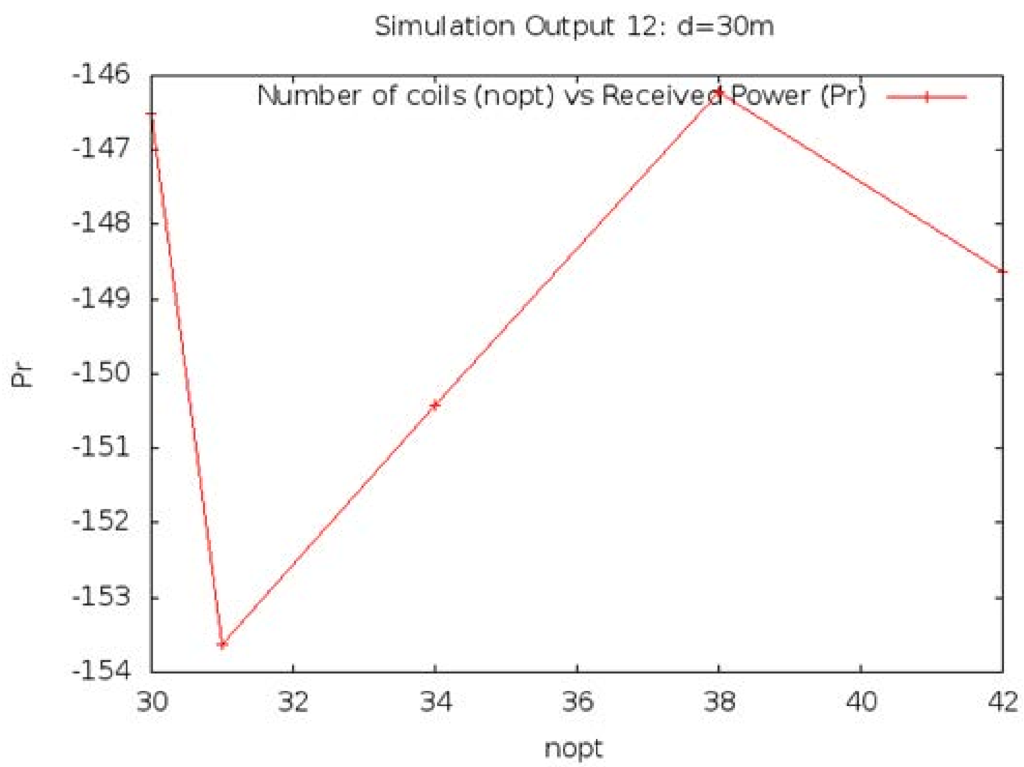

Figure 7.17: Simulation 2, Test suite 4: $\theta_t = 40°$, $\theta_r = 45°$, d = 30 m

However, within this uniformity of the results, there are subtle differences as well. The impact of θ_j, and the variations in θ_t and θ_r, can been seen in the differences observed among the different outputs.

The optimum number of coils shown for the very moderate range chosen for the RFID ARPT model, does not present an economical deployment option. This can be partially attributed to the impact of the angular displacement on the system performance, and the resultant increase in the requisite number of relay coils. Earlier during the discussion on simulation specific data, the author had hinted at the relatively small coil displacement range considered; it is thus clearly evident from the simulation results that even such small displacement can have a marked detrimental impact on the deployment economy.

NOTE

The displacement range chosen for the simulation was proportionately scaled down to make it more congenial for the feasibility study undertaken as part of this simulation. In reality, the displacement range based on the actual field conditions could be much higher, in which case even the impact of lateral displacement too would come into play.

Viewed in this light, the notion of uniform mutual inductance considered by many of the theoretical simulations reviewed under Chapter 4, is clearly unrealistic in its conceptual import, and so are the corresponding inferences drawn based on such assumption. That said, these results are also clear indicators of the infeasibility of the MI waveguide theoretical model for the chosen application context. In that respect, the results accomplished for the optimum number of requisite relay coils for the ARPT RFID simulation model corroborate the earlier results obtained from Simulation 1.

The results obtained by the second set of simulations involving test suites 3 and 4, are even more striking due to their departure from theoretical prognosis. In (Shamonina et al. 2002*a*) the following observation has been made in relation to power transfer in one-dimensional MI waveguides:

"As mentioned above it makes no difference whether the loops are spaced along a straight line or along a curved line. Hence a line consisting of 21 elements which incorporates the bend ..... would have the same current distribution ....."

This theoretical observation has been updated in (Kisseleff, Gerstacker, Schober, Sun &

Akyildiz 2013), which makes the following observation in relation to horizontal vs. vertical alignment of coils:
"...For vertical axes deployment, $\theta_t = \theta_r = 0$ and for horizontal axes deployment, $\theta_t = \frac{\pi}{2}$ and $\theta_r = \frac{\pi}{2}$ are used, to maintain the correct direction of the current flow in the relay circuits ..."
In addition to the above observations, one would expect based on the theoretical model that the quantum of power transfer should be directly proportional to the number of relay coils. However, the results show a rather "swinging" pattern, which is in spite of the number of relay coils used. A very reasonable justification for such apparent aberration should be the impact of the link deviation on power transfer. This probable conclusion further validates the view that theoretical modelling can be inaccurate in capturing all the factors related to the deployment of the MI waveguide theoretical model, and accompanying performance characteristics. The simulation results for the ARPT RFID model underscore this fundamental fact. The output from the second set of simulation results shows how plugging in the ground data such as possible angular deviation of the relay coils can drastically alter the performance expounded by the theoretical model.
The frequency considered for this simulation is in the UHF range. For this frequency range, the eddy current factor highlighted in (Kisseleff, Gerstacker, Schober, Sun & Akyildiz 2013) would come into play, which would adversely impact the performance of the MI waveguide theoretical model in the soil medium. In this simulation, since the MI waveguide theoretical model proposed in (Sun & Akyildiz 2010*c*) and (Sun & Akyildiz 2013) have been used, the eddy current factor has not been accounted for. If taken into consideration, the eddy current factor would further demote the results of the simulation.
As maintained towards the closure of the theoretical review under Chapter 4, the theoretical assumptions and corresponding framework provide a good starting point. These have to be customized and revised based on the impact of the deployment environment, dependent on the application context. Besides, such emphasis should also bring to the fore any novel workarounds applicable to a specific environment, which could be employed to circumvent the theoretical issues. The discrepancies between the results obtained from this simulation, and the benchmark of the MI waveguide theoretial model, drives home the necessity of this approach. When such approach is rooted in *analogical thinking* (Gassmann & Zeschky 2008), its dependability and efficacy are assured based on proven results from other domains. This aspect was highlighted as part of the case studies presented under

Chapter 6.

7.3.5 Source Code

The source code for the simulation results presented under this section can be viewed under Appendix A. The source code has been authored using C programming language and gnuplot (Williams & Kelley 2015) has been used to generate the graphs from the source code.

7.4 Simulation 3: Numerical Terrain Modelling of the Pecan Farm

7.4.1 Related Publication

The simulation and results discussed under this section have been published in (Parameswaran, Zhou & Zhang 2014). The data and other relevant material from the same publication have been reused in the following discussion.

7.4.2 Description

In the third and final simulation undertaken as part of the preliminary phase, the author focused on numerical terrain modelling of the pecan farm, with the objective of analysing the impact of the terrain on relay coil deployment and consequent MI waveguide performance. This simulation was in many ways a direct fallout of the previous two simulations. Taken together, the previous simulation results demonstrated the relatively large number of relay coils required for coverage with a minimal power transfer efficiency, and the detrimental impact on such efficiency due to coil displacement. Consequently, it was a natural progression to the next step of examining how much of a probability the farm terrain characteristics presented in rendering coil placement on the ground (buried in soil) a non-option, owing to the prospect of angular displacement (or even lateral displacement as applicable), and resulting downgraded system performance. The conclusions drawn from the results of this simulation further corroborated the need for novel workarounds to circumvent theoretical issues, rooted in *analogical thinking* (Gassmann & Zeschky 2008). Before delving into the specifics of the simulation, the author would like to highlight another aspect of innovation accomplished by means of the algorithm developed for terrain modelling of the farm. Terrain modelling is an integral part of the performance evaluation of WUSNs, and is a highly complicated discipline. Typical examples of terrain modelling can be found in (Santamaria-Ibirika, Cantero, Salazar, Devesa & Bringas 2013) and (Yang & Wu 2013). The algorithmic model that was developed in the process of terrain modelling of the pecan farm has the following advantages:

1. The model presents a very simple underlying framework, and enables a clear demarcation of the various underground terrain components.
2. The model is generic yet flexible to customization in accordance with particular underground terrain characteristics.
3. The model facilitates direct and clear-cut evaluation of MI waveguide related performance aspects such as coil placement, wave propagation, bit rate and power efficiency et al., by means of extension.

The terrain modelling algorithm has been built on two distinct terrain components:

- terrain attributes
- soil properties

The author shall use the following subsidiary sections to detail on each component.

7.4.2.1 Terrain Attributes

Since the farm is very large in area spreading across several hundreds of hectares and home to tens of thousands of trees, a representative area of 100 hectares was chosen for modelling the farm terrain in accordance with the typical area of a large nut tree plantation ((IAC) 2013). Based on the typical planting pattern in pecan farming (Plantation 2002), this area was further subdivided into units each comprising of a hectare in area.

Each unit was represented on a grid scale of 1:10, and the grid scale was adapted to a Cartesian coordinate system by means of points 1 – 10 on the X – Y coordinate axes. The actual land area denoted by each grid unit (point of the coordinate system) thus amounted to 100×100 square metres (m^2).

A layered approach is usually adopted in evaluating soil moisture content, and since the feeder roots of the pecan tree are located at the upper 12 inches of the soil (Andersen & Crocker 2015), the sensor nodes would have to be deployed in the 0 – 30 cm depth range. Accordingly, the applicable burial depth was considered in three layers of 10, 20 and 30 cm respectively.

In terms of terrain modelling, Table 7.7 lists all the primary terrain attributes (adapted from (Moore, Grayson & Ladson 1991)) considered for the model. Table 7.8 lists the equations borrowed from (Mitasova & Hofierka 1993) for approximating the first and second derivatives of the Digital Elevation Model (DEM) of a grid cell (i,j), and the corresponding equations taken from (Erskine, Green, Ramirez & MacDonald 2007) for all the primary terrain attributes other than *Aspect*.

Considering the elevation range, the slope values should be infinitesimal. Since *gentle* slope values could contribute to large spikes in aspect angles (James R Carter 1992), the value of aspect angle was restricted to the 0°– 90°range by means of the adapted algorithm (Hodgson 1998) listed under Table 7.9.

7.4.2.2 Soil Properties

The soil properties have been assumed to display covariance across a range of 10 hectares, analogical to the concept of *pedotransfer functions* (PTFs) (Grunwald 2006). The range has been based on the pecan farm characteristics. The grid scale adopted is similar to that of the terrain attributes, viz., 1:10. Each grid unit should represent a land area of 10 hectares, considering the total land area of 100 hectares. Table 7.10 lists the range of soil physical properties and their corresponding value range (Lal & Shukla 2004) considered for modelling the topsoil region.

Attribute	Attribute	Hydrological Significance
Altitude	Elevation	Climate, vegetation type, potential energy
Slope	Gradient	Overland and subsurface flow velocity and run-off rate
Aspect	Slope azimuth	Solar irradiation
Profile Curvature	Slope profile curvature	Flow acceleration, erosion/deposition rate
Plan Curvature	Contour curvature	Converging/diverging flow, soil water content

Table 7.7: Primary Terrain Attributes considered for the Numerical Terrain Model in Simulation 3

7.4.2.3 Modelling Algorithm

The farm land area has been modelled as a combination of terrain attributes and soil properties. The following is a brief description of the modelling particulars:

- A unit area of 1 hectare has been taken as the basic classification unit. This is in accordance with the typical plantation paradigm (Plantation 2002).
- There are two aspects to the model, as mentioned above. These are the terrain attributes and soil properties representative of the total area of 100 hectares considered for the model.
- Only the topsoil region is relevant for modelling on account of soil moisture sensor deployment in the rhizosphere region of pecan trees. This region falls between 0 – 30 cm depth (Andersen & Crocker 2015).
- The author considered only the unit area for terrain modelling since based on the farm topography as well as the plantation paradigm (Plantation 2002), the entire range of recurring terrain variations across the farm can be *figuratively* modelled

Formula	Description
$z_x \cong (z_{i+1,j} - z_{i-1,j})/2d$ $z_y \cong (z_{i,j+1} - z_{i,j-1})/2d$ $z_{xx} \cong (z_{i+1,j} - 2z_{i,j} + z_{i-1,j})/d^2$ $z_{yy} \cong (z_{i,j+1} - 2z_{i,j} + z_{i,j-1})/d^2$ $z_{xy} \cong (z_{i-1,j+1} - z_{i+1,j+1} - z_{i-1,j-1} + z_{i+1,j-1})/4d^2$	These formulae borrowed from (Mitasova & Hofierka 1993) have been used for approximating the first and the second derivatives of the DEM for a grid cell (i,j). Here z denotes the primary terrain attribute *Altitude*, listed under Table 7.7, and d denotes the grid cell distance. The value of altitude corresponds to the elevation of a particular layer. These approximated values have been used in the calculation of the other primary terrain attributes, except altitude and aspect.
$\left[z_x^2 + z_y^2\right]^{1/2}$	The formula used for calculating *Slope* (Erskine et al. 2007).
$\left(z_{xx}z_x^2 + 2z_{xy}z_xz_y + z_{yy}z_y^2\right)/\left[S_{FD}^2\left(z_x^2 + z_y^2 + 1\right)^{3/2}\right]$	The formula for calculating *Profile Curvature* (K_p) (Erskine et al. 2007). Here S_{FD} denotes slope.
$\left(z_{xx}z_y^2 - 2z_{xy}z_xz_y + z_{yy}z_x^2\right)/S_{FD}^3$	The formula for calculating *Plan Curvature* (K_c) (Erskine et al. 2007). Here S_{FD} denotes slope.

Table 7.8: Equations used in Simulation 3 for Terrain Modelling

within the unit area. For this reason, the total farm area has been considered as *concatenations* of the unit area.

- For modelling the soil properties, the entire farm area has been taken into consideration. Based on the farm land features, the soil properties display variations over each ten hectare area.

Algorithm for Calculating Aspect Angle
$if \quad S_{FD-WE} == 0 \quad AND \quad S_{FD-SN} == 0$
$\qquad Aspect = Undefined$
$else\ if \quad S_{FD-WE} == 0 \quad AND \quad S_{FD-SN} < 0$
$\qquad Aspect = 180$
$else$
$\qquad Aspect = 0$

Table 7.9: Algorithm used in Simulation 3 for Calculating Aspect Angle

Soil Physical Property	**Range**	**Units**
Particle Density (ρ_s)	2.6 – 2.8	Mg/m^3
Dry Bulk Density (ρ_b)	0.7 – 1.8	Mg/m^3
Porosity (f_t)	0.3 – 0.7	Fraction, m^3/m^3
Air Porosity (f_a)	$0 - f_t$	Fraction, m^3/m^3
Void Ratio (e)	0.4 – 2.2	Fraction
Gravimetric Soil Moisture Content (w)	0 – 0.3	Fraction, kg/kg
Volumetric Soil Moisture Content (Θ)	0 – 0.7	Fraction, m^3/m^3
Degree of Saturation (s)	0 – 1	Fraction
Dry Specific Volume (v_b)	0.5 – 1	Fraction, m^3/Mg
Air Ratio (α)	0 – 1	Dimensionless
Liquid Ratio (θ_p)	0 – 1	Dimensionless
Wet Bulk Density ($\rho_b{}'$)	1 – 2	Mg/m^3

Table 7.10: Range of Soil Physical Properties considered for the Numerical Model in Simulation 3

- A *covariance* model has been used to represent the terrain attribute changes across the unit farm area for the three layers of the topsoil region, viz., 0 – 10 cm, 10 – 20 cm, and 20 – 30 cm respectively.

- Another *covariance* model has been employed to characterize the variations in soil properties manifesting on a 10 hectare frequency across the land area.

- A grid scale of 1:10 has been used in the case of both the covariance models. In the case of the terrain, each unit of the grid scale corresponds to 100×100 square metres (m^2). In the case of soil, each unit of the grid scale corresponds to 10 hectares of land area.
- For both the terrain and soil properties, mean values taken across the respective applicable range have been used as indicators of the degree of covariance.

7.4.3 Simulation Specific Data

The simulations were conducted in two distinct phases. To begin with, only the topsoil region (0 – 30 cm depth) was modelled based on ground data to understand the terrain fluctuations, which would have a detrimental impact on coil placement underground. The numerical data obtained for this phase has been presented under Table 7.11 (all values rounded to four decimal digits).

Subsequently, the topsoil terrain model was integrated with the soil properties for the entire farm area, and a Mean Index Value (MIV) was arrived at to reflect the average overall covariance of both the terrain and soil properties across the farm area under consideration. The numerical data obtained for this phase has been presented under Table 7.12.

Elevation (in cm)	**Slope ($S_F D$)**	**Profile Curvature (K_p)**	**Plan Curvature (K_c)**
10	0.7953	0.4296	-1.3141[1]
20	0.9457	0.1970	-0.6202
30	1.0466	0.1872	-0.5996

[1] Positive curvature values are concave upward and are characterized by decelerating and converging flows (Mitasova & Hofierka 1993). So the opposite should hold good for negative values.

Table 7.11: Numerical Values obtained under Simulation 3 for Terrain Modelling in the Topsoil Region

Mean Index Value (MIV)	**Land Area (in square metres (m^2))**	**Grid Scale**
0.485366139055406	100000	1
0.553999705676076	200000	2
0.539066595719894	300000	3
0.616663070460352	400000	4
0.62050275221743	500000	5
0.587469156002179	600000	6
0.448202846958238	700000	7
0.65721179032837	800000	8
0.727667452615117	900000	9
0.619841938258119	1000000	10

Table 7.12: Mean Index Values (MIVs) Obtained Under Simulation 3 for Covariant Terrain and Soil Properties in the Pecan Farm

7.4.4 Simulation Results

Figure 7.18 displays the 3D rendering of the numerical model of the covariant topsoil terrain using MATLAB. Similarly, Figure 7.19 displays the 3D rendering of the numerical model of the covariant terrain and soil properties using MATLAB, for the considered farm land area of 100 hectares for the simulation.

7.4.4.1 Commentary

Fig. 7.18 clearly shows the fluctuation of slope, profile curvature, and planar curvature even for the topsoil region. This result implies that deploying coils directly in the soil is bound to degrade MI waveguide system performance drastically even for very small elevations, due to the irregularities presented by the terrain structure.
In Table 7.7, the hydrological significance of these terrain attributes have been highlighted. Of the three attributes, it has been mentioned that plan curvature influences soil moisture content. During the course of the theoretical review under Chapter 4, the author discussed

about the study undertaken in (Kisseleff, Gerstacker, Schober, Sun & Akyildiz 2013) which considered the impact of eddy current factor on MI waveguide performance in the soil medium. The eddy current factor is tightly coupled with the soil moisture content. Thus it is a reasonable conclusion that fluctuations in planar curvature values of the topsoil terrain, as observed in Fig. 7.18, can pose serious problems to the uniformity of the MI waveguide performance underground. It is often impossible to predict or even approximate on the peculiarities of the terrain topography, based on theoretical calculations alone; this being so, theoretical modelling founded on the assumption of uniform terrain should not yield the same results once transplanted to the actual field.

NOTE

The reader is referred back to the review of the state-of-the-art theoretical work on MI based WUSNs undertaken in Chapter 4, wherein none of the works reviewed have considered the impact due to the vagaries of the terrain on system performance. Additionally, a good number of works have also assumed uniform soil characteristics.

The result underscores this fundamental aspect of any deployment environment underground. Consequently, it becomes necessary to complement theoretical modelling with novel workarounds of a practical nature, to circumvent theoretical issues.

The result highlighted in Fig. 7.19 shows random fluctuations in the MIV with increasing land area. This is a very solid indicator of how it is quite reasonable to expect unforeseeable variations in both terrain attributes and soil properties on average in most considerably large areas of coverage. There are four key implications to this result.

The first implication pertains to relay coil deployment. Deploying the relay coils directly underground in the face of such unpredictable flux in the terrain attributes and soil properties could clearly interfere with the optimum MI waveguide system performance, as mentioned above. Thus any assumption about uniform mutual inductance between adjacent coils, as in the case of the original MI waveguide model (Sun & Akyildiz 2010*c*), does not fit the actual deployment conditions.

Secondly, the deployment complexity visiting any such land area subject to irregular variation in terrain attributes and soil properties can be humongous. In Chapter 4, the author mentioned during the review of (Sun & Akyildiz 2010*b*) how most of the algorithms presented therein do not pass the simplicity requirements of a practicable deployment scenario. The result shown in Fig. 7.19 is a further corroboration of that assessment. Given a terrain with irregular topographical characteristics and soil features as shown in the figure, considering anything other than a simple yet complete deployment algorithm could augment the deployment complexity by several orders of magnitude, not to mention the subsequent maintenance and troubleshooting difficulties.

The importance of dividing any large deployment area into small, self-contained units is another implication that could be taken away from the simulation result. Such demarcation is necessary for easy deployment, troubleshooting and maintenance, in the light of the terrain complexity presented in the simulation results.

Last but not the least, during the course of the theoretical review on MI waveguide in Chapter 4, the author had pointed to the assumption adopted by many recent theoretical research outputs about the uniformity of the soil medium. In this context, the author had even quoted a recent study (Stadler et al. 2015) to disprove this conception. The simulation result evinced in Fig. 7.19 is a further repudiation of the theoretical notion. This fact, alongside other incorrect assumptions underlying many current theoretical findings such as uniform mutual inductance mentioned above, point clearly to the marked discrepancy between theory and deployment conditions.

NOTE

All of these inferences have been translated to related novel workarounds or models rooted in *analogical thinking* (Gassmann & Zeschky 2008) , which will be discussed under the next chapter.

7.4.5 Source Code

The source code for the simulation results presented under this section can be viewed under Appendix A. MATLAB has been used for the simulations.

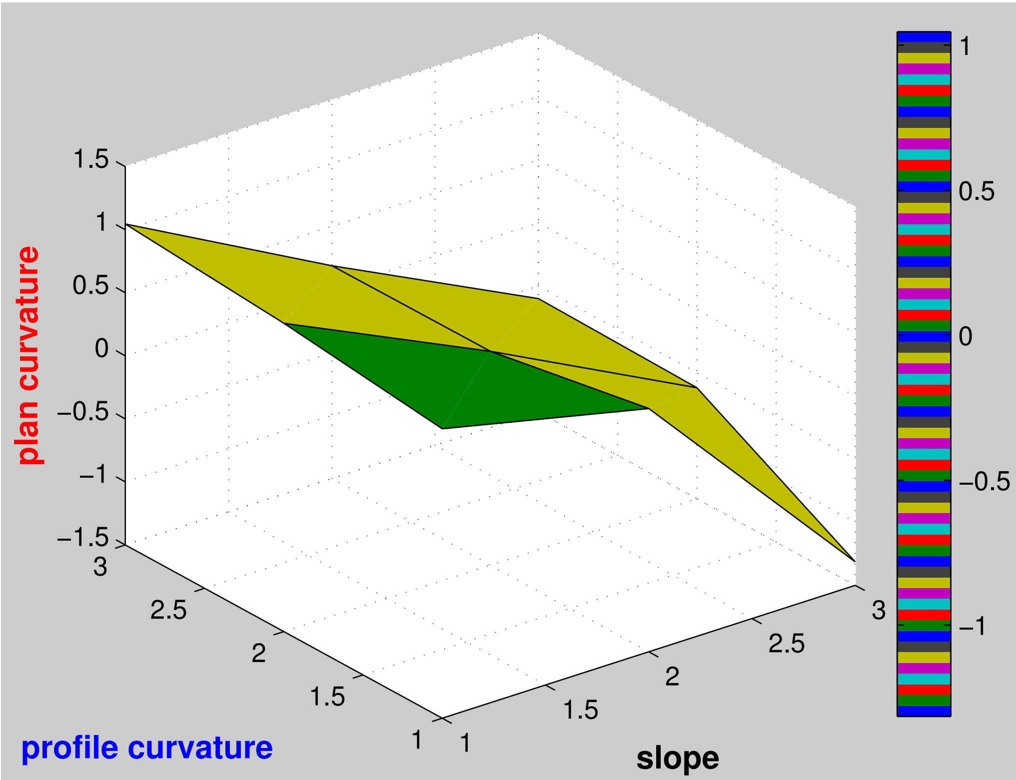

Figure 7.18: Simulation 3 - 3D Surface Mesh Grid of Covariant Terrain Attributes for the Farm Topsoil

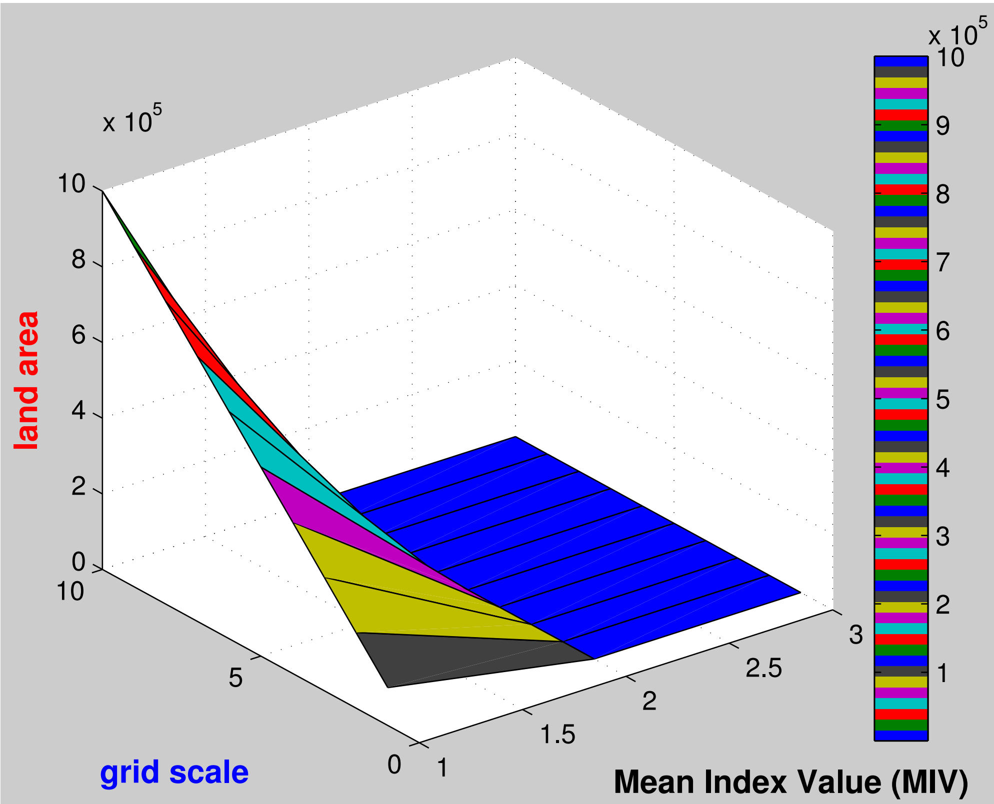

Figure 7.19: Simulation 3 - 3D Surface Mesh Grid of Covariant Terrain Attributes and Soil Properties for the Farm Land Area

7.5 Chapter Summary

In this very critical chapter, the author presented simulations and corresponding results validating the feasibility of the MI waveguide theoretical models against the chosen application context. The following is a gist of the simulations and the corresponding results obtained:

- In Simulation 1, the power transfer efficiency vs. the optimum number of relay coils was validated for the MI waveguide theoretical model (Sun & Akyildiz 2010*c*) using a minimal configuration, suitable for a feasibility study related to the chosen application context. The results showed the non-feasibility of the model for the chosen application context, in terms of the generated power vs. the optimum number of relay coils required for a minimum receiver sensitivity threshold. The results also demonstrated the delicate balance among the various components of the model, which limited the optimal configuration possible.
- In Simulation 2, the question of power transfer efficiency vs. optimum number of relay coils was revisited, in the light of an ARPT RFID model. The factor of coil displacement was also taken into consideration for this simulation, which had not been addressed in Simulation 1. The validation used the MI waveguide theoretical model proposed in (Sun & Akyildiz 2010*c*) and (Sun & Akyildiz 2013). The results showed that the power transfer efficiency did not strictly adhere to the theoretical predictions, and displayed a rather fluctuating pattern against the number of relay coils considered. This discrepancy is attributed to the impact of coil displacement on the MI waveguide theoretical model performance. The result showed clearly that the assumption of uniform mutual inductance in the theoretical model does not fit a deployment scenario. In addition, it was also mentioned the the eddy current factor highlighted in (Kisseleff, Gerstacker, Schober, Sun & Akyildiz 2013) had not been accounted for in the simulation using a UHF range, which would have further demoted the results obtained.
- In Simulation 3, terrain and soil covariance modelling was presented using a novel numerical modelling algorithm, based on ground data for the chosen application context. The objective of the simulation was to determine the impact of the to-

pographical characteristics on coil displacement, and the consequent impact on the MI waveguide theoretical models. The results showed that the topographical fluctuations would severely impact the performance of the MI waveguide theoretical model due to coil displacement, including both angular and lateral displacements; the latter had been excluded from the limited scope of Simulation 2. This further confirmed the error in the assumption about unifrom mutual inductance, and the consequent non-feasibility of any MI waveguide theoretical model for deployment. The topographical fluctuations also dispelled the assumption of uniform soil characteristics inherent to many MI waveguide theoretical models; in the absence of such assumption, the eddy current factor outlined in (Kisseleff, Gerstacker, Schober, Sun & Akyildiz 2013) would have a more pronounced impact on the performance of the MI waveguide theoretical model.

The bottom-line is clear as far as the larger takeaway from all the various results presented in this chapter are concerned: *it is impossible to construct an acceptable deployment model using the MI waveguide theoretical models. In order to have any realistic progress in that direction, it is imperative to consider alternate novel workarounds that circumvent the key issues inherent to these models.*

Additionally, many theoretical models are based on incorrect assumptions such as uniform mutual inductance and soil characteristics. A more grounded theoretical approach has to account for both coil displacement aspects as well as the eddy current factor, and base the model on these premises as well. However, as pointed out during the review under Chapter 4, the existing theoretical models start showing severe performance degradation once these factors are accounted for.

The simulation results highlighted in this chapter were catalytic to the direction adopted by this research, in finding novel workarounds rooted in *analogical thinking* (Gassmann & Zeschky 2008), to the key theoretical issues. In this sense, this chapter served as a precursor to the next chapter wherein the author would delve more into the alternate solution approaches based on analogical thinking, positioned against the backdrop of the simulation results presented in this chapter, and the theoretical analysis covered in the preceding chapters.

Chapter 8

Innovations based on Analogical Thinking

8.1 Chapter Overview

This chapter marks the culmination of the work accomplished as part of this research. In this chapter, the author would describe the innovative workarounds rooted in *analogical thinking* (Gassmann & Zeschky 2008) to the issues in the MI waveguide theoretical models. These issues had been analysed at length, during the course of the discussion under the preceding chapters. In addition to the innovative workarounds, the author would also present a novel longevity model for MI based WUSNs, and certain novel communication concepts and models. These aspects have also been based on analogical thinking. Additionally, the author would present a heuristic deployment model for the chosen application context, based on the above innovations.

The analysis and simulations presented in the previous chapters underscore the purely theoretical nature of the research on MI waveguide based WUSNs thus far, and its shortcomings. However, it is possible to identify certain key bottlenecks to the improvement of the MI waveguide theoretical models, and examine how these could be overcome by means of ingenious workarounds. The resultant solution approaches presented in this chapter have been documented in the form of novel ideas and models, solution pointers based on previous research output, or novel hypothetical propositions, akin in spirit to the Request for Comments (RFC) ((IETF) 2015) memorandum published by the Internet Engineering Task Force (IETF).

Towards the end of the chapter, the author would revert to the theory of MI waveguide WUSNs and show by means of selective simulations the validity of certain innovative workarounds presented hereunder, which are directly related to the theoretical MI waveguide WUSN model (Sun & Akyildiz 2010*c*), and its subsequent improvements. In the case of the other propositions, such exercise has been refrained from either due to the fact that the validity of the proposed model or solution approach is self-evident, or has been proven in a previous research output. In the latter case, explicit reference has been provided to the corresponding work.

Another overriding tenor of all of the solution approaches, models and hypothetical propositions provided in the chapter, apart from their theoretical origin, is the fact that they have all been derived or devised using the concept and method of analogical thinking. Thus in addition to demonstrating how novel workarounds could break the ice of theoretical stalemate in MI based WUSNs, these innovations also drive home the significance of outside the box thinking in order to arrive at such workarounds or novel ideas in the first place. And in doing so, they also throw wide open the research space and the consequent possibilities for MI based WUSNs, hitherto confined to the rather restricted environs of pure theoretical research.

In the following section, the author would begin with an overview of the novel workarounds or models presented in this chapter, and expand on each in the ensuing sections. A final section has been devoted to the previously stated selective simulations and corresponding results.

8.1.1 Related Prospective Publication

An article based on the innovations and the consequent heuristic deployment model discussed under this chapter, has been submitted for review and publication in the IEEE Sensors Journal.

8.2 Overview of the Innovations

The innovations proposed have been aimed at working around several key issues identified by the state-of-the-art theoretical research on MI waveguide WUSNs. In addition, a certain aspect of the innovations has resonance with a core issue identified by WUSN research in general.

The key issues for which innovative workarounds, solution pointers or models have been proposed, are as outlined below:

NOTE

No description of the issues have been given hereunder, since all of these factors have been adequately dealt with in the corresponding preceding chapters.

1. Coil misalignment and consequent performance degradation of MI waveguide WUSNs.
2. Eddy current factor in the soil medium and its adverse impact on the performance of MI waveguide WUSNs.
3. Coil parasitic capacitance and its restrictive impact on the MI waveguide resonance parameters.
4. Generic complexity of the deployment model and corresponding algorithms hitherto presented in the related theoretical research on MI waveguide WUSNs.
5. The preoccupation about self-sustained WUSNs, due to the extreme difficulty involved in both node troubleshooting and replacement post deployment (this is a generic research area, and is not confined to MI based WUSNs).

The author does acknowledge that a lot of other factors can be added to the above list such as innovative coil or waveguide design, or the prospect of experimenting with alternate metamaterial solution approaches. These topics were discussed during the course of the review of the preliminary research on MI waveguide. However, the author has hand-picked certain key issues (theoretical and otherwise) pertaining to MI based WUSNs.

Fig. 8.1 presents an overview of the proposed innovations with the individual components, to be detailed under the subsequent sections.

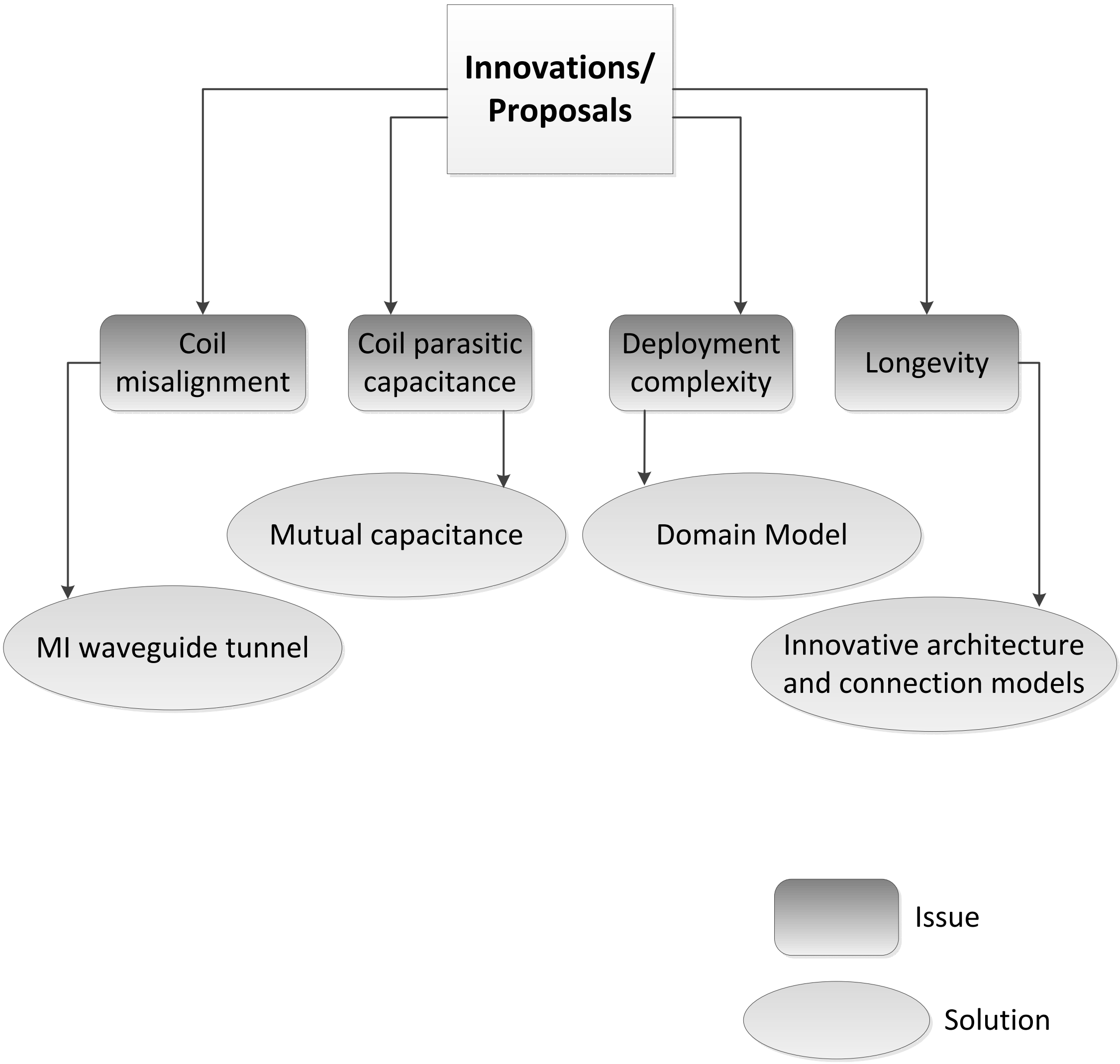

Figure 8.1: Overview of the Proposed Innovations

8.3 Novel Workarounds or Proposals to Circumvent or Eliminate Theoretical Issues

8.3.1 MI Waveguide Tunnel

One of the fundamental requirements for the realization of an MI waveguide is the accurate alignment of coils so as to achieve resonance at a central frequency. In the previous chapter, it was shown by means of simulations how terrain irregularities could impact such alignment. In addition, often there are lumps of hard mass such as stones, vegetation and root undergrowth that create further impediments. A maximum coil misalignment to the tune of 10% has been assumed in the simulation results presented in (Sun & Akyildiz 2010*c*), but in reality the deviation could be much higher, and anywhere between 25% to 50% or even more, depending on the terrain.

In the simulation results presented under the previous chapter, the incapability of the theoretical MI waveguide model (Sun & Akyildiz 2010*c*) was demonstrated in precisely accounting for the extent of impact on the system due to coil misalignment. It was also demonstrated by means of terrain modelling how the assumption of 10% coil misalignment probability does not coincide with actual field conditions.

Based on this research study, there are two major factors that are key to overcoming the coil misalignment issue in MI waveguide deployment underground:

- the coils of the waveguide have to be embedded in the soil
- the coils should be *physically linked* to the sensors

NOTE

The phrase *physically linked* implies that the coils have to be connected to the sensors by means of a suitable mechanism, which can be even wireless; there are no existing physical implementations of a device model integrating the sensor nodes and the MI waveguide.

If the above two factors could be addressed, the problem of coil misalignment could be effectively resolved without impacting integration with sensor nodes. Towards this end, the author proposes the novel concept of the composite framework of a MI waveguide tunnel (*vide* Fig. 8.2). The concept is analogous to the practice of undergrounding used in power transmission.

Fig. 8.2 highlights the diagrammatic representation of the origination side of the waveguide tunnel. This framework would coexist underground with a soil moisture sensor connected by means of long cable to an underground data logger, as shown in the figure. The MI waveguide tunnel has been envisaged as a composite tube made of non-conducting material (such as PVC), and each coil would be fixed on the inside of the tube at the required orientation.

The main advantage of the tunnel is that it would facilitate deployment of the waveguide at a convenient depth, *irrespective of the sensing depth*. By fixing the coils on to the inner walls of the tube, the problem of coil misalignment or position deviation can be effectively addressed. In addition, since the coils are shielded from the environment by the outer sheath of the tunnel (not shown in the diagram), the fluctuations in the environment should not impact the optimal functioning of the coils either. This very fact should also render the impact of the eddy current factor null and void. *Thus using the same contrivance, it should be possible to resolve two key theoretical issues confronting the MI waveguide theoretical model (Sun & Akyildiz 2010*c*) at the same time.*

A very striking analogy can be drawn to the physical layout of a mineral-insulated copper-clad cable (MICC), which is a NFPA® recommended standard for undergrounding ((NFPA)® 2014). In the case of the proposed MI waveguide, the inner layer of the cable would be replaced by the aligned array of coils in required orientations.

The notion of a composite tunnel has been suggested for reasons of flexibility. Due to the peculiarities of the underground terrain, as demonstrated by means of the simulations presented under the previous chapter, it may not be possible to have a continuous stretch of the tunnel from a source point to the sink, especially in the case of relatively longer transmission distances. In such cases, it should be possible to break up the tunnel at suitable points, without impacting the coil orientation in those locations. This can be achieved using the notion of a composite tunnel, joined together at multiple locations. Fig. 8.3 shows the schematic representation of a composite MI waveguide tunnel formed of two distinct tubes joined together at the ends. In the figure, the relay distance traversing the joints, as well as the orientation angle between the coils bordering the joints are also discernible. It is evident from the diagram that both the orientation angle and the relay distance between adjacent coils could vary at the joints of the composite MI waveguide tunnel. The inter-coil alignment at each joint can be tuned for maximum resonance.

The concept of the MI waveguide tunnel enables a futuristic scenario, wherein a customer could provide the vendor of a waveguide tunnelling solution with the layout of the deployment site complete with break-up points, along with the required coil specifications, coil orientations, relay distance and other applicable technical details, in order to get a custom solution delivered, and even possibly deployed on site.

8.3.1.1 Advantages

The following are the key advantages provided by the MI waveguide tunnel:

- The MI waveguide tunnel provides the flexibility to deploy the waveguide at a suitable depth, irrespective of the sensing depth. This often can make a significant difference to real world application contexts. For instance, in the case of the chosen application context for this research, the waveguide tunnel could be laid as a single continuous stretch across each hectare unit of the farm area, at a depth of approximately 5 m below ground, considering the maximum root penetration of pecan trees (Andersen & Crocker 2015).

- The framework of the MI waveguide tunnel analogous to that of MICC should offer total insulation for the waveguide coils from the fluctuations of the underground environment. As shown in Fig. 8.2, the coils can be fixed to the inner wall of the tunnel and thus be protected from the surrounding environment vagaries by means of the outer sheath (not shown in the diagram).

- The MI waveguide tunnel offers a flawless solution approach to the problem of coil misalignment or deviation, which can cause a significant dent in the performance of the MI waveguide system (Sun & Akyildiz 2010*c*), (Sun & Akyildiz 2012).

- The framework of the MI waveguide tunnel analogous to the MICC totally eliminates the prospect of the eddy current factor, highlighted in the theoretical research as a major performance bottleneck (Kisseleff, Gerstacker, Schober, Sun & Akyildiz 2013) for MI waveguide WUSNs. In a later section, the author shall provide further evidence to this fact by means of simulation results.

- The MI waveguide tunnel should be easy to install and maintain, as the paradigm is not novel in its entirety and takes after the standard practice of using MICC undergrounding ((NFPA)® 2014). This fact should lend additional guarantee to the practicality of the proposed approach.

- Perhaps the single biggest advantage of the waveguide tunnel stems from the fact that it enables a stable environment for the MI waveguide system, irrespective of the possible variations of the underground environment (including soil) across space and time. Soil characteristics can vary subject to both time of the day and physical location, and these variations can impact MI communication (Kisseleff, Gerstacker, Schober, Sun & Akyildiz 2013). In addition to the simulation results of terrain modelling presented under the previous chapter to evidence the variation of soil characteristics with physical location, further examples of the variation of the soil characteristics with the time of the day has been presented in (Dursun & Ozden 2014), and a study of the variation of the soil characteristics with seasonal changes can be found in (Kurnik, Louwagie, Erhard, Ceglar & Bogataj Kajfez 2014).

- Since the MI waveguide tunnel deprives the communication medium of all the uncertainties associated with the conductive medium (soil), the system should achieve better bit rate efficiency based on (Kisseleff, Gerstacker, Schober, Sun & Akyildiz 2013), and consequently better power efficiency.

- In terms of cost, even though the MI waveguide tunnel could be more expensive than the MI waveguide coils deployed or embedded directly in the soil, such cost should be more than a fair trade-off considering the system stability that ensues due to the MI waveguide tunnel option.

- The MI waveguide tunnel model provides a concrete visual representation and related pointers to possible future commercial directions for MI waveguide WUSN deployment.

NOTE

Recall the observation in (da Silva et al. 2014) mentioned under Chapter 5, about the lack of implementation guidelines for MI communication underground. Based on the above discussion, the author would like to suggest that the MI waveguide tunnel constitutes a clear-cut guideline in that direction.

8.3.2 Mutual Capacitance

The coils of the MI waveguide are loaded with a suitable capacitor to achieve resonance (Sun & Akyildiz 2010*c*), whose value is given by the equation presented under Chapter 4.

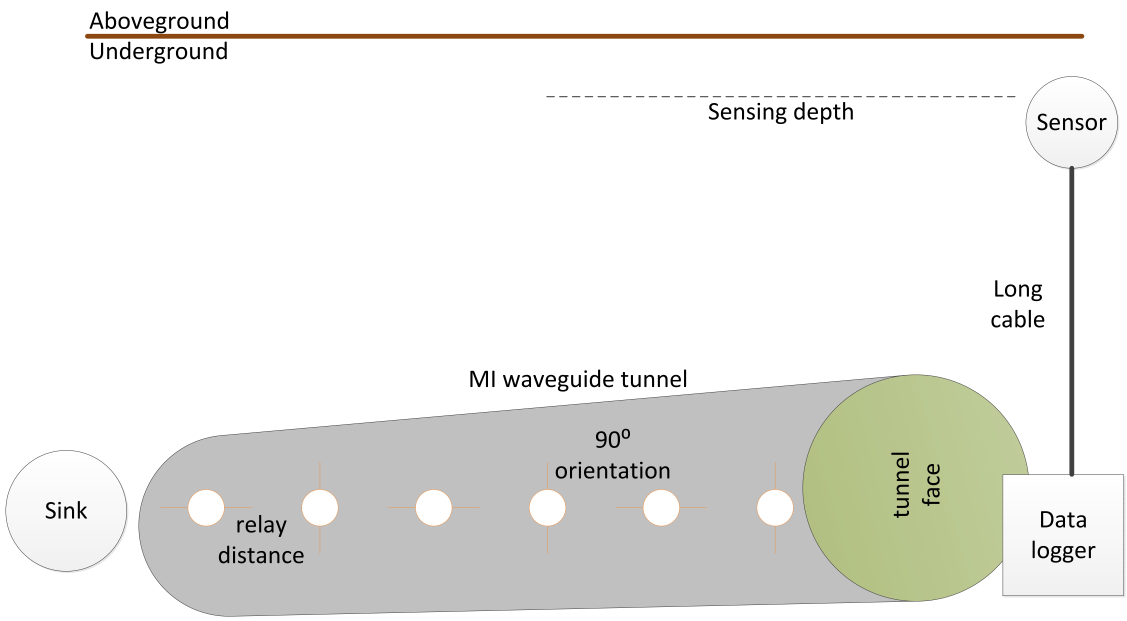

Figure 8.2: MI waveguide tunnel with underground data logger

Figure 8.3: Schematic representation of prototypical composite MI waveguide tunnel

For the sake of the reader's convenience, the same has been reproduced below:

$$C = \frac{2}{\omega^2 N^2 \mu \pi a} \tag{8.1}$$

This value of the capacitor imposes restrictions on the operational frequency of the system, and the number of turns of the coil. The theoretical result in (Kisseleff, Gerstacker, Schober, Sun & Akyildiz 2013) draws the conclusion that in effect, capacitor constrained MI waveguide would have highly degraded channel capacity at high frequencies, depending on the soil conductivity (dry soil vs. wet soil). However capacitor constraint is also imposed by the factor of parasitic capacitance, which could dominate the coil circuitry if the value of the loaded capacitor falls below a certain minimum value (Sun & Akyildiz 2010*c*). Accordingly, a minimum value of 1 pF capacitor load has been set in the theoretical simulations related to MI waveguide improvements (Kisseleff, Gerstacker, Schober, Sun & Akyildiz 2013), (Kisseleff, Akyildiz & Gerstacker 2013).

In this research, operational frequencies in the UHF band have been considered for the MI waveguide system, as mentioned in the context of the discussion pertaining to ARPT RFID simulation in the previous chapter. Consequently, the value of the capacitor load could fall below that of parasitic capacitance as per equation 8.1.

In order to address this issue, in the vein of the purported *analogical thinking* (Gassmann & Zeschky 2008) based approach, the author explored the relevant research on the minimization or elimination of parasitic capacitance for wound inductor coils. Early research (Massarini & Kazimierczuk 1997) on parasitic capacitance for wound inductor coils had identified the following classes:

- turn-to-turn capacitance between turns of the same layer
- turn-to-turn capacitance between turns of adjacent layers
- turn-to-core capacitance
- turn-to shield capacitance

Of these classes, only the first one is relevant for MI waveguide coils (Sun et al. 2013).

NOTE

The fact that a stream of the current theoretical research continues to be based on single layered coils, despite the observation in (Syms, Young & Solymar 2006), had been indicated during the course of the discussion under Chapter 4. The author shall revisit this specification of single layered coils outlined in (Sun et al. 2013) while concluding this dissertation, within the context of possible future improvements to the MI waveguide theoretical model (Sun & Akyildiz 2010*c*) for WUSNs.

The problem of parasitic capacitance reduction has been a recent preoccupation in the design of Electro-Magnetic Interference (EMI) filters in power electronics. Accordingly, there has been some innovative research output in this direction. The author would like to point out one such research output (Wang, Lee & van Wyk 2006) due to its close similarity and relevance to the problem in hand.

The solution approach outlined in the above research output is based on the concept of *mutual capacitance*, which had been originally presented in an earlier research (ling Yang 1992). In (ling Yang 1992), the concept of mutual capacitance has been presented as the *dual* of mutual inductance. Just as in the case of mutual inductance, mutual capacitance can be either positive or negative.

In (Wang et al. 2006), this notion of mutual capacitance has been used to eliminate the parasitic winding capacitance (same as intra-layer turn-to-turn capacitance (Massarini & Kazimierczuk 1997)) of coupled inductor coils wound on a toroidal core, by means of loading suitable additional diminutive capacitors in each coil. Simulation results in keeping with suitable coil parameters for the chosen EMI filter show considerable performance improvement in terms of increased resonant frequency of the coupled inductor coils. In addition, practical suggestions pertaining to how such diminutive coils can be integrated into large scale coil manufacturing have also been provided.

The result of this approach is encouraging and can be adopted for cancellation of parasitic capacitance in the case of MI waveguide coils at higher frequency ranges. However, the differences between the MI waveguide system model and the power electronics device model considered in (Wang et al. 2006) should be taken into account as well. For instance there are vast differences between the two system models in terms of the intended functionality, the operational frequency, and the coil specifications and parameters.

In spite of the contrasts, using the mutual capacitance concept in designing circuitry to mitigate or cancel winding parasitic capacitance of MI waveguide coils can be a viable approach, based on the results presented in (Wang et al. 2006), with suitable modifications. The author shall wind up with this pointer to future researchers in this area, as the specifics of such design are well beyond the scope of this dissertation, and would consume an entire dissertation by itself. However, before closing this section, the author would like to point to the lack of consideration of this highly viable solution approach in the theoretical research related to MI waveguide WUSNs thus far. This is another typical example of how the theoretical research has been largely oblivious to very relevant solution pointers both within and outside the domain of MI waveguides, to certain critical issues derailing progress in this research area.

8.3.3 Domain Network Model

Before proceeding to the discussion about the network model, the author would like to redraw the reader's attention to certain preoccupations in the theoretical research related to MI and MI waveguide WUSNs. These preoccupations have formed the basis for the network model that is the topic of discussion under this section.

One of the key preoccupations of the theoretical research on MI and MI waveguide WUSNs has been the notion of multi-node transmissions (Kisseleff, Akyildiz & Gerstacker 2013), (Kisseleff, Gerstacker, Sun & Akyildiz 2013), (Lin et al. 2014), and the inter-node interference (Kisseleff, Gerstacker, Sun & Akyildiz 2013) caused thereof. The basis of such theoretical inclination has been the communication paradigm in traditional wireless networks. However, it has also been pointed out categorically that the MI and MI waveguide WUSNs differ quintessentially from the traditional wireless networks in terms of channel and network models (Sun & Akyildiz 2012), (Kisseleff, Gerstacker, Sun & Akyildiz 2013). Another preoccupation pertains to the deployment algorithms for WUSNs. The deployment algorithms considered in (Sun & Akyildiz 2010*b*) do not lend themselves easily to a network plan based on a practical deployment strategy, except for the MST algorithm. The MST algorithm verges on a random deployment strategy, as the only criterion is the shortest distance between two nodes.

In this report the author proposes a network model for MI waveguide WUSNs within the chosen application context, which addresses both of the theoretical snags highlighted above. The model has been based, in accordance with *analogical thinking* (Gassmann & Zeschky 2008), on the concept of a *domain* inherent to many Voice over Internet Protocol (VoIP) networks such as H.323 (ITU-T 2009) and the Session Initiation Protocol (SIP) (Rosenberg, Schulzrinne, Camarillo, Johnston, Peterson, Sparks, Handley & Schooler 2002).

NOTE

The author would like to clearly emphasize at this point that although there are similarities to the star network model in WSNs (Karl & Willig 2005), the concept of a domain is original and intrinsically disparate from the star network model in its details.

The proposed network model based on the domain concept has been centred on the following premises:

- elimination of inter-node interference along with the optimization of channel and system usage, by means of quelling multi-node transmissions without losing out on efficiency.
- emphasizing on a highly localized deployment strategy, which is easy to implement, maintain and troubleshoot.

From hereupon, the author shall refer to this network model as the *domain network model*. The analogical solution approaches related to network longevity outlined under the next section assume the domain network model as the underlying WUSN architecture.

NOTE

It is a very reassuring coincidence that during the course of the work on this dissertation, the author came across two recent research outputs (Silva et al. 2014), (Silva, Liu & Moghaddam 2013), which have proposed network models for WSNs akin in spirit to the domain network model proposed and detailed hereunder.

8.3.3.1 Salient Features

NOTE

In the following discussion on the domain network model, the sensor node design has been envisaged analogous to the EC-5 Soil Moisture Sensor (Decagon 2014*b*); similarly, the aggregator node design has been envisaged analogous to the Em50 Series Data Collection System (Decagon 2014*c*). All the relevant specifications for the chosen reference prototypes, including power and baud rate, are adaptable to the corresponding sensor or aggregator nodes, respectively.

The following are the salient features of the domain network model:

- The domain model represents a highly localized communication paradigm. The domain is the basic unit of classification. Each domain is a standalone entity, and all the elements therein can be uniquely identified by means of a suitable addressing logic. Each domain consists of a single sink node, multiple aggregator nodes, and a set of sensor nodes attached to each aggregator node. This clear demarcation helps to manage the network deployed over a large area very efficiently. In addition, it also facilitates a rapid turnaround time for both maintenance and troubleshooting tasks. Moreover, the domain model is also easily scalable to accommodate network growth.
- Communication is highly organized within each domain. There is no direct communication between the sensor nodes and the sink node within a domain. Instead, based on the current application context requirements, communication is confined only between the sensor nodes and the aggregator node, and each aggregator node and the sink node.
- Communication between the aggregator node and the corresponding sensor nodes can either be using a dedicated serial port connection as per the current practice (Decagon 2014*c*), or by means of another innovative method to achieve both data and power transfer between the sensor and the aggregator node simultaneously. This has been detailed under the next section.
- Communication between each aggregator node and the sink node happens by means

of the MI waveguide tunnel. A cable connection is envisaged between each underground sink node and aboveground sink node. The nature of this connection has been detailed under the next section.

NOTE

Although this design infringes on the notion of a wireless connection, this arrangement has been envisaged as a stopgap until more nuanced methods to achieve the same functionality can be identified. The author shall dwell more on this aspect while concluding this dissertation.

Moreover, the wired connection has been deemed to be suitable as a temporary workaround. The placement of the aboveground sink nodes in the domain model has been envisaged at appropriate boundaries earmarked, so as not to interfere with normal operations in the chosen application context.

- A polling mechanism has been envisaged for data collection between the aboveground sink node and the underground sink node, the underground sink node and the aggregator nodes, and the aggregator node and the corresponding sensor nodes. The aggregator node should periodically excite each sensor node in turn with a requisite voltage for sensing the rhizosphere soil moisture and communicating the reading, similar to the existing practice (Decagon 2014*b*). An hourly sensing interval is deemed to be sufficient, similar to a previous research on soil moisture sensing discussed under Chapter 3 (Tiusanen 2009). The underground sink node should poll data from each aggregator node in a round-robin fashion, for every update interval of 1 hour. A similar round-robin polling schedule is envisaged among the aboveground sink node and the associated underground sink nodes across multiple domains.

- Even though the current application requirement is met by means of the master/slave communication paradigm between all the relevant network elements, a future requirement could necessitate communication among aggregator nodes, thus bringing in the peer-peer dimension. This requirement can also be addressed by extending the communication mechanism and protocol currently envisaged between the aggregator node and the underground sink node.

- The notion of a well-defined communication protocol in VoIP networks (the analogy since the domain model has been derived from VoIP protocols as stated previously) has been substituted in this model with the notion of a *representative data model*. This is an improvement on the retention and transmission of sensor readings in raw format by the aggregator (Decagon 2014*c*). Using the representative data model, the aggregator could map the raw data to a highly reduced bit pattern or a code word which could even be indicative of a particular range of sensor output, and communicate only the reduced bit pattern or the code to the sink node. This variant of data modelling is also analogous to the specific set of protocol messages inherent to either H.323 (ITU-T 2009) or SIP (Rosenberg et al. 2002), wherein each message encodes a particular stage or event associated with the system operation. In scenarios wherein the sensor readings are ultimately meant for human consumption, the usage of such nuanced data processing can drastically reduce the volume of data exchanged over the network without losing any of its significance, and thus enable power, as well as network traffic and resource efficiency. Even in systems wherein the sensor readings are intended to drive actuators, there could be intermediary systems or even in-built systems with the actuators, which could decipher the bit pattern or code to get at the sensor output.

NOTE

The design proposed for the chosen application context is also intended to be interworking with an actuator system to regulate water pumps based on an event-triggered model (Mazo & Tabuada 2011).

Moreover, the representative data model can also enable enhanced network security and integrity of data sent over the network.

- The domain network model obviates the need for multi-node transmissions and consequent inter-node interference, since the envisaged polling mechanism effectively addresses the coordination problem among multiple nodes. In addition, due to the fact that no direct communication is required between the sensor nodes and the underground sink node, and because of the fact that the representative data model drastically reduces the number of bits corresponding to the readings performed by a group of sensor nodes, the prospect of interference is further reduced.

  The MAC layer design concepts outlined above eliminate the impact of multi-node transmissions and ensuing interference. The network efficiency is still maintained, due to the envisaged polling mechanism and directed communication. This addresses the first preoccupation of theoretical research highlighted at the beginning of this section.

- The domain network model affords a very simple yet highly organized deployment strategy, which as mentioned above also enables the prospect of easy maintenance and troubleshooting post deployment. This is a huge advantage compared to the deployment algorithms presented in (Sun & Akyildiz 2010*b*), most of which are highly complex and unsuitable to a practical deployment scenario. Moreover, the domain network model is preferable to the MST algorithm as well, since it is robust to node failures due to its inherently different network architecture. Besides, the domain network model is more amenable to the notion of a planned deployment strategy than the MST algorithm.

  The domain network model also enhances the prospect of immediate node failure detection, as the representative data model from a node group can be designed to highlight such eventualities. This also sheds light on the flexibility offered by the domain network model, and the alternate options for accomplishing specific objectives in a deployed system.

  On these accounts, the domain network model also addresses the second preoccupation of the theoretical research highlighted at the beginning of this section.

8.3.3.2 Delineation of the Domain Network Model for the Chosen Application Context

Fig. 8.4 shows a representative sketch of the proposed domain network model for 1/4 hectare (2500 square meters) in the pecan farm.

The typical planting pattern of the farm allows for roughly 40 trees per 1/4 hectare. Each sensor node is deployed in the middle of the rhizosphere region of a row of 4 trees planted diagonally across one another. The proposed design envisages a minimum of 5 serial connections to an aggregator node, thus covering a total number of 20 planted trees. Thus a minimal network configuration would require 10 sensor nodes and 2 aggregator nodes to cover a single domain. The single underground sink node would be positioned at the edge of the domain. Depending on the coverage area stipulated for a domain, the lateral length of the wire-link between the sensor node and the aggregator node also needs to be taken into account. This has not been highlighted in Fig. 8.4.

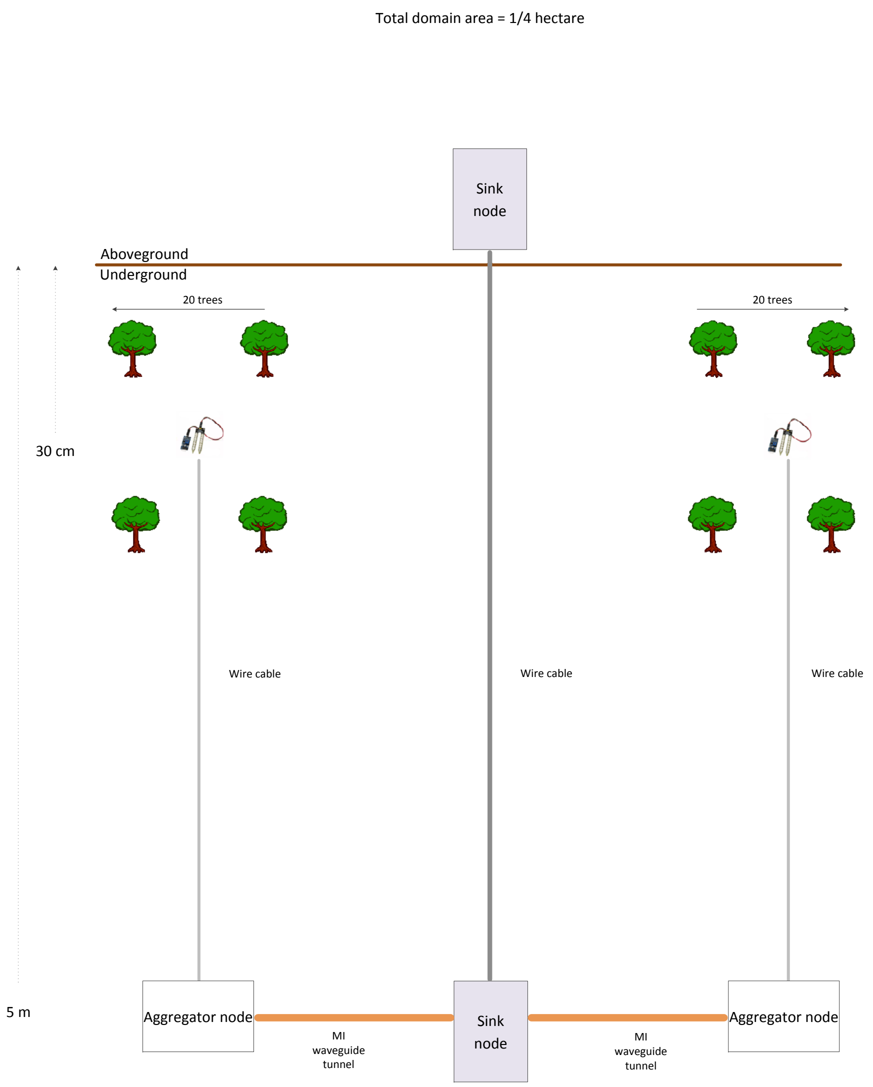

Figure 8.4: Domain network in a section of the pecan farm

8.4 Novel Longevity Model and Communication Concepts

The innovation model presented under this section is more hypothetical in its elements than the rest of the novel solution approaches detailed in this chapter. Despite this fact, the model has been founded on pragmatic analysis and conceptualized using previously proven solution models. This model is a more profound example of the *analogical thinking* (Gassmann & Zeschky 2008) concept. The model and all the related components detailed hereunder have been customized for the chosen application context.

The following discussion has been classified under two subsections. In the first subsection, the author discusses about power generation and storage. In the second subsection, power distribution design has been explained.

8.4.1 Power Generation and Storage

One of the major concerns related to WUSNs is about the longevity of the sensor nodes deployed underground, due to the fact that replacement of the nodes or recharging the nodes may not be easily accomplished after deployment (Akyildiz & Stuntebeck 2006). Thus conservation of battery power of sensor nodes is of primary concern in WUSNs. Current sensor node designs are mostly powered by a battery included as part of their operational mechanism (Dewan, Ay, Karim & Beyenal 2014). Although battery powered devices are easier to deploy, especially in the difficult underground terrain, the longevity of battery powered devices is limited. Moreover, the preoccupation with saving battery power also often restricts the optimal usage of such devices.

In order to overcome the dependency on battery, recent research has focused on novel methods of power harvesting for sensor nodes using ambient energy sources (Dewan et al. 2014). Such research is in its preliminary stage, and there are various sources that can be tapped into for harvesting power, depending on the location of deployment of the sensor nodes (Dewan et al. 2014). Considering the difficulty involved in replacing the battery of sensor nodes post deployment, the model outlined below has considered a rechargeable battery (Vinoy & Prabhakar 2014) for the WUSN nodes, which could be powered using energy harvested from ambient sources.

The following source categories can be considered for harvesting ambient energy:

- sources underground, from which power could be harvested and supplied to the WUSN nodes by means of a suitable mechanism.
- sources aboveground, from which power could be harvested and supplied to the WUSN nodes by means of a suitable mechanism.
- a combination of the above.

There has been very little research output on power harvesting underground using ambient energy sources. An earlier research output (Lawrence & Snyder 2002) examined the possibility of using a thermoelectric micro-generator to harvest power underground, leveraging on the temperature difference between air and underground. This study was conducted in a feasibility mode, and the practical deployment implications have been omitted. Besides, the amount of power harvested falls way short of the required power for soil moisture sensors (Decagon 2014*b*). The piezoelectric method for harvesting power underground has gained attention due to its capability to leverage on ambient mechanical vibrations such as thunder and aboveground activity. A recent study (Singh, Kumar & Weber 2014) reports the design of a non-linear bistable piezoelectric harvester and synchronized extraction model with significant output gain compared to other existing models. However, the resultant power output still falls short of the minimum required power for current soil moisture sensors (Decagon 2014*b*).

In spite of the above facts, there is a certain uncertainty factor associated with underground power harvesting innovations that have not been tested under field conditions, even though the simulation results are highly encouraging. This stems from the potential problem that any practical issues encountered would be hard to resolve in the case of underground deployment, after the fact. In view of this uncertainty, the model has excluded underground power harvesting and focused on aboveground power harvesting, and the feasibility of storing and transferring the generated power underground.

The weather condition in the northern part of New South Wales (where the farm is located) around the year on the average verges on medium-hot temperatures (Bureau of Meteorology 2015) with plenty of sunlight. In addition, the farm region is characterized by medium to strong winds averaging to 9 m/s (Resources & Energy 2014), with the maximum wind during the night.

NOTE

Based on the wind speed the calculated wind class is **7** at 80 m, which corresponds to the hub height of modern 77-m diameter, 1500 kW turbines (Archer & Jacobson 2005).

Since solar energy is the best ambient power source during bright days in an open environment (Tan & Panda 2010), it can be effectively complemented during the night time by means of power harvested from wind energy. Besides, since the farm is subject to intense aboveground vibrations during the day time due to human activity including operation of agricultural and transportation machinery, *augmented* piezoelectric conversion methods can be exploited to advantage for harvesting additional power during daytime.

NOTE

By augmented piezoelectric conversion methods, the author implies design options analogical to that outlined in (Worthington 2010).

These options led to the natural concerns about how to methodically and effectively scatter the power harvesting infrastructure across the land area, and how to collate the generated power for an organized local distribution. Considering the domain network model, the schematic of the proposed arrangement for distributive power harvesting, and collated localized storage and distribution is shown in Fig. 8.5.

The entire architecture displayed in Fig. 8.5 revolves around the domain network model. The underlying principle has been to localize power storage and distribution required for a given domain within the domain itself, so that the domain concept becomes essentially self-contained in all respects, not just in terms of the network architecture alone. The following distinct architectural facets were amalgamated, towards this end:

Localized Power Harvesting and Collation: A hybrid microgrid (Majumder 2014) installed on the farm is proposed to meet this requirement. All the distributed power harvesting sources scattered across all domains would interface and upload to the microgrid (Jiang & Yu 2009).

Localized Power Storage for Distribution: In order to meet this requirement, a storage mechanism co-existent with the aboveground sink node in each domain is proposed. The storage associated with the aboveground sink node is envisaged as an array of suitably large batteries or supercapacitors (Patrice Simon & Dunn 2014).

Uninterrupted Power Supply: Ambient power sources can be subject to fluctuations in terms of the quantum of power generated (Dewan et al. 2014). In order to ensure an uninterrupted power supply around the year, the solution proposed is to integrate the hybrid microgrid with the power grid supplying power to the farm.

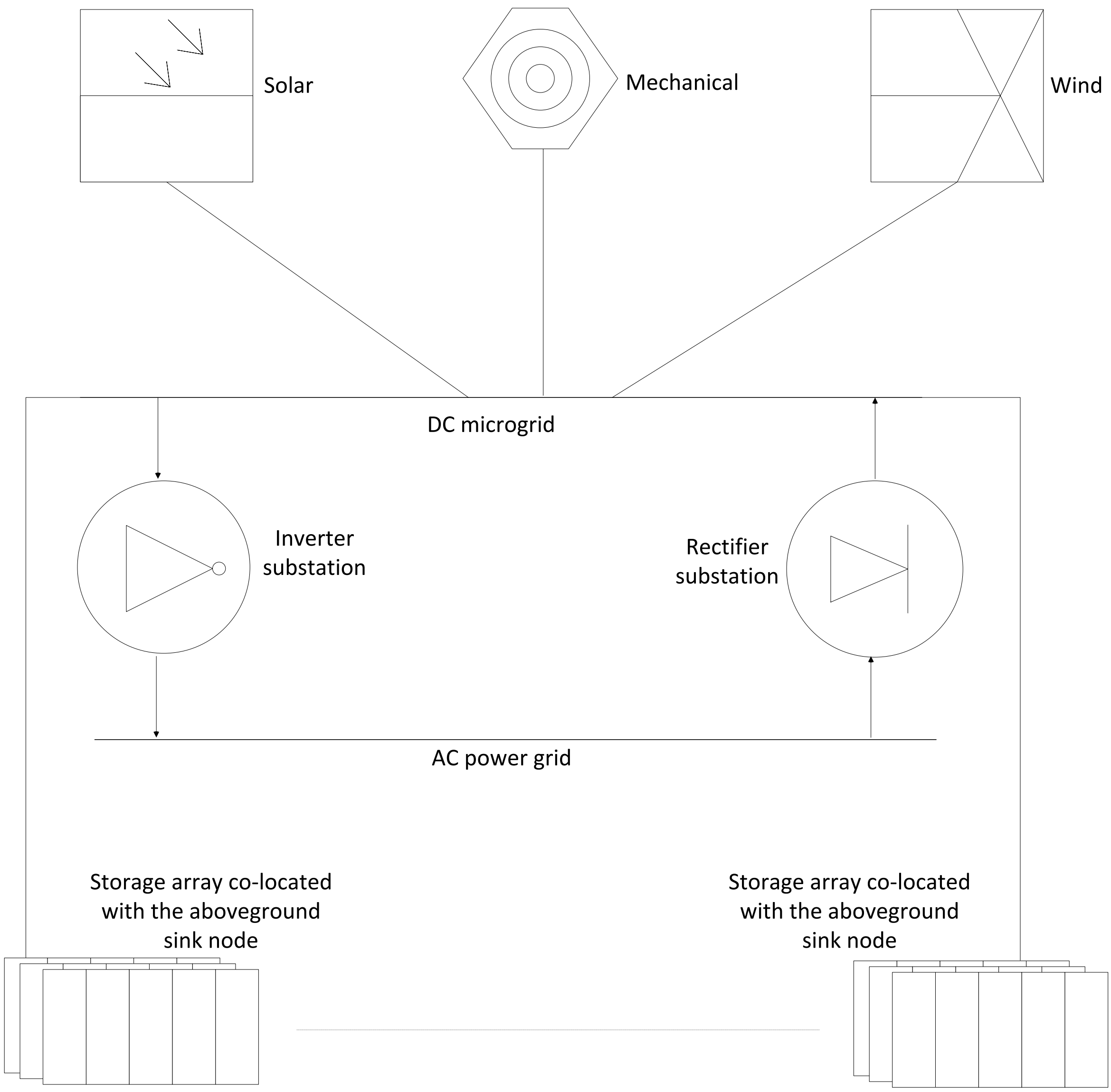

Figure 8.5: Schematic layout of the hybrid microgrid structure envisaged for localized power storage and distribution

NOTE

Integration with the power grid was the major decider in choosing the hybrid microgrid design (Majumder 2014) in the first place.

The microgrid could both tap into the power grid for additional power, as well as deposit excess power generated onto the power grid (Jiang & Yu 2009). This arrangement would ensure an undying supply of power to the WUSN around the year.

8.4.2 Combined Power and Data Distribution Model

Power distribution based on the domain network model has three distinct components:

- power delivered from the aboveground sink node to each underground sink node
- power delivered from the underground sink node to each aggregator node
- power delivered from the aggregator node to each associated sensor node

A combined power and data transfer model has been envisaged for each of the above components. The author ties together several previous innovations in the power distribution model, in order to enable simultaneous power and data transfer in the case of each of the above components. The following subsections cover each of the above components in detail.

8.4.2.1 Aboveground to Underground Sink Node Link

In order to realize simultaneous power and data transfer between the aboveground and the underground sink nodes, a link design is proposed analogical to the model presented in (Fisher, Burns & Muther 1999). In the case of the link, the coupler de-coupler mechanism in the model would have to be powered by the aboveground sink node. The link is envisaged as a two way communication channel.

8.4.2.2 Underground Sink Node to Aggregator Node Link

The following models have been integrated in the proposed link between the underground sink node and each aggregator node within a given domain, for simultaneous power and data transfer:

- Conceptually, the link between the underground sink node and the aggregator node is an active-passive RFID link, analogical to the innovation proposed in (Posamentier 2013). In this case however, the dual sense is imparted to the link because of the fact that a portion of the signal power from the underground sink node (reader) is used to recharge the battery of the aggregator node (tag). Thus even though the aggregator node is active because of the presence of a battery, since power is harvested from the underground sink node signal for recharging it is passive as well.

NOTE

A quick observation about the ARPT RFID design approach employed in the case of this link; the simulation results presented under the previous chapter showed the non-feasibility of the model for MI waveguide WUSNs. However, in the case of the current link, since the communication between the underground sink node and each aggregator node within a domain is envisaged by means of the MI waveguide tunnel, it has been assumed with reasonable cause that the performance impediments caused due to coil misalignment evident in the simulation results would be rendered null and void.

- In terms of actual implementation specifics, for maximum Power Transfer Efficiency (PTE) in the UHF band, the forward link can be modelled analogical to the Wireless Power Transfer (WPT) design proposed in (Cato & Lim 2014). The WPT design comprises of a 4-W transmitter connected to a 6-dBi Yagi antenna, a 4-W receiver with a miniature bi-quad antenna, a matching network constructed using an L-network topology (Sobot 2014), a low-voltage booster circuit, and a large capacitor for energy storage. These design nuggets can be incorporated into the design of the underground sink node and aggregator node respectively. The capacitor specified in the design could be substituted by a suitable battery for the aggregator node. In the case of the reverse link, a similar model proposed in (Kadil & Adane 2012) using a parabolic reflector can be adapted for maximum transmission efficiency. Thus in effect, the proposed implementation model of the two way transmission/reception link combines the approaches outlined in (Cato & Lim 2014) and (Kadil & Adane 2012). In keeping with the 4-W transmitter design (Cato & Lim 2014), an improved basic circuitry necessary for RF (UHF band) low power/extremely low power harvesting at the aggregator can be modelled analogical to the design proposed in (Le, Mayaram & Fiez 2008) for >44 m transmission range, which is greater than the maximum transmission range attempted in the ARPT RFID MI waveguide model simulations presented under Chapter 7, and the maximum range of 110 ft. (33.528 m) reported in (Cato & Lim 2014). The high sensitivity passive rectifier circuit design presented in (Le et al. 2008) for RF to DC conversion can be used to harvest energy from even extremely low power transmissions. In turn, this can lead to optimal power transmission efficiency for the forward link.

- Recall the rotating antenna design (Barber & III 2000) discussed in the context of ARPT RFID simulation under Chapter 7. The same design can be reused for communication between the underground sink node and multiple aggregator nodes in a domain.

8.4.2.3 Aggregator Node to Underground Sensor Node Link

As stated previously, existing models (Decagon 2014*c*) make use of dedicated serial port communication for the link between sensor nodes and the data aggregator. In contrast, the author proposes a novel connection model for this link analogical to the recent Universal Serial Bus (USB) Power Delivery ((USB-IF) 2014) framework. The author would like to term this connection model as the *Aggregator Sensor Serial Bus Communication Protocol (ASBCP)*. The ASBCP could render the interface between the sensor node and the aggregator node analogous to that between a USB flash drive and the computer. The ASBCP should customize the USB standard in the following respects (suggestive not comprehensive):

- Supported delivered power, which is drastically different for sensor nodes than the 5V specified for USB Power Delivery ((USB-IF) 2014).
- Support a hub-like architecture for the aggregator interface so as to enable a large (practically unlimited) number of simultaneous sensor node connections.
- Support ideally unlimited cable length, considering the fact that the 5 m limit should not be applicable to the link due to the much reduced expected data rate. Besides, this should meet the additional requirement of the lateral length of the cables in the case of large coverage areas.

Using the ASBCP connection it should be possible to simultaneously transfer data and power between the aggregator node and the sensor node. *Thus the aggregator node could* *recharge the sensor battery while extracting the sensor reading by means of an excitation voltage.* Fig. 8.6 shows a schematic representation of the ASBCP link between an aggregator node and a group of attached sensor nodes in a domain.

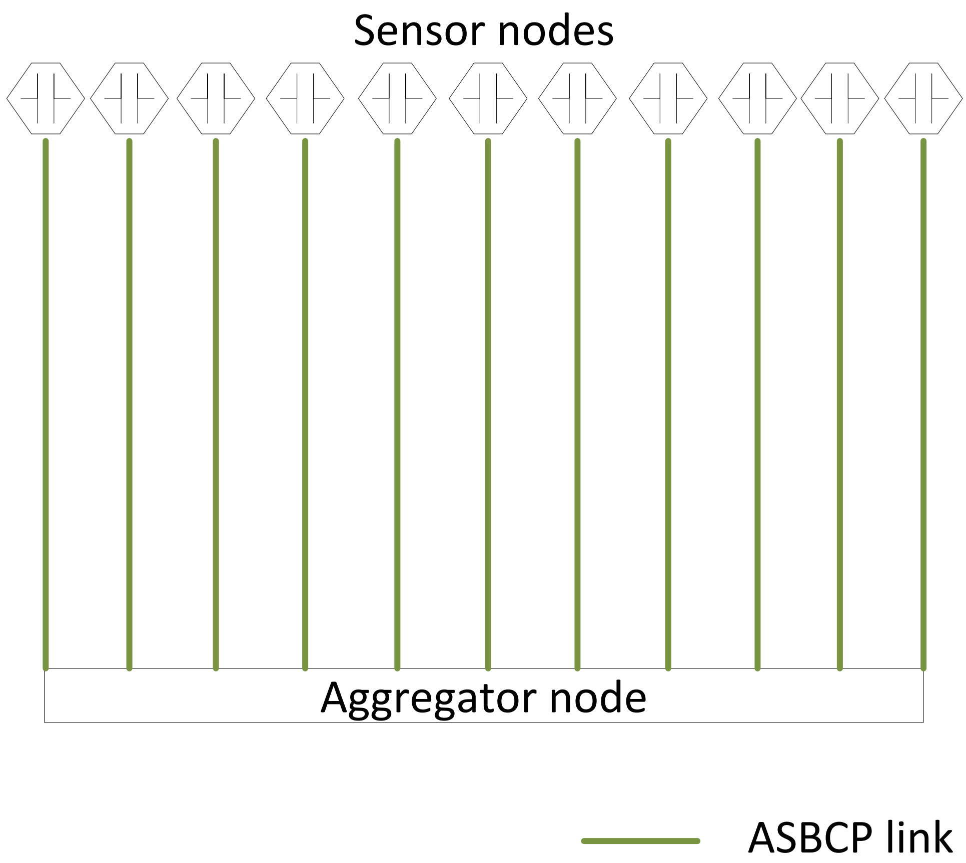

Figure 8.6: Schematic of the proposed ASBCP link between the aggregator node and sensor nodes

8.4.2.4 Synchronization of Power and Data Transfer for a Cycle

A cycle denotes a complete communication procedure with an hourly frequency (repeats every hour), during which data would be exchanged and power would be transferred between the nodes. The flowchart shown in Fig. 8.7 captures a complete communication cycle.

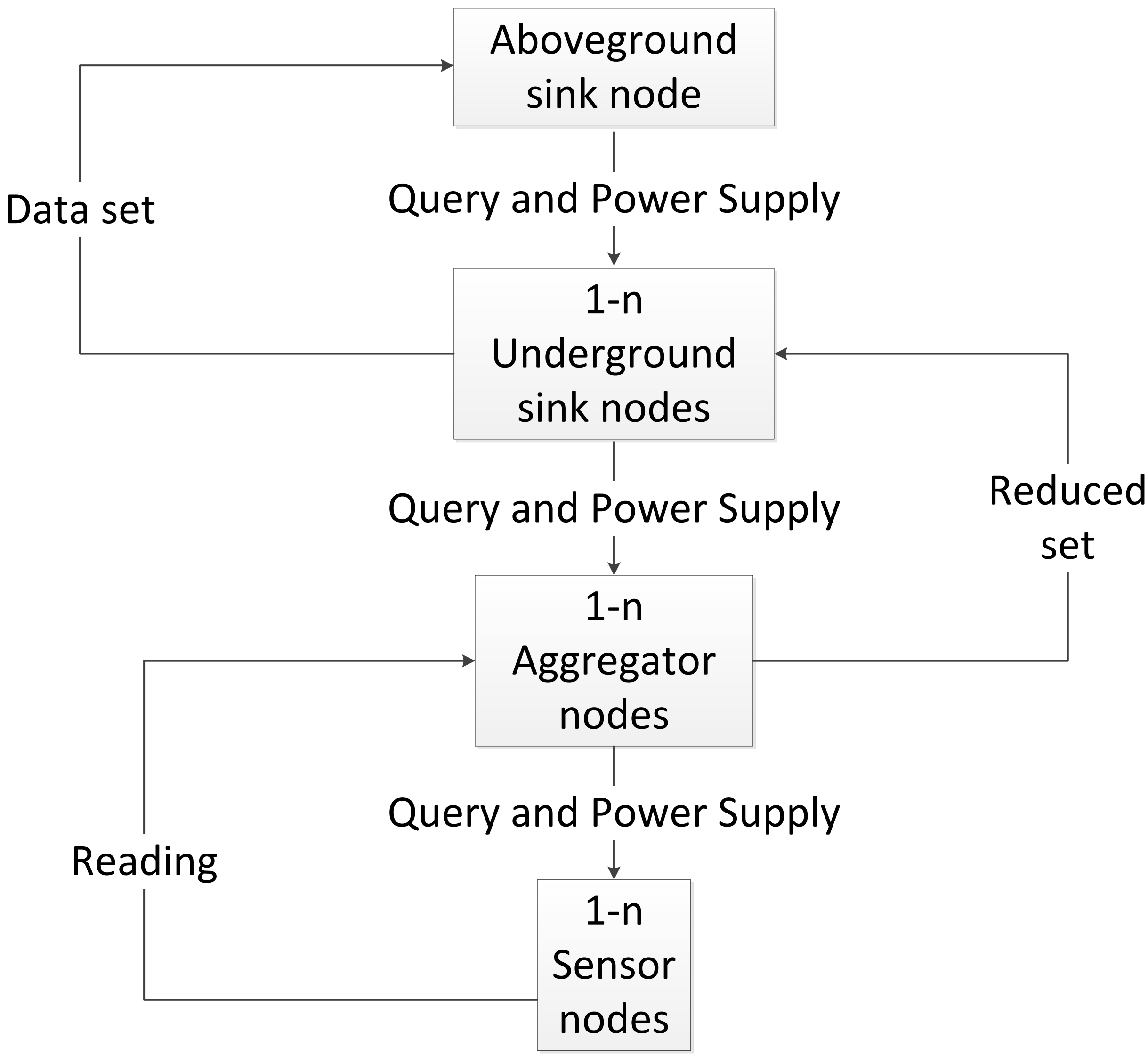

Figure 8.7: Flowchart for a typical hourly communication cycle

Each cycle would start with the aboveground sink node polling each underground sink node in turn, while transferring power to the underground sink node. The underground sink node would use a portion of the power to recharge its battery, and in turn poll each aggregator node through the MI waveguide tunnel. The aggregator node circuitry would capture the power in the signal, recharge its battery using a portion of the power and poll each sensor node in turn for a short duration (milliseconds), recharging the sensor node battery. The data read from each sensor node is mapped to the reduced bit pattern which is communicated to the underground sink node through the MI waveguide tunnel.

The cycle is completed with each underground sink node returning the data to the above-ground sink node. This synchronization of both data and power transfer ensures that the battery charge level of the underground nodes is always maintained above a certain minimum threshold. *Since the microgrid is supplemented by the power grid, this synchronization should ensure that the WUSN can operate indefinitely without any mediation after successful deployment.* The quantum of power transferred between each point-point communication in the cycle can be customized based on the power requirements of each receiving node.

8.5 Simulation and Results

The following analogical solution approaches were proposed under the previous section:

(a) The MI waveguide tunnel

(b) Mutual capacitance

(c) The domain network model

(d) Underground power distribution architecture and innovative connection models

The author considers the benefit of (b) to be self-deductive, based on the limiting impact of parasitic capacitance on the MI waveguide system performance (Sun & Akyildiz 2010*c*), (Kisseleff, Gerstacker, Schober, Sun & Akyildiz 2013), and the simulation results presented in (Wang et al. 2006). As observed within the context of the discussion on mutual capacitance, the purported solution in (Wang et al. 2006) needs to be adapted to the operational system specifications of the MI waveguide WUSNs.
Likewise, the impact of (d) on the longevity of the MI waveguide WUSN system should be evident based on the proposed architecture. The author believes that the cost aspects of (d), which should not be prohibitive for application contexts involving a substantial revenue turnover, should be overridden by the prospect of an enduring solution to uninterrupted WUSN system power supply.
In this section, the author uses simulation results from MATLAB to further drive home the validity of (a) and (c). All the simulations have been customized for the application

of MI waveguide WUSN within the chosen application context.

8.5.1 Simulation Scenarios

The different scenarios considered for the simulations have been listed below.

Scenario 1 Path Loss: In this scenario, the author considers the following theoretical issues associated with the MI waveguide model:

- Path loss impacted by soil characteristics (eddy current factor) (Kisseleff, Gerstacker, Schober, Sun & Akyildiz 2013)
- Path loss impacted by coil misalignment (Sun & Akyildiz 2010*c*), (Sun & Akyildiz 2012)
- Path loss impacted by large operational frequencies (Kisseleff, Gerstacker, Schober, Sun & Akyildiz 2013)

The author does not consider the impact of thermal noise aspect (Kisseleff, Gerstacker, Schober, Sun & Akyildiz 2013), as it is not impacted by the MI waveguide tunnel. The author investigates how for fixed transmission power and system bandwidth, the MI waveguide tunnel impacts the path loss and hence the SNR at the receiver end, and consequently the channel capacity. Unless otherwise specified, all the relevant simulation parameters in (Kisseleff, Gerstacker, Schober, Sun & Akyildiz 2013) have been reused.

Scenario 2 Deployment Complexity: In this scenario, the author examines how the domain network model facilitates a much simplified deployment strategy when compared to the simplest deployment strategy considered in (Sun & Akyildiz 2010*b*).

NOTE

In addition to the the domain network model being simpler than MST (Sun & Akyildiz 2010*b*), it is also qualitatively different in the sense that it is a highly organized architecture; MST verges on a random deployment strategy. This difference was noted within the context of the discussion on the domain network model.

8.5.2 Simulation Analysis

A brief analysis of the simulation scenarios listed under the previous subsection has been provided below.

NOTE

The simulation numbering continues from the previous chapter.

Scenario 1 Path Loss:

Unless otherwise specified, all the relevant simulation parameters in (Kisseleff, Gerstacker, Schober, Sun & Akyildiz 2013) have been reused.

Simulation 4: In (Sun & Akyildiz 2010*c*), the path loss of the MI waveguide WUSN has been mentioned as a monotonously increasing function of the variable $\frac{R}{\omega M}$. Thus it is obvious that the larger the value of the mutual inductance M, the lesser the path loss of the system. In (Kisseleff, Gerstacker, Schober, Sun & Akyildiz 2013), the impact of the eddy current factor of the soil on mutual inductance has been highlighted. *Since the MI waveguide tunnel obviates the need for the deployment of the coils in the soil medium, the eddy current factor can be omitted.*

The author shall demonstrate by means of the first simulation the fact that deployment using the MI waveguide tunnel increases mutual inductance, which in turn should decrease the path loss and improve the channel capacity.

Simulation 5: The impact of coil misalignment on path loss and channel capacity as highlighted in (Sun & Akyildiz 2010*c*) and (Sun & Akyildiz 2012), was detailed during the course of the theoretical review under Chapter 4. The author shall demonstrate by means of the second simulation and corresponding logic how the MI waveguide tunnel mitigates the path loss and augments channel capacity, by eliminating the prospect of coil misalignment after installation. In this simulation, the author has ignored the eddy current effect (Kisseleff, Gerstacker, Schober, Sun & Akyildiz 2013) on mutual inductance in order to curtail the extent of the simulation.

Simulation 6: In the third simulation, the author shall contrast the system performance as a function of path loss and consequently channel capacity (Sun & Akyildiz 2010*c*), for a range of operational frequencies with and without the MI waveguide tunnel. The range of frequencies considered for the simulation is from 10 MHz to 300 MHz, inclusive.

Scenario 2 Deployment Complexity:

Simulation 7: The author shall use the simulation results to show how the domain network model facilitates a much simpler deployment strategy in comparison with the MST algorithm for a 2D network proposed in (Sun & Akyildiz 2010*b*). A reduction in the complexity of the network structure should also positively impact the aspects of inter-node interference and network throughput (Shang, Huang, Mao & Liu 2014).

8.5.3 Simulation Results

The results obtained for the simulations outlined under the previous two sections have been reproduced below.

Scenario 1 Path Loss:

Unless otherwise specified, all the relevant simulation parameters in (Kisseleff, Gerstacker, Schober, Sun & Akyildiz 2013) have been reused.

Simulation 4: Fig. 8.8 shows the results of the first simulation which highlight the difference in the mutual inductance between two adjacent coils in dry soil, in the presence and absence of the MI waveguide tunnel. As can be observed from the figure, the mutual inductance is a flat line for the number of turns of the coil given by the X-axis, in the absence of the MI waveguide tunnel. ***This is due to the eddy current factor which impacts the coils deployed directly in the soil.*** On the contrary, the mutual inductance is mostly much higher in the case of the coils deployed by means of the MI waveguide tunnel. A similar effect is observed in the case wet soil as well, as shown in Fig. 8.9.

From Fig. 8.8 and Fig. 8.9, the impact of parasitic capacitance on mutual inductance with the increasing number of coil turns (Sun & Akyildiz 2010*c*)

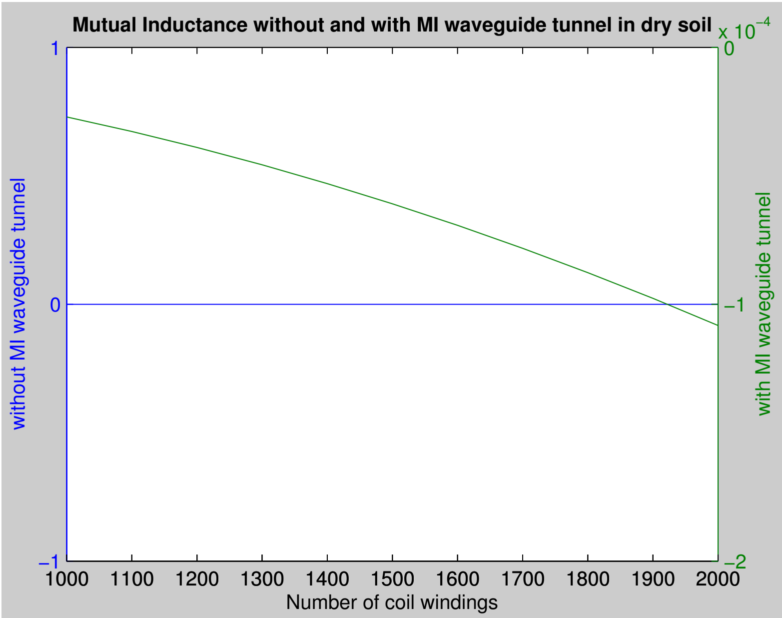

Figure 8.8: Difference in the mutual inductance between adjacent coils in dry soil without and with the MI waveguide tunnel

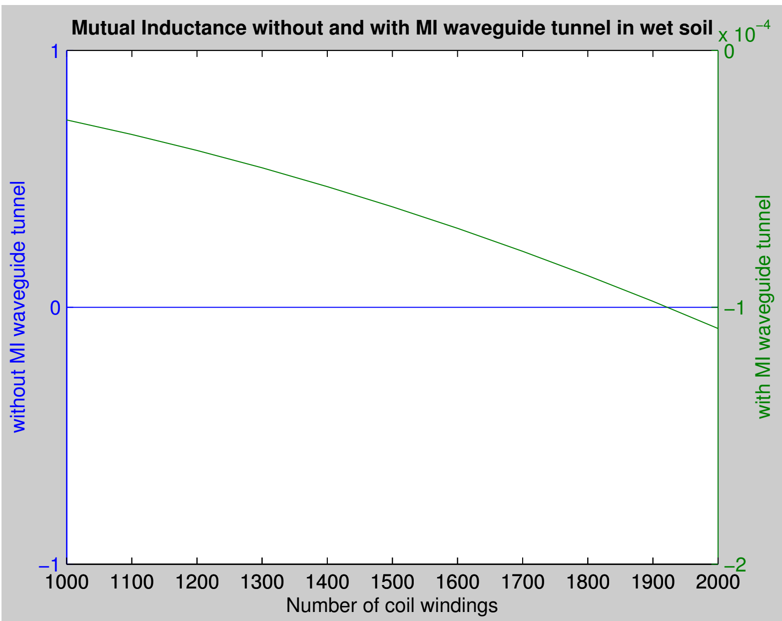

Figure 8.9: Difference in the mutual inductance between adjacent coils in wet soil without and with the MI waveguide tunnel

is also evident. The proposed solution approach based on mutual capacitance (Wang et al. 2006) thus holds the key to further improvement of the mutual inductance between adjacent coils deployed by means of the MI waveguide tunnel.

Simulation 5: For this simulation, the range of values for the orientation angle between two adjacent coils has been chosen from the vertical alignment (θ_t = θ_r = 0°) (Sun & Akyildiz 2012) to the horizontal alignment (θ_t = 90°; θ_r = −90°) (Kisseleff, Gerstacker, Schober, Sun & Akyildiz 2013), both inclusive. The author has ignored the negative angle values in this simulation, as the purpose is to demonstrate the impact of angular deviation on mutual inductance. A value of 5° has been chosen as the average variation between successive coil orientations. In this simulation, the author has also ignored the eddy current effect (Kisseleff, Gerstacker, Schober, Sun & Akyildiz 2013) on mutual inductance in order to curtail the extent of the simulation.

Fig. 8.10 shows the impact of coil orientation on the mutual inductance between adjacent coils. From Fig. 8.10, it is evident that the angle of orientation between the adjacent coils has a major impact on their mutual inductance.

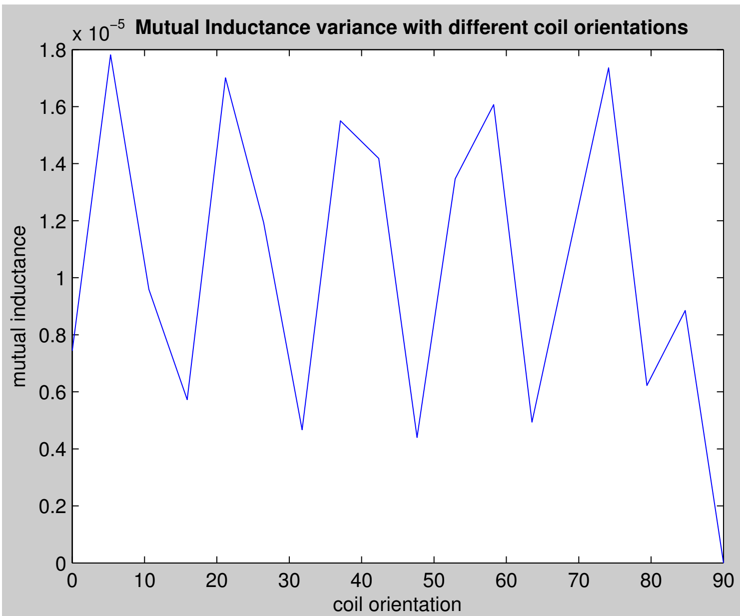

Figure 8.10: Impact of coil misalignment on mutual inductance

NOTE

As an aside, the simulation result also shows how the variance of mutual inductance with coil orientation angles does not strictly adhere to the theoretical notion of horizontal coil alignment for maximum mutual inductance (Kisseleff, Gerstacker, Schober, Sun & Akyildiz 2013). This is yet another example of how the theoretical assumptions do not coincide with deployment aspects. The result of this simulation further corroborates the results and the corresponding conclusions presented in the case of the ARPT RFID solution model for MI waveguide WUSNs under the previous chapter.

Since the coils are fixed to the inside of the MI waveguide tunnel at orientation angles for maximizing mutual inductance (vide. Fig.8.2), any fluctuation of the mutual inductance after deployment due to coil misalignment or displacement can be eliminated. Thus the problem of network planning and optimization is highly simplified as the performance of the system can be anticipated to a fair degree of accuracy, even before the actual deployment.

NOTE

Note that in Fig.8.2, the horizontal axis alignment has been shown for adjacent coils, wherein they are oriented mutually at 90° angle. However, the adjacent coils can be fixed inside the MI waveguide tunnel at a suitable mutual orientation for maximizing their mutual inductance.

Simulation 6: The derivations in (Kisseleff, Gerstacker, Schober, Sun & Akyildiz 2013) show the path loss as directly proportional to the following function:

$$F(x,n) = \frac{\left(\frac{x+\sqrt{x^2-4}}{2}\right)^{n+1} - \left(\frac{x-\sqrt{x^2-4}}{2}\right)^{n+1}}{\left(\sqrt{x^2-4}\right)} \tag{8.2}$$

where

$$x = \frac{Z}{j2\pi fM} \tag{8.3}$$

$$Z = j2\pi fL + \frac{1}{j2\pi fC} + R \tag{8.4}$$

and inversely proportional to $I_m\{\mathrm{x}_L\}$, where

$$x_L = \frac{Z_L}{j2\pi f M} \tag{8.5}$$

NOTE

In the above equations, Z denotes the coil impedance, M denotes the mutual inductance between adjacent coils, L denotes the coil self-inductance, C denotes the value of the capacitance loaded in the coil, R denotes the resistance of the coil material, f denotes the signal frequency, and n denotes the nth relay coil.

Based on equation 8.2, it can be observed that the path loss is an increasing function of x. Since x is shown to be inversely proportional to frequency and mutual inductance in equations 8.3 and 8.5, the path loss should be diminished by an increase in either of the two. In Fig. 8.11, the value of x for the MI waveguide has been shown for the range of frequencies in dry soil.

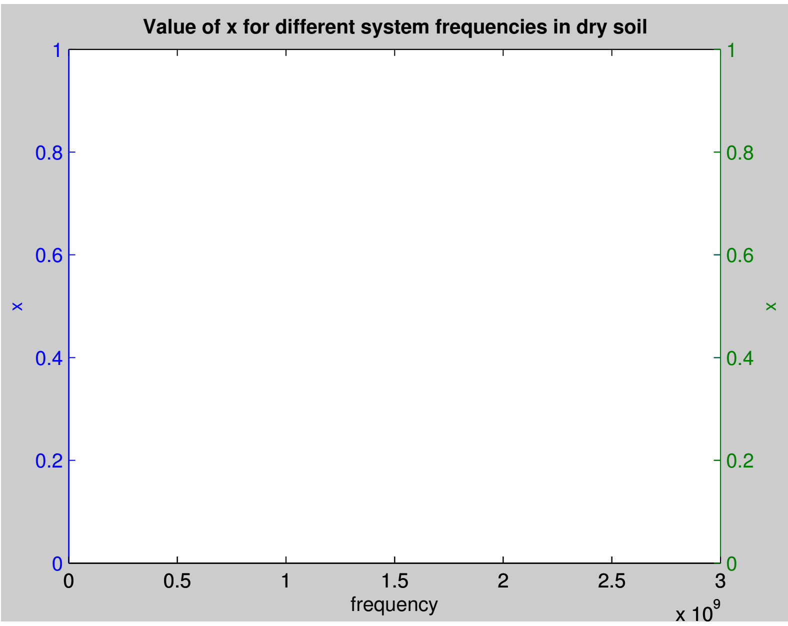

Figure 8.11: Value of x for the chosen frequency range in dry soil

As can be observed from the figure, the value of x swings between negative and positive infinities for different frequency values, due to the eddy current factor. A similar behaviour can be observed for the value of x in wet soil, as shown in Fig. 8.12.

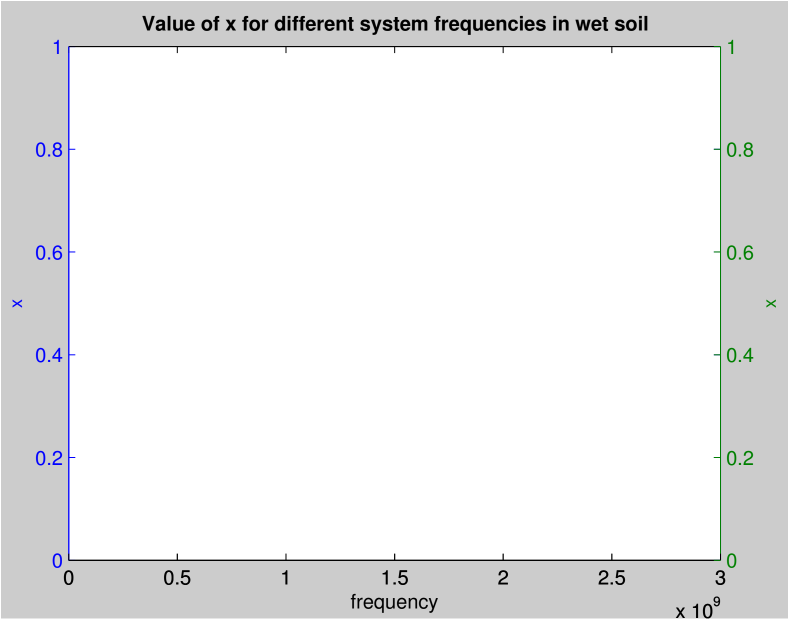

Figure 8.12: Value of x for the chosen frequency range in wet soil

In contrast, Fig. 8.13 shows the behaviour of x for the range of frequencies using the MI waveguide tunnel.

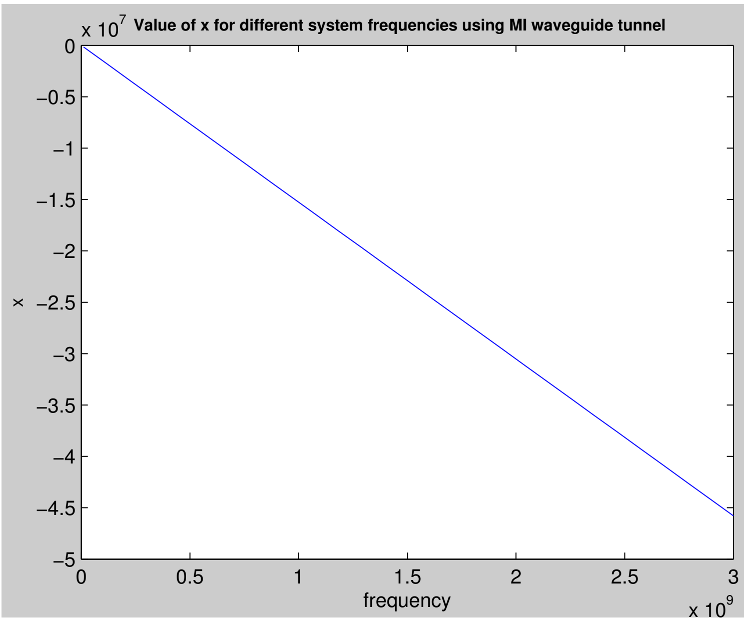

Figure 8.13: Value of x for the chosen frequency range using the MI waveguide tunnel

Since the eddy current factor is totally eliminated by the MI waveguide tunnel, the value of x now declines steadily with increasing frequency, as seen from Fig. 8.13. The results of the simulation conclusively demonstrate the positive impact of the MI waveguide tunnel on the system path loss, and consequently channel capacity.

Scenario 2 Deployment Complexity:

Simulation 7: The fundamental difference between the domain network model and the MST (Sun & Akyildiz 2010*b*) stems from the fact that while the latter is a representation of a random graph (Erdos & Renyi 1960), the former is not. The relationship between the number of edges and the number of vertices in a random graph is given by the following equation (Erdos & Renyi 1959):

$$N_c = [\frac{1}{2}nlogn + cn] \tag{8.6}$$

NOTE

In the above equation, N_c denotes the number of edges (links), n denotes the number of vertices (transceiver or relay nodes), c denotes any arbitrary fixed real number, and the square brackets denote the integer value of N_c.

In the case of the domain network model however, the number of MI waveguide links do not scale with the number of sensor nodes; rather the connection between each sensor node and the aggregator node in the domain is through a single independent cable link. *Due to this fact, the complexity of the network remains unchanged for a domain, irrespective of the scaling of the number of (sensor) nodes within in the maximum range allowed per aggregator node.*

This contrast is highlighted in Fig. 8.14 and Fig. 8.15, which show the network scaling factor as a function of the number of sensor nodes, and the corresponding number of MI waveguide links, for the MST and the domain network respectively.

In Fig. 8.14 and Fig. 8.15, a scaling of the network from 1 to 100 nodes has been considered. In Fig. 8.15, it has also been assumed that a maximum of 5 sensor nodes can be connected to the aggregator node, which should be the lowest limit applicable. This is also the underlying logic based upon which the linear progression pattern in Fig. 8.15 has been generated. The line connecting the peaks of the chart also indicates the number of links for number of nodes that are not a multiple of 5.

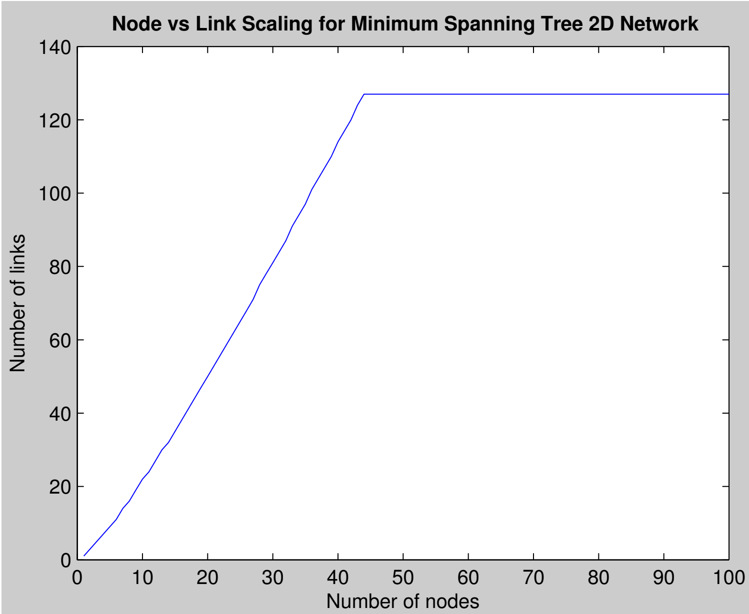

Figure 8.14: Number of MI waveguide links corresponding to nodes for the MST network

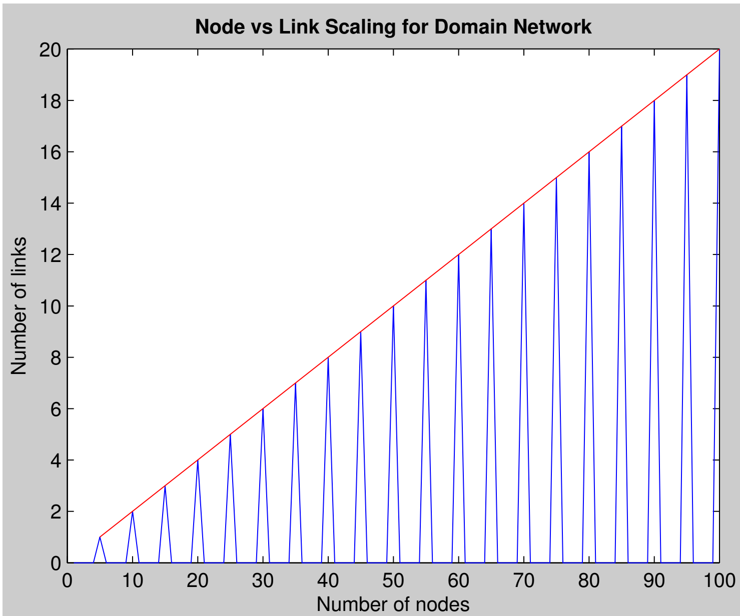

Figure 8.15: Number of MI waveguide links corresponding to nodes for the domain network

For the domain network model, an increment in the number of MI waveguide links is synonymous only with the increment in the number of aggregator nodes, since the MI communication is confined only between each aggregator node and the underground sink node for the domain. This is observable from the simulation output in Fig. 8.15. Even this increment in the number of links does not degrade the system performance, due to the segregation of each link by the MI waveguide tunnel.

In contrast, the scaling of the number of MI waveguide links is more pronounced in the case of MST, as shown in Fig. 8.14. Moreover, additional algorithms would be needed to mitigate the effect of interference in the case of multi-node transmissions. Even in the absence of multi-node transmissions, complex channel scheduling algorithms would be required to co-ordinate transmission between various sensor nodes on the same MST network.
A corresponding difference between the domain network and the MST is that in the case of the domain network, the number of relay coils do not scale with the increase only in the number of sensor nodes. Of course, it is a possibility that a new aggregator node is deployed to accommodate the additional sensor nodes, in which case there would be a one-time increase in the number of relay coils needed to connect the new aggregator node to the underground sink node in the corresponding domain. However, the author expects the frequency of such increase to be much lesser compared to that of the increase in the number of relay coils for the MST network.
Finally, unlike in the case of the MST network, the scaling factor for the number of MI waveguide links in the domain network is bound by the size of the domain. There can only be so many maximum number of MI waveguide links accommodated in a given domain, according to the specific network design.

8.5.4 Commentary

The author presented the alternate solution approaches based on *analogical thinking* (Gassmann & Zeschky 2008) to theoretical snags in the MI waveguide model (Sun & Akyildiz 2010*c*) under the previous sections. The results speak for themselves. The simulation results show how the concept of the MI waveguide tunnel drastically improves the performance characteristics of the MI waveguide WUSN system. In fact, the contrivance of the MI waveguide tunnel immediately eliminates two of the most apparently insurmountable impediments stated in the theoretical research on MI waveguide WUSNs till date: coil misalignment and eddy current factor.
The simulation results also convey the efficacy of the alternate solution approaches based on analogical thinking, in circumventing theoretical issues. The proposed analogical solu-

tion approach of the MI waveguide tunnel based on undergrounding is an example of how proven solution approaches could be borrowed from other domains, to circumvent theoretical issues in MI waveguide WUSNs. In a previous chapter, the author had indicated the need for a balanced approach in the research on MI waveguide WUSNs, which combines theoretical understanding with novel solution models rooted in analogical thinking. These models could be innovative workarounds, or conceptual paradigm shifts. The results of the simulations presented in this chapter corroborate the need for such a balanced approach. The scope for extensibility of the analogical solution models is also a point worth noting. It should be possible to adapt and transpose the innovations achieved using such models within one application context, to another similar or distant application context. For instance, the concept of the MI waveguide tunnel can be transposed to any application context involving MI waveguide WUSNs, with suitable adaptation.

The concept of mutual capacitance discussed under this chapter is another direction that has the potential to upgrade the performance benchmark of MI waveguide WUSNs. The introduction of this concept is also a very conspicuous example of analogical thinking, and its possible advantages.

The proposed innovation of the domain network model presents distinct advantages over existing deployment algorithms in MI waveguide WUSNs, as indicated by the simulation results. The larger import of the model is also the efficacy of analogical solution approaches in circumventing key theoretical issues, such as issues pertaining to multi-node transfer and consequent congestion and interference.

The longevity model presented stems from the domain network model. The model presents important paradigm shifts in the solution approach to the longevity issue in WUSNs. These include aboveground power generation and underground power transfer, and simultaneous power and data transfer. Both these novel concepts have been introduced for enabling sustained, uninterrupted power supply for WUSNs.

The wired connection paradigm used in the longevity model is contrary to the notion of a purely wireless paradigm in MI waveguide WUSNs. However, the author believes that the notion of a wired paradigm is equally worth pursuing in the context of MI waveguide WUSNs, *if the paradigm itself can be revolutionized by means of suitable innovations.* It is in this context that the research on MI waveguide WUSNs needs to pay close attention to the research on metamaterials and other such novel solution approaches, and borrow and adapt suitably from the respective domains. A more elaborate discussion on these aspects has been provided under the next chapter, as part of pointers to future research directions in MI waveguide WUSNs.

8.5.5 Source Code

The source code for the simulation results presented under this chapter can be viewed under Appendix A. MATLAB has been used for the simulations.

8.6 Chapter Summary

In this chapter, the author presented innovative workarounds and proposals rooted in analogical thinking, to theoretical impediments in MI waveguide WUSNs. The following distinct innovations or proposals were presented in improving the MI waveguide theoretical models:

- MI waveguide tunnel
- Mutual Capacitance
- Domain network model

A novel power generation and distribution model for MI waveguide WUSNs was also presented, with the following conceptual innovations:

- Aboveground power generation and underground transfer
- Simultaneous power and data transfer

Simulations were also presented to drive home the validity of selective innovations.
This chapter marks the culmination of this research. By means of the proposed analogical thinking based solution approach and corresponding innovations, the author believes that this research has opened a hitherto closed door in the research on MI waveguide WUSNs. What does the future hold in terms of possibilities by stepping through this door? What could be the challenges and which directions could be more rewarding? The author would attempt to answer these questions in the next (concluding) chapter.

Part III

Parting Thoughts

Chapter 9

Conclusion

9.1 Chapter Overview

In this chapter, the author summarizes the analyses, observations, results and inferences outlined in the preceding chapters. This chapter provides a synopsis of the value addition brought to the existing body of work by this research, in terms of both concepts and corresponding results. In addition, this chapter also dwells on the paradigm shift enunciated by this research, in the approach to research on MI based WUSNs.

In the process of outlining the above two aspects, the author draws on the numerous specific observations, instances, analogies and takeaways documented across the preceding chapters. Thus the discussion in this chapter also provides a summary of this dissertation.

9.2 Concluding Remarks

Throughout the course of this dissertation, a recurring theme has formed the central thread of argument for the *raison d'etre* of this research: *the aspect of the purely theoretical nature of the research on MI based WUSNs thus far, and how novel workarounds to theoretical stalemates have not been attempted as alternate solutions to issues; additionally, there has been no conscious initiative to look for such alternatives in other related or distant domains, adhering to the principle and practice of analogical thinking (Gassmann & Zeschky 2008).*

In the attempt to drive home this argument with conviction, the author carried out an exhaustive review the state-of-the-art literature on theoretical research in the domain. In this process of drawing on current literature to prove this point, the author followed a very deliberate and apt methodology, progressively interconnecting all the vital pieces in this subject matter:

- The author started off with discussing the issues confronting WSNs themselves, in spite of having been around as a technological entity at least for more than a decade and a half when compared to WUSNs. This exercise served to position the discussion on WUSNs and associated problems in the right spotlight, and how those problems were rendered even more intricate owing to the fact that WUSNs have originated from WSNs.
- Once the author was done with adequately highlighting the problems visiting WUSNs, the stage had been set to introduce MI based communication for WUSNs, which had emerged as the obvious alternative to EM waves. The author subsequently spent quite a bit of time reviewing the progress of research on this topic over the years, starting from its very origins. The author followed up with a thorough analysis of the state-of-the-art theoretical research on MI based WUSNs, throwing light on its pros and cons. This analysis also pointed to the critical theoretical issues in MI based WUSNs, which came in the way of deployment in any application context.
- The author then reviewed a cross-section of recent application of WUSNs in irrigation control. This review showed that the prospect of UG2UG communication has not been attempted in any of the contexts. This review also substantiated the issues confronting WUSNs outlined previously, which prevented UG2UG communication.
- The author subsequently prepared the context for the paradigm shift enunciated by this research, by introducing the principle of analogical thinking. The author also produced examples from both recent and not so recent scientific discoveries and technological innovations, to demonstrate how analogical thinking has or had been the pivot in such breakthroughs.
- The author then discussed at length the preliminary work done as part of this research. Simulations based on the state-of-the-art theoretical research models on

MI waveguide WUSNs were presented, and their results were used to demonstrate how such models were restricted by certain theoretical assumptions and key theoretical issues. The author also made it a point to outline another dimension of these simulations and their corresponding results; they marked a turning point in the alternate approach adopted by this research. The alternate approach embodied finding novel workarounds to certain key theoretical issues in MI waveguide WUSNs using analogical thinking.

- The author followed up with a detailed discussion of the innovative solution approaches rooted in analogical thinking. The author also demonstrated by means of selective simulations and their results, how the proposed innovations enabled effective workarounds to key theoretical issues in MI waveguide WUSNs.

The course of the above narrative of this dissertation is indicative of the prospect presented by such alternate solution approach rooted in analogical thinking, in revolutionizing the research on MI based WUSNs. The simulation results obtained for key issues in the theoretical models are suggestive of the enormous potential of such alternate approach, if taken seriously and followed up methodically. In this context, several of the novel solution approaches floated by the original research on MI, such as metamaterials and unique coil designs, all form part of this analogical thinking approach.

NOTE

The author shall elaborate a bit more on how such novel concepts could be used as part of the analogical thinking approach, under the next section.

The scope of analogical thinking extends much beyond the space for solutions to specific problems; in fact, as had been pointed out during the literature review on analogical thinking, often *distant* associations result in more creative ideas. The author would like to point out based on the discussion and results presented in this dissertation, that a radical perceptual change is needed in the envisioning of WUSNs, and their scope and applicability. Such change should be marked by a conscious effort in correlating the technical requirements, solutions and issues, to innovations and breakthroughs in other scientific and technological domains. In order to do so, it is essential to keep track of such innovations and breakthroughs, with the intention to explore their applicability in improving the technology of WUSNs. Such synergy should also enable to reposition the concept and scope of WUSNs; the author is of the view that a radical transformation could result in the very concept of WUSNs due to such repositioning. In order to substantiate this view, the author shall provide certain basic pointers of such repositioning under a following section.

9.3 Summary of Research Contributions

The following are the key contributions of this research to the existing body of work on MI based WUSNs, as outlined in the previous chapters of this dissertation:

I This is the first research output of its kind to technically assess the existing body of literature, with the objective of demonstrating the lack of alternate solution approaches to theoretical issues.

II This is the first research output of its kind to engender a novel paradigm shift, by introducing the concept of *analogical thinking* (Gassmann & Zeschky 2008) into the domain.

III This is the first research output of its kind to introduce novel workarounds to key theoretical issues in the domain; the following were the novel workarounds or pointers introduced:

- i the MI waveguide tunnel
- ii the domain network model
- iii the concept of mutual capacitance

IV This is the first research output of its kind to propose a novel paradigm shift in addressing the longevity issue in WUSNs in general, and present a heuristic model and associated novel communication concepts.

V This is the first research output of its kind to present simulations and corresponding results to validate selective novel workarounds to key theoretical issues in the domain.

VI This is the first research output of its kind to present patterns of a possible standardization option for deployment in the domain; the MI waveguide tunnel and the domain network model embody such options.

VII This is the first research output of its kind to present future directions of research in the domain, engendering the prospect of a paradigm shift in the concept of the domain itself. These directions have been discussed under the next section.

VIII As a by-product, this research output also introduced a novel numerical modelling algorithm for terrain modelling within the domain.

9.4 Future Directions

The author had dwelt on the theoretical stalemate hindering the progress of MI based WUSNs in the preceding chapters. In the process, the author had also emphasized on the need for alternate solution approaches based on analogical thinking. In the previous sections, it was suggested that the extent of such alternate solution approaches can be quite vast, enabling innovative interpretations to the concept of MI based WUSNs. In this regard, the author would like to commence with an aspect that had been dwelt on during the discussion under Chapter 8. This pertained to the replacement of cables used as a stopgap in the proposed heuristic deployment model for the chosen application context, with a suitable alternative.

The author would like to contextually draw the attention of the reader to the design of thin magneto-inductive cables proposed in (Syms, Solymar, Young & Floume 2010). The proposed design modifies a typical planar waveguide structure by serially subdividing the inductor and capacitor elements for large positive coupling within the waveguide, and realization of high-value integrated parallel plate components separated by a substrate of a thin dielectric interlayer, respectively. Since the substrate carries the same design on either side, a thin magneto-inductive cable could be realized by means of cascading substrates. This particular design of the thin magneto-inductive cable has been customized for MRI application, at approximately 100 MHz frequency. The experiment results show low propagation loss effected using the proposed design. There is a very good possibility of adapting this design to MI waveguide WUSNs. The author would go a step further and state that such thin cable design can very well replace the notion of wireless paradigm in WUSNs, even in the case of UG2AG and AG2UG communication. Thus returning to the longevity design that was proposed under Chapter 8, future research effort should be directed at how such thin magneto-inductive cables could be designed for low-loss propagation of a combined power and data signal between the aboveground and the underground nodes.

Intertwined with such a novel concept would be the issue of ensuring that the cables are pliant to the wear and tear of the application environment, particularly for shallow depth deployments in irrigation control. The author believes that the answer lies in biomimetics. The author had reproduced a relevant extract from (Bhushan 2009) under Chapter 6, which is repeated below for refreshing the reader's memory:

"Molecular-scale devices, superhydrophobicity, self-cleaning, drag reduction in fluid flow, energy conversion and conservation, high adhesion, reversible adhesion, aerodynamic lift, materials and fibres with high mechanical strength, biological self-assembly, antireflection, structural coloration, thermal insulation, self-healing and sensory-aid mechanisms are some of the examples found in nature that are of commercial interest."

So it is necessary to look for analogical solutions in nature, and perhaps even other domains, for design clues to low propagation loss, thin yet pliable, magneto-inductive cables that can be customized to the requirements of a given application context, in order to facilitate UG2AG and AG2UG simultaneous power and data transfer. When it comes to this, even metamaterials are an option that holds great promise. And that propels the author to the next proposition.

The author would like to start with an observation from (da Silva et al. 2014):

"While for some applications, the sensor itself needs to be buried (e.g., soil moisture probes can only function when buried among soil), it is not always clear why the transceiver/antenna also needs to be underground."

The author would like to echo a similar sentiment in the case of MI based WUSNs, and propose:

"In order to gauge the soil properties underground, why should it be imperative such readings have to be communicated aboveground through soil medium?"

In other words, the author proposes that there should be intensive research in MI based WUSNs towards divesting sensing performed in soil, from the need for communicating such sensed data through soil. There can be divergent novel solution approaches to effecting this paradigm shift; for instance, the author would like to identify one such innovative model, which the author would like to refer to as a *"colony of tadpoles"*. In this model, the sensors are designed analogous to the shape of a tadpole; the head of the sensor is buried in the soil, whereas the tail end can be analogous to the thin magneto-inductive cable (Syms et al. 2010) enabling interconnection with other neighbouring nodes. A schematic of this model has been presented in Fig. 9.1. These tadpoles could be strewn beneath the ground at selected locations as an interconnected bunch (thus realizing a colony), and could communicate among one another for sharing and uploading data. Further, the colony could be augmented by means of a central collating tadpole, which could in turn communicate with an aboveground node by means of a design analogous to the thin magneto-inductive cable (Syms et al. 2010) for power and/or data transfer.

Another design approach that could be investigated in this context, is that of a *"metamaterial envelope"* conducive to *"near free space"* sensor node communication, but which would not interfere with the natural soil properties. The envelope or layer is envisaged analogous to a dragnet drawn underwater; the mesh fibre can be substituted by the material analogous to the thin magneto-inductive cable (Syms et al. 2010). A schematic of this design is shown in Fig. 9.2. As seen in the figure, the sensors would be *strung* on the dragnet grid at select points, and can perform sensing and communication by means of thin magneto-inductive cables. What could be even more path-breaking is the notion of conceiving the deployment of this dragnet, as if *a spider had spun its cobweb underground.* That would enable casting segments of the dragnet at critical spots underground, connected by means of tenuous yet sturdy magneto-inductive cables criss-crossing the length and breadth of the coverage area.

These are but mere glimpses of the enormous possibilities; the bottom-line is that as we pursue ideation by means of analogies from nature as well as other domains, the solution approaches could be drastically ingenious and produce dexterous and durable workarounds to the theoretical bottlenecks.

Next, the author would wish to expend some thoughts on how innovative coil designs and waveguide structures, also facilitated by means of applying novel metamaterials, could enable a paradigm shift as well in MI based communication. In fact, the author had expanded on this topic during the review of preliminary research on MI under Chapter 4. During the course of this review, the author had pointed out that many of the novel ideas that sprung from the early research have not been considered in the ongoing theoretical research on MI based WUSNs.

NOTE

For further details, the reader is directed to Chapter 4.

During the course of the discussion under Chapter 8, the author had again touched upon the aspect of single layered coils for WUSNs. While reviewing the earlier research on MI waveguides, the author had reproduced a relevant extract from (Syms, Young & Solymar 2006), highlighting the advantage presented by double layered coils. The extract has been repeated below for the sake of the reader's convenience:

"... for single- and double-sided coils operating at.....frequencies in the range 50-400 MHz.....For the single-sided coils, the variation follows an inverse square law, to a reasonable approximation. However, the rate of decay is lower at small separations and higher at larger ones.....Double-layer coils have a consistently higher coupling coefficient than single layer coils over this range. The data were then used to estimate the coupling ratio ξ.....Double-sided coils clearly show a significant reduction in ξ, by around 30%. Based on the above, double-sided coils offer significant advantages for MI waveguides."

In spite of this, a stream of current theoretical research on MI waveguides has been focused on single layered coils (Sun et al. 2013). Similarly, there are bound to be other avenues for improvement (or radical innovation for better), when it comes to coil design, configuration and related structural arrangements (waveguides). This is another research area that needs a lot of careful looking into, without being prejudiced by the patterns being experimented with in ongoing research, with the objective of how analogical solution approaches drawn chiefly from the preliminary research findings, in addition to applicable ideas from other domains, could deliver a drastically augmented performance. A case in point the author had touched upon was the study outlined in (Shamonina & Solymar 2004), contrasting one dimensional MI waveguides with traditional transmission lines. The author believes that as opposed to strictly theoretical study of MI based WUSNs, it is such comparative studies that can expedite the accomplishment of technical breakthroughs in this research area. Especially when it comes to this particular aspect of MI based WUSNs, which is coil design and arrangement (waveguide structures), there is an even enhanced scope to draw on biomimetics as well apart from other domains, in arriving at highly novel designs and solutions. The relevant extract that the author had reproduced from (Bhushan 2009) above bears a much greater significance in this context.

Penultimately, on the point of employing novel workarounds within an application context to complement the theoretical know-how, and vice versa. The aspect of unifying all the research under the umbrella of a consortium is instrumental to achieving this necessary synergy, which could tremendously facilitate this give and take in both directions. During the course of the review of analogical thinking under Chapter 6, the author had highlighted this aspect of how theory and application have always been two sides of the same coin. The author had done so, by means of referencing noteworthy texts on the subject matter from different spheres of science and technology. Also, during the course of the discussion under Chapter 4, the author had highlighted a similar observation from (Bunszel 2001). This sentiment needs to deeply percolate the current research on MI based WUSNs; the author envisages that more often than not, the theoretical research in the coming years should be complemented by the novel workarounds attempted in various application contexts to circumvent the theoretical issues, similar to the MI waveguide tunnel design proposed in this research. The author also would suggest that such novel mechanisms should be rooted in analogical thinking, so as to leverage on the limitless possibilities that exist in other disciplines of study and application. This blend of theoretical research with novel workarounds would bring in more creativity to the domain research than could otherwise be, because of being confined to the theoretical approach to solving the problems.

Ultimately, a departing note on the scope and the application of analogy in creative problem solving in MI based WUSNs as well, as in the case of other engineering and technological domains. The author would like to reproduce excerpts from related research outputs in this context, to begin with. In the work (Dasgupta 1996), there is the following observation on technological creativity:

"...... *To design, is to invent*............ *every act of design is an act of creation*......"

And in another more recent work (Ball, Ormerod & Morley 2004) reporting "the experimental comparison of analogy use by expert and novice design engineers", the authors of the work conclude:

"In this paper, we set out to investigate the extent and nature of spontaneous analogical reasoning associated with novice and expert design activity. In terms of theories of design problem-solving and expert cognition, we believe that our results are important in three main respects.

First, they demonstrate the prevalence of spontaneous analogising in both expert and novice design practice. This finding corroborates the widely-held assumption that analogising plays a fundamental role in creative, real-world problem solving . . . It would appear that analogising is part of the natural behavioural repertoire of industrial designers, and is a form of reasoning that can flourish without directive hints from the experimenter that explicitly request the reuse of prior knowledge and experience.. . . . . ."

Taken together, the above two observations attest the undeniable role played by analogical thinking in engineering and technology. Additionally, the above observations complete a full circle in terms of the scope and relevance of analogical thinking in both theoretical and applied science (applied science is synonymous with engineering and technology); it wouldn't be an exaggeration at all, considering also the portrayal of creative thinking itself as analogical in its essentials by Hadamard (Hadamard 1954), to maintain that practically all ideation in science, engineering and technology has always been, and continues to be, rooted in analogical thinking. This being so, there is need for a conscious and dedicated research effort in the direction of identifying potential analogies from across scientific disciplines, which could be put to advantageous adaptation and/or application in the domain of MI based WUSNs.

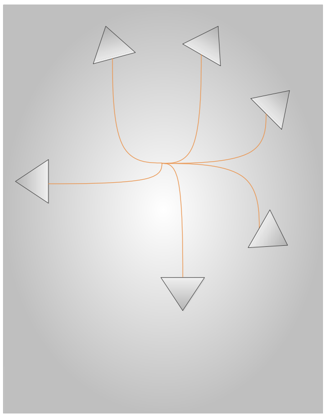

Figure 9.1: A Tadpole Colony of Sensors

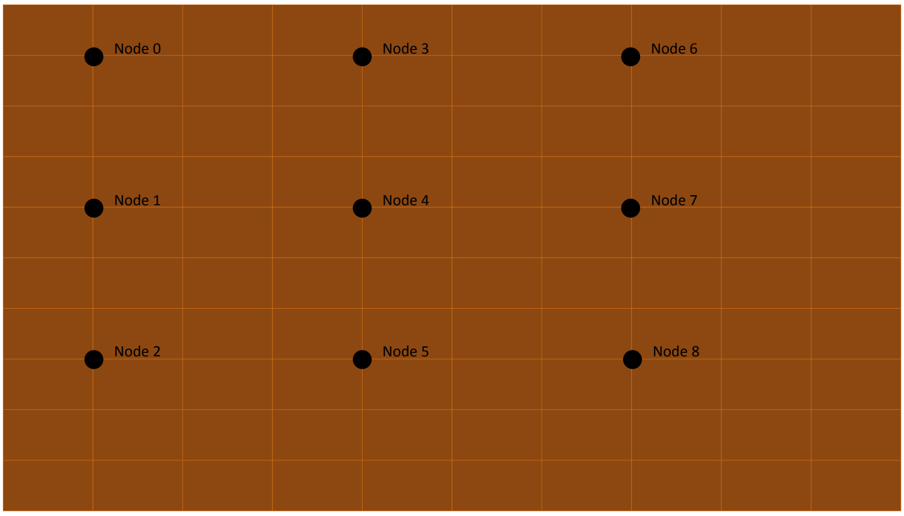

Figure 9.2: A Dragnet of Sensors

9.5 Chapter Summary

In this chapter, the author summarized the contributions of this research. In addition, the author also presented the conclusions and future research directions related to MI based WUSNs. This chapter concludes this dissertation.

References

Abdulla, A., Nishiyama, H., Ansari, N. & Kato, N. (2014), Energy-Aware Routing for Wireless Sensor Networks, *in* H. M. Ammari, ed., 'The Art of Wireless Sensor Networks', Signals and Communication Technology, Springer Berlin Heidelberg, pp. 201–234.

Adel, A. & Norsheila, F. (2013), 'Probabilistic routing protocol for a hybrid wireless underground sensor networks', *Wireless Communications and Mobile Computing* **13**(2), 142–156.

Adler, M. (1974), 'A field-theoretical approach to magnetic induction heating of thin circular plates', *Magnetics, IEEE Transactions on* **10**(4), 1118–1125.

Akyildiz, I. F. & Stuntebeck, E. P. (2006), 'Wireless underground sensor networks: Research challenges', *Ad Hoc Networks* **4**(6), 669 – 686.

Akyildiz, I. F., Sun, Z. & Vuran, M. C. (2009), 'Signal propagation techniques for wireless underground communication networks', *Physical Communication* **2**(3), 167 – 183.

Ammari, H. M., ed. (2014), *The Art of Wireless Sensor Networks*, Vol. Volume 1: Fundamentals, Springer Berlin Heidelberg.

Andersen, P. & Crocker, T. E. (2015), 'The Pecan Tree'.

Archer, C. L. & Jacobson, M. Z. (2005), 'Evaluation of global wind power', *Journal of Geophysical Research: Atmospheres* **110**(D12).

Ball, L. J., Ormerod, T. C. & Morley, N. J. (2004), 'Spontaneous analogising in engineering design: a comparative analysis of experts and novices', *Design Studies* **25**(5), 495–508.

Bar-Cohen, Y. (2006), 'Biomimetics−using nature to inspire human innovation', *Bioinspiration & Biomimetics* **1**(1), P1.

Barber, R. E. & III, W. F. G. (2000), Rotating field antenna with a magnetically coupled quadrature loop, U.S. Patent 6,166,706.

Benyus, J. M. (1997), *Biomimicry*, William Morrow New York.

Bhushan, B. (2009), 'Biomimetics: lessons from nature–an overview', *Philosophical Transactions of the Royal Society A: Mathematical, Physical and Engineering Sciences* **367**(1893), 1445–1486.

Boden, M. A. (1987), *Artificial intelligence and natural man*, MIT press Cambridge, MA.

Boden, M. A. (2004), *The creative mind: Myths and mechanisms*, Psychology Press.

Bogena, H. R., Huisman, J. A., Meier, H., Rosenbaum, U. & Weuthen, A. (2009), 'Hybrid Wireless Underground Sensor Networks: Quantification of Signal Attenuation in Soil', *VADZONE* .

Bunszel, C. (2001), 'Magnetic induction: A low-power wireless alternative', *RF DESIGN* **24**(11), 78–80.

Bureau of Meteorology (2015), 'Monthly Weather Review'. Retreived from http://www.bom.gov.au/climate/mwr/.

Cato, C. & Lim, S. (2014), UHF far-field wireless power transfer for remotely powering wireless sensors, *in* 'Antennas and Propagation Society International Symposium (APSURSI), 2014 IEEE', pp. 1337–1338.

Chen, C.-J., Chu, T.-H., Lin, C.-L. & Jou, Z.-C. (2010), 'A Study of Loosely Coupled Coils for Wireless Power Transfer', *Circuits and Systems II: Express Briefs, IEEE Transactions on* **57**(7), 536–540.

Chen, Y. & Zhao, Q. (2005), 'On the lifetime of wireless sensor networks', *Communications Letters, IEEE* **9**(11), 976–978.

Crossbow (2007), *MPR-MIB Users Manual*, Crossbow Technology. Revision A.

Crossbow (2013), 'TELOSB Mote Platform', "http://www.willow.co.uk/TelosB_Datasheet.pdf". Document Part Number: 6020-0094-01 Rev B Datasheet hosted by Willow Technologies.

da Silva, A. R., Moghaddam, M. & Liu, M. (2014), The Future of Wireless Underground Sensing Networks Considering Physical Layer Aspects, *in* 'The Art of Wireless Sensor Networks', Springer, pp. 451–484.

Dasgupta, S. (1996), *Technology and creativity*, Oxford University Press New York.

De Vita, G. & Iannaccone, G. (2005), 'Design criteria for the RF section of UHF and microwave passive RFID transponders', *Microwave Theory and Techniques, IEEE Transactions on* **53**(9), 2978–2990.

Decagon (2008), ECH2O-TE/EC-TM Water Content, EC and Temperature Operator's Manual, Technical report, Decagon Devices Inc., Pullman, Washington, USA. Version 7 (discontinued).

Decagon (2014*a*), 10HS Soil Moisture Sensor Manual, Technical report, Decagon Devices Inc., Pullman, Washington, USA. Version: December 1, 2014—14:29:39.

Decagon (2014*b*), EC-5 Soil Moisture Sensor Operator's Manual, Technical report, Decagon Devices Inc., Pullman, Washington, USA. Version: June 20, 2014—09:43:53.

Decagon (2014*c*), Em50/Em50R/Em50G Em50 Series Data Collection System Operator's Manual, Technical report, Decagon Devices Inc., Pullman, Washington, USA. Version: August 12, 2014—10:02:24.

Dewan, A., Ay, S. U., Karim, M. N. & Beyenal, H. (2014), 'Alternative power sources for remote sensors: A review', *Journal of Power Sources* **245**(0), 129–143.

Dietrich, I. & Dressler, F. (2009), 'On the Lifetime of Wireless Sensor Networks', *ACM Trans. Sen. Netw.* **5**(1), 5:1–5:39.

Dong, X. & Vuran, M. C. (2011), A Channel Model for Wireless Underground Sensor Networks Using Lateral Waves, *in* 'Global Telecommunications Conference (GLOBECOM 2011), 2011 IEEE', pp. 1–6.

Dong, X., Vuran, M. C. & Irmak, S. (2013), 'Autonomous precision agriculture through integration of wireless underground sensor networks with center pivot irrigation systems', *Ad Hoc Networks* **11**(7), 1975–1987.

Dursun, M. & Ozden, S. (2014), 'An efficient improved photovoltaic irrigation system with artificial neural network based modeling of soil moisture distribution - A case study in Turkey', *Computers and Electronics in Agriculture* **102**(0), 120–126.

Erdos, P. & Renyi, A. (1959), 'On random graphs I.', *Publ. Math. Debrecen* **6**, 290–297.

Erdos, P. & Renyi, A. (1960), On the Evolution of Random Graphs, *in* 'PUBLICATION OF THE MATHEMATICAL INSTITUTE OF THE HUNGARIAN ACADEMY OF SCIENCES', Vol. 5, pp. 17–61.

Erskine, R. H., Green, T. R., Ramirez, J. A. & MacDonald, L. H. (2007), 'Digital Elevation Accuracy and Grid Cell Size: Effects on Estimated Terrain Attributes', *Soil Science Society of America Journal* **71**(4), 1371–1380.

Evans-Pughe, C. (2005), 'Close Encounters of the Magnetic Kind.', *IEE Review* **51**(5), 38–42.

Fisher, D. A., Burns, L. M. & Muther, S. E. (1999), 'Power transfer apparatus for concurrently transmitting data and power over data wires'.

Fotopoulou, K. & Flynn, B. (2011), 'Wireless Power Transfer in Loosely Coupled Links: Coil Misalignment Model', *Magnetics, IEEE Transactions on* **47**(2), 416–430.

Freire, M. J., MarquÃľs, R., Medina, F., Laso, M. A. G. & MartÃŋn, F. (2004), 'Planar magnetoinductive wave transducers: Theory and applications', *Applied Physics Letters* **85**(19).

Fu, B., Xiao, Y., Deng, H. & Zeng, H. (2014), 'A Survey of Cross-Layer Designs in Wireless Networks', *Communications Surveys Tutorials, IEEE* **16**(1), 110–126.

Gassmann, O. & Zeschky, M. (2008), 'Opening up the Solution Space: The Role of Analogical Thinking for Breakthrough Product Innovation', *Creativity and Innovation Management* **17**(2), 97–106.

Gick, M. L. & Holyoak, K. J. (1980), 'Analogical problem solving', *Cognitive Psychology* **12**(3), 306–355.

Gordon, W. J. (1961), *Synectics: The development of creative capacity.*, Harper.

Grunwald, S. (2006), *Environmental Soil-landscape Modeling: Geographic Information Technologies and Pedometrics.*, CRC Press, New York, NY, USA, chapter What do we really know about the space-time continuum of soil-landscapes?

Gupta, P. & Kumar, P. (2000), 'The capacity of wireless networks', *Information Theory, IEEE Transactions on* **46**(2), 388–404.

Hadamard, J. (1954), *An essay on the psychology of invention in the mathematical field*, Courier Corporation.

Hamrita, T. K. & Hoffacker, E. C. (2005), 'Development of a "smart" wireless soil monitoring sensor prototype using RFID technology', *Applied Engineering in Agriculture* **21**(1), 139–143.

Hesmer, F., Tatartschuk, E., Zhuromskyy, O., Radkovskaya, A. A., Shamonin, M., Hao, T., Stevens, C. J., Faulkner, G., Edwards, D. J. & Shamonina, E. (2007), 'Coupling mechanisms for split ring resonators: Theory and experiment', *physica status solidi (b)* **244**(4), 1170–1175.

Hodgson, M. E. (1998), 'Comparison of Angles from Surface Slope/Aspect Algorithms', *Cartography and Geographic Information Systems* **25**(3), 173–185.

Holyoak, K. J. (1996), *Mental leaps: Analogy in creative thought*, MIT press.

Huang, J., Kumar, R., El-Sayed Kamal, A. & Eber, R. (2008), Development of a wireless soil sensor network, *in* 'Proceeding of the ASABE annual meeting 2008'.

Huang, P., Xiao, L., Soltani, S., Mutka, M. & Xi, N. (2013), 'The Evolution of MAC Protocols in Wireless Sensor Networks: A Survey', *Communications Surveys Tutorials, IEEE* **15**(1), 101–120.

(IAC), I. A. C. (2013), 'Macademia'.

(IETF), I. E. T. F. (2015), 'Request for Comments (RFC)'.

ITU-T (2009), *H.323 Packet-based multimedia communications systems*, ITU-T.

James R Carter (1992), 'The Effect Of Data Precision On The Calculation Of Slope And Aspect Using Gridded DEMs', *Cartographica: The International Journal for Geographic Information and Geovisualization* **29**(1).

Jiang, Z. & Yu, X. (2009), Power electronics interfaces for hybrid DC and AC-linked microgrids, *in* 'Power Electronics and Motion Control Conference, 2009. IPEMC '09. IEEE 6th International', pp. 730–736.

Kadil, V. & Adane, D. (2012), Maximizing range of signal strength by homemade Wi-Fi booster antenna, *in* 'Information and Communication Technologies (WICT), 2012 World Congress on', pp. 389–393.

Karl, H. & Willig, A. (2005), *Protocols and Architectures for Wireless Sensor Networks*, John Wiley & Sons Ltd.

Kisseleff, S., Akyildiz, I. & Gerstacker, W. (2013), Interference polarization in magnetic induction based Wireless Underground Sensor Networks, *in* 'Personal, Indoor and Mobile Radio Communications (PIMRC Workshops), 2013 IEEE 24th International Symposium on', pp. 71–75.

Kisseleff, S., Akyildiz, I. & Gerstacker, W. (2014*a*), On modulation for magnetic induction based transmission in wireless underground sensor networks, *in* 'Communications (ICC), 2014 IEEE International Conference on', pp. 71–76.

Kisseleff, S., Akyildiz, I. & Gerstacker, W. (2014*b*), Transmitter-side channel estimation in magnetic induction based communication systems, *in* 'Communications and Networking (BlackSeaCom), 2014 IEEE International Black Sea Conference on', pp. 16–21.

Kisseleff, S., Gerstacker, W., Schober, R., Sun, Z. & Akyildiz, I. (2013), Channel capacity of magnetic induction based Wireless Underground Sensor Networks under practical constraints, *in* 'Wireless Communications and Networking Conference (WCNC), 2013 IEEE', pp. 2603–2608.

Kisseleff, S., Gerstacker, W., Sun, Z. & Akyildiz, I. (2013), On the throughput of Wireless Underground Sensor Networks using magneto-inductive waveguides, *in* 'Global Communications Conference (GLOBECOM), 2013 IEEE', pp. 322–328.

Knight, D. W. (2013), *An Introduction to the Art of Solenoid Inductance Calculation with Emphasis on Radio-Frequency Applications*, version 0.19 edn.

Kopetz, H. (2011), Internet of Things, *in* 'Real-Time Systems', Real-Time Systems Series, Springer US, pp. 307–323.

Kurnik, B., Louwagie, G., Erhard, M., Ceglar, A. & Bogataj Kajfez, L. (2014), 'Analysing Seasonal Differences between a Soil Water Balance Model and in Situ Soil Moisture Measurements at Nine Locations Across Europe', *Environmental Modeling & Assessment* **19**(1), 19–34.

Kurs, A., Karalis, A., Moffatt, R., Joannopoulos, J. D., Fisher, P. & Soljacic, M. (2007), 'Wireless Power Transfer via Strongly Coupled Magnetic Resonances', *Science* **317**(5834), 83–86.

Kusy, B., Abbott, D., Richter, C., Huynh, C., Afanasyev, M., Hu, W., Brünig, M., Ostry, D. & Jurdak, R. (2014), 'Radio Diversity for Reliable Communication in Sensor Networks', *ACM Trans. Sen. Netw.* **10**(2), 32:1–32:29.

Lal, R. & Shukla, M. K. (2004), *Principles of soil physics*, CRC Press.

Lawrence, E. & Snyder, G. (2002), A study of heat sink performance in air and soil for use in a thermoelectric energy harvesting device, *in* 'Thermoelectrics, 2002. Proceedings ICT '02. Twenty-First International Conference on', pp. 446–449.

Le, T., Mayaram, K. & Fiez, T. (2008), 'Efficient Far-Field Radio Frequency Energy Harvesting for Passively Powered Sensor Networks', *Solid-State Circuits, IEEE Journal of* **43**(5), 1287–1302.

Li, L., Vuran, M. C. & Akyildiz, I. F. (2007), 'Characteristics of underground channel for wireless underground sensor networks'.

Li, X. & Wu, J. (2014), Utility-Based Routing in Wireless Sensor Networks, *in* H. M. Ammari, ed., 'The Art of Wireless Sensor Networks', Signals and Communication Technology, Springer Berlin Heidelberg, pp. 235–270.

Li, Z., Wang, N., Franzen, A., Taher, P., Godsey, C., Zhang, H. & Li, X. (2014), 'Practical deployment of an in-field soil property wireless sensor network', *Computer Standards & Interfaces* **36**(2), 278–287.

Li, Z., Wang, X. & Liang, Q. (2014), Physical Layer Communications in Wireless Sensor

Networks, *in* H. M. Ammari, ed., 'The Art of Wireless Sensor Networks', Signals and Communication Technology, Springer Berlin Heidelberg, pp. 97–127.

Lin, S.-C., Akyildiz, I., Wang, P. & Sun, Z. (2014), Optimal energy-throughput efficiency for magneto-inductive underground sensor networks, *in* 'Communications and Networking (BlackSeaCom), 2014 IEEE International Black Sea Conference on', pp. 22–27.

ling Yang, Z. (1992), 'Mutual capacitance-duality principle evolved from planar network', *Circuits and Systems I: Fundamental Theory and Applications, IEEE Transactions on* **39**(12), 1005–1006.

Majumder, R. (2014), 'A Hybrid Microgrid With DC Connection at Back to Back Converters', *Smart Grid, IEEE Transactions on* **5**(1), 251–259.

Mandelbrot, B. B. (1983), *The fractal geometry of nature*, Macmillan.

Martinez, K., Ong, R. & Hart, J. (2004), Glacsweb: a sensor network for hostile environments, *in* 'Sensor and Ad Hoc Communications and Networks, 2004. IEEE SECON 2004. 2004 First Annual IEEE Communications Society Conference on', pp. 81–87.

Massarini, A. & Kazimierczuk, M. (1997), 'Self-capacitance of inductors', *Power Electronics, IEEE Transactions on* **12**(4), 671–676.

Mayordomo, I., Berenguer, R., Garcia-Alonso, A., Fernandez, I. & Gutierrez, I. (2009), 'Design and Implementation of a Long-Range RFID Reader for Passive Transponders', *Microwave Theory and Techniques, IEEE Transactions on* **57**(5), 1283–1290.

Mazo, M. & Tabuada, P. (2011), 'Decentralized Event-Triggered Control Over Wireless Sensor/Actuator Networks', *Automatic Control, IEEE Transactions on* **56**(10), 2456–2461.

McCulloch, C. E. & Cain, M. L. (1989), 'Analyzing Discrete Movement Data as a Correlated Random Walk', *Ecology* **70**(2), pp. 383–388.

Mitasova, H. & Hofierka, J. (1993), 'Interpolation by regularized spline with tension: II. Application to terrain modeling and surface geometry analysis', *Mathematical Geology* **25**(6), 657–669.

Moore, I. D., Grayson, R. B. & Ladson, A. R. (1991), ‘Digital terrain modelling: A review of hydrological, geomorphological, and biological applications’, *Hydrological Processes* **5**(1), 3–30.

(NFPA)®, N. F. P. A. (2014), *NFPA® 70 National Electrical Code*, 2014 edn, National Fire Protection Association (NFPA)®, NFPA, 1 Batterymarch Park, Quincy, MA 02169-7471.

Oppermann, F., Boano, C. & RÃűmer, K. (2014), A decade of wireless sensing applications: Survey and taxonomy, *in* H. M. Ammari, ed., ‘The Art of Wireless Sensor Networks’, Signals and Communication Technology, Springer Berlin Heidelberg, pp. 11–50.

Pandey, G., Kumar, R. & Weber, R. J. (2014), A low profile, low-RF band, small antenna for underground, in-situ sensing and wireless energy-efficient transmission, *in* ‘Networking, Sensing and Control (ICNSC), 2014 IEEE 11th International Conference on’, IEEE, pp. 179–184.

Parameswaran, V., Zhou, H. & Zhang, Z. (2012), Irrigation control using Wireless Underground Sensor Networks, *in* ‘Sensing Technology (ICST), 2012 Sixth International Conference on’, pp. 653–659.

Parameswaran, V., Zhou, H. & Zhang, Z. (2013), Wireless underground sensor network design for irrigation control: Simulation of RFID deployment, *in* ‘Sensing Technology (ICST), 2013 Seventh International Conference on’, pp. 842–849.

Parameswaran, V., Zhou, H. & Zhang, Z. (2014), Numerical Terrain Modelling for Wireless Underground Sensor Networks, *in* ‘Sensing Technology (ICST), 2014 Eighth International Conference on’, pp. 296–300.

Patrice Simon, Y. G. & Dunn, B. (2014), ‘Where Do Batteries End and Supercapacitors Begin?’, *Science* **343**(6176), 1210–1211.

Pendry, J., Holden, A., Robbins, D. & Stewart, W. (1999), ‘Magnetism from conductors and enhanced nonlinear phenomena’, *Microwave Theory and Techniques, IEEE Transactions on* **47**(11), 2075–2084.

Plantation, T. (2002), ‘Nut trees’. Accessed at http://www.treeplantation.com/nut-trees.html Latest Update 2002.

Popovic, Z. & Popovic, B. D. (2000), *Introductory electromagnetics*, Prentice Hall.

Posamentier, J. (2013), 'Switchable active-passive RFID tag'.

Resources & Energy (2014), 'The New South Wales Wind Atlas'. Retrieved from http://www.resourcesandenergy.nsw.gov.au/energy-consumers/sustainable-energy/wind/sustain_renew_wind_atlas_poster.pdf on 17.03.2015.

Ritsema, C. J., Kuipers, H., Kleiboer, L., van den Elsen, E., Oostindie, K., Wesseling, J. G., Wolthuis, J.-W. & Havinga, P. (2009), 'A new wireless underground network system for continuous monitoring of soil water contents', *Water Resources Research* **45**(4).

Rosenberg, J., Schulzrinne, H., Camarillo, G., Johnston, A., Peterson, J., Sparks, R., Handley, M. & Schooler, E. (2002), *RFC 3261 SIP: Session Initiation Protocol.*

Roundy, S., Steingart, D., Frechette, L., Wright, P. & Rabaey, J. (2004), Power Sources for Wireless Sensor Networks, *in* H. Karl, A. Wolisz & A. Willig, eds, 'Wireless Sensor Networks', Vol. 2920 of *Lecture Notes in Computer Science*, Springer Berlin Heidelberg, pp. 1–17.

Rowaihy, H., Eswaran, S., Johnson, M., Verma, D., Bar-Noy, A., Brown, T. & La Porta, T. (2007), A survey of sensor selection schemes in wireless sensor networks, *in* 'Proc. SPIE', Vol. 6562, pp. 65621A–65621A–13.

Santamaria-Ibirika, A., Cantero, X., Salazar, M., Devesa, J. & Bringas, P. (2013), Volumetric Virtual Worlds with Layered Terrain Generation, *in* 'Cyberworlds (CW), 2013 International Conference on', pp. 20–27.

Shamonina, E., Kalinin, V. A., Ringhofer, K. H. & Solymar, L. (2002*a*), 'Magnetoinductive waves in one, two, and three dimensions', *Journal of Applied Physics* **92**(10).

Shamonina, E., Kalinin, V., Ringhofer, K. & Solymar, L. (2002*b*), 'Magneto-inductive waveguide', *Electronics Letters* **38**(8), 371–373.

Shamonina, E. & Solymar, L. (2004), 'Magneto-inductive waves supported by metamaterial elements: components for a one-dimensional waveguide', *JOURNAL OF PHYSICS D: APPLIED PHYSICS* **37**(3), 362–367.

Shang, T., Huang, F.-H., Mao, K.-F. & Liu, J.-W. (2014), 'The effect of hexagonal grid topology on wireless communication networks based on network coding', *International Journal of Communication Systems* **27**(9), 1319–1337.

Showers, R. M., Schulz, R. & Lin, S.-Y. (1981), 'Fundamental limits on EMC', *Proceedings of the IEEE* **69**(2), 183–195.

Silva, A. R. d., Moghaddam, M. & Liu, M. (2014), Design of Low Data-Rate Environmental Monitoring Applications, *in* H. M. Ammari, ed., 'The Art of Wireless Sensor Networks', Signals and Communication Technology, Springer Berlin Heidelberg, pp. 51–94.

Silva, A. R., Liu, M. & Moghaddam, M. (2013), 'Ripple-2: A Non-collaborative, Asynchronous, and Open Architecture for Highly-scalable and Low Duty-cycle WSNs', *SIGMOBILE Mob. Comput. Commun. Rev.* **17**(1), 55–60.

Silva, A. R. & Vuran, M. C. (2010*a*), (CPS)ˆ 2: integration of center pivot systems with wireless underground sensor networks for autonomous precision agriculture, *in* 'Proceedings of the 1st ACM/IEEE International Conference on Cyber-Physical Systems', ACM, pp. 79–88.

Silva, A. R. & Vuran, M. C. (2010*b*), 'Development of a Testbed for Wireless Underground Sensor Networks', *EURASIP J. Wirel. Commun. Netw.* **2010**, 9:1–9:12.

Silva, A. & Vuran, M. (2009), Empirical Evaluation of Wireless Underground-to-Underground Communication in Wireless Underground Sensor Networks, *in* B. Krishnamachari, S. Suri, W. Heinzelman & U. Mitra, eds, 'Distributed Computing in Sensor Systems', Vol. 5516 of *Lecture Notes in Computer Science*, Springer Berlin Heidelberg, pp. 231–244.

Silva, A. & Vuran, M. C. (2010*c*), Communication with Aboveground Devices in Wireless Underground Sensor Networks: An Empirical Study, *in* 'Communications (ICC), 2010 IEEE International Conference on', pp. 1–6.

Singh, K., Kumar, R. & Weber, R. (2014), Piezoelectric-based broadband bistable vibration energy harvester and SCE/SSHI-based high-power extraction, *in* 'Networking, Sensing and Control (ICNSC), 2014 IEEE 11th International Conference on', pp. 197–202.

Sobot, R. (2014), Matching Networks: Solutions, *in* 'Wireless Communication Electronics by Example', Springer International Publishing, pp. 183–199.

Sojdehei, J., Wrathall, P. & Dinn, D. (2001), Magneto-inductive (MI) communications, *in* 'OCEANS, 2001. MTS/IEEE Conference and Exhibition', Vol. 1, pp. 513–519 vol.1.

Soontornpipit, P., Furse, C. M., Chung, Y. C. & Lin, B. M. (2006), 'Optimization of a buried microstrip antenna for simultaneous communication and sensing of soil moisture', *Antennas and Propagation, IEEE Transactions on* **54**(3), 797–800.

Stadler, A., Rudolph, S., Kupisch, M., Langensiepen, M., van der Kruk, J. & Ewert, F. (2015), 'Quantifying the effects of soil variability on crop growth using apparent soil electrical conductivity measurements', *European Journal of Agronomy* **64**(0), 8–20.

Stratton, S. W. (1914), Copper Wire Tables, Circular of the Bureau of Standards 31, Department of Commerce, United States of America.

Stuntebeck, E., Pompili, D. & Melodia, T. (2006), Wireless underground sensor networks using commodity terrestrial motes, *in* 'Wireless Mesh Networks, 2006. WiMesh 2006. 2nd IEEE Workshop on', pp. 112–114.

Sun, Z. & Akyildiz, I. (2009), Underground Wireless Communication Using Magnetic Induction, *in* 'Communications, 2009. ICC '09. IEEE International Conference on', pp. 1–5.

Sun, Z. & Akyildiz, I. (2010*a*), Connectivity in Wireless Underground Sensor Networks, *in* 'Sensor Mesh and Ad Hoc Communications and Networks (SECON), 2010 7th Annual IEEE Communications Society Conference on', pp. 1–9.

Sun, Z. & Akyildiz, I. (2010*b*), Deployment Algorithms for Wireless Underground Sensor Networks Using Magnetic Induction, *in* 'Global Telecommunications Conference (GLOBECOM 2010), 2010 IEEE', pp. 1–5.

Sun, Z. & Akyildiz, I. (2010*c*), 'Magnetic Induction Communications for Wireless Underground Sensor Networks', *Antennas and Propagation, IEEE Transactions on* **58**(7), 2426–2435.

Sun, Z. & Akyildiz, I. (2012), On capacity of magnetic induction-based wireless underground sensor networks, *in* 'INFOCOM, 2012 Proceedings IEEE', pp. 370–378.

Sun, Z. & Akyildiz, I. F. (2013), 'Optimal Deployment for Magnetic Induction-Based Wireless Networks in Challenged Environments', *Wireless Communications, IEEE Transactions on* **12**(3), 996–1005.

Sun, Z., Akyildiz, I. & Hancke, G. (2011), 'Dynamic Connectivity in Wireless Underground Sensor Networks', *Wireless Communications, IEEE Transactions on* **10**(12), 4334–4344.

Sun, Z., Akyildiz, I., Kisseleff, S. & Gerstacker, W. (2013), 'Increasing the Capacity of Magnetic Induction Communications in RF-Challenged Environments', *Communications, IEEE Transactions on* **61**(9), 3943–3952.

Syms, R. R. A., Shamonina, E., Kalinin, V. & Solymar, L. (2005), 'A theory of metamaterials based on periodically loaded transmission lines: Interaction between magnetoinductive and electromagnetic waves', *Journal of Applied Physics* **97**(6), 064909.

Syms, R. R. A., Young, I. R. & Solymar, L. (2006), 'Low-loss magneto-inductive waveguides', *JOURNAL OF PHYSICS D: APPLIED PHYSICS* **39**(18), 3945−3951.

Syms, R., Shamonina, E. & Solymar, L. (2006), 'Magneto-inductive waveguide devices', *IEE Proceedings-Microwaves, Antennas and Propagation* **153**(2), 111–121.

Syms, R., Solymar, L. & Shamonina, E. (2005), 'Absorbing terminations for magneto-inductive waveguides', *Microwaves, Antennas and Propagation, IEE Proceedings* **152**(2), 77–81.

Syms, R., Solymar, L., Young, I. & Floume, T. (2010), 'Thin-film magneto-inductive cables', *Journal of Physics D: Applied Physics* **43**(5), 055102.

Tan, Y. K. & Panda, S. K. (2010), *Sustainable Wireless Sensor Networks*, InTech, chapter Review of Energy Harvesting Technologies for Sustainable WSN.

Tiusanen, J. (2005), 'Attenuation of a soil scout radio signal', *Biosystems Engineering* **90**(2), 127–133.

Tiusanen, J. (2007), 'Validation and results of the soil scout radio signal attenuation model', *Biosystems Engineering* **97**(1), 11–17.

Tiusanen, J. (2009), 'Wireless Soil Scout prototype radio signal reception compared to the attenuation model', *Precision Agriculture* **10**(5), 372–381.

Tiusanen, M. J. (2013), 'Soil Scouts: Description and performance of single hop wireless underground sensor nodes', *Ad Hoc Networks* **11**(5), 1610–1618.

udea (2011), UFM-M11 Product Guide, Technical report, udea wireless technologies. Version 1.3.0 Retrieved from http://www.udea.com.tr/english/home_assets/documents/UFM-M11.pdf Latest Update June 2011.

udea (2014), Antennas UGP A-434. Accessed at http://www.udeashop.com/UGPA-434Kablo-ucu-bos,PR-22.html Latest Update 12/25/2014 11:42:32.

(USB-IF), U. I. F. (2014), *Universal Serial Bus Power Delivery Specification*, version 1.0 edn.

Vinoy, K. & Prabhakar, T. (2014), A Universal Energy Harvesting Scheme for Operating Low-Power Wireless Sensor Nodes Using Multiple Energy Resources, *in* K. J. Vinoy, G. K. Ananthasuresh, R. Pratap & S. B. Krupanidhi, eds, 'Micro and Smart Devices and Systems', Springer Tracts in Mechanical Engineering, Springer India, pp. 453–466.

von Gleich, A., Pade, C., Petschow, U. & Pissarskoi, E. (2010), *Potentials and Trends in Biomimetics*, Springer Science & Business Media.

Vosniadou, S. & Ortony, A. (1989), *Similarity and analogical reasoning*, Cambridge University Press.

Vuran, M. & Akyildiz, I. (2008), Cross-Layer Packet Size Optimization for Wireless Terrestrial, Underwater, and Underground Sensor Networks, *in* 'INFOCOM 2008. The 27th Conference on Computer Communications. IEEE', pp. 13–18.

Vuran, M. C. & Akyildiz, I. F. (2010), 'Channel model and analysis for wireless underground sensor networks in soil medium', *Physical Communication* **3**(4), 245–254.

Wang, C., George, D. & Green, P. R. (2014), Development of plough-able RFID sensor network systems for precision agriculture, *in* 'Wireless Sensors and Sensor Networks (WiSNet), 2014 IEEE Topical Conference on', IEEE, pp. 64–66.

Wang, S., Lee, F. & van Wyk, J. (2006), 'Inductor winding capacitance cancellation using mutual capacitance concept for noise reduction application', *Electromagnetic Compatibility, IEEE Transactions on* **48**(2), 311–318.

Weaver, R. (2012), 'Numerical Methods for Inductance Calculation', Accessed at http://electronbunker.ca/CalcMethods.html Latest update June 29, 2012.

Williams, T. & Kelley, C. (2015), *gnuplot 5.0 An Interactive Plotting Program*, Vol. 5.0, GNU General Public License.

Wiltshire, M. C. K., Shamonina, E., Young, I. R. & Solymar, L. (2004), 'Experimental and theoretical study of magneto-inductive waves supported by one-dimensional arrays of "swiss rolls"', *Journal of Applied Physics* **95**(8).

Wiltshire, M., Shamonina, E., Young, I. & Solymar, L. (2003), 'Dispersion characteristics of magneto-inductive waves: comparison between theory and experiment', *Electronics Letters* **39**, 215–217(2).

Worthington, E. L. (2010), Piezoelectric Energy Harvesting: Enhancing Power Output by Device Optimisation and Circuit Techniques, PhD thesis, School of Applied Sciences, Cranfield University.

Yang, W. & Wu, S. (2013), Data Modeling and Visualization of Guangzhou Underground Space, *in* 'Information Technology and Applications (ITA), 2013 International Conference on', pp. 343–347.

Yoon, S.-U., Cheng, L., Ghazanfari, E., Pamukcu, S. & Suleiman, M. (2011), A Radio Propagation Model for Wireless Underground Sensor Networks, *in* 'Global Telecommunications Conference (GLOBECOM 2011), 2011 IEEE', pp. 1–5.

Younis, M., Lee, S., Senturk, I. & Akkaya, K. (2014), Topology Management Techniques for Tolerating Node Failure, *in* H. M. Ammari, ed., 'The Art of Wireless Sensor Networks', Signals and Communication Technology, Springer Berlin Heidelberg, pp. 273–311.

Yu, X., Wu, P., Han, W. & Zhang, Z. (2012), 'The research of an advanced wireless sensor networks for agriculture', *African Journal of Agricultural Research* **7**(5), 851–858.

Zhang, Z., Wu, P., Han, W. & Yu, X. (2012), 'Design of wireless underground sensor network nodes for field information acquisition', *African Journal of Agricultural Research* **7**(1), 82–88.

Zhou, G., He, T., Stankovic, J. & Abdelzaher, T. (2005), RID: radio interference detection in wireless sensor networks, *in* 'INFOCOM 2005. 24th Annual Joint Conference of the IEEE Computer and Communications Societies. Proceedings IEEE', Vol. 2, pp. 891–901 vol. 2.

Appendix A

Source Code for Simulations

A.1 Overview of Addendum

This appendix has been used to reproduce source code related to the entire gamut of simulation results presented under Chapters 7 and 8, for the range of simulations conducted. A section has been devoted to one particular simulation, and the simulations have been listed in the same order as found under each respective chapter. A sequential numbering has been followed for the sections, starting with the first simulation detailed under Chapter 7. A sequential numbering has been adhered to for the simulations as well, in spite of their chapter affiliation.

A.2 Source Code for Simulation 1

The source code for the C program used in Simulation 1 presented under Chapter 7, has been reproduced under the following subsections.

A.2.1 Header File

```
#include<stdio.h>
#include<stdlib.h>
```

```
#include<math.h>
#include<string.h>
#include<assert.h>
#include <fcntl.h>

/* constants */
#define R0 0.01 // ohms per meter
#define PI 3.142
#define B 1 //in MHz
#define BUFFER 2
#define TMPBUF 7

/* total number of disparate configurations */
#define NUM_CONFIG 3

/* double space */
#define DOUBLE_SPACE "  "

/* assumed value */
#define J 1

struct list
{
 struct list* next;
 double d;
 double Pt_Pth[BUFFER];
 int n_opt[BUFFER];
};
struct list test_results[BUFFER];

struct IE
{
 int N;
```

```
  double a;
  double Pt;
  double Pth;
  double omega;
  double omega0;
  double R;
  double M;
  double L;
  double Z;
  double mu;
  double d;
  int n_opt; // optimum number of coils to be calculated
  double values_d[BUFFER]; // array to hold variable d values for a configuration
  double values_PT_PTH[BUFFER]; // array to hold variable PT or PTH values for a configuration
};

enum configuration
{
 STANDARD,
 VARIABLE_PT,
 VARIABLE_PTH
};
void write_binary_to_disk(enum configuration, struct list*);
void write_to_disk(enum configuration, struct list*);
void run_testcase(enum configuration, struct IE*);
void set_constants(enum configuration, struct IE*);
void set_variables(enum configuration, struct IE*);
int estimate_opt_num_coils (double Pt, double d, double omega0, int N, double a, double mu, double Z, double Pth);
double estimate_soil_permeability (void);
double estimate_resistance (int N, double a);
```

```
double estimate_mutual_induction (double mu, double N, double a, double r);
double estimate_self_induction (double mu, int N, double a);
double estimate_self_impedance (double R, double omega, double L);
double estimate_path_loss (double R, double omega, double M, int n);
double find_nth_order_polynomial (double Z, double omega, double M, int n);
```

A.2.2 Source File

```
#include "code.h"

int main (void)
{
 struct IE parameters;
 enum configuration c;
 int count = 0;

 /* uncomment to run different test cases in iteration */
#if 0
 for(; count < NUM_CONFIG; ++count)
 {
  switch(count)
  {
    case 0:
    c = VARIABLE_PT;
    break;
    case 1:
    c = VARIABLE_PTH;
    break;
    default:
```

```
      break;
    }
    run_testcase(c, &parameters);
  }
#endif

  c = VARIABLE_PTH;
  run_testcase(c, &parameters);

return 0;
}

void run_testcase (enum configuration c, struct IE* parameters)
{
    unsigned short i = 0;
    unsigned short j = 0;

    set_constants(c, parameters);
    set_variables(c, parameters);

  switch(c)
  {
   case STANDARD:
     test_results[i].Pt_Pth[0] = parameters->Pt;
     test_results[i].Pt_Pth[1] = parameters->Pth;

   for(; i < BUFFER; ++i)
   {
     parameters->d = parameters->values_d[i];
     test_results[i].d = parameters->d;
     parameters->n_opt = estimate_opt_num_coils(
                                                   parameters->Pt,
                                                   parameters->d,
```

```
                                                                    parameters->omega0,
                                                                    parameters->N,
                                                                    parameters->a,
                                                                    parameters->mu,
                                                                    parameters->Z,
                                                                    parameters->Pth
                                                                  );
      test_results[i].n_opt[i] = parameters->n_opt;
   }
   break;
   case VARIABLE_PT:

   for(; i < BUFFER; ++i)
   {
    parameters->d = parameters->values_d[i];
    test_results[i].d = parameters->d;
    j = 0;
    for(; j < BUFFER; ++j)
    {
       parameters->Pt = parameters->values_PT_PTH[j];
       test_results[i].Pt_Pth[j] = parameters->Pt;
       parameters->n_opt = estimate_opt_num_coils(
                                                                  parameters->Pt,
                                                                  parameters->d,
                                                                  parameters->omega0,
                                                                  parameters->N,
                                                                  parameters->a,
                                                                  parameters->mu,
                                                                  parameters->Z,
                                                                  parameters->Pth
                                                                );
      test_results[i].n_opt[j] = parameters->n_opt;
    }
```

```
  }
  break;
  case VARIABLE_PTH:
  for(; i < BUFFER; ++i)
  {
   parameters->d = parameters->values_d[i];
   test_results[i].d = parameters->d;
   j = 0;
   for(; j < TMPBUF; ++j)
   {
     parameters->Pth = parameters->values_PT_PTH[j];
     test_results[i].Pt_Pth[j] = parameters->Pth;
     parameters->n_opt = estimate_opt_num_coils(
                                                parameters->Pt,
                                                parameters->d,
                                                parameters->omega0,
                                                parameters->N,
                                                parameters->a,
                                                parameters->mu,
                                                parameters->Z,
                                                parameters->Pth
                                              );
    test_results[i].n_opt[j] = parameters->n_opt;
   }
  }
  break;
  default:
  break;
 }

  write_to_disk(c, test_results);

 return;
```

```
}

void write_to_disk(enum configuration c, struct list* table)
{
 FILE *fp;
 long offset;
 unsigned short i, j;
 struct list *ptr;

 /* open a file on the disk for writing the data */
 fp = fopen("./test_results.txt", "w+");

 if(NULL != fp)
 {
   offset = ftell(fp);
   if(0 == fseek(fp, offset, SEEK_CUR))
   {
     switch(c)
     {
     case STANDARD:
     ptr = table;

      for(i = 0; i < BUFFER; ++i)
      {
       fprintf(fp, "d = %f  Pt = %f  Pth = %f\n", (ptr+i)->d, (
           ptr+0)->Pt_Pth[0], (ptr+0)->Pt_Pth[1]);
       fprintf(fp, "nopt = %d\n", (ptr+i)->n_opt[i]);
      }
     break;
      case VARIABLE_PT:
      ptr = table;

      for(i = 0; i < BUFFER; ++i)
```

```
          {
            fprintf(fp, "d = %f\n", (ptr+i)->d);
            for(j = 0; j < BUFFER; ++j)
            {
              fprintf(fp, "Pt = %f   ", (ptr+i)->Pt_Pth[j]);
              fprintf(fp, "nopt = %d\n", (ptr+i)->n_opt[j]);
            }
          }
          break;
          case VARIABLE_PTH:
          ptr = table;

          for(i = 0; i < BUFFER; ++i)
          {
            fprintf(fp, "d = %f\n", (ptr+i)->d);
            for(j = 0; j < TMPBUF; ++j)
            {
              fprintf(fp, "Pth = %f   ", (ptr+i)->Pt_Pth[j]);
              fprintf(fp, "nopt = %d\n", (ptr+i)->n_opt[j]);
            }
          }
          break;
          default:
          break;
        }
      }
  }
  fclose(fp);

return;
}


```

```
void set_constants(enum configuration c, struct IE* parameters)
{
 unsigned short count = 0;

 for(; count < (BUFFER - 1); ++count)
 {
   test_results[count].next = &test_results[count+1];
 }

 test_results[count].next = (struct list*) NULL;

   if(STANDARD == c)
   {
    parameters->Pt = 10.0;
    parameters->Pth = -80.0;
   }
   else if(VARIABLE_PT == c)
   {
    parameters->Pth = -80.0;
   }
   else if(VARIABLE_PTH == c)
   {
    parameters->Pt = 10.0;
   }
   parameters->mu = estimate_soil_permeability();
   parameters->N = 5;
   parameters->a = 0.15;
   parameters->omega = 10; //in MHz
   parameters->omega0 = parameters->omega + 0.5 * B; //in MHz
   parameters->R = estimate_resistance(parameters->N, parameters
       ->a);
   parameters->L = estimate_self_induction (parameters->mu,
       parameters->N, parameters->a);
```

```
    parameters->Z = estimate_self_impedance (parameters->R, parameters->omega, parameters->L);

    memset((void*)parameters->values_d, 0, sizeof(double) * BUFFER);
    memset((void*)parameters->values_PT_PTH, 0, sizeof(double) * BUFFER);

    /* configurable values for d */
     parameters->values_d[0] = 150.0;
    //parameters->values_d[0] = 25.0;
    //parameters->values_d[1] = 50.0;
    //parameters->values_d[2] = 75.0;
    //parameters->values_d[3] = 100.0;
    //parameters->values_d[4] = 125.0;
    //parameters->values_d[5] = 150.0;
    //parameters->values_d[6] = 175.0;

  return;
}

void set_variables (enum configuration c, struct IE* parameters)
{
  switch (c)
  {
   case VARIABLE_PT:
   /* all values are in dBm units */
   parameters->values_PT_PTH[0] = 4.0;
   parameters->values_PT_PTH[1] = 5.0;
   parameters->values_PT_PTH[2] = 6.0;
   parameters->values_PT_PTH[3] = 7.0;
   parameters->values_PT_PTH[4] = 8.0;
   parameters->values_PT_PTH[5] = 9.0;
```

```
    parameters->values_PT_PTH[6] = 10.0;
    break;
    case VARIABLE_PTH:
    /* all values are in dBm units */
    parameters->values_PT_PTH[0] = -80.0;
    parameters->values_PT_PTH[1] = -70.0;
    parameters->values_PT_PTH[2] = -60.0;
    parameters->values_PT_PTH[3] = -50.0;
    parameters->values_PT_PTH[4] = -40.0;
    //parameters->values_PT_PTH[5] = -30.0;
    //parameters->values_PT_PTH[6] = -20.0;
    break;
    default:
    break;
  }

  return;
}

int estimate_opt_num_coils (double Pt, double d, double omega0,
    int N, double a, double mu, double Z, double Pth)
{
    int n;
    double Pr = -200;;
    double r = 0;
    double M = 0;
    double LMI = 0;

      for(n=1; Pr < Pth; ++n)
      {
        /* estimate the relay interval between two adjacent coils */
          r = d/n;
        /* estimate the mutual induction between two adjacent coils*/
```

```
        M = estimate_mutual_induction(mu, N, a, r);
       /* estimate the path loss incurred for n adjacent coils */
       /*  We assume the same resistance, self and mutual inductions
           ↪ between
        *  two adjacent coils for the entire distance d.
        */
         LMI = estimate_path_loss(Z, omega0, M, n);

        /* estimate the received power */
         Pr = Pt - LMI;
     }

  return (n);
}


double estimate_soil_permeability (void)
{
  return (4 * PI * pow(10,1.0/7.0));
}


double estimate_resistance (int N, double a)
{
  return (N * 2 * PI * a * R0);
}


double estimate_mutual_induction (double mu, double N, double a,
     ↪ double r)
{
  double numerator = mu * PI * pow(N, 2) * pow(a, 4);
  double denominator = 4 * pow(r, 3);
```

```
    return (numerator/denominator);
}

double estimate_self_impedance (double R, double omega, double L)
{

    return (R + J * omega * L);
}

double estimate_self_induction (double mu, int N, double a)
{

    return (1/2 * mu * PI * pow(N, 2) * a);
}


double estimate_path_loss (double Z, double omega, double M, int
    ↪ n)
{

    /*
    *   As per reference, path loss has to be 50 dB when r= 5m,
    *   R0 = 0.01 ohms/m, N = 5 and a = 0.15m
    *
    */

    double temp = find_nth_order_polynomial(Z, omega, M, n);
    double log = log10(temp);
    double result = 6.02 + 20 * log;
    return result;
}

```

```
double find_nth_order_polynomial (double Z, double omega, double
    ↪ M, int n)
{

 if(0 == n)
 {
  return 1;
 }

else if(1 == n)
 {
  double temp = Z/(omega * M);
  return (temp);
 }

else
 {
  double temp1 = Z/(omega * M);
  double temp2 = find_nth_order_polynomial(Z, omega, M, n-1);
  double temp3 = find_nth_order_polynomial(Z, omega, M, n-2);
  return temp1 * (temp2 + temp3);
 }
}
```

A.3 Source Code for Simulation 2

The source code for the C program used in Simulation 2 presented under Chapter 7, has been reproduced under the following subsections.

A.3.1 Header File

```
#include<stdio.h>
```

```
#include<stdlib.h>
#include<math.h>
#include<time.h>
#include<complex.h>
#include<assert.h>
#include<string.h>
#include<stdbool.h>

#define UNITRo 0.15328
#define Pth -150.0L
#define PI 3.14159265359
#define Q 100

/*
 * the range of values for OMEGA and Pt are dependent
 * for OMEGA in the range 865.6 ~ 868 MHz, Pt has to be
 * in the vicinity of 500 mw
 * for OMEGA in the range 902 ~ 928 MHz, Pt has to be
 * in the vicinity of 4 w
 */

//range for transmission frequency
#define MIN_OMEGA_EUR 865.6 //in MHz
#define MAX_OMEGA_EUR 868 //in MHz

#define MIN_OMEGA_USA 902 //in MHz
#define MAX_OMEGA_USA 916 //in MHz

//range for Pt
#define MIN_PT_OMEGA_EUR 26.020599913 //in dBm
#define MAX_PT_OMEGA_EUR 26.989700043 //in dBm

#define MIN_PT_OMEGA_USA 35.797835966 //in dBm
```

```
#define MAX_PT_OMEGA_USA 36.020599913 //in dBm

//range for required bandwidth
#define MIN_BW 1.0 //in KHz
#define MAX_BW 3.0//in KHz

struct point
{
 long double x;
 long double y;
};

union turn
{
 bool left;
 bool right;
};

long double calculateMu ();
long double calculateRo (long double);
long double approximate_angledl (long double, double, double,
    ↪ double, union turn);
long double approximate_ri (long double, int);
int approximate_nri (long double, long double, int);
long double calculateMi (double, long double, int , long double,
    ↪ double, double);
long double calculateK (long double, long double, double);
long double calculateKsd (long double, double);
long double calculatedelta (long double);
long double approximateLMi (long double, long double, double);
int approximate_nOpt (long double, double);
double pow (double, double);
long double power (long double, double);
```

```

/* function for generating random integer within a range */
int getRandomNum (int , int );

/* function for generating random double within a range */
double getRandomDouble (double , double );
```

A.3.2 Source File

```
#include "header.h"

int main ()
{
  long double Mu;
  long double dr = 200.0L;
  long double linedl = 30.0L; //average straight-line link distance
  long double angledl; //link distance considering displacement and deviation
  int n = 35; //average number of coils per link distance
  int nri; //number of relay intervals
  double theta_t = 30;
  double theta_r = 35;
  double theta_j = 30;
  union turn direction;
  long double a = 0.2L;
  //int N = 20;
  //int N = 25;
  int N = 30;
  //int N = 35;
  //int N = 40;
  //long double L = 11.9481L;
  //long double L = 18.1878L;
```

```
long double L = 25.7610L;
//long double L = 34.6719L;
//long double L = 44.9236L;
//long double l = 2.5136L;
//long double l = 3.1418L;
long double l = 3.7701L;
//long double l = 4.3984L;
//long double l = 5.0267L;
long double Ro = 0.0L;
double omega;
double pt;
double bw;
long double pr;
long double ri = 0L;
long double Mi = 0L;
long double K = 0L;
long double Ksd = 0L;
long double delta = 0L;
long double LMi = 0L;
int nOpt = 0;

//omega = getRandomDouble(MIN_OMEGA_EUR, MAX_OMEGA_EUR);
omega = MIN_OMEGA_EUR;
//pt = getRandomDouble(MIN_PT_OMEGA_EUR, MAX_PT_OMEGA_EUR);
pt = MIN_PT_OMEGA_EUR;
//bw = getRandomDouble(MIN_BW, MAX_BW);
bw = 1.0;

Mu = calculateMu();
Ro = calculateRo(l);

direction.left = 1;
direction.right = 0;
```

```
  angledl = approximate_angledl(linedl, theta_t, theta_r, theta_j, direction);
  ri = approximate_ri(angledl, n);
  nri = approximate_nri(dr, angledl, n);

  Mi = calculateMi(a, Mu, N, ri, theta_t, theta_r);
  K =  calculateK(Mi, L, omega);
  Ksd = calculateKsd(K, omega);
  delta = calculatedelta(Ksd);

  LMi = approximateLMi(Ro, Mi, omega);
  pr = pt - LMi;

  //for a link
  //nOpt =  approximate_nOpt(LMi, pt);

 printf("##########################\n");
 printf("\n");
 printf("Simulation Run Output\n");
 printf("=========================\n");
 printf("Field Parameters:\n");
 printf("====================\n");
 printf("Mu: %Lf\n", Mu);
 printf("dr: %Lf\n", dr);
 printf("linedl: %Lf\n", linedl);
 printf("angledl: %Lf\n", angledl);
 printf("n: %d\n", n);
 printf("nri: %d\n", nri);
 printf("theta_t: %f\n", theta_t);
 printf("theta_r: %f\n", theta_r);
 printf("theta_j: %f\n", theta_j);
 printf("ri: %Lf\n", ri);
 printf("Mi: %Lf\n", Mi);
```

```
 printf("K: %Lf\n", K);
 printf("Ksd: %Lf\n", Ksd);
 printf("delta: %Lf\n", delta);
 printf("\n");
 printf("Coil Parameters:\n");
 printf("==================\n");
 printf("a: %Lf\n", a);
 printf("N: %d\n", N);
 printf("l: %Lf\n", l);
 printf("Ro: %Lf\n", Ro);
 printf("L: %Lf\n", L);
 printf("\n");
 printf("Transmission Parameters:\n");
 printf("========================\n");
 printf("omega: %f\n", omega);
 printf("pt: %f\n", pt);
 printf("pr: %Lf\n", pr);
 printf("\n");
 //printf("Results:\n");
 //printf("========\n");
 printf("LMi: %Lf\n", LMi);
 //printf("aggregateLMi: %Lf\n", aggregateLMi);
 //printf("nOpt: %d\n", nOpt);
 printf("\n");
 printf("########################\n");
 printf("\n");

return 0;
}

long double calculateMu (void)
{
 return (4 * PI * pow(10, -7));
```

```
}

long double calculateRo (long double l)
{
 return (UNITRo * l);
}

long double approximate_angledl (long double linedl, double theta_t, double theta_r, double theta_j, union turn direction)
{
  struct point t, r;
  long double deltaX, deltaY;
  double angledl;

  t.x =  cos(theta_t);
  t.y =  sin(theta_t);

  if(direction.right)
  theta_j *= -1.0;

  r.x =  cos(theta_r + theta_j);
  r.y =  sin(theta_r + theta_j);

  deltaX = r.x - t.x;
  deltaY = r.y - t.y;

  angledl = linedl + sqrt((power(deltaX, 2) + power(deltaY, 2)));

  return (angledl);
}

long double approximate_ri (long double angledl, int n)
```

```
{
   return (angledl/n);
}

int approximate_nri (long double dr, long double angledl, int n)
{
   int nri;

   nri = (dr/angledl) * n;

  return (nri);
}

long double calculateMi (double a, long double Mu, int N, long double ri, double theta_t, double theta_r)
{
  long double Mi;
  long double temp1;
  long double temp2;

   temp1 = Mu * PI * pow(N,2);
   temp2 = power(a,4)/(2 * power(ri,3));
   Mi = temp1 * temp2;

  return(Mi);
}

long double calculateK (long double Mi, long double L, double omega)
{
   double temp;

   temp = ( 2 * power(power(L,2), 1/2));
```

```

  return ((omega * Mi) / temp);
}

long double calculateKsd (long double K, double omega)
{
 return ((2 * K) / omega);
}

long double calculatedelta (long double Ksd)
{
 return (power(Ksd,2) * pow(Q,2));
}

long double approximateLMi (long double Ro, long double Mi,
    ↪ double omega)
{
  double product = 1.0;
  long double LMi;

  product *= Ro / (omega * Mi);
  LMi = 6.02 * 20 * (log10(product));

 return (LMi);
}

//nOpt
int approximate_nOpt (long double LMi, double pt)
{
 long double temp;
 int nOpt = 0;

 temp = LMi + Pth;
```

```
 nOpt = (int) fminl(pt,temp);

 return (nOpt);
}
double pow (double b, double e)
{
  double result = 1;
  if(0 < e)
 {
  do
  {
   result *= b;

  }while(e-- > 0);
 }
 else
 {
  do
  {
   result /= b;

  }while(e++ < 0);
 }

return result;
}

long double power (long double b, double e)
{
  long double result = 1L;
  if(0 < e)
 {
  do
```

```
    {
      result *= b;

    }while(e-- > 0);
  }
  else
  {
    do
    {
      result /= b;

    }while(e++ < 0);
  }

return result;
}

/* function for generating random double value within a range */
double getRandomDouble (double low, double high)
{
  srand((unsigned)time(NULL));

  return ( ( double )rand() * ( high - low ) ) / ( double )
      RAND_MAX + low;
}

/* function for generating random integer value within a range */
int getRandomNum(int min, int max)
{
  int i;
  srand((unsigned)time(NULL));
  i = (rand() % max) + min;

```

```
    return i;
}
```

A.3.3 Sample Run Output

```
########################

Simulation Run Output
=====================
Field Parameters:
=================
Mu: 0.000001
dr: 200.000000
linedl: 30.000000
angledl: 32.368436
n: 35
nri: 216
theta_t: 30.000000
theta_r: 35.000000
theta_j: 30.000000
ri: 0.924812
Mi: 0.000023
K: 172.505994
Ksd: 0.398581
delta: 633.214443

Coil Parameters:
================
a: 0.200000
N: 30
l: 3.770100
Ro: 0.577881
L: 25.761000
```

```
Transmission Parameters:
========================
omega: 865.600000
pt: 26.020600
pr: -149.389237

LMi: 175.409836

########################
```

A.4 Source Code for Simulation 3

The source code for the MATLAB program used in Simulation 3 presented under Chapter 7, has been reproduced under the following subsections.

NOTE

The author would like to advise the reader that there are repetitions in the source code related to the two simulations belonging to Simulation 3, reproduced under the following subsections. This is due to the rigid correlation of field data for the two simulations.

A.4.1 Topsoil Terrain Covariance

The author presented the first part of the simulation and its results pertaining to the covariance of the terrain attributes for the topsoil region. The MATLAB source code for the same has been reproduced below.

```
function unit_code( )
% This function serves the following purposes:
```

```
% a) Models the altitude/elevation across the topsoil region within a
% fractal using the concept of 'fractal layers'
%
% b) Models the primary terrain attributes (altitude, slope,
% profile curvature and plan curvature) for the fractal layer of the
% topsoil region using the equations provided in the following reference:
%
% Erskine, R. H., Green, T. R., Ramirez, J. A., & MacDonald, L. H. (2007).
% Digital elevation accuracy and grid cell size: Effects on estimated
% terrain attributes.Soil Science Society of America Journal, 71(4),
% 1371-1380.
%
% In the case of the primary terrain attribute aspect, there could be
% large spikes in the case of mild slopes, as in the case of this
% simulation. This fact has been noted in the following reference (see
% Paras 1 and 2 of the section "Identifying the Effect of Precision on
% Aspect" on P 1
%
% CARTER, J. R. (1992). The effect of data precision on the calculation of
% slope and aspect using gridded DEMs. Cartographica: The International
% Journal for Geographic Information and Geovisualization, 29(1), 22-34.
```

```
%
% Based on the data reproduced in the above reference, a nominal range for
% aspect angle should fall within the range 0-90 degrees.
% In order to restrict the aspect angle within this range, the algorithm
% outlined in Figure 2 P 3 of the following reference has been adopted:
% Hodgson, M. E. (1998). Comparison of angles from surface slope/aspect
% algorithms. Cartography and Geographic Information Systems, 25(3),
% 173-185.
%
% c) Models the soil properties for each fractal layer (the soil properties
% do not vary within a fractal).
%
% d) Models the topology in terms of adjacent fractals with covariant soil
% properties
%
% d) Creates a 3D mesh grid model of the topology in terms of the
% adjacent fractals, their terrain attributes and their soil properties.
%
% Assumptions
%
% 1) A fractal is assumed to represent a hectare (100 m x 100 m) in keeping
% with the plantation density outlined in the following link:
%
% http://www.treeplantation.com/nut-trees.html
```

```
%
% 2) The total farm area is assumed to fall within the range 10-100
% hectares, based on the statistics provided in the following link:
%
% The average plantation size for Macademia trees can be found in the
% following link (ranging between less than 10 hectares for small farms to
% more than 100 hectares in the case of large farms)
% https://www.google.com.au/url?sa=t&rct=j&q=&esrc=s&source=web&cd=2&cad
% =rja&uact=8&ved=0CDAQFjAB&url=http%3A%2F%2Fwww.australian-macadamias.org%
% 2Fdownload.php%3Ffile%3DMacadamia_industry_benchmark_report2009-2012
% seasons.pdf&ei=lho9U8ftCcrrkAWPhIGQAw&usg=AFQjCNEPGDy2e6vzfah-j-
% zfZ0M8YFV2HQ
% The above range is assumed to be generic for nut trees for the sake of
% this simulation.
%
% 3) The maximum elevation for topsoil region is assumed to be 30 cm, in
% accordance with the following reference:
%
% %Silva, A. R., & Vuran, M. C. (2009). Empirical evaluation of wireless
% underground-to-underground communication in wireless underground sensor
```

```
% networks. In Distributed Computing in Sensor Systems (pp. 231-244).
% Springer Berlin Heidelberg.
%
% The topsoil region is assumed to vary in primary terrain attributes for
% the range of the above elevation, in 10 cm gradients. In addition, the
% primary terrain attributes also vary across the fractal distance of the
% topsoil region (100 m x 100 m), as the grid size d changes in accordance
% with the ground distance. The primary terrain attributes are calculated
% using the grid derivatives, which depend both on the elevation and grid
% size at a given point ( see the following reference):

% Erskine, R. H., Green, T. R., Ramirez, J. A., & MacDonald, L. H. (2007).
% Digital elevation accuracy and grid cell size: Effects on estimated
% terrain attributes.Soil Science Society of America Journal, 71(4),
% 1371-1380.
%
% 4) The soil properties are assumed to display covariance between
% neighboring fractals, as should the terrain attributes. On the contrary,
% the soil properties do not vary within a fractal, but the terrain
```

```
% attributes are assumed to display covariance across the topsoil depth
% considered for the simulation.
%
% 5) The grid scale has been taken as 1 cm = 10 m
% (for the horizontal and vertical distances - X,Y coordinates).

% the terrain has been modelled as follows:
%
% I) the matrix array TOPSOIL_FRACTAL_TERRAIN_GRID models the complete
% numerical representation  of all the layers of the topsoil fractal region
% in terms of the following:
%
% 1. the fractal ground distance in terms of the X, Y coordinates
% (2 columns) cols 1-2
% 2. the corresponding grid coordinates for fractal ground distance
% (2 columns) cols 3-4
% 3. the grid cell size for the corresponding fractal ground distance of
% the topsoil layer (100 m x 100 m) (1 column) col 5
% 4. the grid derivatives for the fractal ground distance of the
% topsoil layer (5 columns) cols 6-10
% 5. the primary terrain attributes for the fractal topsoil layer (4
% columns)cols 11-14
% 7. the soil properties of the fractal topsoil layer (12 columns) cols
% 15-26
% 8. since each fractal represents a distance on the ground of 1 hectare
```

```
% (100 m x 100 m), and since the grid scale assumed has been 1 cm = 10 m on
% the ground, there would be 10 rows to represent the entire range of the
% fractal ground distance
%
% II) the entire topsoil region is represented by three fractal layers, one
% above the other. thus TOPSOIL_FRACTAL_TERRAIN_GRID would be an array of
% three identical matrices of 10 X 26 dimension
%
% III) the function creatematrixarray, implemented based on the algorithm
% provided in the following link, would be used to create the matrix array
% TOPSOIL_FRACTAL_TERRAIN_GRID:

% http://stackoverflow.com/questions/466972/array-of-matrices-in-matlab

% Note that elevation is not stored within the matrix, as the range of
% elevations can span only three rows. Instead, each elevation value is
% used on the fly in the calculation of one dimension of the grid
% derivatives and the other primary terrain attributes.
%
% the grid derivatives are the following as per the reference mentioned as
% part of Step b above:
% Zx
% Zy
```

```
% Zxx
% Zyy
% Zxy
% each of the above derivatives is dependent on the elevation and the grid
% cell(i,j) size d
% the grid cell has been modelled as representing 10 square meters of
% actual ground distance of the topsoil region, using the scale 1 cm = 10 m
% the grid cell (i,j) size d is determined using an algorithm
% outlined in the following link:
%
%  http://geospatialmethods.org/documents/ppgc/ppgc.html
%
% "A grid cell (i,j) is defined as the area between grid coordinates
% i-.5 and i+.5, and j-.5 and j+.5."
%
% since the unit grid is a square grid of 1cm x 1cm resolution, the grid
% area is approximated based on the algorithm provided in the above
% link, without the 0.5 round off
% thus i and j values have been used directly in the approximation of the
% grid cell size d
% Note that since the grid is always square, i = j
%
% Although the topsoil region has been modelled in elevation gradients of
% 10 cm, the actual ground distance would remain unchanged in the case of
```

```
% all the elevation gradients. Consequently, the grid cell size would
% remain the same as well.

% array of 3 matrices, where each matrix denotes one fractal layer of the
% topsoil region
% each matrix size would be 10 X 26, as explained above
% variables pertaining to creation of a matrix array
narrays = 3;
arraysz = [10,26];

%nested functions
%function to create an array of matrices, where each matrix denotes one
%fractal layer of the topsoil region
creatematrixarray (narrays, arraysz);
% function to model the fractal distance encompassing 1 hectare
% (100 x 100 m)
modelfractaldist;
% function to model the topsoil region within a fractal as ascending
% fractal layers with covariant primary terrain attributes
modelfractalayers;
% function to model the neighboring fractals encompassing the entire
% topology with covariant soil properties and primary terrain attributes
% modelneighborfractals;
% function to create a 3D mesh grid of the entire topology in terms of
% neighboring fractals
% creat3dmeshtopology;
```

```
%globals
global TOPSOIL_FRACTAL_TERRAIN_GRID
TOPSOIL_FRACTAL_TERRAIN_GRID = creatematrixarray (narrays, arraysz);

% Covariance terrain matrix for the topsoil region within the fractal
%global COVFRACTALS_TOPOLOGY_TERRAIN_GRID

% function to create TOPSOIL_FRACTAL_TERRAIN_GRID
% code segment borrowed from the following web reference:
%
%http://stackoverflow.com/questions/466972/array-of-matrices-in-matlab

function result = creatematrixarray (narrays, arraysz)
result = cell(1, narrays);
for i = 1 : narrays
result{i} = zeros(arraysz);
end
end

% FROM HERE ON TERRAIN MODELLING CODE BEGINS
%-------------------------------------------------------
% the terrain has been modelled as follows:
%
% I) the matrix array TOPSOIL_FRACTAL_TERRAIN_GRID models the complete
% numerical representation of all the layers of the topsoil fractal region
% in terms of the following:
%
```

```
% 1. the fractal ground distance in terms of the X, Y coordinates
% (2 columns) cols 1-2
% 2. the corresponding grid coordinates for fractal ground distance
% (2 columns) cols 3-4
% 3. the grid cell size for the corresponding fractal ground distance of
% the topsoil layer (100 m x 100 m) (1 column) col 5
% 4. the grid derivatives for the fractal ground distance of the
% topsoil layer (5 columns) cols 6-10
% 5. the primary terrian attributes for the fractal topsoil layer (4
% columns)cols 11-14
% 7. the soil properties of the fractal topsoil layer (12 columns) cols
% 15-26
%------------------------------------------------------------
function [] = modelfractaldist ()
%  this function models the terrain distance for the fractal in
% terms of the X and Y coordinates, and the corresponding grid cell
% (i,j)
% the grid cell has been constructed according to the scale 1 cm =
% 10 m
 % for the additional matrix dimesnions
for k = 1:3
% for X and Y distance coordinates
for i=1:10
switch i
case 1
    TOPSOIL_FRACTAL_TERRAIN_GRID {k}(i,i) = i * 10;
    TOPSOIL_FRACTAL_TERRAIN_GRID {k}(i,i+1) = i * 10;
```

```
case 2
    TOPSOIL_FRACTAL_TERRAIN_GRID {k}(i,i-1) = i * 10;
    TOPSOIL_FRACTAL_TERRAIN_GRID {k}(i,i) = i * 10;
otherwise
    a = i - 1;
    b = a - 1;
    TOPSOIL_FRACTAL_TERRAIN_GRID {k}(i,i-a) = i * 10;
    TOPSOIL_FRACTAL_TERRAIN_GRID {k}(i,i-b) = i * 10;
end
end
% for corresponding grid cell (i,j) coordinates
for i = 1:10
switch i
case 1
    TOPSOIL_FRACTAL_TERRAIN_GRID {k}(i,i+2) = i;
    TOPSOIL_FRACTAL_TERRAIN_GRID {k}(i,i+3) = i;
case 2
    TOPSOIL_FRACTAL_TERRAIN_GRID {k}(i,i+1) = i;
    TOPSOIL_FRACTAL_TERRAIN_GRID {k}(i,i+2) = i;
case 3
    TOPSOIL_FRACTAL_TERRAIN_GRID {k}(i,i) = i;
    TOPSOIL_FRACTAL_TERRAIN_GRID {k}(i,i+1) = i;
case 4
    TOPSOIL_FRACTAL_TERRAIN_GRID {k}(i,i-1) = i;
    TOPSOIL_FRACTAL_TERRAIN_GRID {k}(i,i) = i;
case 5
    TOPSOIL_FRACTAL_TERRAIN_GRID {k}(i,i-2) = i;
    TOPSOIL_FRACTAL_TERRAIN_GRID {k}(i,i-1) = i;
case 6
    TOPSOIL_FRACTAL_TERRAIN_GRID {k}(i,i-3) = i;
    TOPSOIL_FRACTAL_TERRAIN_GRID {k}(i,i-2) = i;
case 7
    TOPSOIL_FRACTAL_TERRAIN_GRID {k}(i,i-4) = i;
```

```
    TOPSOIL_FRACTAL_TERRAIN_GRID {k}(i,i-3) = i;
case 8
    TOPSOIL_FRACTAL_TERRAIN_GRID {k}(i,i-5) = i;
    TOPSOIL_FRACTAL_TERRAIN_GRID {k}(i,i-4) = i;
case 9
    TOPSOIL_FRACTAL_TERRAIN_GRID {k}(i,i-6) = i;
    TOPSOIL_FRACTAL_TERRAIN_GRID {k}(i,i-5) = i;
case 10
    TOPSOIL_FRACTAL_TERRAIN_GRID {k}(i,i-7) = i;
    TOPSOIL_FRACTAL_TERRAIN_GRID {k}(i,i-6) = i;
end
end
end
end

% the nested function to model the topsoil region as covariant
    ↪ fractal
% terrain layers, with each layer signifying a higher elevation
% the soil properties remain the same across the layers

function [] = modelfractalayers ()

% nested functions in relation to approximation of primary
    ↪ terrain
% attributes

% function to approximate grid cell size for the distance of the
% topsoil region, which is the distance encompassed by the
    ↪ fractal,
% i.e., i hectare
approxgridcellsize;
% function to approximate the grid derivatives for the distance
```

```
%  of the topsoil region, which is the distance encompassed by the
% fractal, i.e., 1 hectare and also the corresponding soil
% properties
% note that the soil properties do not vary within a fractal region
approxgriderivatives_terrainattributes_nd_soilproperties;

% nested helper functions
% this function will be used for writing the cell array
% TOPSOIL_FRACTAL_TERRAIN_GRID to a text file on the disk for
% the sake of data analysis
% the analysis involves removing all the redundant data, so as
% to retain only data essential for generating 3D meshgrid
% code snippet for writing cell array to a file on the
% disk has been borrowed from the following reference:
% http://stackoverflow.com/questions/8565617/print-a-cell-array-as-txt-
% in-matlab
writecellarray2fileondisk;

% this function will be used to plot the three dimensional
% fractal terrain comprising of three layers, in terms of the
% mean values for elevation, profile curvature and plan
% curvature. only these three values are relevant for plotting
% the terrain.
plot3dfractalterrain;

function [] = approxgridcellsize ()
%nested function to calculate grid cell (i,j) size d, which does
%not change with the different layers of the topsoil region.
% the grid cell (i,j) size d is determined using an algorithm
% outlined in the following link:
```

```
%
%  http://geospatialmethods.org/documents/ppgc/ppgc.html
%
% "A grid cell (i,j) is defined as the area between grid coordinates
% i-.5 and i+.5, and j-.5 and j+.5."
%
% since the unit grid is a square grid of 1cm x 1cm resolution, the
% grid area is approximated based on the algorithm provided in the
% above link, without the 0.5 round off
% thus i and j values have been used directly in the approximation
% of the grid cell size d
% Note that since the grid is always square, i = j

% for additional fractal dimensions
for k = 1:3
j = 5;
for i = 1:10
TOPSOIL_FRACTAL_TERRAIN_GRID{k}(i,j) = ...
    TOPSOIL_FRACTAL_TERRAIN_GRID{k}(i,j - 2) * ...
    TOPSOIL_FRACTAL_TERRAIN_GRID{k}(i,j - 1);
end
end
end

function [] = approxgriderivatives_terrainattributes_nd_soilproperties()
% the grid cell derivatives are the following as per the reference
% mentioned as part of Step b above:
```

```
% Zx
% Zy
% Zxx
% Zyy
% Zxy
% since each of the above is dependent both on the
% grid cell (1,j) size d and the elevation, they are calculated
% independently for the different layers of the topsoil region.
% To approximate the the grid derivatives across the topsoil
% region, the grid derivatives are calculated
%
% Since z denotes the elevation in all of the equations related to
% the approximation of the grid derivatives, the notation z(i,j) in
% the equations is assumed to refer to the grid cell in the z axis,
% which corresponds to a fractal layer. Thus z(i+1,j) should refer
% to the next fractal layer above. Both the ground distance for the
% topsoil fractal region (X,Y) and the corresponding grid cell size
% do not vary for a given z(i,j) for a particular approximation.
% This should  not be cause for concern, as the approximation is
% done over the entire range of the fractal distance of the
% topsoil region.
%
% the layer which corresponds to 0 elevation (ground layer) has not
% been considered as a unique case in the approximation of the
% grid derivatives, as in the case of the three layers
% corresponding to increasing elevation in 10 cm steps. However,
```

```
% the ground layer is included in the equations pertaining to the
% approximation of the grid derivatives in the immediate layer
% above, which corresponds to a height of 10 cm.
%
% in the equations pertaining to the approximation of grid
% derivatives in the reference mentioned under Step b above, the
% coordinates Zi+1,j/Zi,j+1 should denote elevation gradients in
% the horizontal/vertical directions (X/Y). But since the topsoil
% region is assumed to be of uniform elevation in a fractal layer,
% with only increasing horizontal/vertical distances, and since the
% coordinates have been used in the reference as approximations to
% partial differentiation of the z coordinate (elevation) wrt
% either x coordinate (horizontal distance) or y coordinate
% (vertical distance), or both, the notion of clamping
% Zi+1,j/Zi,j+1 on hierarchical layers should be identical in its
% implication, especially since the entire range of
% horizontal/vertical distance for the fractal region of the
% topsoil have been accounted for.
%
% zi-1,j/zi,j-1 has been approximated as zi,j in the simulation.
% The reason being that both of the coordinates imply increase in
% one direction and a corresponding decrease in the other. Since
% the coordinates are clamped on the Z axis in the simulation for
% reasons stated above, this should have the net effect of
% retaining the same layer in the current simulation.
%
% By the same logic as above, zi+1,j+1 denotes two layers above the
% current layer, since zi+1,j/zi,j+1 denotes the layer immediately
```

```
% above the current layer. Similarly, zi-1,j-1 denotes two layers
% below the current layer, since zi,j-1/zi-1,j denotes the layer
% immediately below the current layer.
%
% zx and zy are considered as zc for the simulation, for the reason
% that both denote a distance in one axis (X,Y) at a given point
% in time, and since the distance is mapped to the Z axis in this
% simulation, the distance should effectively denote the current
% layer of the topsoil region.

% nested function to generate a matrix of soil properties of the
% current fractal layer of the topsoil region
soil;

% for the additional matrix dimensions
for k = 1:3
switch k
case 1
%case corresponds to 10 cm elevation
% Zx = (zi+1, j - zi-1, j) / 2d
% zu denotes the upper layer
% zl denotes the lower layer
% zc denotes the current layer
% zuu denotes two layers above the current layer
% zll denotes two layers below the current layer
zu = 0.2; % denotes zi+1,j/zi,j+1
zc = 0.1; % denotes zi,j/zi-1,j/zi,j-1/zx/zy
zl = 0; % denotes zi-1,j/zi,j-1 i.e., the ground layer
zuu = 0.3; % denotes zi+1,j+1
zll = -0.2; % denotes zi-1,j-1
zx_y = 0; % denotes zx/zy
zxx_yy = 0; % denotes zxx/zyy
```

```
zxy = 0; % denotes zxy
xindex = 6; % matrix column Zx index
yindex = 7; % matrix column Zy index
xxindex = 8; % matrix column Zxx index
yyindex = 9; % matrix column Zyy index
xyindex = 10; % matrix column Zxy index
dxindex = xindex - 1; % difference between xindex and
                      % matrix column index for grid
                      % cell size d
dyindex = yindex - 2; % difference between yindex and
                      % matrix column index for grid
                      % cell size d
dxxindex = xxindex - 3; % difference between xxindex and
                      % matrix column index for grid
                      % cell size d
dyyindex = yyindex - 4; % difference between yyindex and
                      % matrix column index for grid
                      % cell size d
dxyindex = xyindex -5; %difference between xyindex and
                      % matrix column index for grid
                      % cell size d
sfd = 0; % denotes slope
sfdindex = 11; % matrix column sfd index
theta_fd = 0; % dentoes aspect
theta_fd_index = 12; % matrix column theta_fd index
kp = 0; % denotes the profile curvature
kpindex = 13; % matrix column kp index
kc = 0; % denotes the plan curvature
kcindex = 14; % matrix column kc index
for j = 1:10
TOPSOIL_FRACTAL_TERRAIN_GRID{k}(j,xindex) = (zu - zl)/2 * ...
    TOPSOIL_FRACTAL_TERRAIN_GRID{k}(j,dxindex);
TOPSOIL_FRACTAL_TERRAIN_GRID{k}(j,yindex) = (zu - zl)/2 * ...
```

```
    TOPSOIL_FRACTAL_TERRAIN_GRID{k}(j,dyindex);
zx_y = TOPSOIL_FRACTAL_TERRAIN_GRID{k}(j,yindex);
TOPSOIL_FRACTAL_TERRAIN_GRID{k}(j,xxindex) = (zu - 2 * zc + zl)/ ...
    nthroot(TOPSOIL_FRACTAL_TERRAIN_GRID{k}(j,dxxindex), 2);
TOPSOIL_FRACTAL_TERRAIN_GRID{k}(j,yyindex) = (zu - 2 * zc + zl)/ ...
    nthroot(TOPSOIL_FRACTAL_TERRAIN_GRID{k}(j,dyyindex), 2);
zxx_yy = TOPSOIL_FRACTAL_TERRAIN_GRID{k}(j,yyindex);
TOPSOIL_FRACTAL_TERRAIN_GRID{k}(j,xyindex) = (zu - zuu - zll + zc)/ ...
    4 * nthroot(TOPSOIL_FRACTAL_TERRAIN_GRID{k}(j,dxyindex), 2);
zxy = TOPSOIL_FRACTAL_TERRAIN_GRID{k}(j,xyindex);
sfd = sqrt(nthroot(zc,2) + nthroot(zc,2));
TOPSOIL_FRACTAL_TERRAIN_GRID{k}(j,sfdindex) = sfd;
% Note that aspect is calculated using a
% restrictive algorithm, in order to eliminate
% spikes for mild slopes under consideration, and
% confine the aspect angle within the
% nominal range 0-90 degrees. See the explanation
% provided as part of Step b.
%theta_fd = 180 - atand(zc/zc) + 90 * (zc/zc);
theta_fd = 90 - atand (sfd/sfd);
TOPSOIL_FRACTAL_TERRAIN_GRID{k}(j,theta_fd_index) = theta_fd;
temp1 = (zxx_yy * nthroot(zx_y, 2) + 2 * zxy * nthroot(zx_y, 2) + ...
    zxx_yy * nthroot(zx_y, 2));
temp2 = 2 * nthroot(zx_y, 2) + 1;
temp3 = nthroot(sfd, 2) * nthroot(temp2, 3/2);
kp = temp1/temp3;
TOPSOIL_FRACTAL_TERRAIN_GRID{k}(j,kpindex) = kp;
temp1 = (zxx_yy * nthroot(zx_y, 2) - 2 * zxy * nthroot(zx_y, 2) + ...
```

```
    zxx_yy * nthroot(zx_y, 2));
temp2 = nthroot(sfd, 3);
kc = temp1/temp2;
TOPSOIL_FRACTAL_TERRAIN_GRID{k}(j,kcindex) = kc;
end
% soil(); the function call has been commented
% out here, since there has to be a single
% invocation of this function to get the loop
% iteration right for writing to successive
% dimensions of the matrix struture
case 2
%case corresponds to 20 cm elevation
% Zx = (zi+1, j - zi-1, j) / 2d
% zu denotes the upper layer
% zl denotes the lower layer
% zc denotes the current layer
% zuu denotes two layers above the current layer
% zll denotes two layers below the current layer
zu = 0.3; % denotes zi+1,j/zi,j+1
zc = 0.2; % denotes zi,j/zi-1,j/zi,j-1/zx/zy
zl = 0.1; % denotes zi-1,j/zi,j-1 i.e., the ground layer
% note that the value of 0.4 for zuu has been
% specified merely following a logical order
% since this value denotes a region above the
% topsoil, the implications of the same have to
% be decided and the appropriateness of the
% value has to be ascertained
zuu = 0.4; % denotes zi+1,j+1
zll = 0; % denotes zi-1,j-1
zx_y = 0; % denotes zx/zy
zxx_yy = 0; % denotes zxx/zyy
zxy = 0; % denotes zxy
xindex = 6; % matrix column Zx index
```

```
yindex = 7; % matrix column Zy index
xxindex = 8; % matrix column Zxx index
yyindex = 9; % matrix column Zyy index
xyindex = 10; % matrix column Zxy index
dxindex = xindex - 1; % difference between xindex and
                   % matrix column index for grid
                   % cell size d
dyindex = yindex - 2; % difference between yindex and
                   % matrix column index for grid
                   % cell size d
dxxindex = xxindex - 3; % difference between xxindex and
                   % matrix column index for grid
                   % cell size d
dyyindex = yyindex - 4; % difference between yyindex and
                   % matrix column index for grid
                   % cell size d
dxyindex = xyindex -5; %difference between xyindex and
                   % matrix column index for grid
                   % cell size d
sfd = 0; % denotes slope
sfdindex = 11; % matrix column sfd index
theta_fd = 0; % dentoes aspect
theta_fd_index = 12; % matrix column theta_fd index
kp = 0; % denotes the profile curvature
kpindex = 13; % matrix column kp index
kc = 0; % denotes the plan curvature
kcindex = 14; % matrix column kc index
for j = 1:10
TOPSOIL_FRACTAL_TERRAIN_GRID {k}(j,xindex) = (zu - zl)/2 * ...
    TOPSOIL_FRACTAL_TERRAIN_GRID {k}(j,dxindex);
TOPSOIL_FRACTAL_TERRAIN_GRID {k}(j,yindex) = (zu - zl)/2 * ...
    TOPSOIL_FRACTAL_TERRAIN_GRID {k}(j,dyindex);
% this variable will be used in later calculation
```

```
zx_y = TOPSOIL_FRACTAL_TERRAIN_GRID {k}(j,yindex);
TOPSOIL_FRACTAL_TERRAIN_GRID {k}(j,xxindex) = (zu - 2 * zc + zl)/ ...
    nthroot(TOPSOIL_FRACTAL_TERRAIN_GRID {k}(j,dxxindex), 2);
TOPSOIL_FRACTAL_TERRAIN_GRID {k}(j,yyindex) = (zu - 2 * zc + zl)/ ...
    nthroot(TOPSOIL_FRACTAL_TERRAIN_GRID {k}(j,dyyindex), 2);
% this variable will be used in later calculation
zxx_yy = TOPSOIL_FRACTAL_TERRAIN_GRID {k}(j,yyindex);
TOPSOIL_FRACTAL_TERRAIN_GRID {k}(j,xyindex) = (zu - zuu - zll + zc)/ ...
    4 * nthroot(TOPSOIL_FRACTAL_TERRAIN_GRID {k}(j,dxyindex), 2);
% this variable will be used in later calculation
zxy = TOPSOIL_FRACTAL_TERRAIN_GRID {k}(j,xyindex);
sfd = sqrt(nthroot(zc,2) + nthroot(zc,2));
TOPSOIL_FRACTAL_TERRAIN_GRID {k}(j,sfdindex) = sfd;
% Note that aspect is calculated using a
% restrictive algorithm, in order to eliminate
% spikes for mild slopes under consideration, and
% confine the aspect angle within the
% nominal range 0-90 degrees. See the explanation
% provided as part of Step b.
%theta_fd = 180 - atand(zc/zc) + 90 * (zc/zc);
theta_fd = 90 - atand (sfd/sfd);
TOPSOIL_FRACTAL_TERRAIN_GRID {k}(j,theta_fd_index) = theta_fd;
temp1 = (zxx_yy * nthroot(zx_y, 2) + 2 * zxy * nthroot(zx_y, 2) + ...
    zxx_yy * nthroot(zx_y, 2));
temp2 = 2 * nthroot(zx_y, 2) + 1;
temp3 = nthroot(sfd, 2) * nthroot(temp2, 3/2);
kp = temp1/temp3;
TOPSOIL_FRACTAL_TERRAIN_GRID {k}(j,kpindex) = kp;
```

```
temp1 = (zxx_yy * nthroot(zx_y, 2) - 2 * zxy * nthroot(zx_y, 2) +
    ↪ ...
      zxx_yy * nthroot(zx_y, 2));
temp2 = nthroot(sfd, 3);
kc = temp1/temp2;
TOPSOIL_FRACTAL_TERRAIN_GRID{k}(j,kcindex) = kc;
end
% soil(); the function call has been commented
% out here, since there has to be a single
% invocation of this function to get the loop
% iteration right for writing to successive
% dimensions of the matrix struture
case 3
%case corresponds to 30 cm elevation
% Zx = (zi+1, j - zi-1, j) / 2d
% zu denotes the upper layer
% zl denotes the lower layer
% zc denotes the current layer
% zuu denotes two layers above the current layer
% zll denotes two layers below the current layer
zu = 0.4; % denotes zi+1,j/zi,j+1
zc = 0.3; % denotes zi,j/zi-1,j/zi,j-1/zx/zy
zl = 0.2; % denotes zi-1,j/zi,j-1 i.e., the ground layer
% note that the value of 0.5 for zuu has been
% specified merely following a logical order
% since this value denotes a region above the
% topsoil, the implications of the same have to
% be decided and the appropriateness of the
% value has to be ascertained
zuu = 0.5; % denotes zi+1,j+1
zll = 0.1; % denotes zi-1,j-1
zx_y = 0; % denotes zx/zy
zxx_yy = 0; % denotes zxx/zyy
```

```
zxy = 0; % denotes zxy
xindex = 6; % matrix column Zx index
yindex = 7; % matrix column Zy index
xxindex = 8; % matrix column Zxx index
yyindex = 9; % matrix column Zyy index
xyindex = 10; % matrix column Zxy index
dxindex = xindex - 1; % difference between xindex and
                   % matrix column index for grid
                   % cell size d
dyindex = yindex - 2; % difference between yindex and
                   % matrix column index for grid
                   % cell size d
dxxindex = xxindex - 3; % difference between xxindex and
                   % matrix column index for grid
                   % cell size d
dyyindex = yyindex - 4; % difference between yyindex and
                   % matrix column index for grid
                   % cell size d
dxyindex = xyindex -5; %difference between xyindex and
                   % matrix column index for grid
                   % cell size d
sfd = 0; % denotes slope
sfdindex = 11; % matrix column sfd index
theta_fd = 0; % dentoes aspect
theta_fd_index = 12; % matrix column theta_fd index
kp = 0; % denotes the profile curvature
kpindex = 13; % matrix column kp index
kc = 0; % denotes the plan curvature
kcindex = 14; % matrix column kc index
for j = 1:10
TOPSOIL_FRACTAL_TERRAIN_GRID {k}(j,xindex) = (zu - zl)/2 * ...
    TOPSOIL_FRACTAL_TERRAIN_GRID {k}(j,dxindex);
TOPSOIL_FRACTAL_TERRAIN_GRID {k}(j,yindex) = (zu - zl)/2 * ...
```

```
    TOPSOIL_FRACTAL_TERRAIN_GRID {k}(j,dyindex);
% this variable will be used in later calculation
zx_y = TOPSOIL_FRACTAL_TERRAIN_GRID {k}(j,yindex);
TOPSOIL_FRACTAL_TERRAIN_GRID {k}(j,xxindex) = (zu - 2 * zc + zl)/ ...
    nthroot(TOPSOIL_FRACTAL_TERRAIN_GRID {k}(j,dxxindex), 2);
TOPSOIL_FRACTAL_TERRAIN_GRID {k}(j,yyindex) = (zu - 2 * zc + zl)/ ...
    nthroot(TOPSOIL_FRACTAL_TERRAIN_GRID {k}(j,dyyindex), 2);
% this variable will be used in later calculation
zxx_yy = TOPSOIL_FRACTAL_TERRAIN_GRID {k}(j,yyindex);
TOPSOIL_FRACTAL_TERRAIN_GRID {k}(j,xyindex) = (zu - zuu - zll + zc)/ ...
    4 * nthroot(TOPSOIL_FRACTAL_TERRAIN_GRID {k}(j,dxyindex), 2);
% this variable will be used in later calculation
zxy = TOPSOIL_FRACTAL_TERRAIN_GRID {k}(j,xyindex);
sfd = sqrt(nthroot(zc,2) + nthroot(zc,2));
TOPSOIL_FRACTAL_TERRAIN_GRID {k}(j,sfdindex) = sfd;
% Note that aspect is calculated using a
% restrictive algorithm, in order to eliminate
% spikes for mild slopes under consideration, and
% confine the aspect angle within the
% nominal range 0-90 degrees. See the explanation
% provided as part of Step b.
%theta_fd = 180 - atand(zc/zc) + 90 * (zc/zc);
theta_fd = 90 - atand (sfd/sfd);
TOPSOIL_FRACTAL_TERRAIN_GRID {k}(j,theta_fd_index) = theta_fd;
temp1 = (zxx_yy * nthroot(zx_y, 2) + 2 * zxy * nthroot(zx_y, 2) + ...
    zxx_yy * nthroot(zx_y, 2));
temp2 = 2 * nthroot(zx_y, 2) + 1;
temp3 = nthroot(sfd, 2) * nthroot(temp2, 3/2);
kp = temp1/temp3;
```

```
TOPSOIL_FRACTAL_TERRAIN_GRID{k}(j,kpindex) = kp;
temp1 = (zxx_yy * nthroot(zx_y, 2) - 2 * zxy * nthroot(zx_y, 2) + ...
    zxx_yy * nthroot(zx_y, 2));
temp2 = nthroot(sfd, 3);
kc = temp1/temp2;
TOPSOIL_FRACTAL_TERRAIN_GRID{k}(j,kcindex) = kc;
end
soil();
end
end

% nested function to generate a matrix of soil properties of the current
% fractal layer of the topsoil region
function soil()
%function to generate a matrix of soil properties of the current fractal
%layer of the topsoil region
%
% this routine writes to the last 12 columns of  the
% TOPOLOGY_FRACTAL_TERRAIN_GRID matrix defined in the file terrain.m
%
% algorithm
% inside a loop generate a random value within the applicable range
% for each soil property (column), and then use these values for assigning
% a specific row in TOPOLOGY_FRACTAL_TERRAIN_GRID
% generate the covariance matrix COVFRACTALS using TOPOLOGY
% 12 soil properties are considered as per Table 2.3 of the Reference
```

```
% the 12 soil properties represent the soil characteristics of a
    ↪ unit grid
% cell size 1 sq. cm, equivalent to a fractal distance of 10 m x
    ↪ 10 m on
% the ground
% as indicated in the complementary file terrain.m, the soil
    ↪ properties do
% not change within a fractal, and hence the same soil properties
    ↪  would be
% written for the entire range of the fractal distance on the
    ↪ ground, which
% is  100 m x 100 m, represented on the grid as 10 cm x 10 cm
    ↪ according to
% scale.

% Reference for soil properties:
% Principles of Soil Physics (Library reference: 631.43LAL)
% Page # 21 (Table 2.2), 25 (Table 2.3, Section 2.2)
%global variables

global WD % Water Density
WD = 1.0;

x = 0;
y = 0;

%declarations for nested functions
% independent values
calcrandPD;
calcrandDBD;
calcrandWBD;
calcrandVSM;
calcrandDS;
```

```
calcrandDSV;
calcrandAR;

% dependent values
calcrandP(x,y);
calcrandAP(x,y);
calcrandVR(x,y);
calcrandGSM(x,y);
calcrandLR(x,y);

% definition for nested functions
% To calculate random Particle Density
function r = calcrandPD()
%rng(0,'twister');
rng(1); % for repeatability
a = 2.6;
b = 2.8;
r = (b-a).*rand(1,1) + a;
end

% To calculate random Dry Bulk Density
function r = calcrandDBD()
%rng(0,'twister');
rng(1); % for repeatability
a = 0.7;
b = 1.8;
r = (b-a).*rand(1,1) + a;
end

% To calculate random Wet Bulk Density
function r = calcrandWBD()
%rng(0,'twister');
rng(1); % for repeatability
```

```
a = 1.0;
b = 2.0;
r = (b-a).*rand(1,1) + a;
end

% To calculate Volumetric Soil Moisture content
function r = calcrandVSM()
%rng(0,'twister');
rng(1); % for repeatability
a = 0.0;
b = 0.7;
r = (b-a).*rand(1,1) + a;
end

%To calculate random Degree of Saturation
function r = calcrandDS ()
%rng(0,'twister');
rng(1); % for repeatability
a = 0.0;
b = 1.0;
r = (b-a).*rand(1,1) + a;
end

%To calculate random Dry Specific Volume
function r = calcrandDSV()
%rng(0,'twister');
rng(1); % for repeatability
a = 0.5;
b = 1.0;
r = (b-a).*rand(1,1) + a;
end

%To calculate random Air Ratio
```

```
function r = calcrandAR()
%rng(0,'twister');
rng(1); % for repeatability
a = 0.0;
b = 1.0;
r = (b-a).*rand(1,1) + a;
end

% To calculate random Porosity
%the first argument represents particle density
% the second argument represents dry bulk density
function r = calcrandP (x,y)
r = 1 - (x/y);
end

% To calculate random Air Porosity
%the first argument represents porosity
% the second argument represents volumetric soil moisture content
function r = calcrandAP (x,y)
r = x - y;
end

% To calculate random Void Ratio
%the first argument represents particle density
% the second argument represents dry bulk density
function r = calcrandVR (x,y)
r = (x/y) - 1;
end

% To calculate random Gravimetric Soil Moisture content
%the first argument represents wet bulk density
% the second argument represents dry bulk density
function r = calcrandGSM (x,y)
```

```
r = (x - y) / y;
end

%To calculate random Liquid Ratio
%the first argument represents volumetric soil moisture content
% the second argument represents void ratio
function r = calcrandLR (x,y)
r = x .* (1 + y);
end

% loop for generating random values
% the following is the column order for soil properties, constituting a
% single row:
% [pd, dbd, wbd, vsm, ds, dsv, ar, p, ap, vr, gsm, lr]
% a temporary vector for holding the index values
% of parameters to be retrieved from TOPOLOGY
% the column order of temp is as follows:
% [pd, dbd, wbd, vsm, ds, dsv, ar, p, vr]
temp = zeros(1,9);
m = 15; % start column index for soil properties in
% TOPOLOGY_FRACTAL_TERRAIN_GRID
n = 26; % end column index for soil properties in
% TOPOLOGY_FRACTAL_TERRAIN_GRID
c = 1; % variable for indexing temp

% for additional matrix dimensions
for k = 1:3
switch k
case 1
for i = 1:10 % for all rows
for j = m:n % all columns
switch j
```

```
case 15
TOPSOIL_FRACTAL_TERRAIN_GRID {k}(i,j) = calcrandPD();
temp(1,c) = j;
case 16
TOPSOIL_FRACTAL_TERRAIN_GRID {k}(i,j) = calcrandDBD();
temp(1,c+1) = j;
case 17
TOPSOIL_FRACTAL_TERRAIN_GRID {k}(i,j) = calcrandWBD();
temp(1,c+2) = j;
case 18
TOPSOIL_FRACTAL_TERRAIN_GRID {k}(i,j) = calcrandVSM();
temp(1,c+3) = j;
case 19
TOPSOIL_FRACTAL_TERRAIN_GRID {k}(i,j) = calcrandDS();
temp(1,c+4) = j;
case 20
TOPSOIL_FRACTAL_TERRAIN_GRID {k}(i,j) = calcrandDSV();
temp(1,c+5) = j;
case 21
TOPSOIL_FRACTAL_TERRAIN_GRID {k}(i,j) = calcrandAR();
temp(1,c+6) = j;
case 22
x = temp(1,c);
y = temp(1,c+1);
TOPSOIL_FRACTAL_TERRAIN_GRID {k}(i,j) = ...
    calcrandP (TOPSOIL_FRACTAL_TERRAIN_GRID {k}(i,x),...
    TOPSOIL_FRACTAL_TERRAIN_GRID {k}(i,y));
temp(1,c+7) = j;
case 23
x = temp(1,c+7);
y = temp(1,c+3);
TOPSOIL_FRACTAL_TERRAIN_GRID {k}(i,j) = ...
    calcrandAP (TOPSOIL_FRACTAL_TERRAIN_GRID {k}(i,x),...
```

```
    TOPSOIL_FRACTAL_TERRAIN_GRID {k}(i,y));
case 24
x = temp(1,c);
y = temp(1,c+1);
TOPSOIL_FRACTAL_TERRAIN_GRID {k}(i,j) = ...
    calcrandVR (TOPSOIL_FRACTAL_TERRAIN_GRID {k}(i,x),...
    TOPSOIL_FRACTAL_TERRAIN_GRID {k}(i,y));
temp(1,c+8) = j;
case 25
x = temp(1,c+2);
y = temp(1,c+1);
TOPSOIL_FRACTAL_TERRAIN_GRID {k}(i,j) = ...
    calcrandGSM (TOPSOIL_FRACTAL_TERRAIN_GRID {k}(i,x),...
    TOPSOIL_FRACTAL_TERRAIN_GRID {k}(i,y));
case 26
x = temp(1,c+3);
y = temp(1,c+8);
TOPSOIL_FRACTAL_TERRAIN_GRID {k}(i,j) = ...
    calcrandLR (TOPSOIL_FRACTAL_TERRAIN_GRID {k}(i,x),...
    TOPSOIL_FRACTAL_TERRAIN_GRID {k}(i,y));
otherwise
end
end
end
case 2
for i = 1:10 % for all rows
for j = m:n % all columns
switch j
case 15
TOPSOIL_FRACTAL_TERRAIN_GRID {k}(i,j) = calcrandPD();
temp(1,c) = j;
case 16
TOPSOIL_FRACTAL_TERRAIN_GRID {k}(i,j) = calcrandDBD();
```

```
temp(1,c+1) = j;
case 17
TOPSOIL_FRACTAL_TERRAIN_GRID{k}(i,j) = calcrandWBD();
temp(1,c+2) = j;
case 18
TOPSOIL_FRACTAL_TERRAIN_GRID{k}(i,j) = calcrandVSM();
temp(1,c+3) = j;
case 19
TOPSOIL_FRACTAL_TERRAIN_GRID{k}(i,j) = calcrandDS();
temp(1,c+4) = j;
case 20
TOPSOIL_FRACTAL_TERRAIN_GRID{k}(i,j) = calcrandDSV();
temp(1,c+5) = j;
case 21
TOPSOIL_FRACTAL_TERRAIN_GRID{k}(i,j) = calcrandAR();
temp(1,c+6) = j;
case 22
x = temp(1,c);
y = temp(1,c+1);
TOPSOIL_FRACTAL_TERRAIN_GRID{k}(i,j) = ...
    calcrandP(TOPSOIL_FRACTAL_TERRAIN_GRID{k}(i,x),...
    TOPSOIL_FRACTAL_TERRAIN_GRID{k}(i,y));
temp(1,c+7) = j;
case 23
x = temp(1,c+7);
y = temp(1,c+3);
TOPSOIL_FRACTAL_TERRAIN_GRID{k}(i,j) = ...
    calcrandAP(TOPSOIL_FRACTAL_TERRAIN_GRID{k}(i,x),...
    TOPSOIL_FRACTAL_TERRAIN_GRID{k}(i,y));
case 24
x = temp(1,c);
y = temp(1,c+1);
TOPSOIL_FRACTAL_TERRAIN_GRID{k}(i,j) = ...
```

```
    calcrandVR (TOPSOIL_FRACTAL_TERRAIN_GRID {k}(i,x),...
    TOPSOIL_FRACTAL_TERRAIN_GRID {k}(i,y));
temp(1,c+8) = j;
case 25
x = temp(1,c+2);
y = temp(1,c+1);
TOPSOIL_FRACTAL_TERRAIN_GRID {k}(i,j) = ...
    calcrandGSM (TOPSOIL_FRACTAL_TERRAIN_GRID {k}(i,x),...
    TOPSOIL_FRACTAL_TERRAIN_GRID {k}(i,y));
case 26
x = temp(1,c+3);
y = temp(1,c+8);
TOPSOIL_FRACTAL_TERRAIN_GRID {k}(i,j) = ...
    calcrandLR (TOPSOIL_FRACTAL_TERRAIN_GRID {k}(i,x),...
    TOPSOIL_FRACTAL_TERRAIN_GRID {k}(i,y));
otherwise
end
end
end
case 3
for i = 1:10 % for all rows
for j = m:n % all columns
switch j
case 15
TOPSOIL_FRACTAL_TERRAIN_GRID {k}(i,j) = calcrandPD();
temp(1,c) = j;
case 16
TOPSOIL_FRACTAL_TERRAIN_GRID {k}(i,j) = calcrandDBD();
temp(1,c+1) = j;
case 17
TOPSOIL_FRACTAL_TERRAIN_GRID {k}(i,j) = calcrandWBD();
temp(1,c+2) = j;
case 18
```

```
TOPSOIL_FRACTAL_TERRAIN_GRID {k}(i,j) = calcrandVSM();
temp(1,c+3) = j;
case 19
TOPSOIL_FRACTAL_TERRAIN_GRID {k}(i,j) = calcrandDS();
temp(1,c+4) = j;
case 20
TOPSOIL_FRACTAL_TERRAIN_GRID {k}(i,j) = calcrandDSV();
temp(1,c+5) = j;
case 21
TOPSOIL_FRACTAL_TERRAIN_GRID {k}(i,j) = calcrandAR();
temp(1,c+6) = j;
case 22
x = temp(1,c);
y = temp(1,c+1);
TOPSOIL_FRACTAL_TERRAIN_GRID {k}(i,j) = ...
    calcrandP (TOPSOIL_FRACTAL_TERRAIN_GRID {k}(i,x),...
    TOPSOIL_FRACTAL_TERRAIN_GRID {k}(i,y));
temp(1,c+7) = j;
case 23
x = temp(1,c+7);
y = temp(1,c+3);
TOPSOIL_FRACTAL_TERRAIN_GRID {k}(i,j) = ...
    calcrandAP (TOPSOIL_FRACTAL_TERRAIN_GRID {k}(i,x),...
    TOPSOIL_FRACTAL_TERRAIN_GRID {k}(i,y));
case 24
x = temp(1,c);
y = temp(1,c+1);
TOPSOIL_FRACTAL_TERRAIN_GRID {k}(i,j) = ...
    calcrandVR (TOPSOIL_FRACTAL_TERRAIN_GRID {k}(i,x),...
    TOPSOIL_FRACTAL_TERRAIN_GRID {k}(i,y));
temp(1,c+8) = j;
case 25
x = temp(1,c+2);
```

```
y = temp(1,c+1);
TOPSOIL_FRACTAL_TERRAIN_GRID {k}(i,j) = ...
    calcrandGSM (TOPSOIL_FRACTAL_TERRAIN_GRID {k}(i,x),...
    TOPSOIL_FRACTAL_TERRAIN_GRID {k}(i,y));
case 26
x = temp(1,c+3);
y = temp(1,c+8);
TOPSOIL_FRACTAL_TERRAIN_GRID {k}(i,j) = ...
    calcrandLR (TOPSOIL_FRACTAL_TERRAIN_GRID {k}(i,x),...
    TOPSOIL_FRACTAL_TERRAIN_GRID {k}(i,y));
otherwise
end
end
end
end
end
end
end
% display the c array
format shortG; % applicable only to disp, not fprintf
%celldisp (TOPSOIL_FRACTAL_TERRAIN_GRID);
% write the cell array on to a file on the disk
writecellarray2fileondisk();

% nested function for writing cell array to a text file
% on the disk for the sake of data analysis
% the analysis involves removing all the redundant data,
% so as to retain only data essential for generating the
% 3D meshgrid
% code snippet for writing cell array to a file on the
% disk borrowed from the following reference:
% http://stackoverflow.com/questions/8565617/print-a-cell-array-
    as-txt-
```

```
% in-matlab
function writecellarray2fileondisk()
C = TOPSOIL_FRACTAL_TERRAIN_GRID.';
fid = fopen('file.dlm', 'wt');
fprintf(fid, ...
    '"%g"\t"%g"\t"%g"\t"%g"\t"%g"\t"%g"\t"%g"\t"%g"\t"%g"\t"%g"\r\n',...
    C{:}); % write 1 column at a time
fclose(fid);
end

%nested function to plot the 3D meshgrid of the layered
% fractal terrain in terms of the mean values of the
% following primary terrain attributes across the
% fractal distance of 1 hectare (100m x 100m):
%
% a) elevation (sfd) approximated in column 11 of each
% cell of the cell array TOPSOIL_FRACTAL_TERRAIN_GRID
%
% b) profile curvature (kp) approximated in column 13
% of each cell of the cell array
% TOPSOIL_FRACTAL_TERRAIN_GRID
%
% c) plan curvature (kc) approximated in column 14 of
% each cell of the cell array TOPSOIL_FRACTAL_TERRAIN_GRID
function plot3dfractalterrain()
% algorithm
% * extract the relevant columns (11, 13, 14) of each
% cell to a suitable array
% * use the cell array to calculate the mean of the
% column values
% * use the mean values for 3D mesh generation
% cell array definition for extraction
```

```
% since only three columns are required, each
% spanning 10 rows, the requirement is for a 10 x 3
% matrix

% the algorithm for extraction of columns from each
% cell has been adapted from the following link:
%
% http://www.mathworks.com.au/matlabcentral/newsreader/
    ↪ view_thread/242344
narrays = 3;
arraysz = [10,3];
matrix_array = creatematrixarray (narrays, arraysz);

% for additional matrix dimensions
for k = 1:3
for i = 1: 3
switch i
case 1
R = cat(11, TOPSOIL_FRACTAL_TERRAIN_GRID{k});
R = R(:,11);
matrix_array {k}(:,i) = R;
case 2
R = cat(13, TOPSOIL_FRACTAL_TERRAIN_GRID{k});
R = R(:,13);
matrix_array {k}(:,i) = R;
case 3
R = cat(14, TOPSOIL_FRACTAL_TERRAIN_GRID{k});
R = R(:,14);
matrix_array {k}(:,i) = R;
otherwise
end
end
end
```

```
%celldisp(matrix_array);

% now, extract each terrain attribute from each cell
% of the cell array and to a separate matrix for
% calculating mean
submatrix_sfd = zeros(10,3); % for slope values
submatrix_kp = zeros(10,3); % for profile curvature
submatrix_kc = zeros(10,3); % for plan curvature

for k = 1:3
switch k
case 1
for i = 1: 3
switch i
case 1
R = cat(k, matrix_array{i});
R = R(:,i);
submatrix_sfd(:,i) = R;
case 2
R = cat(k, matrix_array{i});
R = R(:,i-1);
submatrix_sfd(:,i) = R;
case 3
R = cat(k, matrix_array{i});
R = R(:,i-2);
submatrix_sfd(:,i) = R;
otherwise
end
end
case 2
for i = 1: 3
switch i
case 1
```

```
R = cat(i, matrix_array{i}(:,k));
R = R(:,i);
submatrix_kp(:,i) = R;
case 2
R = cat(i-1, matrix_array{i}(:,k));
R = R(:,i-1);
submatrix_kp(:,i) = R;
case 3
R = cat(i-2, matrix_array{i}(:,k));
R = R(:,i-2);
submatrix_kp(:,i) = R;
otherwise
end
end
case 3
for i = 1: 3
switch i
case 1
R = cat(i, matrix_array{i}(:,k));
R = R(:,i);
submatrix_kc(:,i) = R;
case 2
R = cat(i-1, matrix_array{i}(:,k));
R = R(:,i-1);
submatrix_kc(:,i) = R;
case 3
R = cat(i-2, matrix_array{i}(:,k));
R = R(:,i-2);
submatrix_kc(:,i) = R;
otherwise
end
end
end
```

```
end

% now, extract the mean values
% mean values for sfd
M_sfd = mean(submatrix_sfd);
disp(M_sfd);

% mean values for kp
M_kp = mean(submatrix_kp);
disp(M_kp);

% mean values for kc
M_kc = mean(submatrix_kc);
disp(M_kc);

%convert the vectors to a single matrix for
% plotting
% transpose the vectors for concatenation
M_sfd = permute(M_sfd, [2,1]);
disp(M_sfd);

M_kp = permute(M_kp, [2,1]);
disp(M_kp);

M_kc = permute(M_kc, [2,1]);
disp(M_kc);

% now horizontally concatenate the vectors
Z = horzcat(M_sfd, M_kp, M_kc);
disp(Z);

% now convert the concatenation of vectors to a
% matrix
```

```
Z = vec2mat(Z, 3);
disp(Z);

% now plot the 3D surface mesh-grid
surf(Z);
xlabel('slope', 'Color', 'k', 'FontSize',12, 'FontWeight','bold')
    ↪ ;
ylabel('profile curvature', 'Color', 'b', 'FontSize',12, ...
    'FontWeight','bold');
zlabel('plan curvature', 'Color', 'r', 'FontSize',12, 'FontWeight
    ↪ ','bold');
%xlabel('slope', 'Color', 'k');
%ylabel('profile curvature', 'Color', 'b');
%zlabel('plan curvature', 'Color', 'r');
colormap lines
colorbar
end
end
end
```

A.4.2 Covariance of Terrain Attributes and Soil Properties

The second part of the simulation concerned itself with covariance of the terrain attributes and soil properties across the chosen farm land of 100 hectares. It was mentioned in this context under Chapter 7 about the notion of a MIV for characterizing the average covariance of both of these factors. The corresponding MATLAB source code has been reproduced below.

```
function soil_topography_code( )
% code segment borrowed from the following web reference:
%
%http://stackoverflow.com/questions/466972/array-of-matrices-in-
    ↪ matlab
```

```

function result = creatematrixarray (narrays, arraysz)
result = cell(1, narrays);
for i = 1 : narrays
result{i} = zeros(arraysz);
end
end

function flowcontrol ()
% dummy, to be rewritten
data = zeros(10);

% array of decafractals for covdecafractals
%num = 10; % number of entries
%sz = size(array_decafractals);
%array_covdecafractals = creatematrixarray (num, sz);

for v = 1:10
for s = 1:10
unitfractal = modelunitfractaldata (data);
decafractal(s).data = unitfractal;
end
covdecafractal(v).data = decafractal;
end

%write2fileondisk(covdecafractal);
plot3dcovariantdecafractalterrain (covdecafractal);

% nested function to write the entire data to a file on the disk
function write2fileondisk (covdecafractal)

fid = fopen('filecov.dlm', 'wt');
% since there are 10 decafractals in the cell
```

```
% array, and since each decafractal in turn holds
% 10 unitfractals, the data to be written to the
% file should be the unitfractal data for all the
% decafractals

for g = 1:10
fprintf(fid, 'Dec %d\n',g);
fprintf(fid,'=====\r\n');
a = covdecafractal(g).data;

% for each unitfractal inside the decafractal
for h = 1:10
b = a(h).data;
fprintf(fid, 'Unit %d\n',h);
fprintf(fid,'======\r\n');
% for each layer in the unitfractal
%                                        for u = 1:3
for u = 1:1
fprintf(fid, '\r\n');
fprintf(fid, 'Layer %d\n',u);
fprintf(fid,'======\r\n');
% for each column in the unitfractal layer
for l = 1:26
switch l
case 15
fprintf(fid, '\r\n');
fprintf(fid, 'Soil\n');
fprintf(fid, '====\r\n');
fprintf(fid, '\r\n');
fprintf(fid, 'PD\n');
fprintf(fid, '==\r\n');
fprintf(fid, ...
```

```
        '"%g"\t"%g"\t"%g"\t"%g"\t"%g"\t"%g"\n"%g"\t"%g"\t"%g"\t"%g"\r\n',...
        b{u}(:,l));
case 16
fprintf(fid, 'DBD\n');
fprintf(fid, '===\r\n');
fprintf(fid, ...
        '"%g"\t"%g"\t"%g"\t"%g"\t"%g"\t"%g"\n"%g"\t"%g"\t"%g"\t"%g"\r\n',...
        b{u}(:,l));
case 17
fprintf(fid, 'WBD\n');
fprintf(fid, '===\r\n');
fprintf(fid, ...
        '"%g"\t"%g"\t"%g"\t"%g"\t"%g"\t"%g"\n"%g"\t"%g"\t"%g"\t"%g"\r\n', ...
        b{u}(:,l));
case 18
fprintf(fid, 'VSM\n');
fprintf(fid, '===\r\n');
fprintf(fid, ...
        '"%g"\t"%g"\t"%g"\t"%g"\t"%g"\t"%g"\n"%g"\t"%g"\t"%g"\t"%g"\r\n', ...
        b{u}(:,l));
case 19
fprintf(fid, 'DS\n');
fprintf(fid, '==\r\n');
fprintf(fid, ...
        '"%g"\t"%g"\t"%g"\t"%g"\t"%g"\t"%g"\n"%g"\t"%g"\t"%g"\t"%g"\r\n', ...
        b{u}(:,l));
case 20
fprintf(fid, 'DSV\n');
```

```
fprintf(fid, '===\r\n');
fprintf(fid, ...
    '"%g"\t"%g"\t"%g"\t"%g"\t"%g"\t"%g"\n"%g"\t"%g"\t"%g"\t"%g"\r\n', ...
    b{u}(:,l));
case 21
fprintf(fid, 'AR\n');
fprintf(fid, '==\r\n');
fprintf(fid, ...
    '"%g"\t"%g"\t"%g"\t"%g"\t"%g"\t"%g"\n"%g"\t"%g"\t"%g"\t"%g"\r\n', ...
    b{u}(:,l));
case 22
fprintf(fid, 'P\n');
fprintf(fid, '=\r\n');
fprintf(fid, ...
    '"%g"\t"%g"\t"%g"\t"%g"\t"%g"\t"%g"\n"%g"\t"%g"\t"%g"\t"%g"\r\n', ...
    b{u}(:,l));
case 23
fprintf(fid, 'AP\n');
fprintf(fid, '==\r\n');
fprintf(fid, ...
    '"%g"\t"%g"\t"%g"\t"%g"\t"%g"\t"%g"\n"%g"\t"%g"\t"%g"\t"%g"\r\n', ...
    b{u}(:,l));
case 24
fprintf(fid, 'VR\n');
fprintf(fid, '==\r\n');
fprintf(fid, ...
    '"%g"\t"%g"\t"%g"\t"%g"\t"%g"\t"%g"\n"%g"\t"%g"\t"%g"\t"%g"\r\n', ...
    b{u}(:,l));
```

```
case 25
fprintf(fid, 'GSM\n');
fprintf(fid, '===\r\n');
fprintf(fid, ...
    '"%g"\t"%g"\t"%g"\t"%g"\t"%g"\t"%g"\n"%g"\t"%g"\t"%g"\t"%g"\r\n', ...
    b{u}(:,l));
case 26
fprintf(fid, 'LR\n');
fprintf(fid, '==\r\n');
fprintf(fid, ...
    '"%g"\t"%g"\t"%g"\t"%g"\t"%g"\t"%g"\n"%g"\t"%g"\t"%g"\t"%g"\r\n', ...
    b{u}(:,l));
end
end
end
fprintf(fid, '\r\n');
fprintf(fid,...
'**********************END OF DATA SEGMENT **********************\r\n');
fprintf(fid, '\r\n');
fprintf(fid, '\r\n');
end
end
fclose('all');
end

%nested function to plot the covariant mesh-grid
function plot3dcovariantdecafractalterrain (covdecafractal)

% algorithm
% 1. extract the set of decafractals from
```

```
% covdecafractal
% 2. for each decafractal, extract the set of columns
% 15−26 of layer 1 of each of the 10 unitfractals
% 3. calculate the mean of the columns 15−26 of
% unitfractals inside each deacfractals after
% extraction
% 3. plot the mesh as the covariance of the mean value
% across the decafractals in terms of increasing grid
% scale and ground distance
% create arrays of vectors

% nested functions
function [covdeca] = createdatahierarchy()
% create arrays of vectors
num =1;
sz = [1,12];
for c1 = 1: 10
for c2 = 1:10
unit = creatematrixarray (num, sz);
deca(c2).data = unit;
end
covdeca(c1).data = deca;
end
end

function [covdeca] = writedatahierarchy(covdeca, covdecafractal)
for g = 1:10
a = covdecafractal(g).data;
a1 = covdeca(g).data;
% for each unitfractal inside the decafractal
for h = 1:10
b = a(h).data;
b1 = a1(h).data;
```

```
% for each layer of the unitfractal
for layer = 1:1
% for each row of the layer
for row = 1:1
% for columns 15-26 of the
% layer
for col = 15:26
t = 14;
temp = b{layer}(row,col);
b1{layer}(:, col-t) = temp;
end
end
end
a1(h).data = b1;
end
covdeca(g).data = a1;
end
end

function writedatatofile (covdeca)
fid = fopen('filesoilpropextract.dlm', 'wt');
for outer = 1:10
fprintf(fid, 'Decafractal: %d\n',outer);
fprintf(fid, '================\r\n');
for inner = 1:10
fprintf(fid, 'Unitfractal: %d\n', inner);
fprintf(fid, '================\r\n');
fprintf(fid, ...
'"%g"\t"%g"\t"%g"\t"%g"\t"%g"\t"%g"\t"%g"\t"%g"\t"%g"\t"%g"\t"%g"\t"%g"\r\n\r\n', ...
covdeca(outer).data(inner).data{:}(:,:));
fprintf(fid,...
```

```
'===========================================================================\
    ↪ r\n');
end
fprintf(fid,...
'*********************END OF DATA SEGMENT*********************\
    ↪ r\n\r\n');
end
fclose('all');
end

function plotmeshgrid (covdeca)
% algorithm
% 1. generate the mean of each unitfractal inside
% the decafractal, and then use the mean values to
% generate the mean of the decafractal
% 2. plot the covariance of the mean values of the
% conjoined decafractals, in relation to the ground
% distance and the corresponding grid distance
% (recall the ratio of 1:10)
% for outer = 1:10
%  for inner = 1:10
%      celldisp(covdeca(outer).data(inner).data);
%     end
%  end

n = 10;  % number of entries
s =  [1,10]; % size of each entry

mean_unitfractals = creatematrixarray (n,s);
mean_decafractals = [1,10];
for outer = 1:10
for inner = 1:10
mean_unitfractals{outer}(:,inner) = ...
```

```
    mean (covdeca(outer).data(inner).data{:}(:,1:12));
end
mean_decafractals(:,outer) = mean(mean_unitfractals{outer}(:,inner));
end
% X, Y and Z axes for the meshgrid
XYZ = zeros(10,3);
%disp(XYZ);
%X corresponds to the ground distance
%Y corresponds to the proportiaonate distance on
%the grid scale
%Z corresponds to  mean values of the
% soil properties for the conjoined decafractals
% as a function of the ground distance and grid
% scale
% the mean values of the covariant soil
%properties of the conjoined decafractals
%covering the total ground distance, are plotted
% against the distance
%
for i = 1:10
for j = 1:3
switch j
case 1
% ground distance corresponds to 100 hectares or
% 1000000 square meters, in decfractal units or
% 10 hectares
XYZ(i,j)  = i * 100000;
case 2
% on the grid scale, the ground distance of 10
% hectares has been represented using 1 unit, in
% accordance with the ratio of 1:10
XYZ(i,j) = i;
```

```
case 3
% the mean values of the covariant soil
% properties of the conjoined decafractals
% covering the total ground distance, are plotted
% against the distance
XYZ(i,j) =   mean_decafractals(:,i);
end
end
end
format longG;
disp(XYZ);
surf(XYZ);

xlabel('Mean Index Value (MIV)', 'FontSize', 12, ...
'FontWeight','bold', 'color', 'k');
ylabel('grid scale', 'FontSize', 12, 'FontWeight','bold', 'color', 'b');
zlabel('land area', 'FontSize', 12, 'FontWeight','bold', 'color', 'r')
colormap lines
colorbar
%mesh(XYZ);
end

covdeca = createdatahierarchy();
covdeca = writedatahierarchy(covdeca, covdecafractal);
%writedatatofile (covdeca);
plotmeshgrid (covdeca);
end

function [data] = modelunitfractaldata (data)
% the cell array is created here, and reused in
% all the other nested routines
```

```
narrays = 3;
arraysz = [10,26];
data = creatematrixarray(narrays, arraysz);
% nested functions

% to model the terrain distance for the fractal in terms of the
% X and Y coordinates, and the corresponding grid cell (i,j)
distance (data);

% to approximate the grid cell size
grid (data);

% to approximate grid derivatives and terrain attributes
terrain (data);

% to approximate soil properties
soil (data);

% definitions of nested functions
function [data]= distance (data)
for f = 1:3 % for unitfractal layers
% for X and Y distance coordinates
for g=1:10
switch g
case 1
data{f}(g,g) = g * 10;
data{f}(g,g+1) = g * 10;
case 2
data{f}(g,g-1) = g * 10;
data{f}(g,g) = g * 10;
otherwise
a = g - 1;
b = a - 1;
```

```
data{f}(g,g-a) = g * 10;
data{f}(g,g-b) = g * 10;
end
end
% for corresponding grid cell (i,j) coordinates
for g = 1:10
switch g
case 1
data{f}(g,g+2) = g;
data{f}(g,g+3) = g;
case 2
data{f}(g,g+1) = g;
data{f}(g,g+2) = g;
case 3
data{f}(g,g) = g;
data{f}(g,g+1) = g;
case 4
data{f}(g,g-1) = g;
data{f}(g,g) = g;
case 5
data{f}(g,g-2) = g;
data{f}(g,g-1) = g;
case 6
data{f}(g,g-3) = g;
data{f}(g,g-2) = g;
case 7
data{f}(g,g-4) = g;
data{f}(g,g-3) = g;
case 8
data{f}(g,g-5) = g;
data{f}(g,g-4) = g;
case 9
data{f}(g,g-6) = g;
```

```
data{f}(g,g-5) = g;
case 10
data{f}(g,g-7) = g;
data{f}(g,g-6) = g;
end
end
end
end

function [data] = grid (data)
% for additional fractal dimensions
for k = 1:3
n = 5;
for i = 1:10
data {k}(i,n) = data {k}(i,n - 2) * data {k}(i,n - 1);
end
end
end

function [data] = terrain (data)
% for the additional matrix dimensions
for k = 1:3
switch k
case 1
%case corresponds to 10 cm elevation
% Zx = (zi+1, j - zi-1, j) / 2d
% zu denotes the upper layer
% zl denotes the lower layer
% zc denotes the current layer
% zuu denotes two layers above the current layer
% zll denotes two layers below the current layer
zu = 0.2; % denotes zi+1,j/zi,j+1
zc = 0.1; % denotes zi,j/zi-1,j/zi,j-1/zx/zy
```

```
zl = 0; % denotes zi-1,j/zi,j-1 i.e., the ground layer
zuu = 0.3; % denotes zi+1,j+1
zll = -0.2; % denotes zi-1,j-1
zx_y = 0; % denotes zx/zy
zxx_yy = 0; % denotes zxx/zyy
zxy = 0; % denotes zxy
xindex = 6; % matrix column Zx index
yindex = 7; % matrix column Zy index
xxindex = 8; % matrix column Zxx index
yyindex = 9; % matrix column Zyy index
xyindex = 10; % matrix column Zxy index
dxindex = xindex - 1; % difference between xindex and
                      % matrix column index for grid
                      % cell size d
dyindex = yindex - 2; % difference between yindex and
                      % matrix column index for grid
                      % cell size d
dxxindex = xxindex - 3; % difference between xxindex and
                      % matrix column index for grid
                      % cell size d
dyyindex = yyindex - 4; % difference between yyindex and
                      % matrix column index for grid
                      % cell size d
dxyindex = xyindex -5; %difference between xyindex and
                      % matrix column index for grid
                      % cell size d
sfd = 0; % denotes slope
sfdindex = 11; % matrix column sfd index
theta_fd = 0; % denotes aspect
theta_fd_index = 12; % matrix column theta_fd index
kp = 0; % denotes the profile curvature
kpindex = 13; % matrix column kp index
kc = 0; % denotes the plan curvature
```

```
kcindex = 14; % matrix column kc index
for j = 1:10
data {k}(j,xindex) = (zu - zl)/2 * data {k}(j,dxindex);
data {k}(j,yindex) = (zu - zl)/2 * data {k}(j,dyindex);
zx_y = data {k}(j,yindex);
data {k}(j,xxindex) = (zu - 2 * zc + zl)/ ...
    nthroot(data {k}(j,dxxindex), 2);
data {k}(j,yyindex) = (zu - 2 * zc + zl)/ ...
    nthroot(data {k}(j,dyyindex), 2);
zxx_yy = data {k}(j,yyindex);
data {k}(j,xyindex) = (zu - zuu - zll + zc)/ ...
    4 * nthroot(data {k}(j,dxyindex), 2);
zxy = data {k}(j,xyindex);
sfd = sqrt(nthroot(zc,2) + nthroot(zc,2));
data {k}(j,sfdindex) = sfd;
% Note that aspect is calculated using a
% restrictive algorithm, in order to eliminate
% spikes for mild slopes under consideration, and
% confine the aspect angle within the
% nominal range 0-90 degrees. See the explanation
% provided as part of Step b.
%theta_fd = 180 - atand(zc/zc) + 90 * (zc/zc);
theta_fd = 90 - atand (sfd/sfd);
data {k}(j,theta_fd_index) = theta_fd;
temp1 = (zxx_yy * nthroot(zx_y, 2) + 2 * zxy * nthroot(zx_y, 2) ...
    + zxx_yy * nthroot(zx_y, 2));
temp2 = 2 * nthroot(zx_y, 2) + 1;
temp3 = nthroot(sfd, 2) * nthroot(temp2, 3/2);
kp = temp1/temp3;
data {k}(j,kpindex) = kp;
temp1 = (zxx_yy * nthroot(zx_y, 2) - 2 * zxy * nthroot(zx_y, 2) ...
```

```
    + zxx_yy * nthroot(zx_y, 2));
temp2 = nthroot(sfd, 3);
kc = temp1/temp2;
data {k}(j,kcindex) = kc;
end
case 2
%case corresponds to 20 cm elevation
% Zx = (zi+1, j - zi-1, j) / 2d
% zu denotes the upper layer
% zl denotes the lower layer
% zc denotes the current layer
% zuu denotes two layers above the current layer
% zll denotes two layers below the current layer
zu = 0.3; % denotes zi+1,j/zi,j+1
zc = 0.2; % denotes zi,j/zi-1,j/zi,j-1/zx/zy
zl = 0.1; % denotes zi-1,j/zi,j-1 i.e., the ground layer
% note that the value of 0.4 for zuu has been
% specified merely following a logical order
% since this value denotes a region above the
% topsoil, the implications of the same have to
% be decided and the appropriateness of the
% value has to be ascertained
zuu = 0.4; % denotes zi+1,j+1
zll = 0; % denotes zi-1,j-1
zx_y = 0; % denotes zx/zy
zxx_yy = 0; % denotes zxx/zyy
zxy = 0; % denotes zxy
xindex = 6; % matrix column Zx index
yindex = 7; % matrix column Zy index
xxindex = 8; % matrix column Zxx index
yyindex = 9; % matrix column Zyy index
xyindex = 10; % matrix column Zxy index
dxindex = xindex - 1; % difference between xindex and
```

```
                    % matrix column index for grid
                    % cell size d
dyindex = yindex - 2; % difference between yindex and
                    % matrix column index for grid
                    % cell size d
dxxindex = xxindex - 3; % difference between xxindex and
                    % matrix column index for grid
                    % cell size d
dyyindex = yyindex - 4; % difference between yyindex and
                    % matrix column index for grid
                    % cell size d
dxyindex = xyindex -5; %difference between xyindex and
                    % matrix column index for grid
                    % cell size d
sfd = 0; % denotes slope
sfdindex = 11; % matrix column sfd index
theta_fd = 0; % denotes aspect
theta_fd_index = 12; % matrix column theta_fd index
kp = 0; % denotes the profile curvature
kpindex = 13; % matrix column kp index
kc = 0; % denotes the plan curvature
kcindex = 14; % matrix column kc index
for j = 1:10
data {k}(j,xindex) = (zu - zl)/2 * data {k}(j,dxindex);
data {k}(j,yindex) = (zu - zl)/2 * data {k}(j,dyindex);
% this variable will be used in later calculation
zx_y = data {k}(j,yindex);
data {k}(j,xxindex) = (zu - 2 * zc + zl)/ ...
    nthroot(data {k}(j,dxxindex), 2);
data {k}(j,yyindex) = (zu - 2 * zc + zl)/ ...
    nthroot(data {k}(j,dyyindex), 2);
% this variable will be used in later calculation
zxx_yy = data {k}(j,yyindex);
```

```
data {k}(j,xyindex) = (zu - zuu - zll + zc)/ ...
     4 * nthroot(data {k}(j,dxyindex), 2);
% this variable will be used in later calculation
zxy = data {k}(j,xyindex);
sfd = sqrt(nthroot(zc,2) + nthroot(zc,2));
data {k}(j,sfdindex) = sfd;
% Note that aspect is calculated using a
% restrictive algorithm, in order to eliminate
% spikes for mild slopes under consideration, and
% confine the aspect angle within the
% nominal range 0-90 degrees. See the explanation
% provided as part of Step b.
%theta_fd = 180 - atand(zc/zc) + 90 * (zc/zc);
theta_fd = 90 - atand (sfd/sfd);
data {k}(j,theta_fd_index) = theta_fd;
temp1 = (zxx_yy * nthroot(zx_y, 2) + 2 * zxy * nthroot(zx_y, 2)
    ↪ ...
     + zxx_yy * nthroot(zx_y, 2));
temp2 = 2 * nthroot(zx_y, 2) + 1;
temp3 = nthroot(sfd, 2) * nthroot(temp2, 3/2);
kp = temp1/temp3;
data {k}(j,kpindex) = kp;
temp1 = (zxx_yy * nthroot(zx_y, 2) - 2 * zxy * nthroot(zx_y, 2)
    ↪ ...
     + zxx_yy * nthroot(zx_y, 2));
temp2 = nthroot(sfd, 3);
kc = temp1/temp2;
data {k}(j,kcindex) = kc;
end
case 3
%case corresponds to 30 cm elevation
% Zx = (zi+1, j - zi-1, j) / 2d
% zu denotes the upper layer
```

```
% zl denotes the lower layer
% zc denotes the current layer
% zuu denotes two layers above the current layer
% zll denotes two layers below the current layer
zu = 0.4; % denotes zi+1,j/zi,j+1
zc = 0.3; % denotes zi,j/zi-1,j/zi,j-1/zx/zy
zl = 0.2; % denotes zi-1,j/zi,j-1 i.e., the ground layer
% note that the value of 0.5 for zuu has been
% specified merely following a logical order
% since this value denotes a region above the
% topsoil, the implications of the same have to
% be decided and the appropriateness of the
% value has to be ascertained
zuu = 0.5; % denotes zi+1,j+1
zll = 0.1; % denotes zi-1,j-1
zx_y = 0; % denotes zx/zy
zxx_yy = 0; % denotes zxx/zyy
zxy = 0; % denotes zxy
xindex = 6; % matrix column Zx index
yindex = 7; % matrix column Zy index
xxindex = 8; % matrix column Zxx index
yyindex = 9; % matrix column Zyy index
xyindex = 10; % matrix column Zxy index
dxindex = xindex - 1; % difference between xindex and
                      % matrix column index for grid
                      % cell size d
dyindex = yindex - 2; % difference between yindex and
                      % matrix column index for grid
                      % cell size d
dxxindex = xxindex - 3; % difference between xxindex and
                      % matrix column index for grid
                      % cell size d
dyyindex = yyindex - 4; % difference between yyindex and
```

```
                         % matrix column index for grid
                         % cell size d
dxyindex = xyindex -5; %difference between xyindex and
                         % matrix column index for grid
                         % cell size d
sfd = 0; % denotes slope
sfdindex = 11; % matrix column sfd index
theta_fd = 0; % denotes aspect
theta_fd_index = 12; % matrix column theta_fd index
kp = 0; % denotes the profile curvature
kpindex = 13; % matrix column kp index
kc = 0; % denotes the plan curvature
kcindex = 14; % matrix column kc index
for j = 1:10
data {k}(j,xindex) = (zu - zl)/2 * data {k}(j,dxindex);
data {k}(j,yindex) = (zu - zl)/2 * data {k}(j,dyindex);
% this variable will be used in later calculation
zx_y = data {k}(j,yindex);
data {k}(j,xxindex) = (zu - 2 * zc + zl)/ ...
     nthroot(data {k}(j,dxxindex), 2);
data {k}(j,yyindex) = (zu - 2 * zc + zl)/ ...
     nthroot(data {k}(j,dyyindex), 2);
% this variable will be used in later calculation
zxx_yy = data {k}(j,yyindex);
data {k}(j,xyindex) = (zu - zuu - zll + zc)/ ...
     4 * nthroot(data {k}(j,dxyindex), 2);
% this variable will be used in later calculation
zxy = data {k}(j,xyindex);
sfd = sqrt(nthroot(zc,2) + nthroot(zc,2));
data {k}(j,sfdindex) = sfd;
% Note that aspect is calculated using a
% restrictive algorithm, in order to eliminate
% spikes for mild slopes under consideration, and
```

```
% confine the aspect angle within the
% nominal range 0-90 degrees. See the explanation
% provided as part of Step b.
%theta_fd = 180 - atand(zc/zc) + 90 * (zc/zc);
theta_fd = 90 - atand (sfd/sfd);
data {k}(j,theta_fd_index) = theta_fd;
temp1 = (zxx_yy * nthroot(zx_y, 2) + ...
    2 * zxy * nthroot(zx_y, 2) + zxx_yy * nthroot(zx_y, 2));
temp2 = 2 * nthroot(zx_y, 2) + 1;
temp3 = nthroot(sfd, 2) * nthroot(temp2, 3/2);
kp = temp1/temp3;
data {k}(j,kpindex) = kp;
temp1 = (zxx_yy * nthroot(zx_y, 2) - 2 * zxy * nthroot(zx_y, 2) +
   ↪  ...
    zxx_yy * nthroot(zx_y, 2));
temp2 = nthroot(sfd, 3);
kc = temp1/temp2;
data {k}(j,kcindex) = kc;
end
end
end
end

function [data] = soil (data)
% variable controlling the seed input to the rng()
% function based on each invocation
% the increment to this variable can be sequential
% since the covariance of soil properties has been
% implemented for each decafractal, and in turn, for
% the corresponding group of unitfractals
% this variable has been made persistent, as its value
% is incremented from the previous value, before being
% used in the next iteration of this routine
```

```
persistent seed_val;
seed_val = 0;

%global variables
global WD % Water Density
WD = 1.0;

x = 0;
y = 0;

%declarations for nested functions

% independent values
calcrandPD;
calcrandDBD;
calcrandWBD;
calcrandVSM;
calcrandDS;
calcrandDSV;
calcrandAR;

% dependent values
calcrandP(x,y);
calcrandAP(x,y);
calcrandVR(x,y);
calcrandGSM(x,y);
calcrandLR(x,y);

% helper functions
% increases the seed value by 1 for each iteration
% of the function
add1toseedvalue;

```

```
% to add 1 to the seed value for each iteration
function add1toseedvalue ()
seed_val = seed_val + 1;
rng(seed_val, 'combRecursive');
rng('shuffle');
end

% increase the seed here
add1toseedvalue();

% definition for nested functions
%rng(0, 'combRecursive');
% To calculate random Particle Density
function r = calcrandPD()
%rng(seed, 'combRecursive'); % for repeatability
%rng(seed, seed_val); % for repeatability
%rng('default');
a = 2.6;
b = 2.8;
r = (b-a).*rand(1,1) + a;
end

% To calculate random Dry Bulk Density
function r = calcrandDBD()
%rng(seed,'combRecursive'); % for repeatability
%rng(seed_val); % for repeatability
%rng('default');
a = 0.7;
b = 1.8;
r = (b-a).*rand(1,1) + a;
end

% To calculate random Wet Bulk Density
```

```
function r = calcrandWBD()
%rng(seed,'combRecursive'); % for repeatability
%rng(seed_val); % for repeatability
%rng('default');
a = 1.0;
b = 2.0;
r = (b-a).*rand(1,1) + a;
end

% To calculate Volumetric Soil Moisture content
function r = calcrandVSM()
%rng(seed,'combRecursive'); % for repeatability
%rng(seed_val); % for repeatability
%rng('default');
a = 0.0;
b = 0.7;
r = (b-a).*rand(1,1) + a;
end

%To calculate random Degree of Saturation
function r = calcrandDS ()
%rng(seed,'combRecursive'); % for repeatability
%rng(seed_val); % for repeatability
%rng('default');
a = 0.0;
b = 1.0;
r = (b-a).*rand(1,1) + a;
end

%To calculate random Dry Specific Volume
function r = calcrandDSV()
%rng(seed,'combRecursive'); % for repeatability
%rng(seed_val); % for repeatability
```

```
%rng('default');
a = 0.5;
b = 1.0;
r = (b-a).*rand(1,1) + a;
end

%To calculate random Air Ratio
function r = calcrandAR()
%rng(seed,'combRecursive'); % for repeatability
%rng(seed_val); % for repeatability
%rng('default');
a = 0.0;
b = 1.0;
r = (b-a).*rand(1,1) + a;
end

% To calculate random Porosity
%the first argument represents particle density
% the second argument represents dry bulk density
function r = calcrandP (x,y)
r = 1 - (x/y);
end

% To calculate random Air Porosity
%the first argument represents porosity
% the second argument represents volumetric soil moisture content
function r = calcrandAP (x,y)
r = x - y;
end

% To calculate random Void Ratio
%the first argument represents particle density
% the second argument represents dry bulk density
```

```
function r = calcrandVR (x,y)
r = (x/y) - 1;
end

% To calculate random Gravimetric Soil Moisture content
%the first argument represents wet bulk density
% the second argument represents dry bulk density
function r = calcrandGSM (x,y)
r = (x - y) / y;
end

%To calculate random Liquid Ratio
%the first argument represents volumetric soil moisture content
% the second argument represents void ratio
function r = calcrandLR (x,y)
r = x .* (1 + y);
end

% loop for generating random values
% the following is the column order for soil properties,
    ↪ constituting a
% single row:
% [pd, dbd, wbd, vsm, ds, dsv, ar, p, ap, vr, gsm, lr]
% a temporary vector for holding the index values
% of parameters to be retrieved from TOPOLOGY
% the column order of temp is as follows:
% [pd, dbd, wbd, vsm, ds, dsv, ar, p, vr]
temp = zeros(1,9);

% a temporary vector for holding the values for soil
% properties generated, outside of any loop, so as to
% ensure repeatability across the layers of a unit
% fractal
```

```
uniform_data = zeros(1,12);
m = 15; % start column index for soil properties in
% data
n = 26; % end column index for soil properties in
% data
c = 1; % variable for indexing temp

% loop to assign all the column values for soil
% properties, so as to ensure repeatability across rows
% and layers
for j = 1:12 % all columns
switch j
case 1
    uniform_data(:,j) = calcrandPD();
    temp(1,c) = j;
case 2
    uniform_data(:,j) = calcrandDBD();
    temp(1,c+1) = j;
case 3
    uniform_data(:,j) = calcrandWBD();
    temp(1,c+2) = j;
case 4
    uniform_data(:,j) = calcrandVSM();
    temp(1,c+3) = j;
case 5
    uniform_data(:,j) = calcrandDS();
    temp(1,c+4) = j;
case 6
    uniform_data(:,j) = calcrandDSV();
    temp(1,c+5) = j;
case 7
    uniform_data(:,j) = calcrandAR();
    temp(1,c+6) = j;
```

```
case 8
    x = temp(1,c);
    y = temp(1,c+1);
    uniform_data (:,j) = calcrandP (uniform_data(:,x),uniform_data (:,y));
    temp(1,c+7) = j;
case 9
    x = temp(1,c+7);
    y = temp(1,c+3);
    uniform_data (:,j) = calcrandAP (uniform_data(:,x), uniform_data(:,y));
case 10
    x = temp(1,c);
    y = temp(1,c+1);
    uniform_data (:,j) = calcrandVR (uniform_data(:,x), uniform_data(:,y));
    temp(1,c+8) = j;
case 11
    x = temp(1,c+2);
    y = temp(1,c+1);
    uniform_data (:,j) = calcrandGSM (uniform_data(:,x), uniform_data(:,y));
case 12
    x = temp(1,c+3);
    y = temp(1,c+8);
    uniform_data (:,j) = calcrandLR (uniform_data(:,x), uniform_data(:,y));
otherwise
end
end

% for additional matrix dimensions
for k = 1:3
```

```
% for all rows
for i = 1:10
% for all columns
for j = m:n
  t = j - 14;
  data {k}(i,j) = uniform_data (:,t);
end
end
end
end

% invoke the nested functions in sequence
data =  distance(data);

% to approximate the grid cell size
data = grid(data);

% to approximate grid derivatives and terrain attributes
data = terrain(data);

% to approximate soil properties
data = soil(data);
end
end
% initiate flow
flowcontrol();
end
```

A.5 Source Code for Simulations related to the Proposed Innovations

The following subsections reproduce the MATLAB source code used in Simulations 4 – 7 presented under Chapter 8, as part of the discussion on the proposed innovations based on *analogical thinking* (Gassmann & Zeschky 2008).

A.5.1 Scenario 1: Path Loss

This subsection reproduces the MATLAB source code for Simulations 4 – 6, pertaining to the path loss scenario.

A.5.1.1 Simulation 4: Impact of MI Waveguide Tunnel on Mutual Inductance

This subsidiary section presents the MATLAB source code related to simulation tests highlighting the impact of the MI waveguide tunnel on coil mutual inductance within the MI waveguide theoretical model (Sun & Akyildiz 2010*c*), (Kisseleff, Gerstacker, Schober, Sun & Akyildiz 2013).

```
function simulation4test1 ()
%Reference: Channel Capacity of Magnetic Induction Based Wireless
    ↪ Underground Sensor Networks under Practical Constraints
%  simulation to contrast the mutual inductance between adjacent
    ↪ coils in
%  the absence and presence of the MI waveguide tunnel
%  dry soil medium has been considered for embedding coils in
    ↪ the absence
%  of the MI waveguide tunnel

% set the floating point precision
%DIGITS := 40;
%variables
```

```
%soil conductivity for dry soil
varSIGMAD = 0.01;

%soil conductivity for wet soil
varSIGMAW = 0.077;

%electric constant
varEPSILON0 = 0.00000000000885;

%permittivity for dry soil
varEPSILOND = 0.00000000006195;

%permittivity for wet soil
varEPSILONW = 0.00000000025665;

%skin depth of the soil
global varDELTA;

%permeability of soil
varMU = 0.000001256636;

%eddy current factor
global varG;

%mutual inductance
global varMI;

%angle between successive coil radial directions
varTHETAT = 1.5707963268;
varTHETAR = -1.5707963268;

%frequency
varFRQ = 10000000.0;
```

```

    %inductance
    global varL;

    %capacitance
    varC = 0.000000000001;

    %copper resistivity
    varRHO = 0.000000016780;

    %copper resistance of coil
    varR = 0.0;

    %matched impedance
    varZL = 0.0;

    %impedance
    varZ = 0.0;

    %power transmitted by the transmitter
    varPT = 0.01;

    %power received by the receiver
    varPR = 0.0;

    %coil wire radius
    varCRW = 0.00050000;

    %coil radius
    varCA = 0.15;

    %coil wire radius
    varCWA = 0.0005;
```

```

    %coil length
    varCL = 0.075;

    %assumed value
    %coil winding height
    varCLWNDHGT = 0.01;

    %number of coil windings
    varNUMCLWND = 1000.0;

    %number of relay coils
    varNUMRLYCLS = 15.0;

    %transmission distance
    varTRD = 50.0;

    %relay distance
    varRLD = 3.33;

    %common variables
    varCMN0 = 0.0;
    varCMN1 = 0.0;

    %invocations
    %set the common variables depending on dry or wet soil
    varCMN0 = varSIGMAD;
    varCMN1 = varEPSILOND;
    calcDELTA(varMU, varCMN0, varCMN1, varFRQ);
    calcG(varRLD);
    calcL(varMU, varNUMCLWND, varCA, varCL, varCLWNDHGT);

```

```
%arrays for storing mutual inductance values calculated for
%dry soil for a range of number of coil windings,
% operational frequencies and coil alignment parameters
arrayVARNUMCLWNDDRY = zeros(10,1,1);
arrayVARNUMCLWNDDRYMIWT = zeros(10,1,1);
arrayVARFRQDRY = zeros(10,1,1);
arrayVARTHETATRDRY = zeros(10,1,1);

%calculate the mutual inductance values for a range of coil
%windings without the MI waveguide tunnel
%initially, calculate the mutual inductance with the original
%number of coil windings
calcMI(varMU, varNUMCLWND, varCA, varRLD, varTHETAT, varTHETAR);
arrayVARNUMCLWNDDRY(1,1) = varNUMCLWND;
arrayVARNUMCLWNDDRY(1,2) = varMI;
for i = 2: 11
varNUMCLWND = varNUMCLWND + 100;
calcMI(varMU, varNUMCLWND, varCA, varRLD, varTHETAT, varTHETAR);
arrayVARNUMCLWNDDRY(i,1) = varNUMCLWND;
arrayVARNUMCLWNDDRY(i,2) = varMI;
end

%reset the value of number of coil windings to the original value
varNUMCLWND = 1000;
%calculate the mutual inductance values for a range of coil
%windings with the MI waveguide tunnel
```

```
        %initially, calculate the mutual inductance with the
            ↪ original
        %number of coil windings
        calcMIWT(varMU, varNUMCLWND, varCA, varRLD, varTHETAT,
            ↪ varTHETAR);
        arrayVARNUMCLWNDDRYMIWT(1,1) = varNUMCLWND;
        arrayVARNUMCLWNDDRYMIWT(1,2) = varMI;
        for i = 2: 11
        varNUMCLWND = varNUMCLWND + 100;
        calcMIWT(varMU, varNUMCLWND, varCA, varRLD, varTHETAT,
            ↪ varTHETAR);
        arrayVARNUMCLWNDDRYMIWT(i,1) = varNUMCLWND;
        arrayVARNUMCLWNDDRYMIWT(i,2) = varMI;
        end

        %display results
%           format long;
%           disp('            N               MI')
%           disp(arrayVARNUMCLWNDDRY);
%
%           disp('            N               MI')
%           disp(arrayVARNUMCLWNDDRYMIWT);

        x = double(zeros(1,10));
        y1 = double(zeros(1,10));
        y1 = double(zeros(1,10));

        x = arrayVARNUMCLWNDDRY(:,1);
        y1 = arrayVARNUMCLWNDDRY(:,end);
        y2 = arrayVARNUMCLWNDDRYMIWT(:,end);

%           disp(x);
%           disp(y1);
```

```
%           disp(y2);
          figure % new figure
[hAx,hLine1,hLine2] = plotyy(x,y1,x,y2);
title('Mutual Inductance without and with MI waveguide tunnel in dry soil','fontweight','bold','fontsize',10);
xlabel('Number of coil windings');
ylabel(hAx(1),'without MI waveguide tunnel'); % left y-axis
ylabel(hAx(2),'with MI waveguide tunnel'); % right y-axis
export_fig test.pdf;
%nested at the first level
%function to calculate the skin depth
     function calcDELTA(varMU, varCMN0, varCMN1, varFRQ)
          varTMP1 = 2 * pi * varFRQ;
%           disp(varTMP1);
          varTMP2 = varMU * varCMN1/2;
%           disp(varTMP2);
          varTMP3  = power(varCMN0, 2);
%           disp(varTMP3);
          varTMP4 = power(2 * pi * varFRQ, 2);
%           disp(varTMP4);
          varTMP5 = power(varCMN1, 2);
%           disp(varTMP5);
          varTMP6 = varTMP4 * varTMP5;
%           disp(varTMP6);
          varTMP7 = varTMP3/varTMP6;
%           disp(varTMP7);
          varTMP8 = sqrt(1 + varTMP7);
%           disp(varTMP8);
```

```
        varTMP9 = varTMP8 - 1;
%           disp(varTMP9);
        varTMP10 = sqrt(varTMP2 * varTMP9);
%           disp(varTMP10);
        varDELTA = double(1/varTMP1 * varTMP10);
    end

%function to calculate the eddy current factor
    function calcG(varRLD)
        varTMP1 = double(-varRLD/varDELTA);
%           disp(varTMP1);
        varTMP2 = double(exp(varTMP1));
%           disp(varTMP2);
        varG = varTMP2;
    end

%function to calculate mutual inductance between two coils without MI
%waveguide tunnel
    function calcMI(varMU, varNUMCLWND, varCA, varRLD, varTHETAT, varTHETAR)
     varMI =  double(varMU * pi * (varNUMCLWND.^2) * ((varCA.^4)/(4 * (varRLD.^3))) * ((2* sin(varTHETAT) * sin(varTHETAR)) + (cos(varTHETAT) * cos(varTHETAR))) * varG);
    end

%function to calculate mutual inductance between two coils with MI
%waveguide tunnel
    function calcMIWT(varMU, varNUMCLWND, varCA, varRLD, varTHETAT, varTHETAR)
        varTMP1 = double(varMU * pi);
```

```
        varTMP2 = double(varNUMCLWND.^2);
        varTMP3 = double(varCA.^4);
        varTMP4 = double(4 * (varRLD.^3));
        varTMP5 = double(varTMP1 * varTMP2);
        varTMP6 = double(varTMP3/varTMP4);
        varTMP7 = double((2* sin(varTHETAT) * sin(varTHETAR)) + (cos(varTHETAT) * cos(varTHETAR)));
        varMI = double(varTMP5 * varTMP6 * varTMP7);
        % varMI =  double(varMU * pi * (varNUMCLWND.^2) * ((varCA.^4)/(4 * (varRLD.^3))) * ((2* sin(varTHETAT) * sin(varTHETAR)) + (cos(varTHETAT) * cos(varTHETAR))));
    end

%function to calculate the self inductance of a coil
    function calcL(varMu, varNUMCLWND, varCA, varCL, varCLWNDHGT)
        varTMP1 = 21;
        varL = double(((varTMP1 * varMu * (varNUMCLWND.^2) * varCA)/4 * pi) * ((varCA/(varCL + varCLWNDHGT)).^0.5));
    end

%function to calculate copper resistance of coil
    function calcR(varRHO, varCA, varNUMCLWND, varCRW, varR)
        varR = varRHO * ((2 * varCA * varNUMCLWND)/(varCRW.^2));
    end

end
```

```
function simulation4test2 ()
%Reference: Channel Capacity of Magnetic Induction Based Wireless Underground Sensor Networks under Practical Constraints
%  simulation to contrast the mutual inductance between adjacent coils in
```

```
%   the absence and presence of the MI waveguide tunnel
%   wet soil medium has been considered for embedding coils in
    ↪ the absence
%   of the MI waveguide tunnel

% set the floating point precision
%DIGITS := 40;
%variables
        %soil conductivity for dry soil
        varSIGMAD = 0.01;

        %soil conductivity for wet soil
        varSIGMAW = 0.077;

        %electric constant
        varEPSILON0 = 0.00000000000885;

        %permittivity for dry soil
        varEPSILOND = 0.00000000006195;

        %permittivity for wet soil
        varEPSILONW = 0.00000000025665;

        %skin depth of the soil
        global varDELTA;

        %permeability of soil
        varMU = 0.000001256636;

        %eddy current factor
        global varG;

        %mutual inductance
```

```
        global varMI;

        %angle between successive coil radial directions
        varTHETAT = 1.5707963268;
        varTHETAR = -1.5707963268;

        %frequency
        varFRQ = 10000000.0;

        %inductance
        global varL;

        %capacitance
        varC = 0.000000000001;

        %copper resistivity
        varRHO = 0.000000016780;

        %copper resistance of coil
        varR = 0.0;

        %matched impedance
        varZL = 0.0;

        %impedance
        varZ = 0.0;

        %power transmitted by the transmitter
        varPT = 0.01;

        %power received by the receiver
        varPR = 0.0;

```

```
        %coil wire radius
        varCRW = 0.00050000;

        %coil radius
        varCA = 0.15;

        %coil wire radius
        varCWA = 0.0005;

        %coil length
        varCL = 0.075;

        %assumed value
        %coil winding height
        varCLWNDHGT = 0.01;

        %number of coil windings
        varNUMCLWND = 1000.0;

        %number of relay coils
        varNUMRLYCLS = 15.0;

        %transmission distance
        varTRD = 50.0;

        %relay distance
        varRLD = 3.33;

        %common variables
        varCMN0 = 0.0;
        varCMN1 = 0.0;

        %invocations
```

```
        %set the common variables depending on dry or wet soil
        varCMN0 = varSIGMAW;
        varCMN1 = varEPSILONW;
        calcDELTA(varMU, varCMN0, varCMN1, varFRQ);
        calcG(varRLD);
        calcL(varMU, varNUMCLWND, varCA, varCL, varCLWNDHGT);

        %arrays for storing mutual inductance values calculated for
        %dry soil for a range of number of coil windings,
        % operational frequencies and coil alignment parameters
        arrayVARNUMCLWNDDRY = zeros(10,1,1);
        arrayVARNUMCLWNDDRYMIWT = zeros(10,1,1);
        arrayVARFRQDRY = zeros(10,1,1);
        arrayVARTHETATRDRY = zeros(10,1,1);

        %calculate the mutual inductance values for a range of coil
        %windings without the MI waveguide tunnel
        %initially, calculate the mutual inductance with the original
        %number of coil windings
        calcMI(varMU, varNUMCLWND, varCA, varRLD, varTHETAT, varTHETAR);
        arrayVARNUMCLWNDDRY(1,1) = varNUMCLWND;
        arrayVARNUMCLWNDDRY(1,2) = varMI;
        for i = 2: 11
        varNUMCLWND = varNUMCLWND + 100;
        calcMI(varMU, varNUMCLWND, varCA, varRLD, varTHETAT, varTHETAR);
        arrayVARNUMCLWNDDRY(i,1) = varNUMCLWND;
        arrayVARNUMCLWNDDRY(i,2) = varMI;
        end
```

```

        %reset the value of number of coil windings to the original value
        varNUMCLWND = 1000;
        %calculate the mutual inductance values for a range of coil
        %windings with the MI waveguide tunnel
        %initially, calculate the mutual inductance with the original
        %number of coil windings
        calcMIWT(varMU, varNUMCLWND, varCA, varRLD, varTHETAT, varTHETAR);
        arrayVARNUMCLWNDDRYMIWT(1,1) = varNUMCLWND;
        arrayVARNUMCLWNDDRYMIWT(1,2) = varMI;
        for i = 2: 11
        varNUMCLWND = varNUMCLWND + 100;
        calcMIWT(varMU, varNUMCLWND, varCA, varRLD, varTHETAT, varTHETAR);
        arrayVARNUMCLWNDDRYMIWT(i,1) = varNUMCLWND;
        arrayVARNUMCLWNDDRYMIWT(i,2) = varMI;
        end

        %display results
%         format long;
%         disp('            N              MI')
%         disp(arrayVARNUMCLWNDDRY);
%
%         disp('            N              MI')
%         disp(arrayVARNUMCLWNDDRYMIWT);

        x = double(zeros(1,10));
        y1 = double(zeros(1,10));
        y1 = double(zeros(1,10));
```

```

        x = arrayVARNUMCLWNDDRY(:,1);
        y1 = arrayVARNUMCLWNDDRY(:,end);
        y2 = arrayVARNUMCLWNDDRYMIWT(:,end);

%       disp(x);
%       disp(y1);
%       disp(y2);
        figure % new figure
[hAx,hLine1,hLine2] = plotyy(x,y1,x,y2);

title('Mutual Inductance without and with MI waveguide tunnel in
    ↪ wet soil','fontweight','bold','fontsize',10);
xlabel('Number of coil windings');
ylabel(hAx(1),'without MI waveguide tunnel'); % left y-axis
ylabel(hAx(2),'with MI waveguide tunnel'); % right y-axis

export_fig Figure9.pdf



%nested at the first level

%function to calculate the skin depth
    function calcDELTA(varMU, varCMN0, varCMN1, varFRQ)
        varTMP1 = 2 * pi * varFRQ;
%       disp(varTMP1);
        varTMP2 = varMU * varCMN1/2;
%       disp(varTMP2);
        varTMP3  = power(varCMN0, 2);
%       disp(varTMP3);
        varTMP4 = power(2 * pi * varFRQ, 2);
%       disp(varTMP4);
        varTMP5 = power(varCMN1, 2);
```

```
%           disp(varTMP5);
            varTMP6 = varTMP4 * varTMP5;
%           disp(varTMP6);
            varTMP7 = varTMP3/varTMP6;
%           disp(varTMP7);
            varTMP8 = sqrt(1 + varTMP7);
%           disp(varTMP8);
            varTMP9 = varTMP8 - 1;
%           disp(varTMP9);
            varTMP10 = sqrt(varTMP2 * varTMP9);
%           disp(varTMP10);
            varDELTA = double(1/varTMP1 * varTMP10);
      end

%function to calculate the eddy current factor
      function calcG(varRLD)
            varTMP1 = double(-varRLD/varDELTA);
%           disp(varTMP1);
            varTMP2 = double(exp(varTMP1));
%           disp(varTMP2);
            varG = varTMP2;
      end

%function to calculate mutual inductance between two coils without MI
%waveguide tunnel
      function calcMI(varMU, varNUMCLWND, varCA, varRLD, varTHETAT, varTHETAR)
        varMI = double(varMU * pi * (varNUMCLWND.^2) * ((varCA.^4) /(4 * (varRLD.^3))) * ((2* sin(varTHETAT) * sin(varTHETAR)) + (cos(varTHETAT) * cos(varTHETAR))) * varG);
      end
```

```
%function to calculate mutual inductance between two coils with
    ↪ MI
%waveguide tunnel
    function calcMIWT(varMU, varNUMCLWND, varCA, varRLD,
        ↪ varTHETAT, varTHETAR)
        varTMP1 = double(varMU * pi);
        varTMP2 = double(varNUMCLWND.^2);
        varTMP3 = double(varCA.^4);
        varTMP4 = double(4 * (varRLD.^3));
        varTMP5 = double(varTMP1 * varTMP2);
        varTMP6 = double(varTMP3/varTMP4);
        varTMP7 = double((2* sin(varTHETAT) * sin(varTHETAR)) + (
            ↪ cos(varTHETAT) * cos(varTHETAR)));
        varMI = double(varTMP5 * varTMP6 * varTMP7);
        % varMI =  double(varMU * pi * (varNUMCLWND.^2) * ((varCA
            ↪ .^4)/(4 * (varRLD.^3))) * ((2* sin(varTHETAT) * sin
            ↪ (varTHETAR)) + (cos(varTHETAT) * cos(varTHETAR))));
    end

%function to calculate the self inductance of a coil
    function calcL(varMu, varNUMCLWND, varCA, varCL, varCLWNDHGT)
        varTMP1 = 21;
        varL = double(((varTMP1 * varMu * (varNUMCLWND.^2) *
            ↪ varCA)/4 * pi) * ((varCA/(varCL + varCLWNDHGT))
            ↪ .^0.5));
    end

%function to calculate copper resistance of coil
    function calcR(varRHO, varCA, varNUMCLWND, varCRW, varR)
        varR = varRHO * ((2 * varCA * varNUMCLWND)/(varCRW.^2));
    end
end
```

A.5.1.2 Simulation 5: Impact of MI Waveguide Tunnel on Coil Misalignment

This subsidiary section presents the MATLAB source code related to the simulation test highlighting the impact of the MI waveguide tunnel on coil misalignment (and consequently mutual inductance) within the MI waveguide theoretical model (Sun & Akyildiz 2010*c*), (Kisseleff, Gerstacker, Schober, Sun & Akyildiz 2013). The conclusions drawn based on the simulation result are deductive; the simulation result shows the impact of coil misalignment on mutual inductance, for coils buried directly in the soil. The eddy current factor has been ignored in the case of this simulation.

```
function simulation5 ()
%Reference: Channel Capacity of Magnetic Induction Based Wireless
    ↪ Underground Sensor Networks under Practical Constraints
% simulation models the variance of mutual inductance with coil
% orientation angles in the absence of MI waveguide
% eddy current factor has been ignored

% set the floating point precision
%DIGITS := 40;
%variables
        %soil conductivity for dry soil
        varSIGMAD = 0.01;

        %soil conductivity for wet soil
        varSIGMAW = 0.077;

        %electric constant
        varEPSILON0 = 0.00000000000885;

        %permittivity for dry soil
        varEPSILOND = 0.00000000006195;

        %permittivity for wet soil
```

```
        varEPSILONW = 0.00000000025665;

        %skin depth of the soil
        global varDELTA;

        %permeability of soil
        varMU = 0.000001256636;

        %eddy current factor
        global varG;

        %mutual inductance
        global varMI;

        %angle between successive coil radial directions
        varTHETAT = 1.5707963268;
        varTHETAR = -1.5707963268;

        %frequency
        varFRQ = 10000000.0;

        %inductance
        global varL;

        %capacitance
        varC = 0.000000000001;

        %copper resistivity
        varRHO = 0.000000016780;

        %copper resistance of coil
        varR = 0.0;

```

```
        %matched impedance
        varZL = 0.0;

        %impedance
        varZ = 0.0;

        %power trasmitted by the transmitter
        varPT = 0.01;

        %power received by the receiver
        varPR = 0.0;

        %coil wire radius
        varCRW = 0.00050000;

        %coil radius
        varCA = 0.15;

        %coil wire radius
        varCWA = 0.0005;

        %coil length
        varCL = 0.075;

        %assumed value
        %coil winding height
        varCLWNDHGT = 0.01;

        %number of coil windings
        varNUMCLWND = 1000.0;

        %number of relay coils
        varNUMRLYCLS = 15.0;
```

```
%transmission distance
varTRD = 50.0;

%relay distance
varRLD = 3.33;

%common variables
varCMN0 = 0.0;
varCMN1 = 0.0;

%invocations
%set the common variables depending on dry or wet soil
varCMN0 = varSIGMAW;
varCMN1 = varEPSILONW;
calcDELTA(varMU, varCMN0, varCMN1, varFRQ);
calcG(varRLD);
calcL(varMU, varNUMCLWND, varCA, varCL, varCLWNDHGT);

%note that there is no corresponding array for the MI
    ↪ waveguide
%tunnel as the coil orientations are fixed
%also there is no distinction between dry and wet soils
    ↪ as eddy
%current factor is ignored
arrayVARTHETATR = zeros(18,1);
%array for storing the calculated mutual inductance
    ↪ values for
%different coil orientations
arrayMIVARTHETATR = zeros(18,1);

%calculate the mutual inductance values for a range of
    ↪ theta_t and
```

```
    %theta_r without the MI waveguide tunnel
    % a range from 0 to 90 degrees with a difference of 5 degrees has
    % been used
    arrayVARTHETATR = linspace(0,90,18);
%       disp(arrayVARTHETATR);
    %invoke the routine for calculating the mutual inductance for the
    %MI waveguide tunnel setup, as eddy current factor is ignored
    for i = 1:17
        varTHETAT = arrayVARTHETATR(i);
        varTHETAR = arrayVARTHETATR(i + 1);
        calcMIWT(varMU, varNUMCLWND, varCA, varRLD, varTHETAT, varTHETAR);
        arrayMIVARTHETATR(i) = varMI;
    end
%       disp(arrayMIVARTHETATR);
    x = zeros(18,1);
    y = zeros(18,1);
    x = arrayVARTHETATR;
    y = arrayMIVARTHETATR;
    figure % new figure
    plot(x,y);
    title('Mutual Inductance variance with different coil orientations','fontweight','bold','fontsize',9.5);
    xlabel('coil orientation');
    ylabel('mutual inductance');
    export_fig Figure10.pdf

%nested at the first level

%function to calculate the skin depth
```

```
    function calcDELTA(varMU, varCMN0, varCMN1, varFRQ)
        varTMP1 = 2 * pi * varFRQ;
%           disp(varTMP1);
        varTMP2 = varMU * varCMN1/2;
%           disp(varTMP2);
        varTMP3  = power(varCMN0, 2);
%           disp(varTMP3);
        varTMP4 = power(2 * pi * varFRQ, 2);
%           disp(varTMP4);
        varTMP5 = power(varCMN1, 2);
%           disp(varTMP5);
        varTMP6 = varTMP4 * varTMP5;
%           disp(varTMP6);
        varTMP7 = varTMP3/varTMP6;
%           disp(varTMP7);
        varTMP8 = sqrt(1 + varTMP7);
%           disp(varTMP8);
        varTMP9 = varTMP8 - 1;
%           disp(varTMP9);
        varTMP10 = sqrt(varTMP2 * varTMP9);
%           disp(varTMP10);
        varDELTA = double(1/varTMP1 * varTMP10);
    end

%function to calculate the eddy current factor
    function calcG(varRLD)
        varTMP1 = double(-varRLD/varDELTA);
%           disp(varTMP1);
        varTMP2 = double(exp(varTMP1));
%           disp(varTMP2);
        varG = varTMP2;
    end

```

```
%function to calculate mutual inductance between two coils without MI
%waveguide tunnel
    function calcMI(varMU, varNUMCLWND, varCA, varRLD, varTHETAT, varTHETAR)
     varMI =  double(varMU * pi * (varNUMCLWND.^2) * ((varCA.^4)/(4 * (varRLD.^3))) * ((2* sin(varTHETAT) * sin(varTHETAR)) + (cos(varTHETAT) * cos(varTHETAR))) * varG);
    end

%function to calculate mutual inductance between two coils with MI
%waveguide tunnel
    function calcMIWT(varMU, varNUMCLWND, varCA, varRLD, varTHETAT, varTHETAR)
        varTMP1 = double(varMU * pi);
        varTMP2 = double(varNUMCLWND.^2);
        varTMP3 = double(varCA.^4);
        varTMP4 = double(4 * (varRLD.^3));
        varTMP5 = double(varTMP1 * varTMP2);
        varTMP6 = double(varTMP3/varTMP4);
        varTMP7 = double((2* sin(varTHETAT) * sin(varTHETAR)) + (cos(varTHETAT) * cos(varTHETAR)));
        varMI = double(varTMP5 * varTMP6 * varTMP7);
        % varMI =  double(varMU * pi * (varNUMCLWND.^2) * ((varCA.^4)/(4 * (varRLD.^3))) * ((2* sin(varTHETAT) * sin(varTHETAR)) + (cos(varTHETAT) * cos(varTHETAR))));
    end

%function to calculate the self inductance of a coil
    function calcL(varMu, varNUMCLWND, varCA, varCL, varCLWNDHGT)
        varTMP1 = 21;
```

```
        varL = double(((varTMP1 * varMu * (varNUMCLWND.^2) * varCA)/4 * pi) * ((varCA/(varCL + varCLWNDHGT)).^0.5));
    end

%function to calculate copper resistance of coil
    function calcR(varRHO, varCA, varNUMCLWND, varCRW, varR)
        varR = varRHO * ((2 * varCA * varNUMCLWND)/(varCRW.^2));
    end

end
```

A.5.1.3 Simulation 6: Impact of MI Waveguide Tunnel on Eddy Current Factor

This subsidiary section presents the MATLAB source code related to simulation tests highlighting the impact of the MI waveguide tunnel on the eddy current factor affecting the MI waveguide theoretical model (Kisseleff, Gerstacker, Schober, Sun & Akyildiz 2013), in the case of coils buried directly within the soil medium. The simulation tests consider use cases involving both dry and wet soil.

```
function simulation6test1 ()
%Reference: Channel Capacity of Magnetic Induction Based Wireless Underground Sensor Networks under Practical Constraints
% simulation to model the scaling of x in dry soil

% set the floating point precision
%DIGITS := 40;
%variables
        %soil conductivity for dry soil
        varSIGMAD = 0.01;

        %soil conductivity for wet soil
```

```
varSIGMAW = 0.077;

%electric constant
varEPSILON0 = 0.00000000000885;

%permittivity for dry soil
varEPSILOND = 0.00000000006195;

%permittivity for wet soil
varEPSILONW = 0.00000000025665;

%skin depth of the soil
global varDELTA;

%permeability of soil
varMU = 0.000001256636;

%eddy current factor
global varG;

%mutual inductance
global varMI;

%added for third simulation
global varX;

%angle between succesive coil radial directions
varTHETAT = 1.5707963268;
varTHETAR = -1.5707963268;

%frequency
varFRQ = 10000000.0;

```

```
    %inductance
    global varL;

    %capacitance
    varC = 0.000000000001;

    %copper resistivity
    varRHO = 0.000000016780;

    %copper resistance of coil
    global varR;

    %matched impedance or impedance for a given value of L
    varZL = 0.0;

    %impedance
    global varZ;

    %power trasmitted by the transmitter
    varPT = 0.01;
    %power received by the receiver
    varPR = 0.0;

    %coil wire radius
    varCRW = 0.00050000;

    %coil radius
    varCA = 0.15;

    %coil wire radius
    varCWA = 0.0005;

    %coil length
```

```
        varCL = 0.075;

        %assumed value
        %coil winding height
        varCLWNDHGT = 0.01;

        %number of coil windings
        varNUMCLWND = 1000.0;

        %number of relay coils
        varNUMRLYCLS = 15.0;

        %transmission distance
        varTRD = 50.0;

        %relay distance
        varRLD = 3.33;

        %common variables
        varCMN0 = 0.0;
        varCMN1 = 0.0;

        %invocations
        %set the common variables depending on dry or wet soil
        varCMN0 = varSIGMAD;
        varCMN1 = varEPSILOND;
        calcDELTA(varMU, varCMN0, varCMN1, varFRQ);
        calcG(varRLD);
        calcL(varMU, varNUMCLWND, varCA, varCL, varCLWNDHGT);
        calcR(varRHO, varCA, varNUMCLWND, varCRW);

        %added for third simulation
        %consider frequencies in the range 10 MHz - 300 MHz
```

```
        arrayVARFRQ = zeros(29,1);
        %arrays for storing the calculated Z and X values for
        %different frequencies
        arrayVARZ = zeros(29,1);
        arrayVARX = zeros(29,1);
        %generate the range of frequencies
        arrayVARFRQ = linspace(10000000,3000000000,29);
%           disp('FREQUENCY VALUES');
%           disp('------------------');
%           disp(arrayVARFRQ);
        % calculate the mutual inductance
        calcMI(varMU, varNUMCLWND, varCA, varRLD, varTHETAT, varTHETAR);
        %calculate Z for the range of frequency values and store in the
        %array
        for i = 1:29
        calcZ(arrayVARFRQ(i), varC);
        arrayVARZ(i) = varZ;
        end
%           disp('IMPEDANCE VALUES');
%           disp('------------------');
%           disp(arrayVARZ);
        %calculate X for the range of frequency values and store in the
        %array
        for i = 1:29
            %set varZL to the current value of impedance
            varZL = arrayVARZ(i);
            calcX(varFRQ, varZL);
            arrayVARX(i) = varX;
        end
        % the values of x range from -infinity to infinity
```

```
        disp('X VALUES');
        disp('————————');
        disp(arrayVARX);
%           plot the data
        x = zeros(29,1);
        y = zeros(29,1);
        x = arrayVARFRQ;
        y = arrayVARX;

%           this is a workaround for plotting since the values of x range
%           from -infinity to infinity
          y1 = -(inf(29,1));
          y2 = inf(29,1);

        figure % new figure
        [hAx,hLine1,hLine2] = plotyy(x,y1,x,y2);
        title('Value of x for different system frequencies in dry soil','fontweight','bold','fontsize',10);
        xlabel('frequency');
        ylabel(hAx(1),'x', 'fontsize',9); % left y-axis
        ylabel(hAx(2),'x', 'fontsize',9); % right y-axis


        export_fig Figure11.pdf

%nested at the first level

%function to calculate the skin depth
    function calcDELTA(varMU, varCMN0, varCMN1, varFRQ)
        varTMP1 = 2 * pi * varFRQ;
%           disp(varTMP1);
        varTMP2 = varMU * varCMN1/2;
```

```
%            disp(varTMP2);
          varTMP3  = power(varCMN0, 2);
%            disp(varTMP3);
          varTMP4 = power(2 * pi * varFRQ, 2);
%            disp(varTMP4);
          varTMP5 = power(varCMN1, 2);
%            disp(varTMP5);
          varTMP6 = varTMP4 * varTMP5;
%            disp(varTMP6);
          varTMP7 = varTMP3/varTMP6;
%            disp(varTMP7);
          varTMP8 = sqrt(1 + varTMP7);
%            disp(varTMP8);
          varTMP9 = varTMP8 - 1;
%            disp(varTMP9);
          varTMP10 = sqrt(varTMP2 * varTMP9);
%            disp(varTMP10);
          varDELTA = double(1/varTMP1 * varTMP10);
     end

%function to calculate the eddy current factor
     function calcG(varRLD)
          varTMP1 = double(-varRLD/varDELTA);
%            disp(varTMP1);
          varTMP2 = double(exp(varTMP1));
%            disp(varTMP2);
          varG = varTMP2;
     end

%function to calculate mutual inductance between two coils
    ↪ without MI
%waveguide tunnel
```

```
    function calcMI(varMU, varNUMCLWND, varCA, varRLD, varTHETAT, varTHETAR)
     varMI =  double(varMU * pi * (varNUMCLWND.^2) * ((varCA.^4)/(4 * (varRLD.^3))) * ((2* sin(varTHETAT) * sin(varTHETAR)) + (cos(varTHETAT) * cos(varTHETAR))) * varG);
    end

%function to calculate mutual inductance between two coils with MI
%waveguide tunnel
    function calcMIWT(varMU, varNUMCLWND, varCA, varRLD, varTHETAT, varTHETAR)
        varTMP1 = double(varMU * pi);
        varTMP2 = double(varNUMCLWND.^2);
        varTMP3 = double(varCA.^4);
        varTMP4 = double(4 * (varRLD.^3));
        varTMP5 = double(varTMP1 * varTMP2);
        varTMP6 = double(varTMP3/varTMP4);
        varTMP7 = double((2* sin(varTHETAT) * sin(varTHETAR)) + (cos(varTHETAT) * cos(varTHETAR)));
        varMI = double(varTMP5 * varTMP6 * varTMP7);
        % varMI =  double(varMU * pi * (varNUMCLWND.^2) * ((varCA.^4)/(4 * (varRLD.^3))) * ((2* sin(varTHETAT) * sin(varTHETAR)) + (cos(varTHETAT) * cos(varTHETAR))));
    end

%function to calculate the self inductance of a coil
    function calcL(varMu, varNUMCLWND, varCA, varCL, varCLWNDHGT)
        varTMP1 = 21;
        varL = double(((varTMP1 * varMu * (varNUMCLWND.^2) * varCA)/4 * pi) * ((varCA/(varCL + varCLWNDHGT)).^0.5));
```

```
    end

%function to calculate copper resistance of coil
    function calcR(varRHO, varCA, varNUMCLWND, varCRW)
        varR = varRHO * ((2 * varCA * varNUMCLWND)/(varCRW.^2));
    end
%function to calculate the coil impedance for a given value of
    ↪ coil
%inductance
    function calcZ(varFRQ, varC)
        varTMP1 = sqrt(-1) * 2 * pi * varFRQ * varL;
        varTMP2 = sqrt(-1) * 2 * pi * varFRQ * varC;
        varTMP3 = 1/varTMP2;
        varTMP4 = varTMP1 + varTMP3 + varR;
        varZ = varTMP4;
    end
%function to calculate the value of X for a generated value of Z
    function calcX(varFRQ, varZL)
        varTMP1 = sqrt(-1) * 2 * pi * varFRQ * varMI;
        varTMP2 = varZL/varTMP1;
        varX = varTMP2;
    end

end
```

```
function simulation6test2 ()
%Reference: Channel Capacity of Magnetic Induction Based Wireless
    ↪ Underground Sensor Networks under Practical Constraints
% simulation to model the scaling of x in wet soil

% set the floating point precision
%DIGITS := 40;
%variables
```

```
    %soil conductivity for dry soil
    varSIGMAD = 0.01;

    %soil conductivity for wet soil
    varSIGMAW = 0.077;

    %electric constant
    varEPSILON0 = 0.00000000000885;

    %permittivity for dry soil
    varEPSILOND = 0.00000000006195;

    %permittivity for wet soil
    varEPSILONW = 0.00000000025665;

    %skin depth of the soil
    global varDELTA;

    %permeability of soil
    varMU = 0.000001256636;

    %eddy current factor
    global varG;

    %mutual inductance
    global varMI;

    %added for third simulation
    global varX;

    %angle between successive coil radial directions
    varTHETAT = 1.5707963268;
    varTHETAR = -1.5707963268;
```

```

        %frequency
        varFRQ = 10000000.0;

        %inductance
        global varL;

        %capacitance
        varC = 0.000000000001;

        %copper resistivity
        varRHO = 0.000000016780;

        %copper resistance of coil
        global varR;

        %matched impedance or impedance for a given value of L
        varZL = 0.0;

        %impedance
        global varZ;

        %power transmitted by the transmitter
        varPT = 0.01;
        %power received by the receiver
        varPR = 0.0;

        %coil wire radius
        varCRW = 0.00050000;

        %coil radius
        varCA = 0.15;

```

```
        %coil wire radius
        varCWA = 0.0005;

        %coil length
        varCL = 0.075;

        %assumed value
        %coil winding height
        varCLWNDHGT = 0.01;

        %number of coil windings
        varNUMCLWND = 1000.0;

        %number of relay coils
        varNUMRLYCLS = 15.0;

        %transmission distance
        varTRD = 50.0;

        %relay distance
        varRLD = 3.33;

        %common variables
        varCMN0 = 0.0;
        varCMN1 = 0.0;

        %invocations
        %set the common variables depending on dry or wet soil
        varCMN0 = varSIGMAW;
        varCMN1 = varEPSILONW;
        calcDELTA(varMU, varCMN0, varCMN1, varFRQ);
        calcG(varRLD);
        calcL(varMU, varNUMCLWND, varCA, varCL, varCLWNDHGT);
```

```
        calcR(varRHO, varCA, varNUMCLWND, varCRW);

        %added for third simulation
        %consider frequencies in the range 10 MHz - 300 MHz
        arrayVARFRQ = zeros(29,1);
        %arrays for storing the calculated Z and X values for
        %different frequencies
        arrayVARZ = zeros(29,1);
        arrayVARX = zeros(29,1);
        %generate the range of frequencies
        arrayVARFRQ = linspace(10000000,3000000000,29);
%         disp('FREQUENCY VALUES');
%         disp('------------------');
%         disp(arrayVARFRQ);
        % calculate the mutual inductance
        calcMI(varMU, varNUMCLWND, varCA, varRLD, varTHETAT,
            ↪ varTHETAR);
        %calculate Z for the range of frequency values and store
            ↪ in the
        %array
        for i = 1:29
        calcZ(arrayVARFRQ(i), varC);
        arrayVARZ(i) = varZ;
        end
%         disp('IMPEDANCE VALUES');
%         disp('------------------');
%         disp(arrayVARZ);
        %calculate X for the range of frequency values and store
            ↪ in the
        %array
        for i = 1:29
            %set varZL to the current value of impedance
            varZL = arrayVARZ(i);
```

```
                calcX(varFRQ, varZL);
                arrayVARX(i) = varX;
            end
            % the values of x range from -infinity to infinity
            disp('X VALUES');
            disp('---------------');
            disp(arrayVARX);
%           plot the data
            x = zeros(29,1);
            y = zeros(29,1);
            x = arrayVARFRQ;
            y = arrayVARX;

%               this is a workaround for plotting since the values of x range
%               from -infinity to infinity
              y1 = -(inf(29,1));
              y2 = inf(29,1);

            figure % new figure
            [hAx,hLine1,hLine2] = plotyy(x,y1,x,y2);
            title('Value of x for different system frequencies in wet soil','fontweight','bold','fontsize',10);
            xlabel('frequency');
            ylabel(hAx(1),'x', 'fontsize',9); % left y-axis
            ylabel(hAx(2),'x', 'fontsize',9); % right y-axis

           export_fig Figure12.pdf

%nested at the first level

%function to calculate the skin depth
      function calcDELTA(varMU, varCMN0, varCMN1, varFRQ)
```

```
          varTMP1 = 2 * pi * varFRQ;
%            disp(varTMP1);
          varTMP2 = varMU * varCMN1/2;
%            disp(varTMP2);
          varTMP3  = power(varCMN0, 2);
%            disp(varTMP3);
          varTMP4 = power(2 * pi * varFRQ, 2);
%            disp(varTMP4);
          varTMP5 = power(varCMN1, 2);
%            disp(varTMP5);
          varTMP6 = varTMP4 * varTMP5;
%            disp(varTMP6);
          varTMP7 = varTMP3/varTMP6;
%            disp(varTMP7);
          varTMP8 = sqrt(1 + varTMP7);
%            disp(varTMP8);
          varTMP9 = varTMP8 - 1;
%            disp(varTMP9);
          varTMP10 = sqrt(varTMP2 * varTMP9);
%            disp(varTMP10);
          varDELTA = double(1/varTMP1 * varTMP10);
     end

%function to calculate the eddy current factor
     function calcG(varRLD)
          varTMP1 = double(-varRLD/varDELTA);
%            disp(varTMP1);
          varTMP2 = double(exp(varTMP1));
%            disp(varTMP2);
          varG = varTMP2;
     end

```

```
%function to calculate mutual inductance between two coils without MI
%waveguide tunnel
    function calcMI(varMU, varNUMCLWND, varCA, varRLD, varTHETAT, varTHETAR)
     varMI =  double(varMU * pi * (varNUMCLWND.^2) * ((varCA.^4)/(4 * (varRLD.^3))) * ((2* sin(varTHETAT) * sin(varTHETAR)) + (cos(varTHETAT) * cos(varTHETAR))) * varG);
    end

%function to calculate mutual inductance between two coils with MI
%waveguide tunnel
    function calcMIWT(varMU, varNUMCLWND, varCA, varRLD, varTHETAT, varTHETAR)
        varTMP1 = double(varMU * pi);
        varTMP2 = double(varNUMCLWND.^2);
        varTMP3 = double(varCA.^4);
        varTMP4 = double(4 * (varRLD.^3));
        varTMP5 = double(varTMP1 * varTMP2);
        varTMP6 = double(varTMP3/varTMP4);
        varTMP7 = double((2* sin(varTHETAT) * sin(varTHETAR)) + (cos(varTHETAT) * cos(varTHETAR)));
        varMI = double(varTMP5 * varTMP6 * varTMP7);
        % varMI =  double(varMU * pi * (varNUMCLWND.^2) * ((varCA.^4)/(4 * (varRLD.^3))) * ((2* sin(varTHETAT) * sin(varTHETAR)) + (cos(varTHETAT) * cos(varTHETAR))));
    end

%function to calculate the self inductance of a coil
    function calcL(varMu, varNUMCLWND, varCA, varCL, varCLWNDHGT)
        varTMP1 = 21;
```

```
        varL = double(((varTMP1 * varMu * (varNUMCLWND.^2) *
            ↪ varCA)/4 * pi) * ((varCA/(varCL + varCLWNDHGT))
            ↪ .^0.5));
    end

%function to calculate copper resistance of coil
    function calcR(varRHO, varCA, varNUMCLWND, varCRW)
        varR = varRHO * ((2 * varCA * varNUMCLWND)/(varCRW.^2));
    end
%function to calculate the coil impedance for a given value of
    ↪ coil
%inductance
    function calcZ(varFRQ, varC)
        varTMP1 = sqrt(-1) * 2 * pi * varFRQ * varL;
        varTMP2 = sqrt(-1) * 2 * pi * varFRQ * varC;
        varTMP3 = 1/varTMP2;
        varTMP4 = varTMP1 + varTMP3 + varR;
        varZ = varTMP4;
    end
%function to calculate the value of X for a generated value of Z
    function calcX(varFRQ, varZL)
        varTMP1 = sqrt(-1) * 2 * pi * varFRQ * varMI;
        varTMP2 = varZL/varTMP1;
        varX = varTMP2;
    end

end
```

```
function simulation6test3 ()
%Reference: Channel Capacity of Magnetic Induction Based Wireless
    ↪ Underground Sensor Networks under Practical Constraints
% simulation to model the scaling of x for a given frequency
    ↪ range using the MI waveguide tunnel
```

```

% set the floating point precision
%DIGITS := 40;
%variables
        %soil conductivity for dry soil
        varSIGMAD = 0.01;

        %soil conductivity for wet soil
        varSIGMAW = 0.077;

        %electric constant
        varEPSILON0 = 0.00000000000885;

        %permittivity for dry soil
        varEPSILOND = 0.00000000006195;

        %permittivity for wet soil
        varEPSILONW = 0.00000000025665;

        %skin depth of the soil
        global varDELTA;

        %permeability of soil
        varMU = 0.000001256636;

        %eddy current factor
        global varG;

        %mutual inductance
        global varMI;

        %added for third simulation
        global varX;
```

```

%angle between successive coil radial directions
varTHETAT = 1.5707963268;
varTHETAR = -1.5707963268;

%frequency
varFRQ = 10000000.0;

%inductance
global varL;

%capacitance
varC = 0.000000000001;

%copper resistivity
varRHO = 0.000000016780;

%copper resistance of coil
global varR;

%matched impedance or impedance for a given value of L
varZL = 0.0;

%impedance
global varZ;

%power transmitted by the transmitter
varPT = 0.01;
%power received by the receiver
varPR = 0.0;

%coil wire radius
varCRW = 0.00050000;
```

```

%coil radius
varCA = 0.15;

%coil wire radius
varCWA = 0.0005;

%coil length
varCL = 0.075;

%assumed value
%coil winding height
varCLWNDHGT = 0.01;

%number of coil windings
varNUMCLWND = 1000.0;

%number of relay coils
varNUMRLYCLS = 15.0;

%transmission distance
varTRD = 50.0;

%relay distance
varRLD = 3.33;

%common variables
varCMN0 = 0.0;
varCMN1 = 0.0;

%invocations
%set the common variables depending on dry or wet soil
varCMN0 = varSIGMAW;
```

```
        varCMN1 = varEPSILONW;
        calcDELTA(varMU, varCMN0, varCMN1, varFRQ);
        calcG(varRLD);
        calcL(varMU, varNUMCLWND, varCA, varCL, varCLWNDHGT);
        calcR(varRHO, varCA, varNUMCLWND, varCRW);

        %added for third simulation
        %consider frequencies in the range 10 MHz - 300 MHz
        arrayVARFRQ = zeros(29,1);
        %arrays for storing the calculated Z and X values for
        %different frequencies
        arrayVARZ = zeros(29,1);
        arrayVARX = zeros(29,1);
        %generate the range of frequencies
        arrayVARFRQ = linspace(10000000,3000000000,29);
%         disp('FREQUENCY VALUES');
%         disp('------------------');
%         disp(arrayVARFRQ);
        % calculate the mutual inductance
        calcMIWT(varMU, varNUMCLWND, varCA, varRLD, varTHETAT, varTHETAR);
        %calculate Z for the range of frequency values and store in the
        %array
        for i = 1:29
        calcZ(arrayVARFRQ(i), varC);
        arrayVARZ(i) = varZ;
        end
%         disp('IMPEDANCE VALUES');
%         disp('------------------');
%         disp(arrayVARZ);
        %calculate X for the range of frequency values and store in the
```

```
        %array
        for i = 1:29
            %set varZL to the current value of impedance
            varZL = arrayVARZ(i);
            calcX(varFRQ, varZL);
            arrayVARX(i) = varX;
        end
%           disp('X VALUES');
%           disp('----------');
%           disp(arrayVARX);
%           plot the data
        x = zeros(29,1);
        y = zeros(29,1);
        x = arrayVARFRQ;
        y = arrayVARX;

        figure % new figure
        plot(x,y);
        title('Value of x for different system frequencies using MI waveguide tunnel','fontweight','bold','fontsize',8.25);
        xlabel('frequency');
        ylabel('x', 'fontsize',9);

        export_fig Figure13.pdf

%nested at the first level

%function to calculate the skin depth
    function calcDELTA(varMU, varCMN0, varCMN1, varFRQ)
        varTMP1 = 2 * pi * varFRQ;
%           disp(varTMP1);
        varTMP2 = varMU * varCMN1/2;
```

```
%           disp(varTMP2);
            varTMP3  = power(varCMN0, 2);
%           disp(varTMP3);
            varTMP4 = power(2 * pi * varFRQ, 2);
%           disp(varTMP4);
            varTMP5 = power(varCMN1, 2);
%           disp(varTMP5);
            varTMP6 = varTMP4 * varTMP5;
%           disp(varTMP6);
            varTMP7 = varTMP3/varTMP6;
%           disp(varTMP7);
            varTMP8 = sqrt(1 + varTMP7);
%           disp(varTMP8);
            varTMP9 = varTMP8 - 1;
%           disp(varTMP9);
            varTMP10 = sqrt(varTMP2 * varTMP9);
%           disp(varTMP10);
            varDELTA = double(1/varTMP1 * varTMP10);
      end

%function to calculate the eddy current factor
      function calcG(varRLD)
            varTMP1 = double(-varRLD/varDELTA);
%           disp(varTMP1);
            varTMP2 = double(exp(varTMP1));
%           disp(varTMP2);
            varG = varTMP2;
      end

%function to calculate mutual inductance between two coils
    ↪ without MI
%waveguide tunnel
```

```
    function calcMI(varMU, varNUMCLWND, varCA, varRLD, varTHETAT, varTHETAR)
     varMI =  double(varMU * pi * (varNUMCLWND.^2) * ((varCA.^4)/(4 * (varRLD.^3))) * ((2* sin(varTHETAT) * sin(varTHETAR)) + (cos(varTHETAT) * cos(varTHETAR))) * varG);
    end

%function to calculate mutual inductance between two coils with MI
%waveguide tunnel
    function calcMIWT(varMU, varNUMCLWND, varCA, varRLD, varTHETAT, varTHETAR)
        varTMP1 = double(varMU * pi);
        varTMP2 = double(varNUMCLWND.^2);
        varTMP3 = double(varCA.^4);
        varTMP4 = double(4 * (varRLD.^3));
        varTMP5 = double(varTMP1 * varTMP2);
        varTMP6 = double(varTMP3/varTMP4);
        varTMP7 = double((2* sin(varTHETAT) * sin(varTHETAR)) + (cos(varTHETAT) * cos(varTHETAR)));
        varMI = double(varTMP5 * varTMP6 * varTMP7);
        % varMI =  double(varMU * pi * (varNUMCLWND.^2) * ((varCA.^4)/(4 * (varRLD.^3))) * ((2* sin(varTHETAT) * sin(varTHETAR)) + (cos(varTHETAT) * cos(varTHETAR))));
    end

%function to calculate the self inductance of a coil
    function calcL(varMu, varNUMCLWND, varCA, varCL, varCLWNDHGT)
        varTMP1 = 21;
        varL = double(((varTMP1 * varMu * (varNUMCLWND.^2) * varCA)/4 * pi) * ((varCA/(varCL + varCLWNDHGT)).^0.5));
```

```
    end

%function to calculate copper resistance of coil
    function calcR(varRHO, varCA, varNUMCLWND, varCRW)
        varR = varRHO * ((2 * varCA * varNUMCLWND)/(varCRW.^2));
    end
%function to calculate the coil impedance for a given value of
  ↪ coil
%inductance
    function calcZ(varFRQ, varC)
        varTMP1 = sqrt(-1) * 2 * pi * varFRQ * varL;
        varTMP2 = sqrt(-1) * 2 * pi * varFRQ * varC;
        varTMP3 = 1/varTMP2;
        varTMP4 = varTMP1 + varTMP3 + varR;
        varZ = varTMP4;
    end
%function to calculate the value of X for a generated value of Z
    function calcX(varFRQ, varZL)
        varTMP1 = sqrt(-1) * 2 * pi * varFRQ * varMI;
        varTMP2 = varZL/varTMP1;
        varX = varTMP2;
    end

end
```

A.5.2 Scenario 2: Deployment Complexity

This subsection reproduces the MATLAB source code for Simulation 7, pertaining to deployment complexity. The two simulation tests essentially compare the domain network model and the MST model (Sun & Akyildiz 2010*b*) under the same node range.

```
function simulation7test1 ()
%Reference: On random graphs
```

```
%   simulation to model the node vs link scaling for MST network model

%for MST
arrayNUMNODESMST = zeros(1,100);
arrayNUMLINKSMST = zeros(1,100);

%constant real number c is taken as 1
varC = 1;
for i = 1:100
    arrayNUMNODESMST(i) = i;
    arrayNUMLINKSMST(i) = int8 ( (0.5 * arrayNUMNODESMST(i) * log (arrayNUMNODESMST(i))) + 1 * arrayNUMNODESMST(i));
end
% disp(arrayNUMNODESMST);
% disp(arrayNUMLINKSMST);
% plot the data
    x = zeros(1,100);
    y = zeros(1,100);
    x = arrayNUMNODESMST;
    y = arrayNUMLINKSMST;
    figure % new figure
    plot(x,y);
    title('Node vs Link Scaling for Minimum Spanning Tree 2D Network','fontweight','bold','fontsize',10);
    xlabel('Number of nodes');
    ylabel('Number of links');

    export_fig Figure14.pdf

end
```

```
function simulation7test2 ()
```

```
%Reference: On random graphs
%   simulation to model the node vs. link scaling for the domain
    network
%   model

%for domain network
arrayNUMNODESDN = zeros(1,100);
arrayNUMLINKSDN = zeros(1,20);

% for domain network
% assume 5 nodes per aggregator node
% a new link is calculated per aggregator node, synonymous with
    the MI
% waveguide tunnel
global j;
for i = 1:100
    arrayNUMNODESDN(i) = i;
    if(1 == arrayNUMNODESDN(i))
        j = 1;
        arrayNUMLINKSDN(j) = 1;
        j = j + 1;
    end
    if(0 == rem(arrayNUMNODESDN(i),5))
        if(5 == arrayNUMNODESDN(i))
            continue;
        end
            arrayNUMLINKSDN(j) = arrayNUMLINKSDN(j - 1) + 1;
            j = j + 1;
    end
end
% disp(arrayNUMNODESDN);
% disp(arrayNUMLINKSDN);
%plot the data
```

```
    x = zeros(1,100);
    y = zeros(1,100);
    x = arrayNUMNODESDN;
    j = 1;
    for i = 1: 100
        if(0 == rem(arrayNUMNODESDN(i),5))
            y(i) = arrayNUMLINKSDN(j);
            j = j + 1;
        end
    end
    figure % new figure
    plot(x,y);
    title('Node vs Link Scaling for Domain Network','fontweight',
      'bold','fontsize',10);
    xlabel('Number of nodes');
    ylabel('Number of links');

    export_fig Figure15.pdf


end
```

A.6 Chapter Summary

This addendum reproduced the source code used in the simulations presented under both Chapter 7 and Chapter 8.

Appendix B

A Brief Primer on Electromagnetic Induction

B.1 Overview of Addendum

This addendum has been included to provide a brief primer on Electromagnetic induction. This primer has been intended as a prelude to the more involved discussion on MI waveguide structures, provided under a subsequent addendum.

The discussion below has drawn chiefly on (Popovic & Popovic 2000), besides other references.

B.2 Fundamental Principles of Electromagnetic Induction

B.2.1 Coulomb's Law

Coulomb's law states that two static point charges in space exert a force upon each other which is given by the following vector equation (Popovic & Popovic 2000):

$$F_e 12 = \frac{1}{4\pi\varepsilon_0}\frac{Q_1 Q_2}{r^2} u_r 12 \tag{B.1}$$

In the above equation, F_e12 denotes the magnitude of the force vector exerted by the point charge Q_1 in the direction of Q_2, and r denotes the distance between them. The symbol u_r12 denotes the unit vector in the same direction. The constant ε_0 denotes the *permittivity of free space or vacuum.* It is either expressed in units $C^2/(m^2N)$ or F/m (Farads/metre). The value of ε_0 is approximated as $\frac{1}{36\pi.10^9}F/m$.
Coulomb's law applies to a static electric field or *electrostatic field*, which is the simplest variant of the general electromagnetic field.

B.2.2 Electromagnetic Induction

The fundamental precept about magnetism in classical physics is that *it is the result of moving charges.* In addition to the force expressed by Coulomb's law, two charges moving at constant velocity also exert an additional *magnetic force* on each other. The notion of an *electric field* is complementary to that of a *magnetic field.* In the case of static charges, the force exerted can be explained only in terms of the electric field. In the case of moving charges, however, the force exerted is due to the magnetic field.
From the above precepts, a very important relationship between the two fields can be hypothesized: *a magnetic field that varies with time is also characterized by an electric field that varies accordingly.* This fundamental precept holds the explanation for why moving charged particles are influenced by a magnetic field. The electric field that results due to a variation in the magnetic field is termed as the *induced electric field.*
A corollary to the induced electric field, is that of a magnetic field which varies in accordance with a varying current. This in turn induces an electric field, based on the above explanation. Thus the bottom-line is that a variation of the electric field is always characterized by a variation of the magnetic field, and vice versa.

B.2.2.1 Magnetic Coupling

NOTE

The below description has been adapted from Example 14.1 of (Popovic & Popovic 2000).

The concept of magnetic coupling can be explained based on the above discussion. Consider two concentric circles representing two closed coil loops C_1 and C_2 (represented using dotted lines), as shown in Figure B.1. Assume that a time varying current $i(t)$ exists on C_1 as shown in the figure. In turn, $i(t)$ induces a concentric electric field around C_1. This induced electric field is tangential to C_2, as shown in the figure. Consequently, the line integral of the induced electric field on C_2 is non-zero, and this results in an induced emf around C_2.

Thus going by Figure B.1, the induced electric field enables transport of energy between the loops without any physical contact. In other words, the induced electric field due to a time varying current in C_1 induces a time varying current in C_2. This phenomenon is referred to as *magnetic coupling*, considering the fact that a time varying electric field (which is the induced electric field in C_1) is also characterized by a time varying magnetic field. Magnetic Induction (MI) (Electromagnetic Induction) is yet another phrase for magnetic coupling.

In the above explanation, the shape of the coils is irrelevant. The significant factors impacting MI are the strength of the induced electric field in the primary coil (C_1 Figure B.1), and the distance between two adjacent closed coil loop structures. Thus it is also possible to envisage a relay mechanism using a similar arrangement of closed loop coil structures, comprising of a primary coil (C_1 Figure B.1) and a secondary coil (C_2 Figure B.1), separated by a suitable number of relay coils in accordance with the required power transfer efficiency.

NOTE

The reader can further build on the above fundamentals by gaining familiarity with Faraday's laws of Electromagnetic Induction and Maxwell's equations.

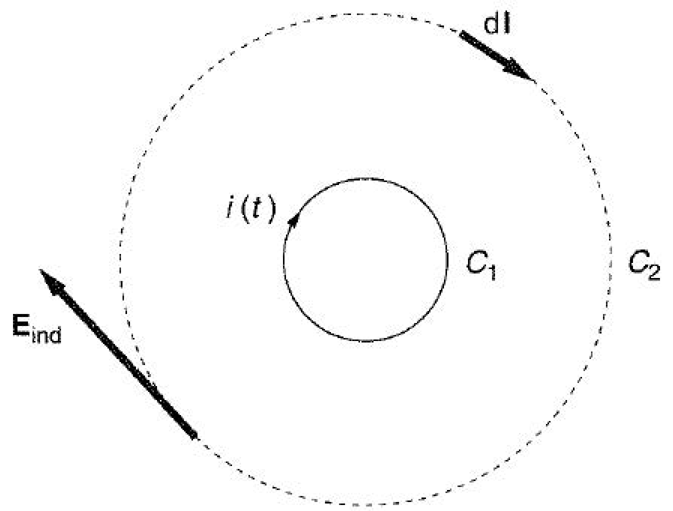

Figure B.1: Magnetic Coupling *Figure copied from Figure 14.3 of (Popovic & Popovic 2000)*

B.3 Chapter Summary

This addendum provided a brief primer on Electromagnetic induction.

Appendix C

A Brief Overview of the MI Waveguide System

C.1 Overview of Addendum

The purpose of this addendum is to provide a more detailed (yet terse) overview of the MI waveguide structures introduced and discussed under Chapter 4. The overview presented under this addendum is in no way a substitute for the description provided in the original reference material for the relevant waveguide structure; rather this overview is intended more as a useful pointer to the relevant MI waveguide structure detailed in the original reference under consideration. A reader of this dissertation short of time to browse through the original reference, would still benefit from the overview presented herein in terms of gaining a basic understanding of the waveguide structure, and is the intended purpose of this addendum as well; however, such reader would have the best foot forward by familiarizing oneself with the original reference under consideration, in order to make most of the technical discussion presented under Chapter 4.

In order to render the following discussion more apt and to the point, a separate section has been devoted to the MI waveguide structure presented under a particular reference publication and discussed under Chapter 4; the author believes that such categorization should also enable the reader to browse through this addendum more efficiently.

C.2 Overview of MI Waveguide Structure from "Magneto-inductive waveguide" (authored by E. Shamonina, V.A. Kalinin, K.H. Ringhofer and L. Solymar) Published in 2002

This work, (Shamonina et al. 2002*b*), introduced the notion of the MI waveguide structure. The prototype design exposited in the work has been reproduced in Figure C.1.

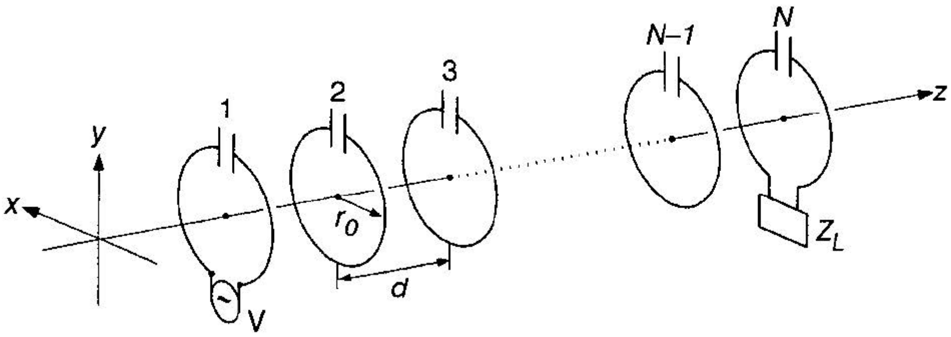

Figure C.1: MI waveguide structure introduced in (Shamonina et al. 2002*b*). *Figure reproduced from original text.*

The structure in the figure consists of a finite array (N elements) of capacitively-loaded loops of radius r_0 placed at a distance d from each other. The waveguide is excited by means of a voltage V of frequency ω in loop 1, and is terminated by a load impedance of $Z_L = R_L + jX_L$ in the last element. The presence of a capacitance in each loop is necessary for the existence of propagating longitudinal waves.

C.3 Overview of MI Waveguide Structure from "Experimental and theoretical study of magneto-inductive waves supported by one-dimensional arrays of "swiss rolls" " (authored by M. C. K. Wiltshire, E. Shamonina, I. R. Young and L. Solymar) Published in 2004

The concept of "swiss rolls" as a magnetic microstructure was introduced in (Pendry, Holden, Robbins & Stewart 1999).

NOTE

The notion of magnetic microstructures as expounded in (Pendry et al. 1999), relates to that of composite materials engineered to generate a desirable effective magnetic permeability (μ_{eff}).

Figure C.2 reproduces the design of a "swiss roll" capacitor proposed in (Pendry et al. 1999). In this design, each turn of a given coil constitutes a cylindrical face formed by winding a metallic sheet. Each turn of the coil is separated by a distance d from the previous sheet.

The design shown in Figure C.2 should be understood as a modification of a metallic cylinder, designed to have magnetic properties in the direction parallel to its axis. A square array of such cylinders is shown in Figure C.3, reproduced from (Pendry et al. 1999).

In (Wiltshire et al. 2004), the 1D waveguide design proposed in (Shamonina et al. 2002*b*) has been combined with the "swiss roll" capacitor design adopted from (Pendry et al. 1999), to produce an 1D array of "swiss rolls". An experimental setup diagram using two elements of such an array as shown in (Wiltshire et al. 2004), has been reproduced in Figure C.4.

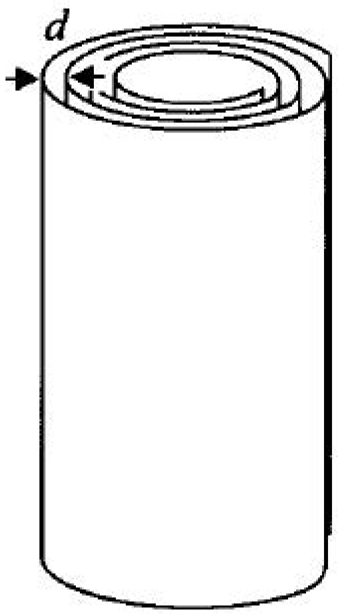

Figure C.2: Swiss roll capacitor design introduced in (Pendry et al. 1999). *Figure reproduced from original text.*

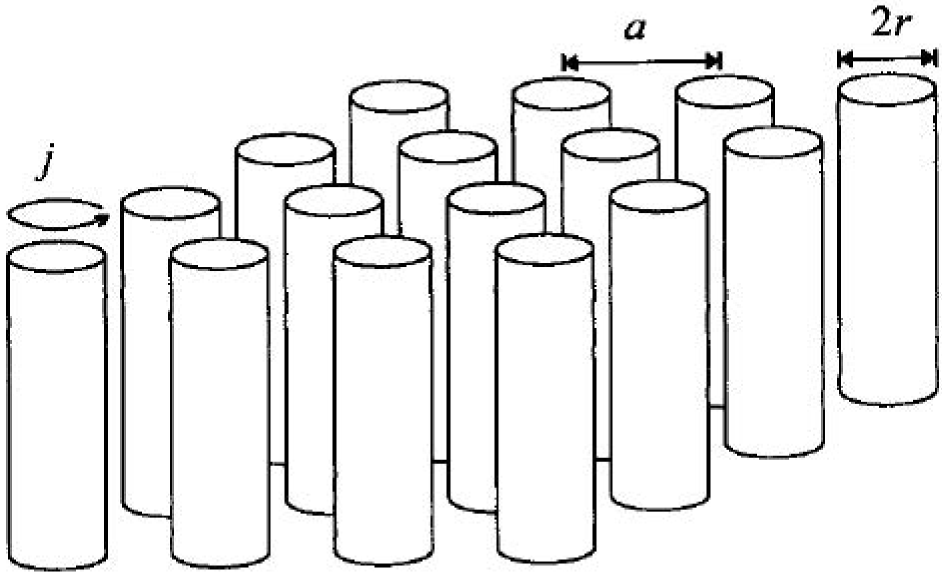

Figure C.3: Square array of metallic cylinders with magnetic properties parallel to their axes as shown in (Pendry et al. 1999). The metallic cylinder design has been modified in the design of a “swiss roll” capacitor. *Figure reproduced from original text.*

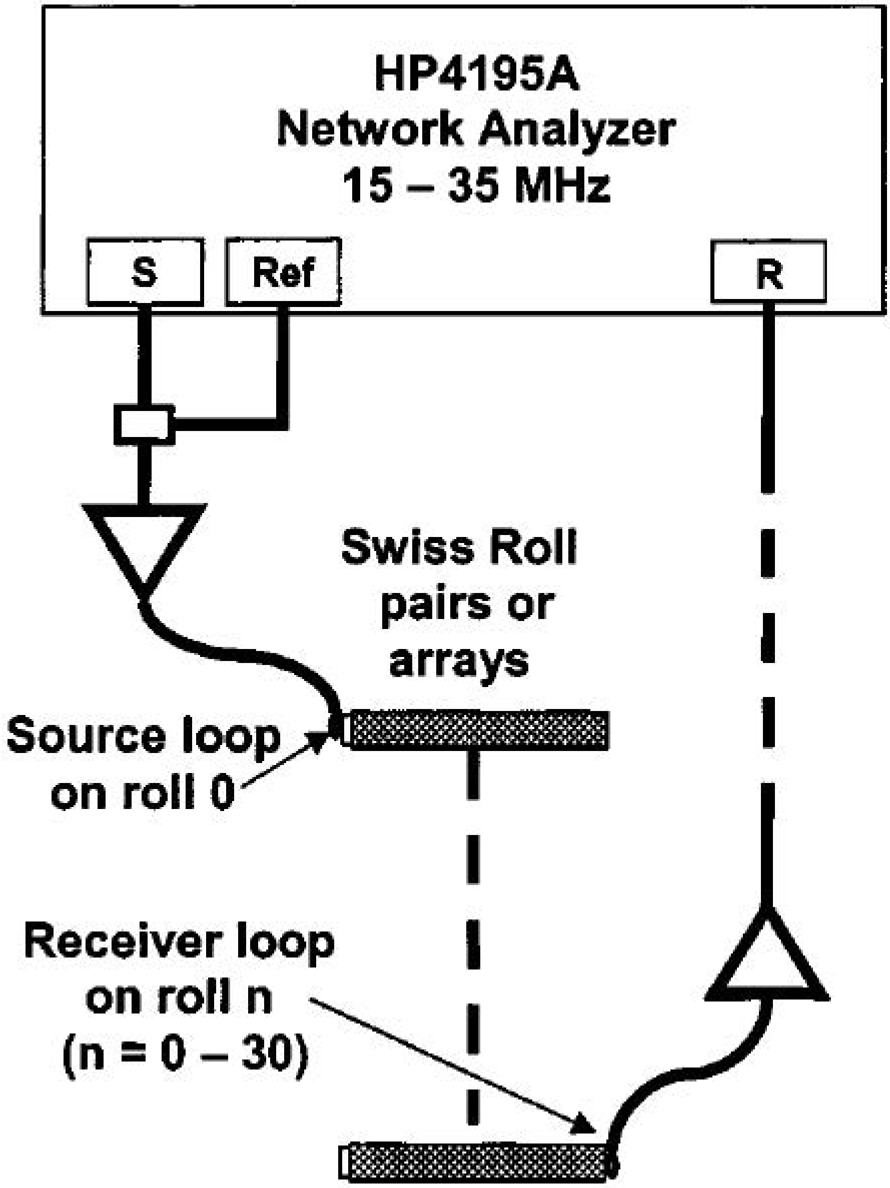

Figure C.4: Experimental setup using a pair of "swiss rolls" as shown in (Wiltshire et al. 2004). *Figure reproduced from original text.*

C.4 Overview of MI Waveguide Structure from "Planar magnetoinductive wave transducers: Theory and applications" (authored by M. J. Freire, R. MarquÃľs, F. Medina, M. A. G. Laso, and F. MartÃŋn) Published in 2004

In (Shamonina et al. 2002*b*), the coil loops of the waveguide are arranged such that the line connecting the centres of the loops is perpendicular to the plane of the loops. This is referred to as the *axial* arrangement of the MI waveguide. On the contrary, in the *planar* waveguide arrangement of coil loops, the line connecting centres of the loops is parallel to (along) the plane of the loops. For the sake of illustrating the planar arrangement, a diagram from (Sun & Akyildiz 2012) has been reproduced in Figure C.5.

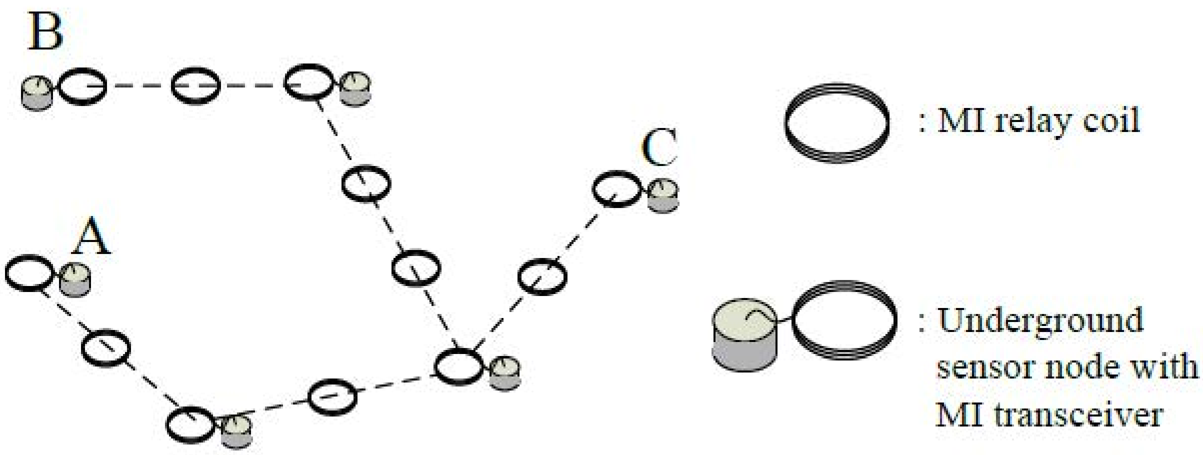

Figure C.5: A planar waveguide arrangement of coil loops as shown in (Sun & Akyildiz 2012). *Figure reproduced from original text.*

In (Freire et al. 2004), the planar MI waveguide is constituted of "a conventional planar circuit board in microstrip technology." The notion of a "split ring" as a magnetic microstructure was introduced in (Pendry et al. 1999), which is a metallic cylinder with an internal structure, reproduced in Figure C.6 from (Pendry et al. 1999).

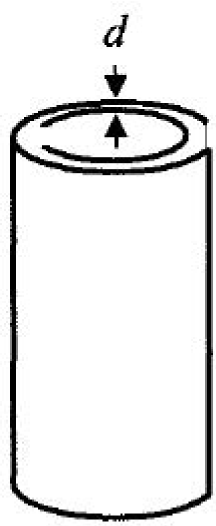

Figure C.6: A "split ring" design as shown in (Pendry et al. 1999). *Figure reproduced from original text.*

C.4 MI Waveguide Structure Introduced by Freire et al., 2004381

The design essentially consists of metallic sheets forming the cylinder separated from each other by a distance *d*. This inter-ring gap prevents current from flowing around a ring, and hence the term "split ring" for the design. The design shown in Figure C.6 should be understood as a modification of a metallic cylinder, designed to have magnetic properties in the direction parallel to its axis. A square array of such cylinders is shown in Figure C.3, reproduced from (Pendry et al. 1999).

The planar waveguide structure introduced in (Freire et al. 2004) modifies the "split ring" design introduced in (Pendry et al. 1999), shown in Figure C.6, to create the *split squared ring resonator* (SSRR). The schematic of the planar MI waveguide with SSRRs has been reproduced in Figure C.7 below from (Freire et al. 2004).

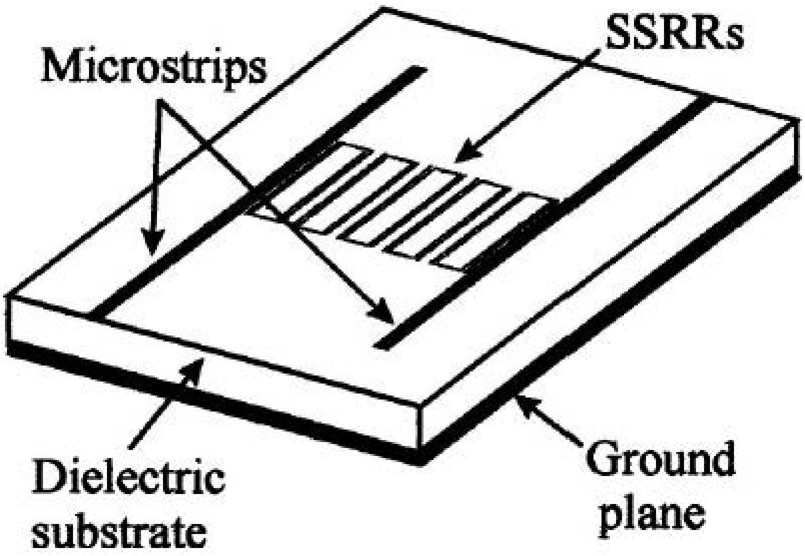

Figure C.7: Schematic of planar MI waveguide with SSRRs as shown in (Freire et al. 2004). *Figure reproduced from original text.*

C.5 Overview of MI Waveguide Structure based on Solenoids from "Low-loss magneto-inductive waveguides" (authored by R R A Syms, I R Young, and L Solymar) Published in 2006

In (Syms, Young & Solymar 2006), MI waveguides supporting forward waves have been presented as a set of L-C resonators separated by a distance a. Figure C.8 reproduces the schematic and the lumped circuit equivalent of such a waveguide, as shown in (Syms, Young & Solymar 2006).

NOTE

In L-C resonators, L stands for inductor and C for capacitor.

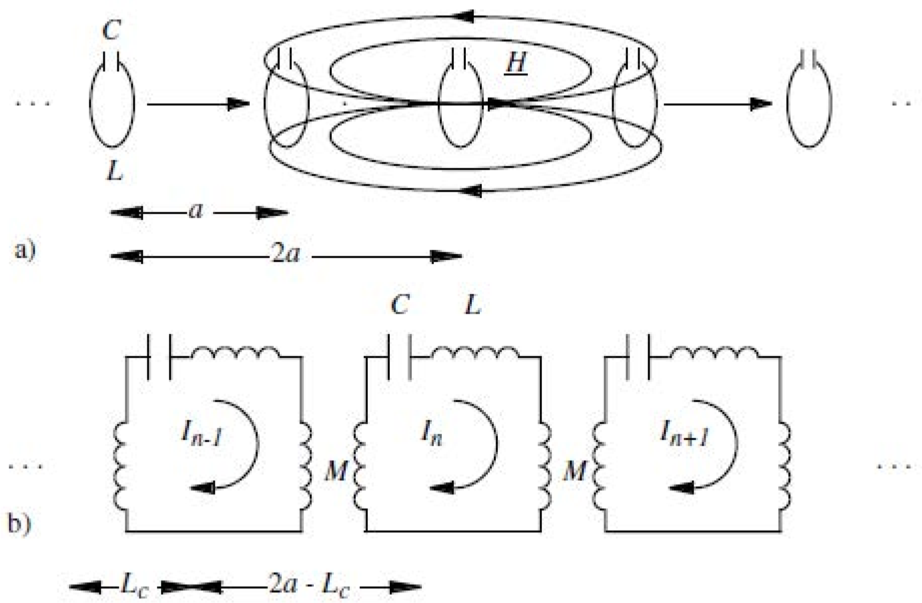

Figure C.8: Schematic and lumped circuit equivalent of MI waveguide as a set of L-C resonators shown in (Syms, Young & Solymar 2006). *Figure reproduced from original text.*

MI waveguides based on solenoids have been presented as one option for structures supporting forward waves whose elements "are coupled strongly to their nearest neighbours and only weakly to non-nearest ones." The idea involved is to replace each inductor in the original MI waveguide as a set of L-C resonators, with a solenoid. To quote (Syms, Young & Solymar 2006) in this context:

"Here the inductors are replaced by solenoids, of length L_c, so the distance between the coil ends is $a - L_c$ for nearest neighbours, $2a - L_c$ for second neighbours, and so on. The effect is to move nearest neighbours relatively closer to each other than higher ones, so that their coupling is enhanced."

Figure C.9 reproduces the schematic of the MI waveguide based on solenoids from (Syms, Young & Solymar 2006).

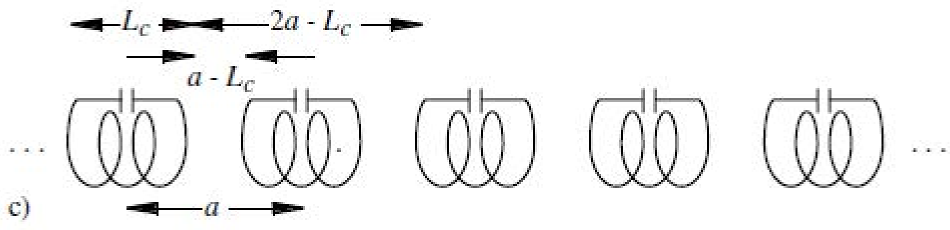

Figure C.9: Schematic of MI waveguide based on solenoids shown in (Syms, Young & Solymar 2006). *Figure reproduced from original text.*

C.6 Overview of MI Waveguide Model Introduced by "Magnetic Induction Communications for Wireless Underground Sensor Networks" (authored by Zhi Sun and Ian F. Akyildiz) Published in 2010

The fundamental MI waveguide model for WUSN was proposed in (Sun & Akyildiz 2010*c*). A detailed technical review of the model has been presented under Section 4.3. All the relevant research reports reviewed under Section 4.4 have also been based on the fundamental MI waveguide model. In this section, the author provides a brief overview of the MI waveguide model proposed in (Sun & Akyildiz 2010*c*).

It would be easier to explain the MI waveguide model proposed in (Sun & Akyildiz 2010*c*), by correlating the model with the model for MI communication outlined in the work. The model for MI communication has been reproduced under Figure C.10. It can be observed from Figure C.10 that in the MI communication model, the MI transmitter and receiver have been modelled as the primary and secondary coils of a transformer.

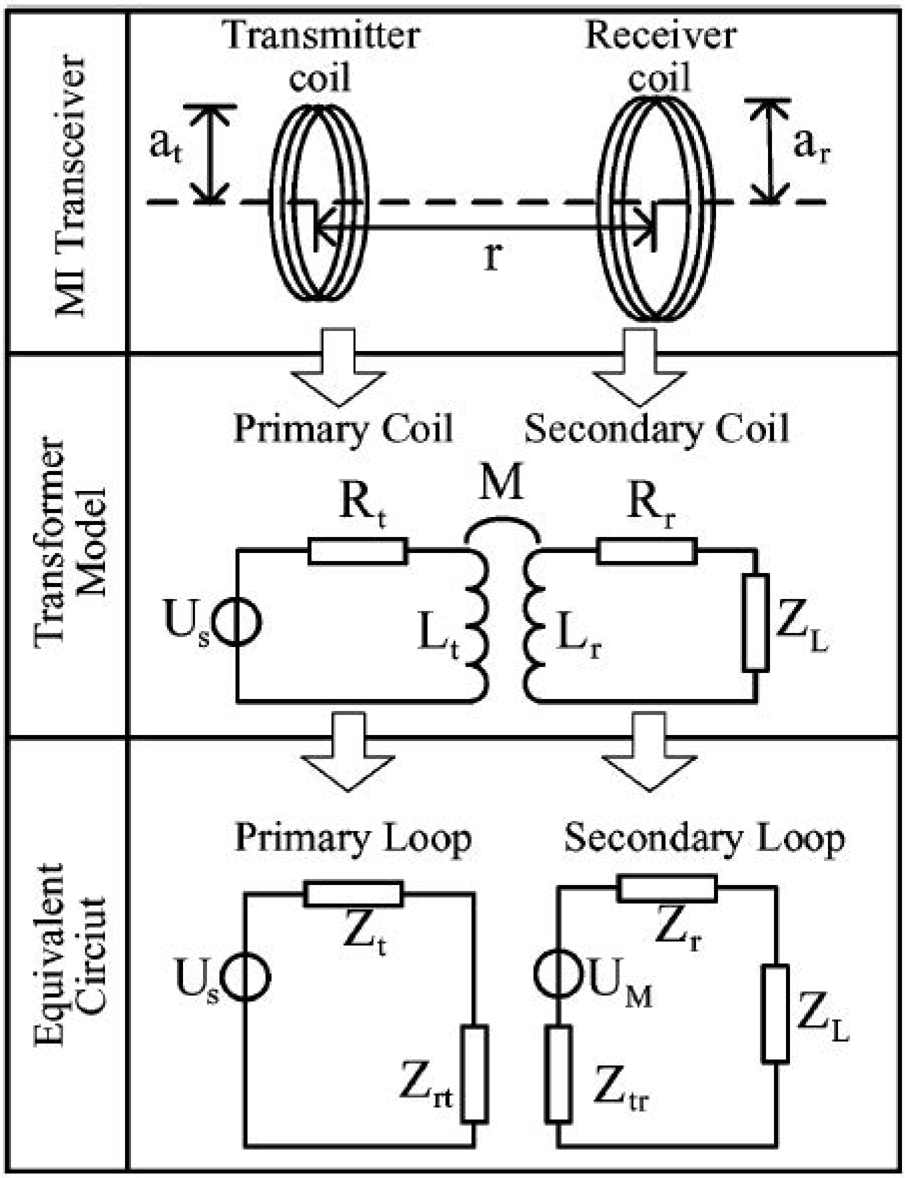

Figure C.10: Schematic of MI communication model shown in (Sun & Akyildiz 2010*c*). *Figure reproduced from original text.*

NOTE

In the figure, M denotes the mutual inductance between the coils, U_s denotes the voltage in the transmitter's battery, L_t and L_r denote the self inductance of the transmitter and the receiver coil respectively, R_t and R_r denote the resistance of the transmitter and the receiver coil respectively, and Z_L denotes the load impedance of the receiver.

The MI waveguide model can be thought of as an extension of the MI communication model, wherein the transmitter and the receiver coil are separated by equally spaced relay coils. The schematic of the MI waveguide model from (Sun & Akyildiz 2010*c*) has been reproduced in Figure C.11.

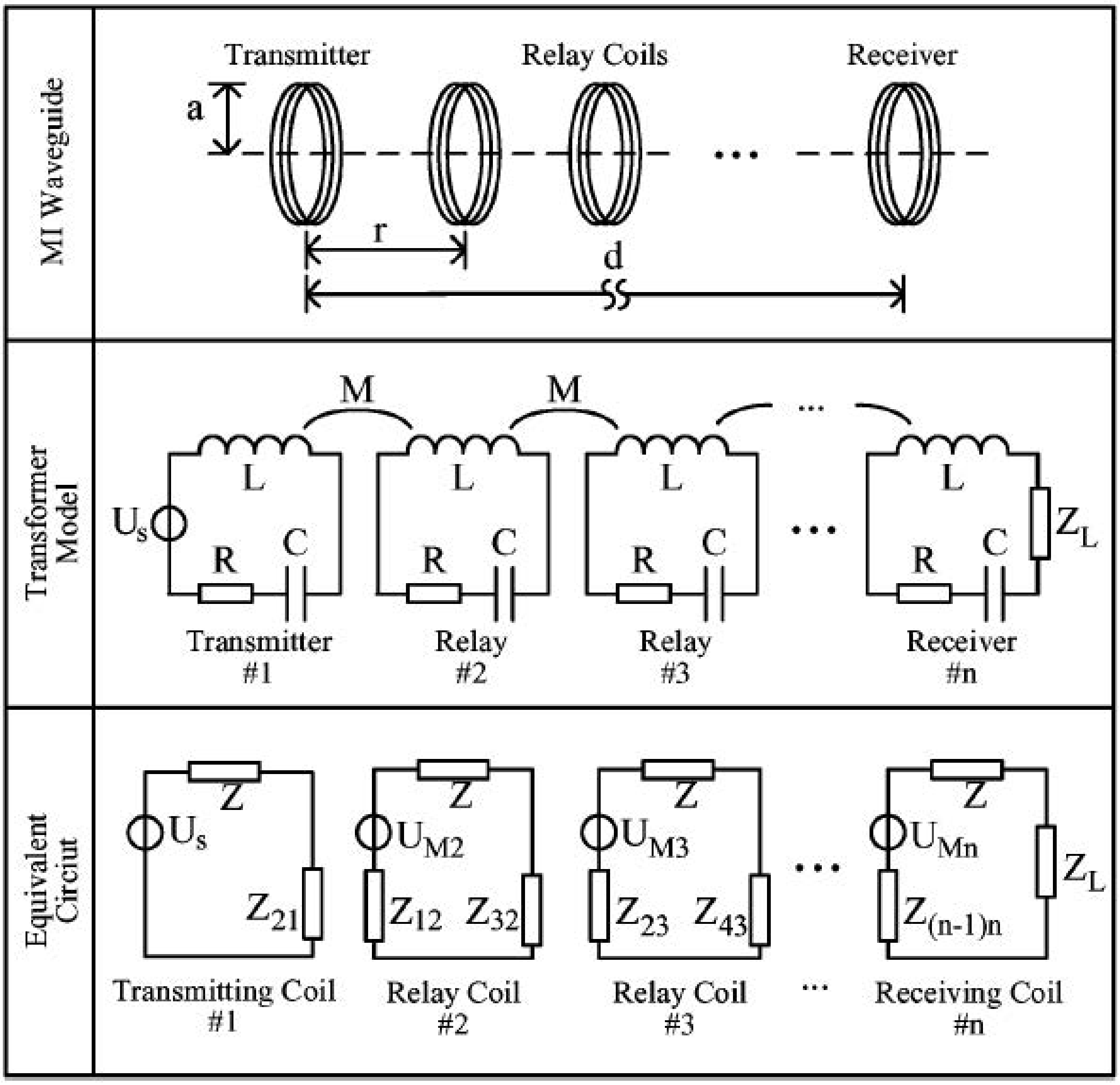

Figure C.11: Schematic of MI waveguide model shown in (Sun & Akyildiz 2010*c*). *Figure reproduced from original text.*

NOTE

It can be observed from Figure C.11 that there exists a mutual inductance M between each pair of coils, whose value is determined by the distance r between them. The distance between the transmitter and the receiver is denoted by d, and the radius of each coil is denoted by a. It can also be observed from the figure that each coil is loaded with a capacitor C, whose value impacts the resonance condition of the MI waveguide. This is also known as the *capacitor constraint* of the MI waveguide. More on the capacitor constraint of the MI waveguide and how it impacts system performance can be found under the review in Chapter 4.

C.7 Chapter Summary

This addendum provided a brief overview of the MI waveguide structures discussed under Chapter 4.